

UC Riverside

UC Riverside Electronic Theses and Dissertations

Title

Biomimetic C-H Oxidation Catalysis in Aqueous Solution

Permalink

<https://escholarship.org/uc/item/4310s4rx>

Author

Djernes, Katherine Elizabeth

Publication Date

2013

Peer reviewed|Thesis/dissertation

UNIVERSITY OF CALIFORNIA
RIVERSIDE

Biomimetic C-H Oxidation Catalysis
in Aqueous Solution

A Dissertation submitted in partial satisfaction
of the requirements for the degree of

Doctor of Philosophy

in

Chemistry

by

Katherine Elizabeth Djernes

June 2013

Dissertation Committee:

Prof. Richard J. Hooley, Chairperson

Prof. Michael Marsella

Prof. Robert C. Haddon

Copyright by
Katherine Elizabeth Djernes
2013

The Dissertation of Katherine Elizabeth Djernes is approved:

Committee Chairperson

University of California, Riverside

ACKNOWLEDGEMENTS

Grad school has had many ups and downs, and I want to thank Pablo Pappano for keeping me sane through all of them. Pablo, I love you, and I wouldn't have made it this far without you.

To Melissa Padilla and Courtney Meyet, we came and we conquered. Grad school would not have been the same without you.

I need to thank my family for their continuous support. Grad school has been a journey, and you have been there for me every step of the way.

Finally, this thesis would not be complete without thanking my advisor, Richard Hooley, for teaching me chemistry.

ABSTRACT OF THE DISSERTATION

Biomimetic C-H Oxidation Catalysis
in Aqueous Solution

by

Katherine Elizabeth Djernes

Doctor of Philosophy, Graduate Program in Chemistry
University of California, Riverside, June 2013
Dr. Richard J. Hooley, Chairperson

The ability to convert feedstock chemicals into synthetically useful derivatives is a major goal in the search for more sustainable and efficient chemical processes. One limitation in the field is the inability of known catalysts to oxidize C-H bonds regioselectively. Traditional synthetic approaches require extreme temperatures and pressures to break the C-H bond; in addition to the high energy cost of these processes, each reaction yields multiple products and over-oxidation is a common problem. In contrast to these harsh reaction conditions, enzymes catalyze C-H oxidations at ambient temperature and pressure with excellent selectivity. More recently, transition metal catalysts have been developed that can oxidize C-H bonds under more mild conditions, but a key difference between enzymes and most synthetic catalysts is that while synthetic catalysts can achieve chemoselectivity based on steric and electronic factors, enzymes exhibit regioselectivity and can selectively oxidize a position on a substrate in the presence of other chemically identical positions.

One problem with using enzymes as catalysts in synthetic organic chemistry is their limited substrate scope. As an alternative, water-soluble synthetic receptors with catalytic functions are an attractive target because they offer the potential to allow regioselective oxidations on a broader range of substrates.

Cavitands provide an alluring scaffold for metalloenzyme mimics because they are capable of displaying four rigid coordinating motifs at defined distances around a hydrophobic cavity that acts as a size-selective recognition motif. A cavitand scaffold is presented that can be smoothly derivatized by CuAAC chemistry to incorporate ligand species at the cavitand rim. The coordination of one or more metals to the scaffold allows self-folding to form a water soluble molecular receptor, without the need for covalent introduction of solubilizing groups such as sulfates or phosphates. Furthermore the hydrophobic binding site allows the cavitands to bind appropriately sized neutral guests. In the presence of a stoichiometric oxidant, the metallocavitands can selectively oxidize unactivated C-H bonds in high yield with good turnover numbers. The catalysts are wide in scope and oxidations are performed cleanly under mild conditions without side oxidation of solvent or catalyst. The cavitands retain the catalytic metal throughout the reaction, and can be recovered from the reaction system by simple filtration. Alternatively, the metallocavitands can be mounted on an SBA-15 solid support, forming highly effective heterogeneous catalysts that can be recovered after reaction in quantitative yield and re-used more than ten times without any decrease in reactivity.

TABLE OF CONTENTS

Acknowledgements	iv
Abstract	v
Table of Contents	vii
List of Figures	x
List of Tables	xiii

Chapter One: Background

1.1	Impact	1
1.2	Cytochrome P450	2
1.3	Rieske Dioxygenases	4
1.4	Methane Monooxygenase	5
1.5	Synthetic Mimics: Chemoselectivity	6
1.6	Biomimetic Catalysis: Regioselectivity	13
1.7	Limitations of Synthetic Mimics	16
1.8	Resorcinarene Based Molecular Receptors	17
1.9	Phase Transfer	25
1.10	References	26

Chapter Two: Synthesis of Cavitands

2.1	Approach	32
2.2	Palladium Catalyzed Cross Coupling Reactions	33
2.3	Click Chemistry	41
2.4	Cavitands from Commercially Available Acetylenes	44
2.5	Amide Cavitands	45

2.6	Molecular Baskets	48
2.7	Amine Cavitands	49
2.8	References	51

Chapter Three: Self-Assembly by Metal Coordination

3.1	Introduction	53
3.2	Selection of Metals	54
3.3	Pyridyl and Phenyl Binding	57
3.4	Increasing Flexibility	60
3.5	Guest Binding Studies	63
3.6	References	65

Chapter Four: Oxidations

4.1	Introduction	66
4.2	Optimization of Conditions	66
4.3	Cyclic Oxidations	69
4.4	Benzylic Oxidations	72
4.5	<i>n</i> -Alkyl Oxidations and Tolerance to Functional Groups	75
4.6	Copper Catalysis	76
4.7	Surface Chemistry	78
4.8	References	80

Chapter Five: Deep Cavitands

5.1	Introduction	81
5.2	Development of a New Cavitand Scaffold	82
5.3	Click Chemistry on the Deepened Scaffold	85
5.4	Future Work	86
5.5	Conclusions	87
5.5	References	88

Chapter Six: Experimental

6.1	General Information	89
6.2	Chapter Two Experimental	90
6.3	Chapter Three Experimental	123
6.4	Chapter Four Experimental	128
6.5	Chapter Five Experimental	128
6.6	Selected NMR Spectra	134
6.7	Selected Mass Spectra	173
6.8	X-ray Crystallographic Data	179
6.9	References	188

List of Figures

1.1	The active site of cytochrome P450	3
1.2	The catalytic cycle for cytochrome P450	4
1.3	(a) The catalytic cycle of Rieske non-heme iron oxygenases (b) The 2-His-1-carboxylate facial triad motif	5
1.4	(a) The catalytic cycle of MMO (b) The binuclear iron active site	6
1.5	The structure of hydrocarbon oxidation catalysts 1.7 and 1.8	8
1.6	The catalytic cycle of 1.7 where L = TPA and 1.8	9
1.7	(a) The structure of catalyst 1.9 (b) The mechanism of oxidation in 1.9	10
1.8	The structure of catalyst 1.10	10
1.9	(a) The structures of catalysts 1.11 and 1.16 (b) The selective oxidation of steroid 1.12 to 1.15	15
1.10	(a) Ibuprofen (1.18) bound to catalyst 1.17 by hydrogen bonding (b) The selective oxidation of 1.18 to form 1.19 rather than 1.20	16
1.11	(a) The synthesis of resorcinarenes 1.21a and 1.21b (b) 2D and 3D renderings of a basic cavitand	18
1.12	Functionalizing tetrabromocavitands 1.22 to make water-soluble hosts	19
1.13	The structure of 1.25 with possible guests and their binding constants	20
1.14	The formation of cavitand 1.29 by metal coordination and some guests	22
1.15	The synthesis of deep cavitand scaffold 1.33 and some possible derivatives	23
1.16	A phase transfer reaction catalyzed by 1.35b	26

2.1	The concept for a biomimetic C-H oxidation catalyst	33
2.2	The synthesis of tetrabromo cavitand scaffold 2.2a from resorcinarene 1.21a	33
2.3	The tuning of scaffold 2.2a to allow water-solubility	34
2.4	The functionalization of scaffold 2.2a,b by Suzuki reactions	35
2.5	(a) ^1H NMR of 2.8b (b) ESI MS of 2.8b	37
2.6	(a) MALDI MS of 2.10b (b) ^1H NMR of 2.10b	38
2.7	The attempted formation of 2.17 by Sonagashira cross-coupling reactions	41
2.8	The synthesis of tetrabromocavitand 2.21 from 2-methylresorcinol 2.18	41
2.9	The crystal structure of azide cavitand 2.22b	42
2.10	(a) The optimization of click conditions to form test cavitand 2.26 (b) Co-catalysts 2.24 and 2.25	44
2.11	The synthesis of cavitands 2.30 – 2.32 from 2.22	45
2.12	The synthesis of the amide and urea ligands used to deepen the cavitands	45
2.13	The synthesis of amide cavitands 2.44-2.48	47
2.14	(a) The synthesis of ligand 2.49 (b) The synthesis of ligand 2.52 (c) A model of a bipyridine-bridged molecular basket binding <i>trans</i> -decalin	48
2.15	The synthesis of the amine ligands used to deepen the cavitands	49
2.16	The synthesis of amine cavitands 2.61-2.65	50
3.1	The cavitands selected for metal binding studies	53
3.2	The preliminary metal-binding screen for 2.31 by ^1H NMR in CD_3CN	55
3.3	The preliminary metal-binding screen for 2.44a by ^1H NMR in CD_3CN	56

3.4	The structure and mass spectra of 2.30•Cu	58
3.5	The structure and mass spectra of 2.30b•Fe₂	59
3.6	(a) The formation of cavitands 2.44•Cu and 2.44•Cu₂ (b) The mass spectra 2.44b•Cu₂	60
3.7	The formation and mass spectra of cavitands 2.44•Fe and 2.44•Fe₂	62
3.8	Guest-binding studies of 2.44•Fe₂ by ¹ H NMR	64
4.1	MALDI mass spectrometry of reclaimed 2.44•Fe_x	71
4.2	Iron control complex 4.4	72
4.3	The mechanisms of oxidation for benzylic substrates	73
4.4	The synthesis of 4.5•Fe and the formation of the heterogeneous catalyst	78
4.5	The oxidation of fluorene by 4.5•Fe over 72 days and 17 reaction cycles	79
5.1	Cavitands 2.30•Fe₂ and 2.44•Fe₂	81
5.2	The synthesis of four-point cavitands	82
5.3	(a) ¹ H NMR spectra of the major bridging product for 5.4 (b) ¹ H NMR spectra of the major bridging product for 5.5	84
5.4	¹ H NMR spectra of 5.7	86
5.5	A model of a deep cavitand built from scaffold 5.8	87

List of Tables

1.1	The substrate scope of catalyst 1.10	11
1.2	The directing effects of catalyst 1.10	12
1.3	The scope of selective secondary oxidations catalyzed by 1.10	13
2.1	A complete list of Suzuki reactions that were tested	40
2.2	A complete list of the Sonagashira reaction conditions that were tested	41
4.1	The optimization of catalyst 2.30•Fe₂ using <i>cis</i> -decalin	68
4.2	The oxidations of hydrocarbon substrates as catalyzed by (a) 2.30•Fe₂ (b) 2.44•Fe_x , and (c) FeSO ₄	70
4.3	The oxidations of benzylic substrates as catalyzed by (a) 2.30•Fe₂ (b) 2.44•Fe_x , (c) FeSO ₄	74
4.4	The oxidations of hydrocarbon substrates as catalyzed by (a) 2.44•Cu_x and (b) CuSO ₄	77
6.1	Crystal data and structure refinement for cavitand 2.22	183
6.2	Atomic coordinates and equivalent isotropic displacement parameters for 2.22b	185

Chapter One: Background

1.1 Impact

The ability to convert feedstock chemicals into their synthetically useful counterparts is an important goal in the search for more sustainable and efficient chemical syntheses.¹ One limitation in the field is the inability of known catalysts to oxidize C-H bonds selectively. Traditional synthetic approaches require extreme temperatures and pressures to break the C-H bond; in addition to the high energy cost of these processes, each reaction yields multiple products and over-oxidation is a common problem.² Mild, generally applicable catalytic methods for hydrocarbon oxidation have been introduced recently that are inspired by enzymes such as cytochrome P-450,³ methane monooxygenase,⁴ or the Rieske non-heme iron oxygenases.⁵⁻¹³ These catalysts are effective at room temperature in protic media,⁸⁻¹¹ and consist of electrophilic metal catalysts capable of chemoselectively oxidizing tertiary¹⁴ or secondary¹⁵ centers with hydrogen peroxide, oxygen^{16,17} or alkylhydroperoxides^{18,19} as oxidant. While the development of these catalysts is a significant accomplishment, they only allow for chemoselectivity and not regioselectivity.

In contrast with chemoselective catalysts that oxidize the most electron rich, least sterically hindered position on a substrate, enzymes regioselectively react a position on a substrate based on its proximity to the active site, regardless of electronic or steric effects.¹⁰ The goal of this project was to mimic the proximity effect of enzymes in a synthetic system by coupling a size-based recognition motif with a catalytic group in

order to selectively bind and oxidize neutral substrates in aqueous solution. This chapter will discuss the field of hydrocarbon oxidation as performed by enzymes and synthetic mimics as well as the development of cavitand-based recognition motifs.

1.2 Cytochrome P450

Studies on drug metabolism during the 1950s led to the discovery of enzymes capable of oxidizing C-H bonds and ultimately inspired chemists to attempt these oxidations using synthetic mimics. It was observed that once administered to rabbits, the drug amphetamine seemed to disappear.²⁰ *In vitro* studies on rabbit liver slices revealed that the liver cells deaminated amphetamine and demethylated other drugs such as codeine, morphine, and methadone in the presence of NADPH and oxygen.²¹ It was determined that multiple enzymes were responsible for these transformations, and the investigation into the isolation and characterization of these enzymes became a central focus in the field of biology. In 1964, a CO binding pigment was observed with a distinctive absorbance maximum at 450 nm, leading to the name cytochrome P450. The first full structure was determined in 1985 from *Pseudomonas putida*, and since that time the term cytochrome P450 has come to include over 11,500 proteins that catalyze the hydroxylation of aliphatic C-H bonds and the epoxidation of C-C double bonds.²² The active sites of the cytochrome P450 family (shown in Figure 1.1) feature an iron porphyrin group with a cysteine residue coordinated to one of the axial positions on iron, anchoring the heme group to the protein. The other axial position on iron is left open, allowing the coordination and activation of O₂.

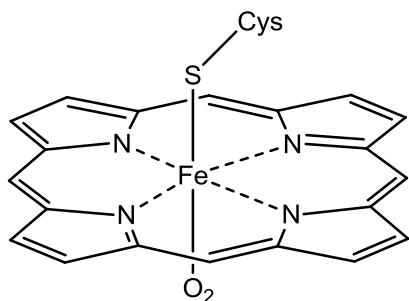


Figure 1.1: The active site of cytochrome P450

The motif of the cytochrome P450 active site is common in nature and is referred to as the heme paradigm. Figure 1.2 outlines the catalytic cycle. **1.1** represents the resting state of the heme paradigm where the low-spin iron (III) center is coordinated to water. Substrate binding generates intermediate **1.2**, which accepts an electron from NADPH thereby forming the iron (II) intermediate **1.3**. Coordination of O₂ forms the superoxo OO[•] **1.4**, and the addition of an electron from NADPH forms the peroxo **1.5**. Cleavage of the O-O bond generates the iron (IV) oxo species **1.6** that carries out the oxidation of the substrate and forms water as a side product.^{3,8}

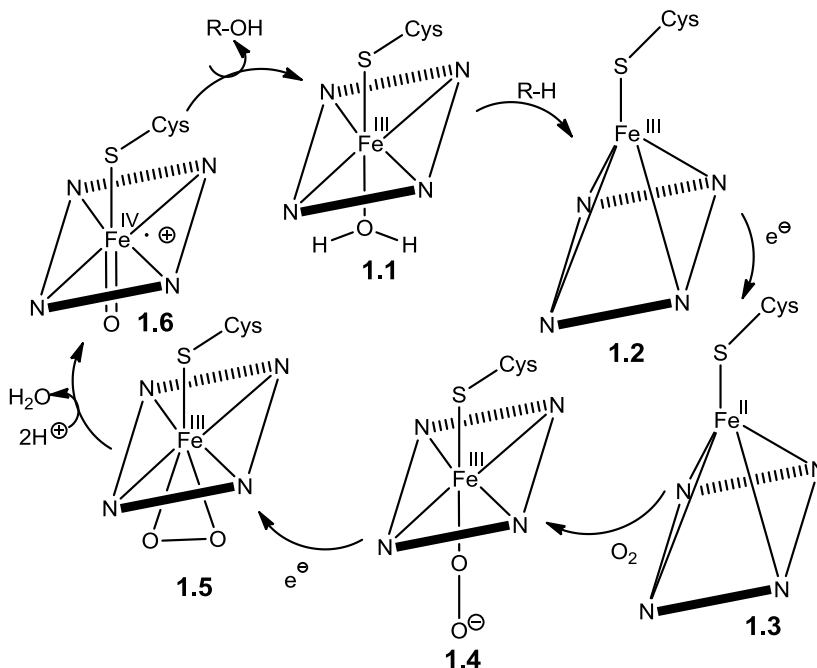


Figure 1.2: The catalytic cycle for cytochrome P450

1.3 Rieske Dioxygenases

Rieske dioxygenases catalyze the cis-dihydroxylation of arene double bonds to initiate the biodegradation of aromatics in the soil.⁶ In the activation of molecular oxygen by Rieske non-heme iron oxygenases, electrons are transported between three protein structures - a reductase, a ferredoxin, and an oxygenase that features both a Rieske [2Fe-2S] cluster domain and a mononuclear iron-containing catalytic domain.

The mononuclear iron catalytic domain is embedded within a hydrophobic binding site and features a 2-His-1-carboxylate facial triad motif found in many non-heme iron enzymes.¹² The 2-His-1-carboxylate facial triad orients the face of the iron towards the hydrophobic binding site, creating an active site for the binding and cleavage of oxygen (Figure 1.3b). This triad allows up to three exogenous ligands to bind to the iron,

allowing Rieske non-heme iron oxygenases to perform not only monohydroxylations and epoxidations that can be performed by heme iron-containing enzymes, but also more complicated reactions such as oxidative ring closure, desaturation, oxidative catechol cleavage, and arene-cis-dihydroxylation.²³ The iron metal coordinates O₂, forming the superoxo iron (III). That superoxo iron gains H⁺ and an electron to generate the peroxo species and then the active iron (V) oxo species (Figure 1.3a).

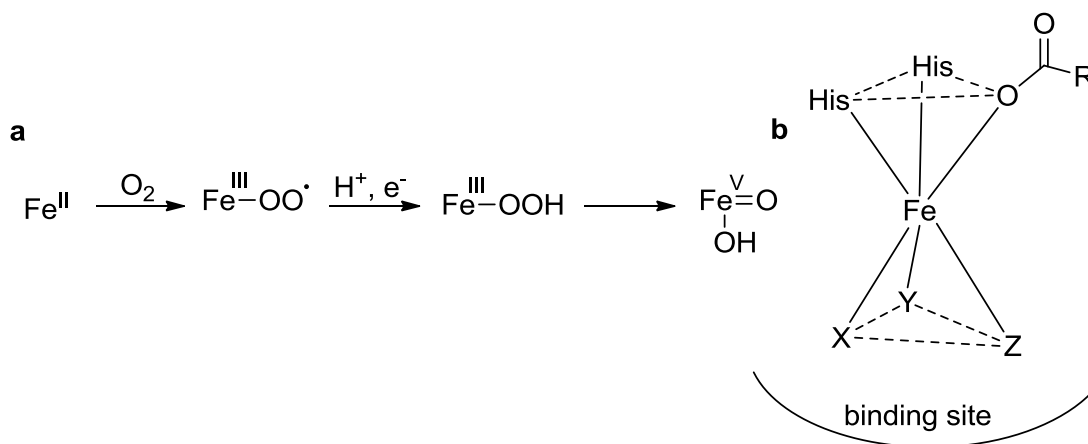


Figure 1.3: (a) The catalytic cycle of Rieske non-heme iron oxygenases and (b) the 2-His-1-carboxylate facial triad motif where x, y, and z are exogenous ligands.

1.4 Methane Monooxygenase

In 1970, it was discovered that *Methylomonas methanica* produced methanol from methane and molecular oxygen.²⁴ This observation led to the discovery of methane monooxygenase (MMO), and since that time, the list of substrates that can be oxidized by MMO has grown to include ammonia, aromatic molecules, and halogenated, cyclic, linear, and branched hydrocarbons up to C₈. Two forms of MMO have been discovered. The soluble form features a catalytic iron center, whereas the particulate form features

catalytic copper. Due to problems with stability and isolation, only the soluble form has been well characterized and for that reason the particulate form will not be discussed at length in this thesis. Crystallization of the protein structures and subsequent mechanistic studies showed that the active site features a bi-nuclear iron core that is coordinated by glutamic acid and histidine residues (Figure 1.4b).

The mechanism of MMO is similar to that of Rieske non-heme iron oxygenases but features a binuclear iron catalytic group. The di-iron(II) resting state is activated by molecular oxygen to form the superoxo species, which forms the di-iron(III) peroxo species and then the active di-iron(IV) oxo species (Figure 1.4a).

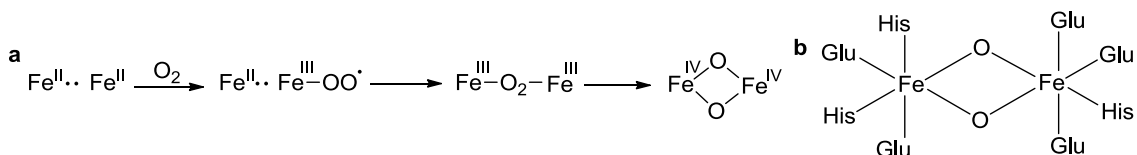


Figure 1.4: (a) The catalytic cycle of MMO and (b) the binuclear iron active site

1.5 Synthetic Mimics: Chemoselectivity

Enzyme catalyzed C-H oxidations are essential for life, but despite their prevalence in nature, these types of reactions are extraordinarily difficult to replicate in synthetic systems. Nevertheless, the usefulness of C-H oxidations in synthetic pathways makes C-H oxidation catalysts a topic of importance. The most commonly used methods for introducing functionality to a molecule rely on the use of pre-oxidized starting materials, despite the fact that preserving those pre-oxidized functional groups throughout a synthesis is challenging and frequently requires additional steps. The ability to introduce

functionality directly onto a molecule late in a synthesis would greatly improve the efficiency within the field of synthetic organic chemistry.

The formation of epoxides from olefins is well known, and oxidations of benzylic substrates or other activated C-H bonds are achievable, but examples allowing the oxidation of simple, unactivated hydrocarbons are very limited. Traditional approaches use high temperatures and pressures to force oxidation,¹ but these approaches only achieve low yields and do not allow for any sort of selectivity. These traditional approaches are in contrast with enzymes that, despite exhibiting very high selectivity, are not ideal for synthetic chemistry because they have a very limited substrate scope. For a synthetic catalyst to be useful it must have both selectivity and scope.

In 2001, a family of non-heme iron catalysts capable of stereospecifically oxidizing alkanes in the presence of H₂O₂ was developed.²⁵ The catalysts have the formula [Fe^{II}(L)XY] where L is a tetradentate ligand and the two cis-oriented monodentate ligands X and Y may be solvent molecules such as CH₃CN and H₂O or anions such as ClO₄⁻ and OTf⁻ (Figure 1.5). TPA [tris(2-pyridylmethyl)-amine] catalyst **1.7** and the similar BPMEN [N,N'-dimethyl-N,N'-bis(2-pyridylmethyl)-1,2-diaminoethane] **1.8** were shown to oxidize hydrocarbons through an iron (V) oxo intermediate. While an iron (V) oxo species is observed in heme and non-heme iron enzymes, it had never previously been observed in a synthetic catalyst.

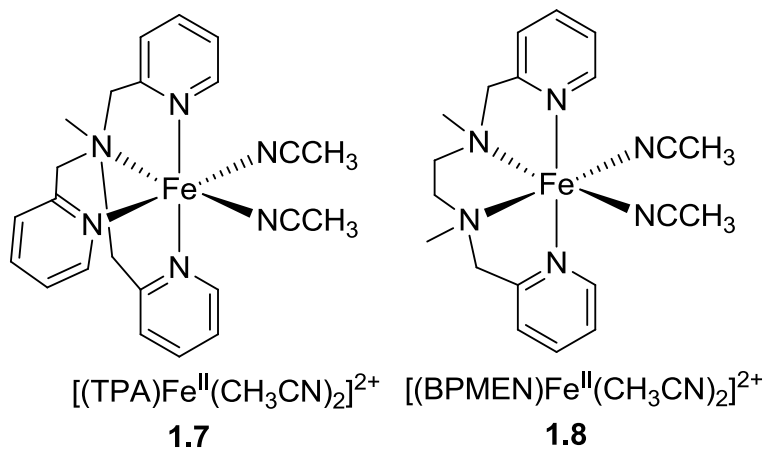


Figure 1.5: The structure of hydrocarbon oxidation catalysts **1.7** and **1.8**

1.7 and **1.8** catalyze the hydroxylation of alkanes to tertiary alcohols with retention of configuration. *Cis*-1,2-dimethylcyclohexane was oxidized to (1*R*,2*R* or 1*S*,2*S*)-1,2-dimethylcyclohexanol where the methyl groups remain *cis* to one another. Likewise *trans*-1,2-dimethylcyclohexane was oxidized to (1*R*,2*S* or 1*S*,2*R*)-1,2-dimethylcyclohexanol where the methyl groups were *trans*. This retention of configuration was also observed in the oxidation of *cis* and *trans*-decalin.

The retention of configuration in *cis* and *trans* substrates indicates that the mechanism of oxidation in catalysts **1.7** and **1.8** is different from previously studied synthetic non-heme iron catalysts where an HO• radical is generated.¹² The HO• radical reacts with alkanes to afford long-lived alkyl radicals that allow the epimerization of *cis* and *trans* stereoisomers. The retention of configuration suggests that a more selective metal-based oxidant catalyzes the reaction, generating instead short-lived alkyl radicals.

The theory of a metal-based oxidant is further supported by the product distribution using **1.7** and **1.8** in the oxidation of cyclohexane. Tertiary alcohols are favored over

ketone products in a ratio of >5:1; whereas in systems proceeding by the formation of HO•, the A/K ration is 1:1.

The mechanism of oxidation for **1.7** and **1.8** is very similar to that of Rieske non-heme iron oxygenases. The two *cis* valences that are weakly coordinated to solvent are critical to the activity of the catalyst. These weakly coordinated ligands can be displaced by H₂O₂ and H₂O to form the Fe^{III} peroxo species and finally the Fe^V oxo species that cleaves the C-H bond and allows the formation of the oxidized substrate.

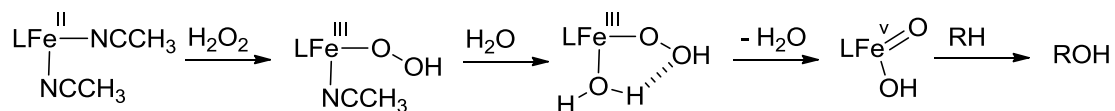


Figure 1.6: The catalytic cycle of **1.7** where L = TPA and **1.8** where L = BPMEN

1.7 and **1.8** were also active towards the olefins cyclooctene and *cis*-2-heptene, allowing the formation of the epoxides and *cis*-diols.⁷ Using **1.7** or **1.8** in the presence of acetic acid co-solvent allowed the epoxidation reaction to be performed preferentially over the *cis*-dihydroxylation reaction. Reactions carried out at 0 °C with 0.5 mol % catalyst and a 1:1.5 olefin/H₂O₂ ratio in a 1:2 CH₃CN/CH₃COOH solvent mixture result in nearly quantitative conversions of cyclooctene to the epoxide within 1 min. It was found that the epoxidation was mediated by the iron (V) oxo intermediate as is shown in Figure 1.6.

Catalysts **1.7** and **1.8** are examples of Rieske dioxygenase mimics. Catalyst **1.9** however is an example of a synthetic MMO mimic.²⁵ The diamond-shaped core of **1.9** can be activated by water or alcohols to allow C-H bond oxidation. In fact, the coordination of hydroxides or alkoxides allows the selective oxidation of alcohol

substrates over non-binding substrates, even when non-binding substrates have weaker C-H bonds.

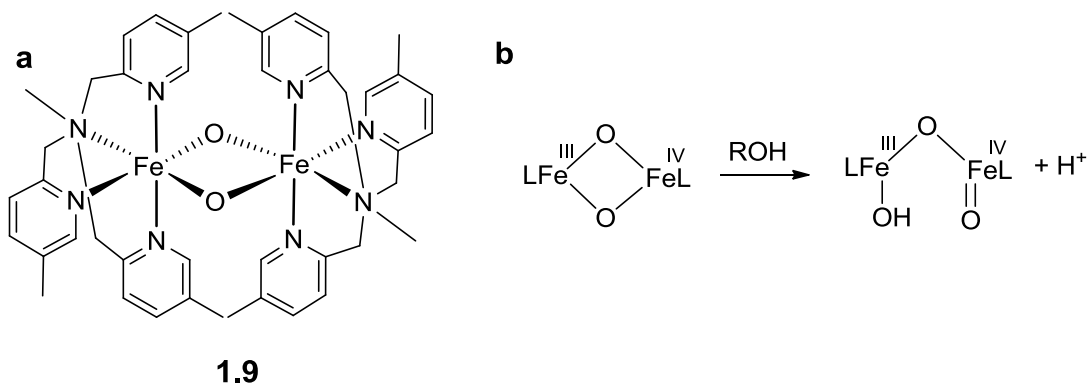


Figure 1.7: (a) The structure of catalyst **1.9** and (b) the mechanism of oxidation in **1.9**

In 2007, iron-based catalyst **1.10** was found to chemoselectively oxidize unactivated sp^3 C-H bonds based on subtle steric and electronic effects with stoichiometric H_2O_2 and substoichiometric acetic acid (Figure 1.8).⁹

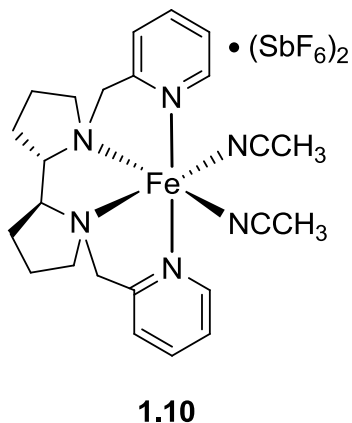


Figure 1.8: The structure of catalyst **1.10**

Using **1.10**, tertiary C-H bonds were preferentially oxidized to the corresponding alcohol, and the catalyst exhibited tolerance for cyclic ethers, esters, carbonates, and electron deficient amides. In the case of substrates containing stereogenic tertiary C-H centers, retention of stereochemistry was observed, allowing access to optically pure

tertiary alcohols. In substrates without tertiary C-H bonds or in substrates where tertiary C-H bonds are sterically inaccessible, oxidation of a secondary position to the corresponding ketone was observed through an alcohol intermediate. In all cases, 40-92% monooxygenated product was observed.

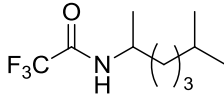
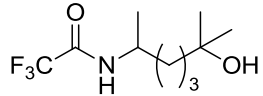
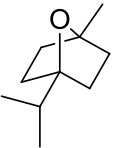
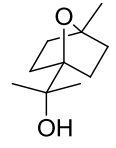
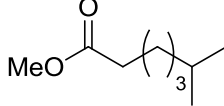
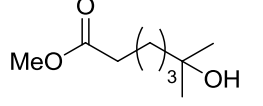
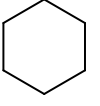
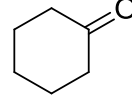
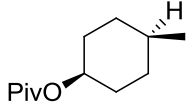
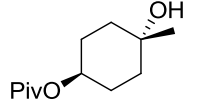
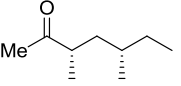
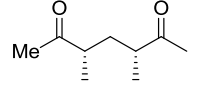
Substrate	Product	Yield	Substrate	Product	Yield
		43%			52%
		60%			92%
		51%			41%

Table 1.1: The substrate scope of catalyst **1.10**. Reactions were performed in CH₃CN at 25°C for 30 min. using 15 mol% **1.10**, 3.6 eq. H₂O₂, and 1.5 eq. AcOH.

The selectivity of the substrate could be increased by the addition of a directing group, allowing one specific tertiary C-H bond to be favored over another. In a substrate containing two tertiary C-H centers and an electron withdrawing group, the tertiary C-H position that was farthest away from the electron withdrawing group (the remote position) was favored over the other (proximal) position as shown in Table 1.2.

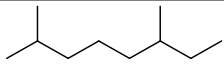
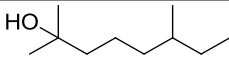
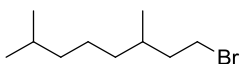
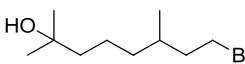
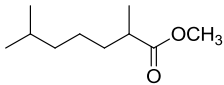
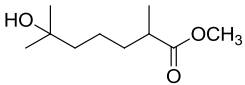
Substrate	Major Product	Remote: Proximal	Yield
		1:1	48%
		9:1	43%
		>99:1	56%

Table 1.2: The directing effects of catalyst **1.10**. Reactions were performed in CH₃CN at 25 °C for 30 min. using 15 mol% **1.10**, 3.6 eq. H₂O₂, and 1.5 eq. AcOH.

The addition of an electron withdrawing group to a substrate could also be used to favor the oxidation of secondary positions over tertiary ones.¹⁸ The proximal C-H groups were effectively deactivated, thereby allowing the most electron-rich secondary position to be oxidized preferentially. The catalyst could also be used to achieve selectivity based on subtle differences in stereoelectronic properties of ring systems and natural products; specifically through hyperconjugative activation as well as relief of torsional strain due to 1,3-diaxial interactions. Desaturation and lactonization reactions were also performed,¹⁴ and these types of reactions can be performed intramolecularly as well as intermolecularly.¹⁵

Substrate	Product	Yield	Substrate	Product	Yield
		54%			52%
		43%			59%
		45%			53%
		49%			56%

Table 1.3: The scope of selective oxidations catalyzed by **1.10**. Secondary C-H bonds can be favored over tertiary ones in the presence of an electron withdrawing group. Selectivity can also be tuned based on hyperconjugation and the alleviation of torsional strain.

The metal-ligand geometry of mimics **1.7-1.10** consistently features an octahedral iron center where four valences are occupied by nitrogen-containing chelating groups and two valences are weakly coordinated to solvent. Stoichiometric oxidant can replace the solvent ligands, allowing the formation of the active iron (V) oxo species.^{25,11,26} Other transition metals, however, also have the potential to perform C-H oxidation reactions including copper,²⁷ manganese,^{28,29} rhenium,³⁰ and ruthenium.³¹

1.6 Biomimetic Catalysis: Regioselectivity

Performing C-H oxidations using a transition metal catalyst in the presence of stoichiometric oxidant has become increasingly popular. While most examples achieve selectivity based on steric and electronic effects, there are a small handful of examples that use a nature-inspired “proximity effect.” **1.11** features cyclodextrin binding pockets

and uses host/guest chemistry to correctly align a steroid substrate with the manganese porphyrin active site.²⁸ The addition of *tert*-butyl groups to steroid **1.12** allowed the steroid to be oxidized selectively when the *tert*-butyl groups were bound to the hydrophobic interior of the cyclodextrin motifs. Upon binding, **1.13** was oriented above the manganese catalytic center so that only one position on the steroid was close enough to the active metal to be oxidized, and that position was reacted preferentially even though other positions on the substrate were more chemically reactive. After the oxidation reaction, the *tert*-butyl groups were removed, allowing access to the site-selectively oxidized **1.15**. The stability of the catalyst could be enhanced by fluorinating the phenyl rings (**1.16**); thereby allowing up to 187 catalyst turnovers.³²

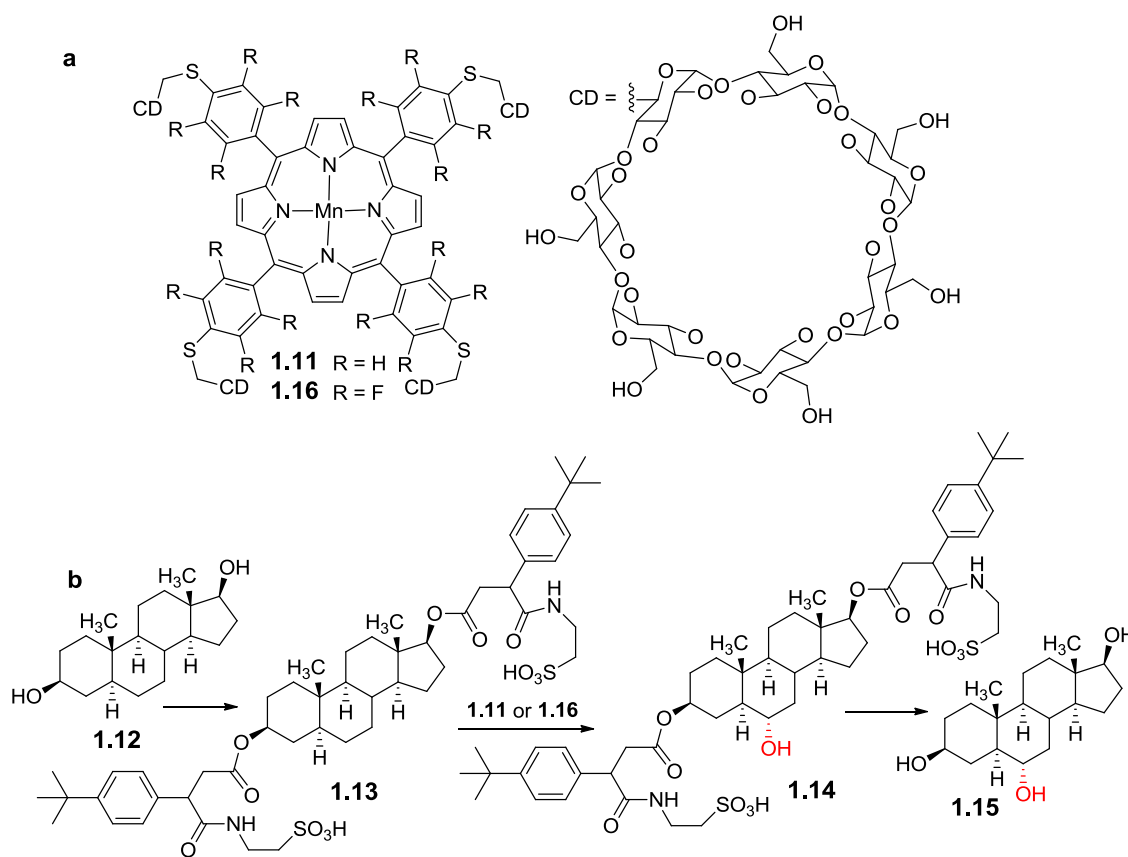


Figure 1.9: (a) The structures of catalysts **1.11** and **1.16** and (b) the selective oxidation of steroid **1.12** to **1.15**

Another example of proximity-based recognition in a synthetic system uses reversible H-bonding between a carboxylic acid group of the catalyst (**1.17**) and a carboxylic acid group of ibuprofen (**1.18**) to correctly align the substrate.³³ Ibuprofen was coordinated to the catalyst via hydrogen bonding (Figure 1.10) and was oxidized in the presence of tetrabutyl ammonium oxone (TBA oxone) at the position closest to the active site, thereby favoring the formation of **1.19** over the formation of **1.20** in a ratio of 99:1.

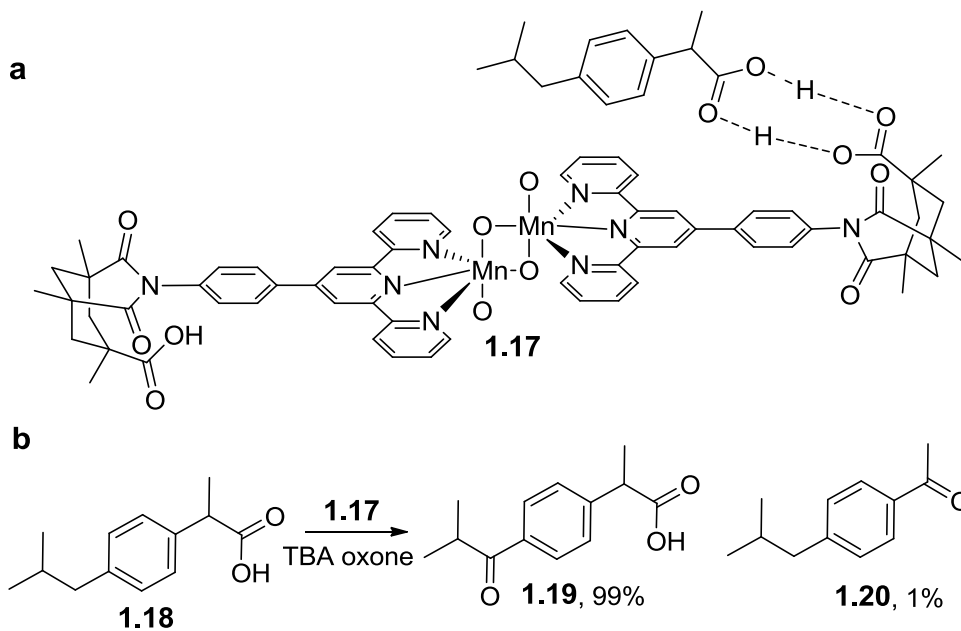


Figure 1.10: (a) Ibuprofen (**1.18**) bound to catalyst **1.17** by hydrogen bonding and (b) the selective oxidation of **1.18** to form **1.19** rather than **1.20**

1.7 Limitations of Synthetic Mimics

While the development of transition metal based C-H oxidation catalysts that work under mild conditions has been a major step forward in the field of catalysis, these oxidations are still underexplored. Chemoselectivity is most commonly achieved based on steric and electronic factors, and this selectivity is controlled by the substrate itself and not the catalyst. Proximity-based catalysts mimic enzymes in the sense that selectivity is the result of precise alignment of the substrate with the catalyst active site, rather than the intrinsic reactivity of the substrate itself; however like enzymes, these catalysts are limited to a very narrow range of substrates. Due to a severely limited pool of synthetic C-H oxidation catalysts, wide scope options for differentiating between positions on a substrate that are sterically and electronically the same simply do not exist. Furthermore,

existing C-H oxidation catalysts tend to be limited by low yields and turnover numbers and the catalysts frequently decompose during the course of the reaction. A particular challenge in this field is the development of C-H oxidation catalysts that are themselves resistant to oxidation and are not limited by product inhibition.^{17, 27}

1.8 Resorcinarene Based Molecular Receptors

Our approach to creating a selective, wide-scope C-H oxidation catalyst is to couple a catalytic group with a tunable recognition motif. Water-soluble synthetic receptors are valuable recognition motifs because they allow the binding of an appropriately sized neutral or cationic guest. The hydrophobic effect controls host:guest binding in water where the entropic benefit of freed water molecules from the clathrate surrounding a hydrophobic molecule is complemented by the enthalpic benefit of London Dispersion forces between the host and the guest. In a similar approach, cationic guests can be bound through cation- π interactions where the cation is enthalpically attracted to the electron density of the π system. Additionally, water is a beneficial solvent for C-H oxidation reactions because it is not prone to oxidation itself.

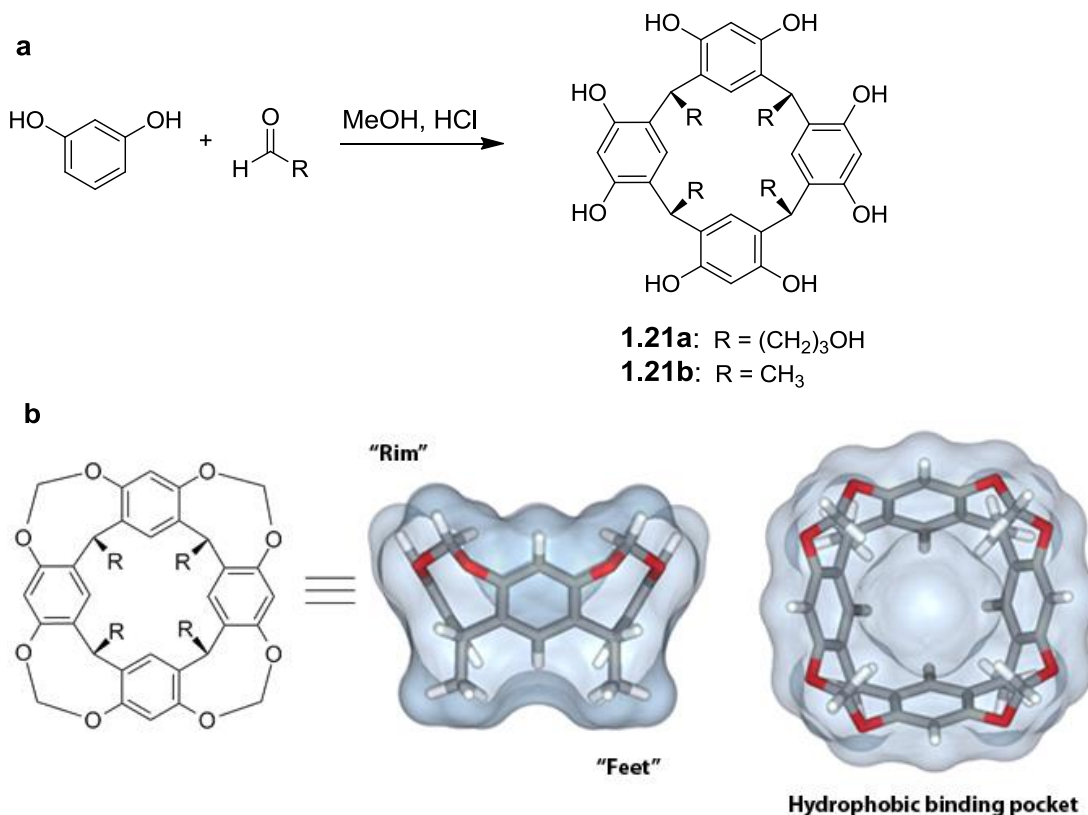


Figure 1.11: (a) The synthesis of resorcinarenes **1.21a** and **1.21b** equipped with different feet and (b) 2D and 3D renderings of a basic cavitand featuring a hydrophobic binding pocket

An early example of a synthetic receptor was the resorcin[4]arene **1.21a** (Figure 1.11).³⁴ Resorcinarenes can be made from a variety of aldehydes thereby allowing “feet” of different lengths. These feet keep the receptor from inverting and also help to control the solubility of the receptor. Additionally, resorcinarenes feature a central cavity that can bind a convex guest; although the hosts are very flexible and exhibit only a weak affinity for guests. Upon treatment with NaOH, four of the eight hydroxyl groups on cavitand **1.21b** are deprotonated so that the negative charges can be stabilized through intramolecular hydrogen bonds with the remaining protonated hydroxyl groups. The partially deprotonated **1.21b** is water-soluble and binds ammonium salts with K_a values

ranging from $5 \times 10^2 \text{ M}^{-1}$ (tetraethylammonium) to $3 \times 10^5 \text{ M}^{-1}$ (tetramethylammonium). In these examples, the binding constants are high because the positive ammonium groups further stabilize the anionic rim.³⁵

In order to improve the receptor's binding ability, the binding pocket can be made less flexible by addition of walls. These walled molecular receptors join a class of molecules known as cavitands – a term referring to structures with an “enforced cavity” (Figure 1.11b).³⁶ The phenyl groups of the resorcinarenes and cavitands give the receptor their hydrophobic character, but other solubilizing groups are needed to dissolve the receptors in water. These solubilizing groups can be added to either the lower feet or the upper rim.

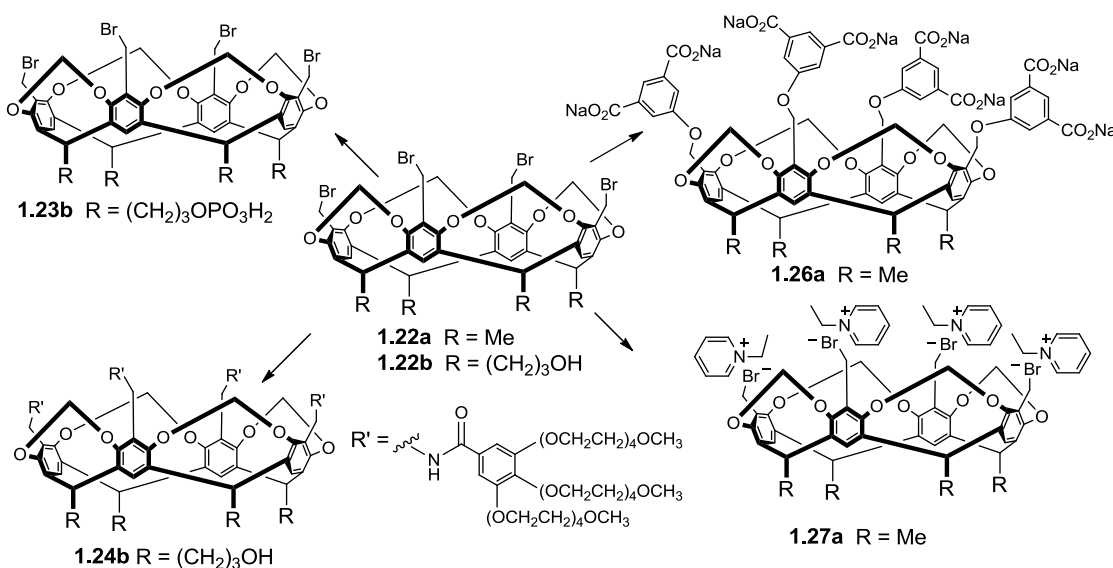


Figure 1.12: Functionalizing tetrabromocavitands **1.22** to make water-soluble hosts

Tetrabromo cavitands **1.22a** and **1.22b** are highly useful building blocks towards the synthesis of more complex cavitands. Water soluble receptors have been built from **1.22** by incorporating sulfates³⁷ and phosphates^{38,39} as feet groups (Figure 1.12). In **1.24b**

(Figure 1.12) and the ethylene bridged **1.25** (Figure 1.13), polyethylene glycol groups are used to solubilize cavitands in water.^{40,41} **1.24b** binds neutral aromatics such as *p*-cresol, toluene and phenol with binding constants in the 10^4 M^{-1} range. The rim **1.25** is functionalized with four amidinium groups that can hydrogen bond with isophthalate guests with $K_a = 1.2 \times 10^4$ and $8.6 \times 10^4 \text{ M}^{-1}$ or nucleotide guests with $K_a = 3.5 \times 10^3$ and $6.6 \times 10^5 \text{ M}^{-1}$ (Figure 1.13). A benefit of adding the solubilizing groups to the feet is that they are then remote from the binding site, thereby preventing the solubilizing groups from interacting with guest molecules. Furthermore, the rim positions can then be optimized for guest binding rather than solubility.

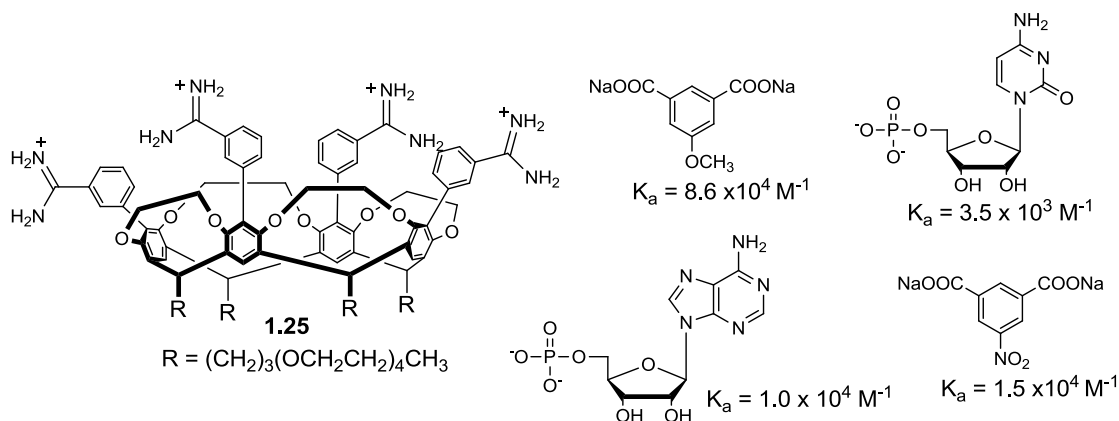


Figure 1.13: The structure of **1.25** with possible guests and their binding constants

The addition of solubilizing groups to the cavitand rim does not, however, prevent the cavitands from being effective hosts. **1.22** can be deepened and solubilized by addition of isophthalates.⁴² Under basic conditions, cavitand **1.26a** binds cationic guests such as *N*-methylpyridinium, acetylcholine, and *N,N,N*-4-tetramethylbenzenaminium with association constants ranging from 10^1 to 10^3 M^{-1} . Binding is favored by both the favorable interactions of the cationic guests with the anionic cavitand rim as well as

hydrophobic interactions between the neutral portion of the guest with the hydrophobic binding pocket. Sufficient solubilizing charge could also be added to the rim of the cavitand by treating the tetrabromocavitand **1.22a** with pyridine forming **1.27a**, which binds *p*-substituted toluene derivatives with association constants between 1.1×10^2 and $5.2 \times 10^2 \text{ M}^{-1}$.⁴³

The shallow water soluble receptors **1.24-1.27** are capable of binding small neutral or cationic guests, but in order for the cavitands to be better receptors, they need to be deeper. One of the challenges in synthesizing deep cavitands is maintaining a well-defined concave shape because large covalent resorcinarene-based structures tend to adopt a more planar orientation. For this reason, weak forces are frequently employed to maintain the shape of larger cavitands.

Cavitand **1.29** is held together by metal-coordinate bonds as shown in Figure 1.14. The uncoordinated pyridyl groups have free rotation but can be locked in a more rigid conformation upon addition of palladium.⁴⁴ The metal coordinated cavitand binds aromatic carboxylates by a combination effect of hydrophobic and electrostatic interactions. Guests with a methyl or methoxy group in the *para* position have an association constant 20-40 times greater than those without the *p*-substituted alkyl group. Likewise 1,4-dimethoxybenzene was bound with $K_a = 4.5 \times 10^3 \text{ M}^{-1}$ whereas the *p*-anisic acid sodium salt had a K_a value of $1.0 \times 10^5 \text{ M}^{-1}$. The carboxylate salt is a better guest due to the electrostatic interactions between the negatively charged carboxylate group and the positively charged palladium center. These association constants are approximately an order of magnitude greater than those for cavitands **1.24 – 1.27**. The increased binding

affinity is the result of the host's larger aromatic surface area available for contact with the guest.

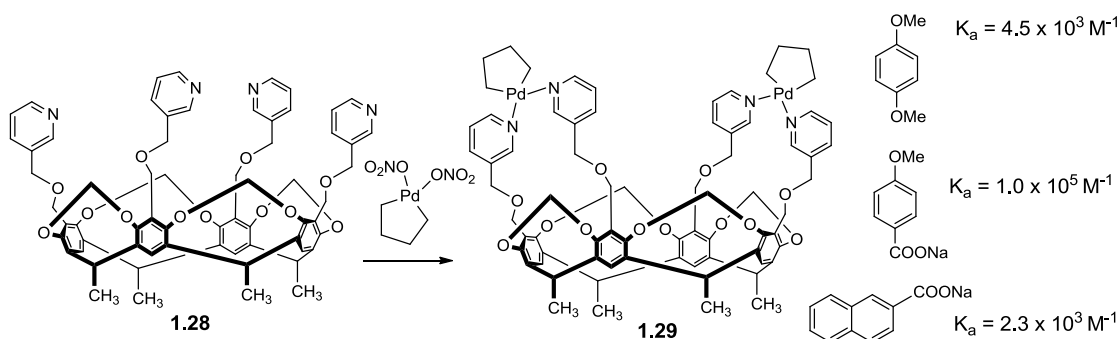


Figure 1.14: The formation of cavitand **1.29** by metal coordination and some guest molecules

Cavitand **1.29** is deeper than previous examples, but the binding site is still not especially rigid or well-defined. Figure 1.15a shows the synthesis of a cavitand scaffold from which well-defined deep cavitands can be made (Figure 1.15b).

Resorcinarene **1.30** undergoes a bridging reaction with 1,2-difluoro-4,5-dinitrobenzene (**1.31**) to form the nitro cavitand (**1.32**), and reduction with SnCl_2 allows access to scaffold **1.33**. Nucleophilic acyl substitution of **1.33** with propionyl chloride followed by derivatization of the feet yields the water-soluble deep cavitand **1.34a**.

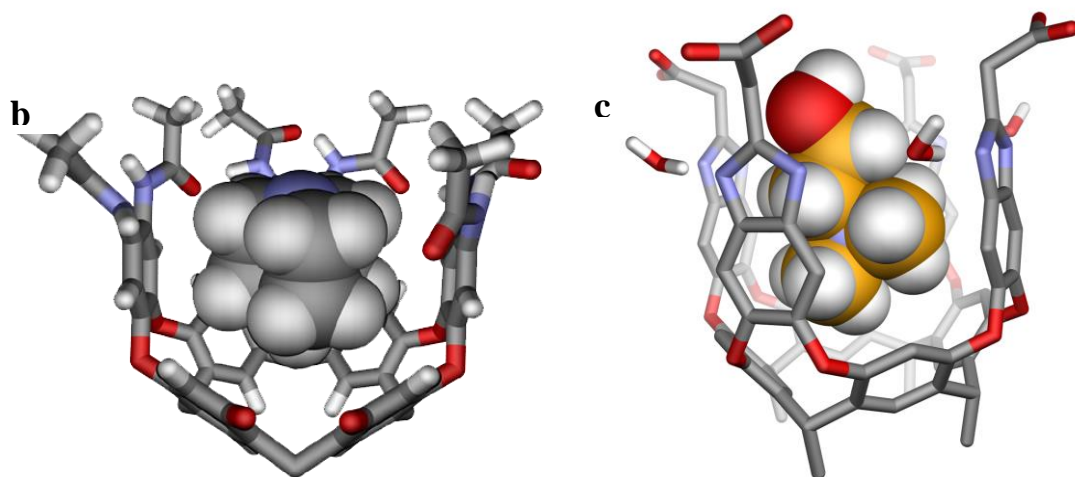
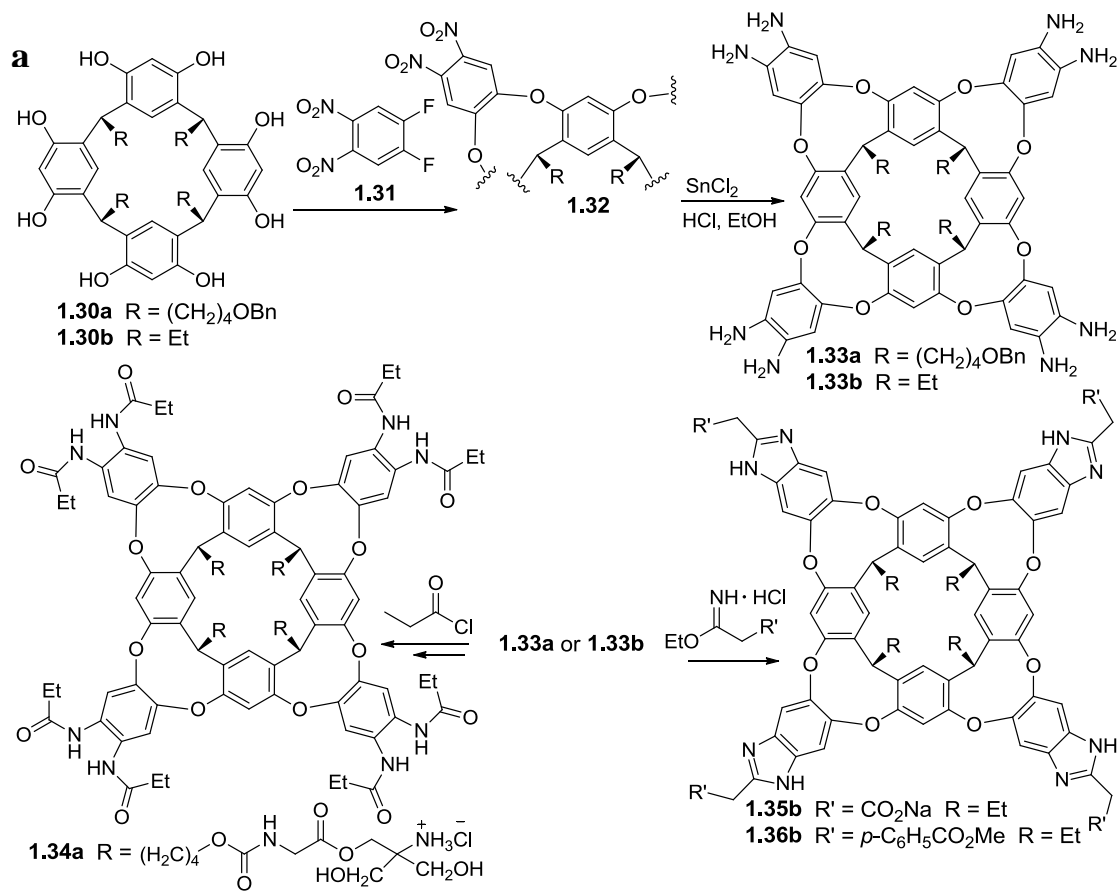


Figure 1.15: (a) The synthesis of deep cavitand scaffold **1.33** and derivatives **1.34** and **1.35**. (b) Model of cavitand **1.34** binding quinuclidine and (c) cavitand **1.35** binding choline

Without the presence of a guest, cavitand **1.34a** takes the flattened C_{2v} kite conformation; however the addition of an appropriate guest such as aminomethyladamantane hydrochloride or *N*-methylquinunclidium trifluoroacetate causes the cavitand to wrap around the guest, forming the C_{4v} vase-shaped conformation.⁴⁵ Guest-binding is favored due to the hydrophobic interactions between the convex neutral portion of the guest and the concave aromatic cavitand interior. The charged portion of the guest interacts favorably with the polar amido groups, and these amido groups form a seam of intramolecular hydrogen bonds that further stabilize the vase-shaped conformation.

Cavitand **1.35b** is also made from scaffold **1.33** but **1.35b** holds a C_{4v} conformation even without an added guest.⁴⁶ The bowl-shaped conformation forms around residual THF solvent molecules that are retained during the synthesis. The concave shape is maintained by hydrogen bonds along the rim of the cavitand between the nitrogen atoms of the benzimidazole groups and four water solvent molecules. **1.35b** can bind large alkyl chains such as those from sodium dodecylsulfate. The alkyl chain of the guest coils into a helix inside the binding site, filling the space of the cavity and leaving the polar group outside of the cavitand where it is stabilized by the aqueous solution and the polar carboxylate groups.⁴⁷ Other guests such as tetramethylammonium salts, choline, and acetylcholine are bound with association constants of 4×10^3 , 2×10^4 , and $1 \times 10^4 \text{ M}^{-1}$, respectively. L-carnitine, on the other hand, only has an association constant of 150 due to the electrostatic interactions between its carboxylate group and the carboxylate groups on the rim of **1.35b**.

Finally the formation of **1.36b** by addition of extra phenyl groups to the rim of the cavity effectively creates doors that significantly slow the in/out exchange rate of a guest.⁴⁸ One of the added phenyl groups fits over the cavity at a time, and this closed-off orientation limits the entrance or exit of a guest and also limits the size of guests that are able to bind. While **1.35b** binds guests up to C₁₂, **1.36b** only binds alkyl chains from pentane to octane.

1.9 Phase Transfer

Resorcinarene-based cavitands have been shown to act as phase-transfer catalysts in two-phase organic/aqueous solutions by pulling neutral, water-insoluble guests into the aqueous layer and allowing the formation of 1:1 host:guest complexes.⁴⁹ While guests featuring a polar group that protrudes from the cavitand opening are effectively anchored in place, neutral guests without this anchor tumble freely within the hydrophobic cavity. Cavitand **1.35b** can fully encapsulate linear alkanes up to octane inside its hydrophobic cavity. Nonane and dodecane can also be bound, but with lower binding constants because the terminal portion of the chain cannot fit into the binding pocket and is therefore exposed to the polar solution.

The phase-transfer properties of **1.35b** can be used to achieve catalytic turnover.⁵⁰ If a neutral guest undergoes a chemical reaction that convert the guest to a more polar species, the hydrophobic stabilization of the guest is weakened and the binding constant is correspondingly lessened. The product is then released from the cavity, allowing the binding of another molecule of starting material. Maleimides (such as **1.37** in Figure

1.16) are insoluble in pure water, but can be extracted into aqueous solution by **1.35b**. ^1H NMR confirmed that the hydrocarbon portions of the maleimides are buried in the hydrophobic binding pocket but that the polar maleimide group itself protrudes from the cavity and is exposed to the aqueous solution. Catalytic turnover is achieved when the 2-mercapto-ethanesulfonic acid sodium salt **1.38** is added and reacts with the exposed maleimide in order to form a water-soluble succinimide (such as **1.39** in Figure 1.16) that has no binding affinity for **1.35b**. The reactions were carried out in a two-phase (1:1) $\text{CD}_2\text{Cl}_2:\text{H}_2\text{O}$ system using only 2 mol% catalyst, and in all instances approximately 80% conversion to the succinimide product was observed, indicating that product inhibition was negligible.

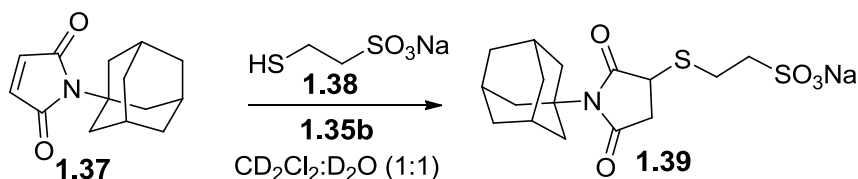


Figure 1.16: A representative phase transfer reaction catalyzed by **1.35b**. Maleimide **1.37** is pulled in the aqueous layer by **1.35b** where it reacts with **1.38** to form succinimide **1.39**

1.10 References

- 1) Shilov, A. E.; Shul'pin, G. B. "Activation of C–H Bonds by Metal Complexes." *Chem. Rev.* **1997**, *97*, 2879-2932.
- 2) De La Mare, H. E.; Rust, F. F. "Intramolecular Radical Reactions. Decomposition of Pure Bis-(2-methyl-2-hexyl) Peroxide in the Liquid Phase." *J. Am. Chem. Soc.* **1959**, *81*, 2691-2694.
- 3) Dawson, J. H. "Probing Structure-Function Relations in Heme-Containing Oxygenases and Peroxidases." *Science* **1988**, *240*, 433-439.

- 4) Merckx, M.; Kopp, D. A.; Sazinsky, M. H.; Blazyk, J. L.; Müller, J.; Lippard, S. J. "Dioxygen Activation and Methane Hydroxylation by Soluble Methane Monooxygenase: A Tale of Two Irons and Three Proteins." *Angew. Chem. Int. Ed.* **2001**, *40*, 2782-2807.
- 5) Taktak, S.; Ye, W.; Herrera, A. M.; Rybak-Akimova, E. V. "Synthesis and Catalytic Properties in Olefin Epoxidation of Novel Iron(II) Complexes with Pyridine-Containing Macrocycles Bearing an Aminopropyl Pendant Arm." *Inorg. Chem.* **2007**, *46*, 2929-2942.
- 6) Ferraro, D. J.; Gakhar, L.; Ramaswamy, S. "Rieske Business: Structure–function of Rieske Non-heme Oxygenases." *Biochem. Biophys. Res. Commun.* **2005**, *338*, 175-190.
- 7) Mas-Ballesté, R.; Que, L. "Iron-Catalyzed Olefin Epoxidation in the Presence of Acetic Acid: Insights into the Nature of the Metal-Based Oxidant." *J. Am. Chem. Soc.* **2007**, *129*, 15964-15972.
- 8) Que, L.; Tolman, W. B. "Biologically Inspired Oxidation Catalysis." *Nature* **2008**, *455*, 333-340.
- 9) Chen, M. S.; White, M. C. "A Predictably Selective Aliphatic C–H Oxidation Reaction for Complex Molecule Synthesis." *Science* **2007**, *318*, 783-787.
- 10) Litvinas, N. D.; Brodsky, B. H.; Du Bois, J. "C-H Hydroxylation Using a Heterocyclic Catalyst and Aqueous H₂O₂." *Angew. Chem. Int. Ed.* **2009**, *48*, 4513-4516.
- 11) Gómez, L.; Garcia-Bosch, I.; Company, A.; Benet-Buchholz, J.; Polo, A.; Sala, X.; Ribas, X.; Costas, M. "Stereospecific C-H Oxidation with H₂O₂ Catalyzed by a Chemically Robust Site-Isolated Iron Catalyst." *Angew. Chem. Int. Ed.* **2009**, *48*, 5720-5723.
- 12) Costas, M.; Mehn, M. P.; Jensen, M. P.; Que, L. "Dioxygen Activation at Mononuclear Nonheme Iron Active Sites: Enzymes, Models, and Intermediates." *Chem. Rev.* **2004**, *104*, 939-986.

- 13) Abu-Omar, M. M.; Loaiza, A.; Hontzas, N. "Reaction Mechanisms of Mononuclear Non-Heme Iron Oxygenases." *Chem. Rev.* **2005**, *105*, 2227-2252.
- 14) Bigi, M. A.; Reed, S. A.; White, M. C. "Diverting Non-haem Iron Catalysed Aliphatic C-H Hydroxylations Towards Desaturations." *Nat. Chem.* **2011**, *3*, 218-224.
- 15) Bigi, M. A.; Reed, S. A.; White, M. C. "Directed Metal (Oxo) Aliphatic C-H Hydroxylations: Overriding Substrate Bias." *J. Am. Chem. Soc.* **2012**, *134*, 9721-9726.
- 16) Barton, D. H. R.; Hay-Motherwell, R. S.; Motherwell, W. B. "Further Studies on the Activation of the C-H Bond in Saturated Hydrocarbons." *Tetrahedron Lett.* **1983**, *24*, 1979-1982.
- 17) Mukherjee, A.; Martinho, M.; Bominaar, E. L.; Münck, E.; Que, L. "Shape-Selective Interception by Hydrocarbons of the O₂-Derived Oxidant of a Biomimetic Nonheme Iron Complex." *Angew. Chem. Int. Ed.* **2009**, *48*, 1780-1783.
- 18) Chen, M. S.; White, M. C. "Combined Effects on Selectivity in Fe-Catalyzed Methylene Oxidation." *Science* **2010**, *327*, 566-571.
- 19) Barton, D. H. R.; Bévière, S. D.; Hill, D. R. "The Functionalization of Saturated Hydrocarbons Part XXIX. Application of *tert*-Butyl Hydroperoxide and Dioxygen Using Soluble Fe(III) and Cu(II) Chelates." *Tetrahedron* **1994**, *50*, 2665-2670.
- 20) Axelrod, J. "The Enzymatic Demethylation of Ephedrine." *J. Pharmacol. Exp. Ther.* **1955**, *114*, 430-438.
- 21) Axelrod, J. "The Enzymatic N-Demethylation of Narcotic Drugs." *J. Pharmacol. Exp. Ther.* **1956**, *117*, 322-330.
- 22) Poulos, T. L.; Finzel, B. C.; Gunsalus, I. C.; Wagner, G. C.; Kraut, J. "The 2.6-Å Crystal Structure of *Pseudomonas putida* Cytochrome P-450." *J. Biol. Chem.* **1985**, *260*, 16122-16130.
- 23) Jouanneau, Y.; Meyer, C.; Jakoncic, J.; Stojanoff, V.; Gaillard, J. "Characterization of a Naphthalene Dioxygenase Endowed with an Exceptionally Broad Substrate

- Specificity toward Polycyclic Aromatic Hydrocarbons." *Biochemistry* **2006**, *45*, 12380-12391.
- 24) Higgins, J. I.; Quayle, J. R. "Oxygenation of Methane by Methane-grown *Pseudomonas methanica* and *Methanomonas methanooxidans*." **1970**, *118*, 201-208.
- 25) Chen, K.; Que, L. "Stereospecific Alkane Hydroxylation by Non-Heme Iron Catalysts: Mechanistic Evidence for an Fe(V)=O Active Species." *J. Am. Chem. Soc.* **2001**, *123*, 6327-6337.
- 26) Company, A.; Gómez, L.; Güell, M.; Ribas, X.; Luis, J. M.; Que, L.; Costas, M. "Alkane Hydroxylation by a Nonheme Iron Catalyst that Challenges the Heme Paradigm for Oxygenase Action." *J. Am. Chem. Soc.* **2007**, *129*, 15766-15767.
- 27) Thiabaud, G.; Guillemot, G.; Schmitz-Afonso, I.; Colasson, B.; Reinaud, O. "Solid-State Chemistry at an Isolated Copper(I) Center with O₂." *Angew. Chem. Int. Ed.* **2009**, *48*, 7383-7386.
- 28) Breslow, R. "An Artificial Cytochrome P450 that Hydroxylates Unactivated Carbons with Regio- and Stereoselectivity and Useful Catalytic Turnovers." *Proc. Natl. Acad. Sci.* **1997**, *94*, 11156-11158.
- 29) Das, S. "Molecular Recognition in the Selective Oxygenation of Saturated C-H Bonds by a Dimanganese Catalyst." *Science* **2006**, *312*, 1941-1943.
- 30) Kuznetsov, M. L.; Pombeiro, A. J. L. "Radical Formation in the [MeReO₃]-Catalyzed Aqueous Peroxidative Oxidation of Alkanes: A Theoretical Mechanistic Study." *Inorg. Chem.* **2009**, *48*, 307-318.
- 31) Carlsen, P. H. J.; Katsuki, T.; Martin, V. S.; Sharpless, K. B. "A Greatly Improved Procedure for Ruthenium Tetroxide Catalyzed Oxidations of Organic Compounds." *J. Org. Chem.* **1981**, *46*, 3936-3938.
- 32) Yang, J.; Gabriele, B.; Belvedere, S.; Huang, Y.; Breslow, R. "Catalytic Oxidations of Steroid Substrates by Artificial Cytochrome P-450 Enzymes." *J. Org. Chem.* **2002**, *67*, 5057-5067.

- 33) Das, S.; Brudvig, G. W.; Crabtree, R. H. "Molecular Recognition in Homogeneous Transition Metal Catalysis: a Biomimetic Strategy for High Selectivity." *Chem. Commun.* **2008**, 413-424.
- 34) Hoegberg, A. G. S. "Two Stereoisomeric Macrocyclic Resorcinol-acetaldehyde Condensation Products." *J. Org. Chem.* **1980**, *45*, 4498-4500.
- 35) Biros, S. M.; Rebek, J., Jr. "Structure and Binding Properties of Water-soluble Cavitands and Capsules." *Chem. Soc. Rev.* **2007**, *36*, 93-104.
- 36) Moran, J. R.; Karbach, S.; Cram, D. J. "Cavitands: Synthetic Molecular Vessels." *J. Am. Chem. Soc.* **1982**, *104*, 5826-5828.
- 37) Yanagihara, R.; Tominaga, M.; Aoyama, Y. "Chiral Host-Guest Interaction. A Water-Soluble Calix[4]resorcarene Having L-Proline Moieties as a Non-Lanthanide Chiral NMR Shift Reagent for Chiral Aromatic Guests in Water." *J. Org. Chem.* **1994**, *59*, 6865-6867.
- 38) Mezo, A. R.; Sherman, J. C. "Water-Soluble Cavitands: Synthesis of Methylene-Bridged Resorcin[4]arenes Containing Hydroxyls and Phosphates at Their Feet and Bromomethyls and Thiomethyls at Their Rims." *J. Org. Chem.* **1998**, *63*, 6824-6829.
- 39) Gui, X.; Sherman, J. C. "Host-guest Binding of Simple Cavitands in Water." *Chem. Commun.* **2001**, 2680-2681.
- 40) Sebo, L.; Diederich, F.; Gramlich, V. "Tetrakis(phenylamidinium)-Substituted Resorcin[4]arene Receptors for the Complexation of Dicarboxylates and Phosphates in Protic Solvents." *Helv. Chim. Acta* **2000**, *83*, 93-113.
- 41) Middel, O.; Verboom, W.; Reinhoudt, D. N. "Water-Soluble Cavitands – Synthesis, Solubilities and Binding Properties." *Eur. J. Org. Chem.* **2002**, *2002*, 2587-2597.
- 42) Park, S. J.; Hong, J.-I. "The Cooperative Effect of Electrostatic and Hydrophobic Forces in the Complexation of Cationic Molecules by a Water-soluble Resorcin[4]arene Derivative." *Tetrahedron Lett.* **2000**, *41*, 8311-8315.

- 43) Grote Gansey, M. H. B.; Bakker, F. K. G.; Feiters, M. C.; Geurts, H. P. M.; Verboom, W.; Reinhoudt, D. N. "Water-soluble Resorcin[4]arene Based Cavitands." *Tetrahedron Lett.* **1998**, *39*, 5447-5450.
- 44) Lim, C. W.; Hong, J.-I. "Intramolecular Binding Site Organization by Pd(II) Complexation with a Resorcin[4]arene Derivative." *Tetrahedron Lett.* **2000**, *41*, 3113-3117.
- 45) Haino, T.; Rudkevich, D. M.; Rebek, J., Jr. "Kinetically Stable Caviplexes in Water." *J. Am. Chem. Soc.* **1999**, *121*, 11253-11254.
- 46) Hof, F.; Trembleau, L.; Ullrich, E. C.; Rebek, J., Jr. "Acetylcholine Recognition by a Deep, Biomimetic Pocket." *Angew. Chem. Int. Ed.* **2003**, *42*, 3150-3153.
- 47) Trembleau, L. "Helical Conformation of Alkanes in a Hydrophobic Cavitand." *Science* **2003**, *301*, 1219-1220.
- 48) Hooley, R. J.; Van Anda, H. J.; Rebek, J., Jr. "Cavitands with Revolving Doors Regulate Binding Selectivities and Rates in Water." *J. Am. Chem. Soc.* **2006**, *128*, 3894-3895.
- 49) Hooley, R. J.; Biroš, S. M.; Rebek, J., Jr. "Normal Hydrocarbons Tumble Rapidly in a Deep, Water-soluble Cavitand." *Chem. Commun.* **2006**, 509-510.
- 50) Hooley, R. J.; Biroš, S. M.; Rebek, J., Jr. "A Deep, Water-Soluble Cavitand Acts as a Phase-Transfer Catalyst for Hydrophobic Species." *Angew. Chem. Int. Ed.* **2006**, *45*, 3517-3519.

Chapter Two: Synthesis of Cavitands

2.1 Approach

In order to achieve regioselective C-H oxidations, an enzyme mimic was designed that featured a water soluble molecular receptor with a hydrophobic binding pocket (Figure 2.1). The purpose of the molecular receptor was to bind an appropriately sized neutral guest via the hydrophobic effect with the intention that the attachment of a catalytic group to the receptor would allow the regioselective oxidation of the bound guest based on its proximity to the catalytic active site. Catalytic turnover is achieved when an oxidized guest is more hydrophilic than the unoxidized starting material.¹ The increased hydrophilicity of the product weakens the binding between host and guest, allowing the product to be released from the binding site.

This chapter focuses on the development of size-selective host molecules built from resorcinarene-based cavitands. The goal of this project was to develop a receptor scaffold that would be tuned to optimally accommodate guests of a specific size. This tunable scaffold would allow size-based selectivity without limiting the receptor to a very narrow pool of substrates, and the molecular receptor could later be attached to a transition metal containing catalytic group to achieve regioselective, as well as size-based, selectivity.

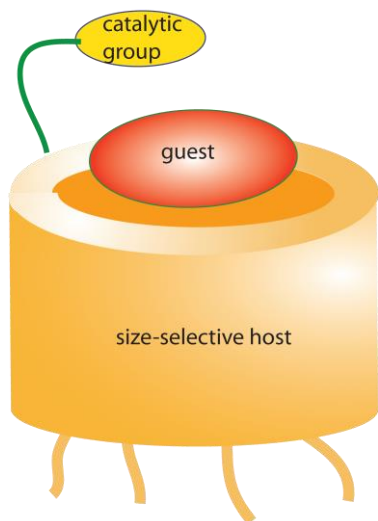


Figure 2.1: The concept for a biomimetic C-H oxidation catalyst

2.2 Palladium Catalyzed Cross Coupling Reactions

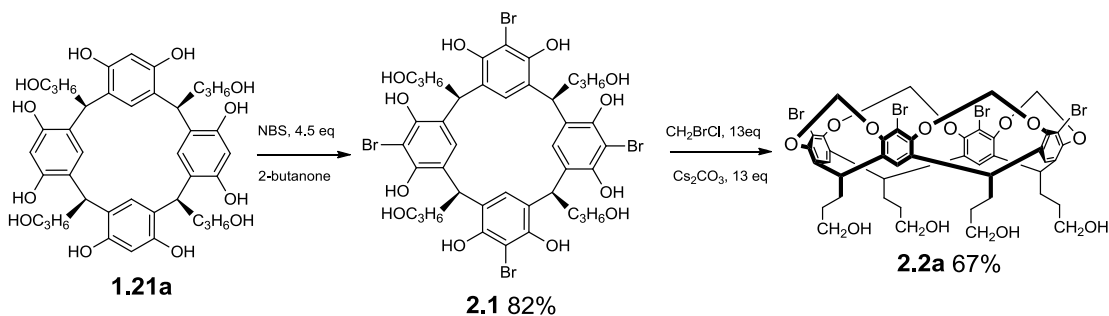


Figure 2.2: The synthesis of tetrabromo cavitand scaffold **2.2a** from resorcinarene **1.21a**

Tetrabromo cavitand **2.2a** is known and has the potential to be functionalized using a variety of cross-coupling reactions.² An advantage to using cavitand **2.2a** is that the rim positions of can be optimized for guest binding and catalysis while the feet positions can be tuned to control water-solubility (Figure 2.3). Since common water-solubilizing groups such as sulfates or carboxylates have the potential to interfere with catalytic groups, having the solubilizing groups remote from the catalytic groups is desirable.

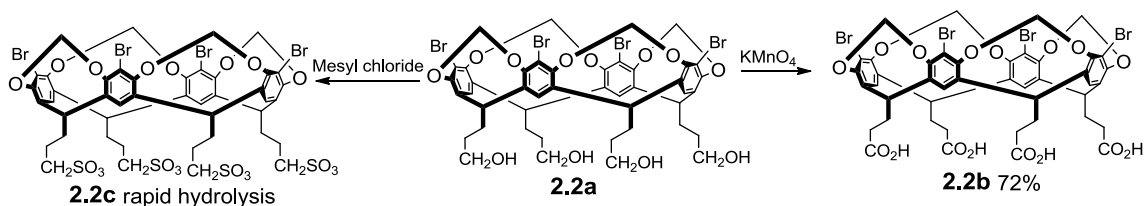


Figure 2.3: The tuning of scaffold **2.2a** to allow water-solubility

When designing the cavitand scaffold, a number of different feet functional groups were considered to solubilize the cavitands in water. Carboxylates, sulfonates, and phosphonates all have precedent as solubilizing groups.³⁻⁵ In the system shown in figure 2.3, the alcohol-footed **2.2a** was smoothly oxidized to the water soluble **2.2b** in 75% yield. Cavitand **2.2b** was of particular interest because it had the potential to form multiple water-soluble products from a single platform. The sulfonate product **2.2c** was also investigated, but it was extremely water sensitive and was hydrolyzed readily back to the alcohol cavitand. Given that the purpose of the sulfonates was to solubilize the cavitand in water, the sensitivity of these groups to water made them unusable.

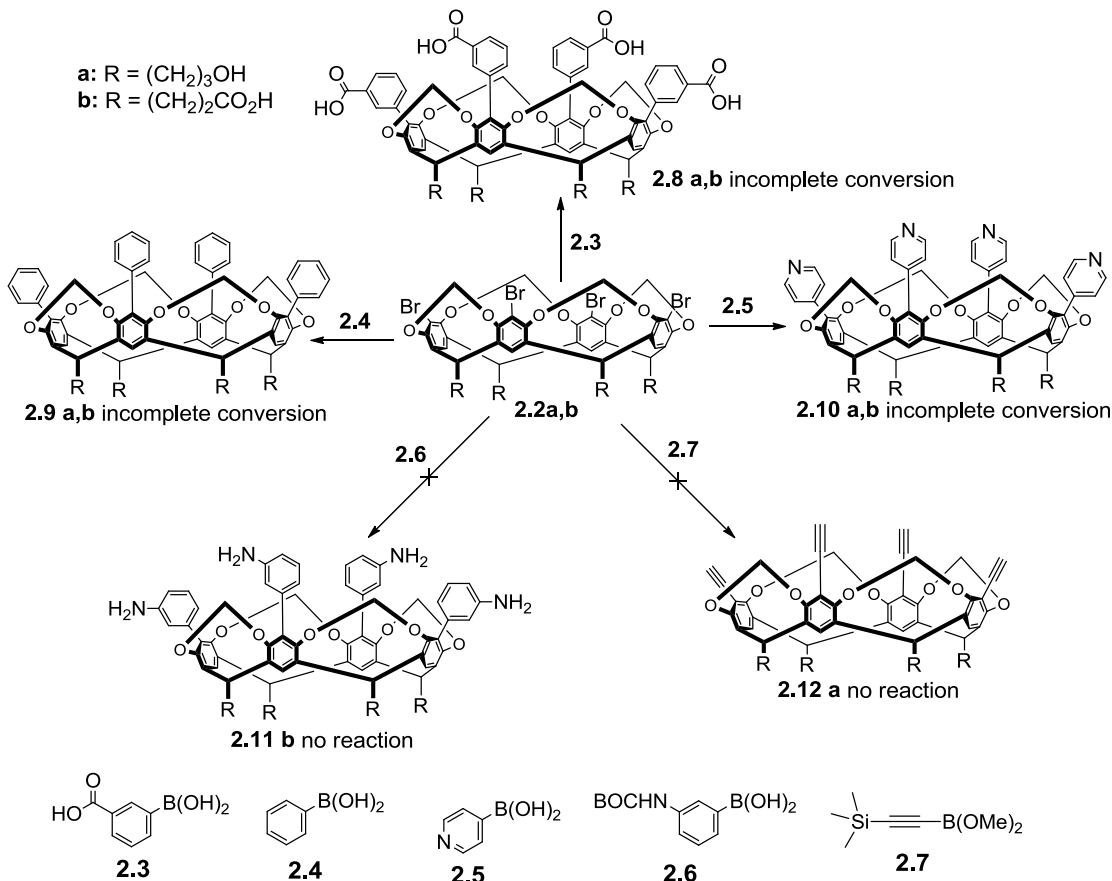


Figure 2.4: The functionalization of scaffold **2.2a,b** with boronic acids **2.3-2.6** and boronic ester **2.7**. None of the Suzuki cross coupling reactions went to completion.

The first attempts to functionalize scaffold **2.2b** utilized Suzuki cross-coupling reactions. Scaffold **2.2** was treated with boronic acids **2.3-2.6** and boronic ester **2.7** (Figure 2.4); however these reactions did not go to completion despite temperatures in excess of 100 °C and reaction times up to 96 hours. Cavitands **2.11b** and **2.12a** were designed to deepen the receptor while providing handles for the attachment of catalytic groups; however the starting bromides were completely unreactive even under forcing conditions. Boronic ester **2.7** had previously been added to a C₁₁-footed, monobrominated cavitand,⁶ but the water soluble **2.2b** proved to be a more challenging scaffold.

Given the synthetic challenges of functionalizing **2.2**, Suzuki cross-coupling reactions were attempted using simpler boronic acids. A clean mass spectrum was obtained for **2.8b** when the reaction was performed using Pd(PPh₃)₂Cl₂ as catalyst, Cs₂CO₃ as base, and water as solvent; however the ¹H NMR showed partially reacted cavitand (Figure 2.5, Table 2.1 entry 1). The two bridging methylene doublets for cavitands built from scaffold **2.2** typically fall between 4 and 6.6 ppm. Rather than the two peaks that are expected from a completely formed cavitand, eight are observed, indicating that multiple, partially formed cavitands are also present. The reaction was repeated using of toluene as an organic co-solvent and triphenylphosphine trisulfonate (TPPTS) as the ligand on palladium in hopes of overcoming problems with solubility; however the complete formation of product was not observed by NMR. Even performing the reaction at 155 °C in a sealed tube did not allow the complete formation of product.

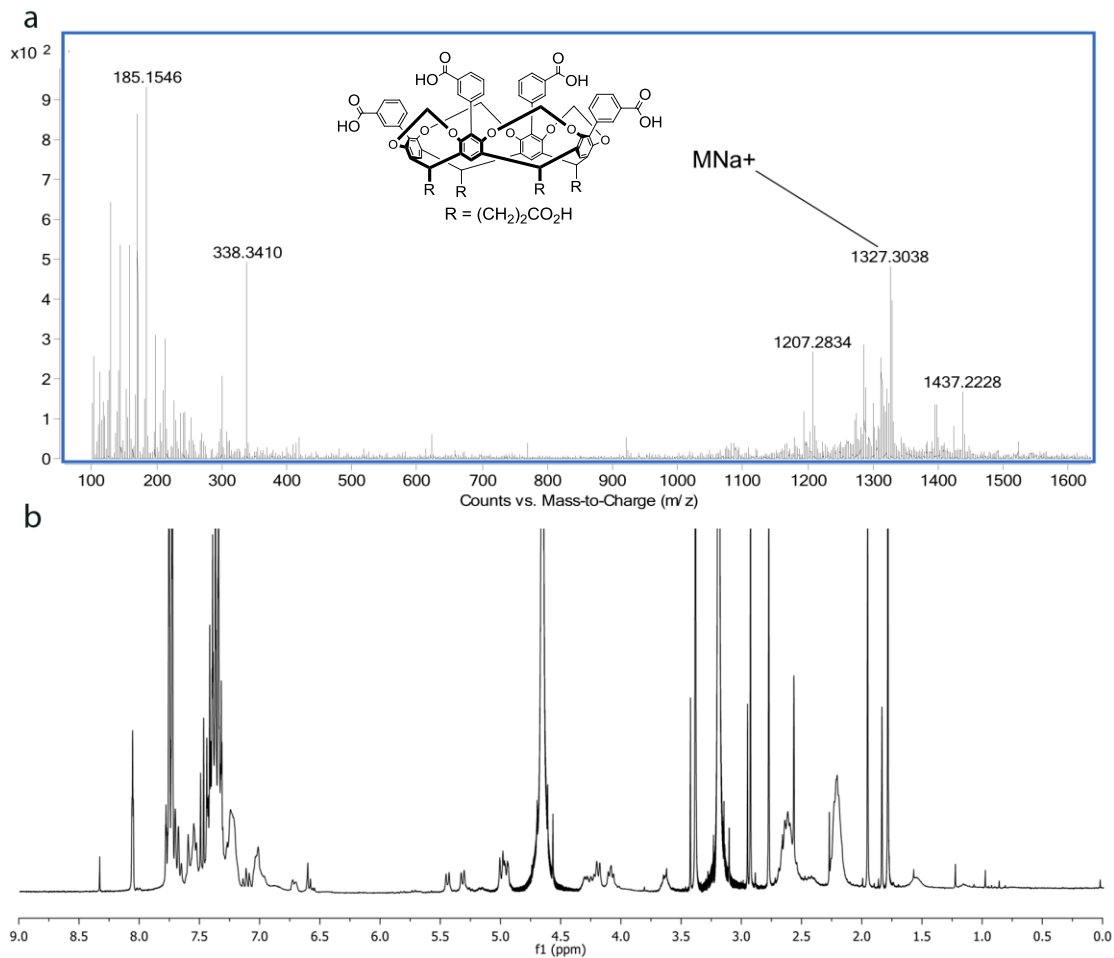
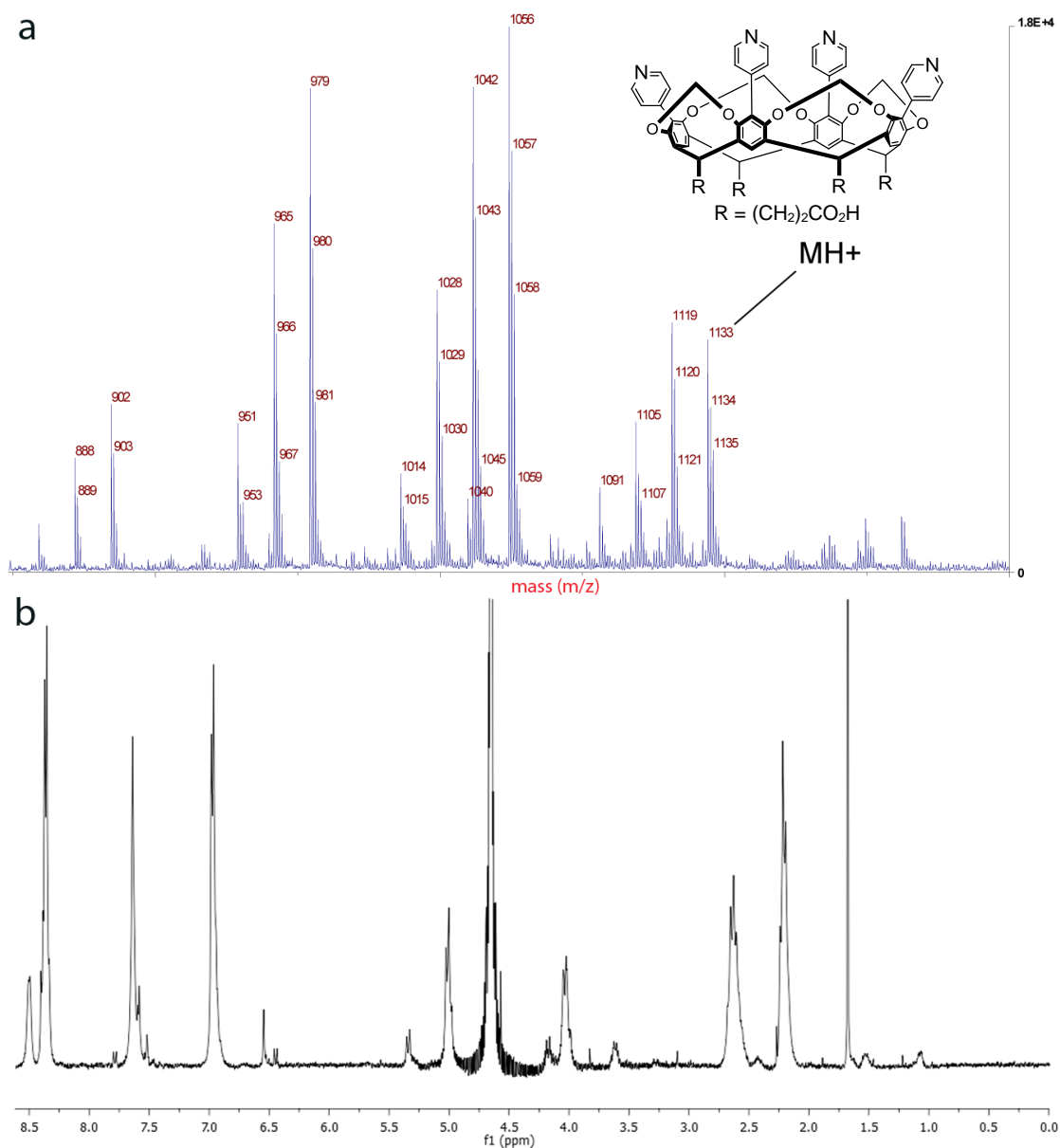


Figure 2.5: (a) ¹H NMR and (b) ESI MS of **2.8b**

The formation of cavitands **2.9b** and **2.10b** was attempted using similar conditions (Table 2.1), but again the reactions never went to completion. The use of tricyclohexylphosphine (PCy₃) ligand and K₃PO₄ base has been known to promote Suzuki cross-coupling reactions on electron rich, sterically hindered systems,^{6,7} and in the synthesis of **2.10b**, some improvement was observed using these conditions. As was the case with **2.8b**, fully formed product was observed by mass, but ¹H NMR spectroscopy showed that the reaction did not reach 100 % completion (Figure 2.6). Due to the polarity

of the carboxylic acid feet, the product mixtures could not be separated using silica gel chromatography, and pure cavitands **2.8b-2.10b** were never obtained.



These cross-coupling reactions were attempted again using scaffold **2.2a**, in hopes that the reactions would be more favorable using the alcohol-footed derivative and that the products could be purified by silica chromatography. Instead the alcohol-footed counterparts were equally problematic. Performing the reaction using Pd(PPh₃)₂Cl₂, K₂CO₃, and water/organic solvent mixtures allowed the observation of fully formed cavitands **2.8a** and **2.9a** by mass, but ¹H NMR of the same samples showed that the reaction had not gone to completion, and the resulting mixtures of products could not be separated.

	Cav.	Boronic acid/ester	Catalyst	Base	Solvent	°C	H
1	2.2b	2.3	Pd(PPh ₃) ₂ Cl ₂	CS ₂ CO ₃	H ₂ O	95	16
2	2.2b	2.3	Pd(PPh ₃) ₂ Cl ₂	K ₂ CO ₃	H ₂ O:PhMe (2:1)	100	72
3	2.2b	2.3	Pd(OAc) ₂ , TPPTS	K ₂ CO ₃	H ₂ O	100	72
4	2.2b	2.3	Pd(PPh ₃) ₂ Cl ₂	K ₂ CO ₃	H ₂ O:PhMe (2:1)	155	48
5	2.2b	2.4	Pd(PPh ₃) ₂ Cl ₂	CS ₂ CO ₃	D ₂ O	100	16
6	2.2b	2.4	Pd(PPh ₃) ₂ Cl ₂	K ₂ CO ₃	H ₂ O:PhMe (4:1)	100	16
7	2.2b	2.4	Pd(PPh ₃) ₂ Cl ₂	K ₂ CO ₃	H ₂ O:PhMe (3:1)	100	16
8	2.2b	2.4	Pd(PPh ₃) ₂ Cl ₂	K ₂ CO ₃	H ₂ O:PhMe	100	48
9	2.2b	2.5	Pd(PPh ₃) ₂ Cl ₂	K ₂ CO ₃	H ₂ O:PhMe (3:1)	100	16
10	2.2b	2.5	Pd(PPh ₃) ₂ Cl ₂	K ₂ CO ₃	H ₂ O:MeOH (4:1)	100	96
11	2.2b	2.5	Pd(OAc) ₂ , PCy ₃	K ₃ PO ₄	Dioxane:H ₂ O	100	16
12	2.2b	2.5	Pd(OAc) ₂ , PCy ₃	K ₃ PO ₄	Dioxane:H ₂ O	155	48
13	2.2b	2.5	Pd(OAc) ₂ , PCy ₃	K ₃ PO ₄	Dioxane	100	16
14	2.2b	2.6	Pd(PPh ₃) ₂ Cl ₂	K ₂ CO ₃	H ₂ O:PhMe (3:1)	100	16
15	2.2b	2.6	Pd(PPh ₃) ₂ Cl ₂	K ₂ CO ₃	H ₂ O:PhMe	100	18
16	2.2b	2.7	Pd(PPh ₃) ₂ Cl ₂	K ₃ PO ₄	THF:H ₂ O	100	16
17	2.2a	2.3	Pd(PPh ₃) ₂ Cl ₂	CS ₂ CO ₃	H ₂ O:PhMe (4:1)	100	16
18	2.2a	2.3	Pd(PPh ₃) ₂ Cl ₂	K ₂ CO ₃	PhMe:MeOH	100	16
19	2.2a	2.3	Pd(PPh ₃) ₂ Cl ₂	K ₂ CO ₃	PhMe:H ₂ O (2:1)	100	16
20	2.2a	2.3	Pd(PPh ₃) ₂ Cl ₂	K ₂ CO ₃	H ₂ O:PhMe	100	16
21	2.2a	2.4	Pd(PPh ₃) ₂ Cl ₂	CS ₂ CO ₃	PhMe:H ₂ O (4:1)	100	16
22	2.2a	2.5	Pd(PPh ₃) ₂ Cl ₂	K ₂ CO ₃	H ₂ O:PhMe:MeOH	100	16
23	2.2a	2.5	Pd(PPh ₃) ₂ Cl ₂	K ₂ CO ₃	H ₂ O:PhMe:MeOH	100	16
24	2.2a	2.5	Pd(OAc) ₂ , TPPTS	K ₂ CO ₃	H ₂ O:PhMe:MeOH	100	16
25	2.2a	2.7	Pd(PPh ₃) ₂ Cl ₂	K ₃ PO ₄	THF:H ₂ O	100	16
26	2.2a	2.7	Pd(PPh ₃) ₂ Cl ₂	K ₃ PO ₄	THF:H ₂ O	100	48

Table 2.1: A complete list of Suzuki reactions that were tested. Solvent mixtures are 1:1 unless otherwise noted. None of the reactions tested went to completion.

While scaffolds **2.2a,b** were not amenable to Suzuki cross-coupling reactions, we wondered if Sonogashira reactions would be more favorable given the steric hindrance of the scaffold. The formation of cavitand **2.17b** was attempted using varying ligands on palladium (examples: PPh₃, Ph₃As, PCy₃), as well as different acetylenes and solvents (Table 2.2, Figure 2.7). The addition of CuI was also tested, but in all cases, no reaction was observed. Performing Sonogashira reactions on the bromocavitand has precedent as being especially difficult due to problems with the oxidative addition step.⁸

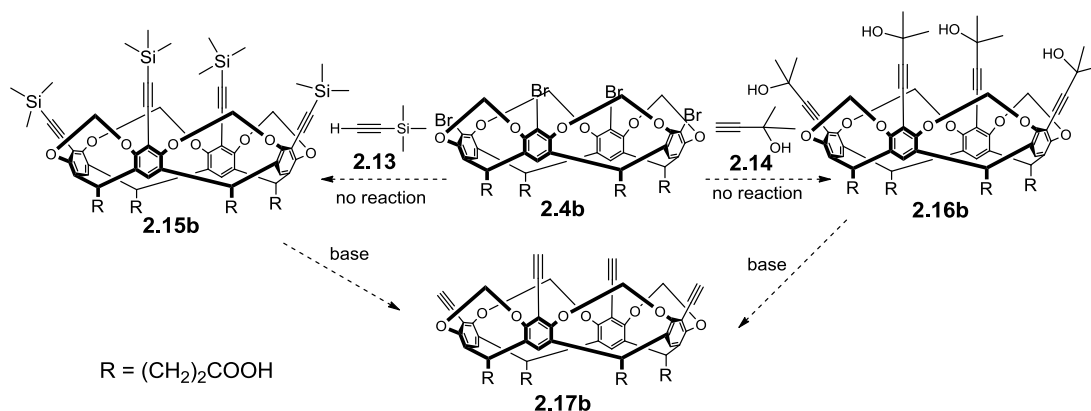


Figure 2.7: The attempted formation of **2.17** by Sonogashira cross-coupling reactions

Entry	Acetylene	Catalyst	Base	CuI	Solvent	°C	Hrs
1	2.13	Pd(PPh ₃) ₂ Cl ₂	Et ₃ N	60%	THF	66	16
2	2.13	Pd(PPh ₃) ₂ Cl ₂	Et ₃ N	16 eq.	THF	25	16
3	2.14	Pd(PPh ₃) ₂ Cl ₂	Et ₃ N	16 eq.	THF	66	16
4	2.14	Pd(OAc) ₂ , Ph ₃ As	Et ₂ NH	0%	MeOH	60	24
5	2.14	Pd(OAc) ₂ , PCy ₃	Et ₂ NH	0%	MeOH	60	24
6	2.14	Pd(OAc) ₂ , Ph ₃ As	Et ₃ N	0%	MeOH	60	16
7	2.14	Pd(PPh ₃) ₂ Cl ₂	Et ₃ N	16 eq.	THF	66	16
8	2.14	Pd(PPh ₃) ₂ Cl ₂	Et ₃ N	16 eq.	THF	66	24

Table 2.2: A complete list of the Sonogashira reaction conditions that were tested

2.3 Click Chemistry

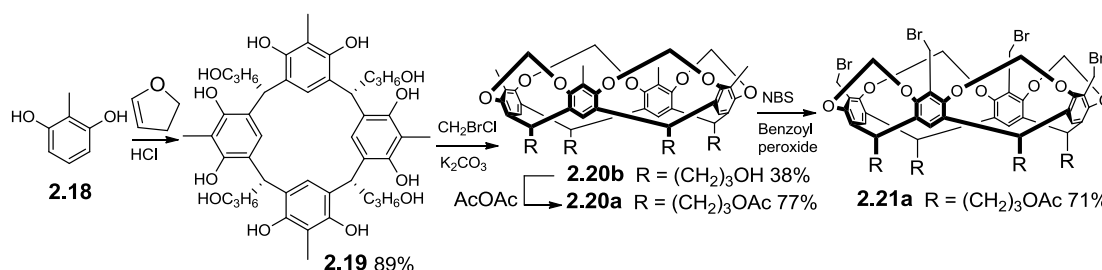


Figure 2.8: The synthesis of tetrabromocavitand **2.21** from 2-methylresorcinol **2.18**

Given the difficulty of palladium catalyzed cross-coupling reactions on this system, an alternate synthesis was designed utilizing click chemistry. Substituting an azide for a bromide directly onto the cavitand proved extremely difficult, so the catalytic scaffold

was modified to tetrabromocavitand **2.21a**, synthesized from 2-methylresorcinol in four steps (Figure 2.8).⁴ The benzylic bromides could be smoothly converted to the corresponding azides via a simple S_N2 reaction, giving the versatile scaffold **2.22** that could be tuned by click chemistry. Cavitand **2.22a** was obtained in 78 % yield, and slow evaporation from chloroform/methanol solution allowed formation of single crystals that were suitable for X-Ray diffraction analysis. During the crystallization process, the acyl groups were cleaved, and crystals were obtained of the OH-footed analogue **2.22b** (Figure 2.9).

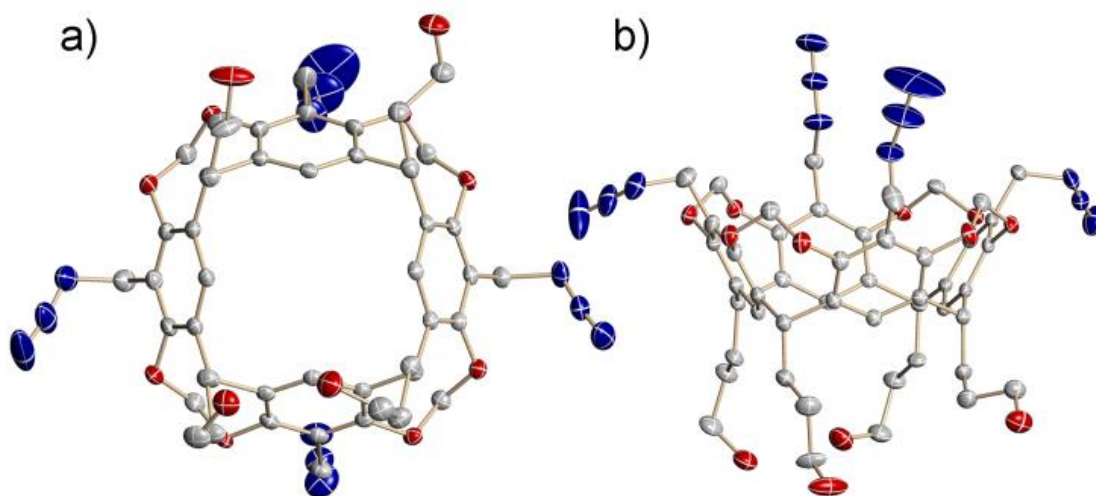


Figure 2.9: The crystal structure of azide cavitand **2.22b**

While accessing scaffold **2.22** was straightforward, the click reactions were surprisingly challenging. Ligand **2.23** was used for click test reactions due to its electronically neutral nature and simple NMR splitting pattern. The initial attempts in THF/H₂O/^tBuOH (3:1:1) at room temperature or 40 °C failed, as did the attempts using a two-phase CH₂Cl₂:H₂O system. The click reactions were repeated in DMSO/H₂O (4:1)

using *p*-tolylacetylene **2.23** (Figure 2.10). At ambient temperature, the reaction went to partial completion, but increasing the temperature to 100 °C allowed the complete formation of product **2.26**. The reaction could be completed at ambient temperature upon addition of 30 mol % TBTA co-catalyst **2.24**, which has been shown previously to enhance the copper-catalyzed cycloaddition.⁹ Benzimidazole co-catalyst **2.25** was also effective for click reactions, and due to its ease of synthesis, was used as the standard co-catalyst for our syntheses. In the reactions that did not go to completion, the incomplete product showed coordination to copper by MALDI mass spectrometry. A potential reason for the sluggish reaction could be the coordination of copper by the incompletely formed product. While the azides in **2.22** are not hindered in their reaction, the four triazole units that result from CuAAC reaction are positioned so that their dipoles can be oriented directly towards the center of the cavitand, allowing coordination of metal ions. When studying the scope of the click reactions, it was determined that the ability of the ligands to coordinate copper frequently limited the reaction progress.

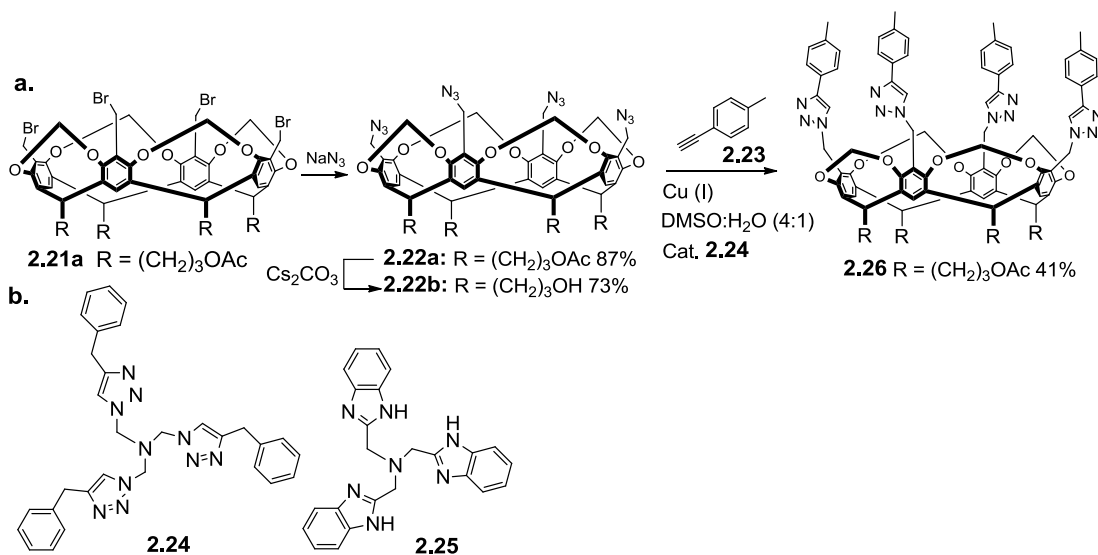


Figure 2.10 (a) Optimization of click conditions to form test cavitand **2.26** and (b) co-catalysts **2.24** and **2.25**

2.4 CavitanDs from Commercially Available Acetylenes

The optimized conditions for the synthesis of **2.26** were applied to other cavitands using simple, commercially available acetylenes **2.27-2.29** (Figure 2.11).¹⁰ Ligand **2.27** was selected in order to form a bidentate between the pyridyl nitrogen and the resulting triazole. Ligands **2.28** and **2.29** lacked the ability to form bidentate ligands with the triazole and therefore were valuable controls. One of the initial challenges was the binding of the copper catalyst by the triazoles. The reactions went to completion at elevated temperatures, but products **2.30-2.32** all contained residual copper from the catalyst. Refluxing the copper-containing cavitand with sodium EDTA did little to remove the copper, which demonstrated the especially strong affinity of the triazoles for the metal. Eventually the residual copper was effectively removed by refluxing the crude

cavitand with sodium hydrosulfide in water for two hours and collecting the insoluble pure product by simple filtration.

The acyl-footed cavitands were readily soluble in organic solvents (ex: methylene chloride, methanol, acetone). Cleaving the acyl groups with base to form the alcohol-footed counterparts allowed access to cavitands **2.30-2.32b** in 70-99 % yield, and the alcohol-footed cavitands were soluble in more polar solvents such as DMSO or DMA (but not water).

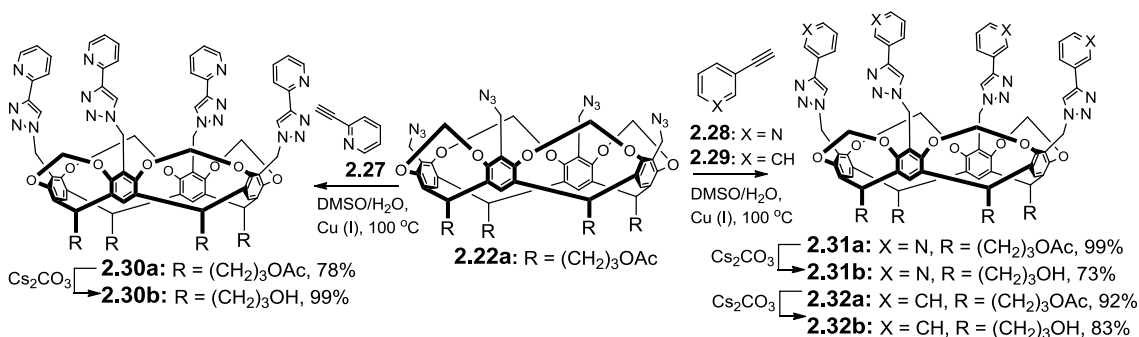


Figure 2.11: The synthesis of cavitands **2.30 – 2.32** from **2.22**

2.5 Amide Cavitands

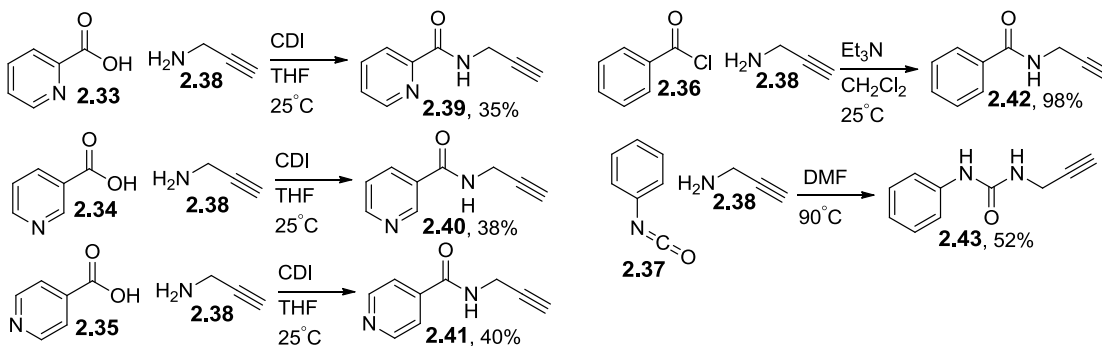


Figure 2.12: The synthesis of the amide and urea ligands used to deepen the cavitands

Once an optimized set of click conditions was established, these conditions were applied to more complex ligands. The purpose of using more complex ligands was the synthesis of more flexible cavitands with multiple potential metal-coordinating groups. Co-catalyst **2.25** was required for reactivity in order to protect the copper source under the forcing conditions. Ligands **2.39-2.41** were all made in 35-40 % yield from the pyridyl carboxylic acids **2.33-2.35** and propargyl amine **2.38** (Figure 2.12), and phenyl amide **2.42** was made from the acid chloride precursor **2.36** in 98 % yield. Only **2.39** and **2.41** allowed the reaction with **2.22a** to go to completion. The reactions of **2.22** with **2.40** and **2.42** went to partial completion, but pure product was never obtained. When **2.22a** was reacting with the phenyl urea ligand **2.43**, however, the reaction proceeded smoothly. The amide or urea functional groups made cavitands **2.44**, **2.46**, and **2.48** more flexible than cavitands **2.30-2.32**, and the amide groups offered potential sites for the coordination of metals in addition to the triazole positions (Figure 2.13).

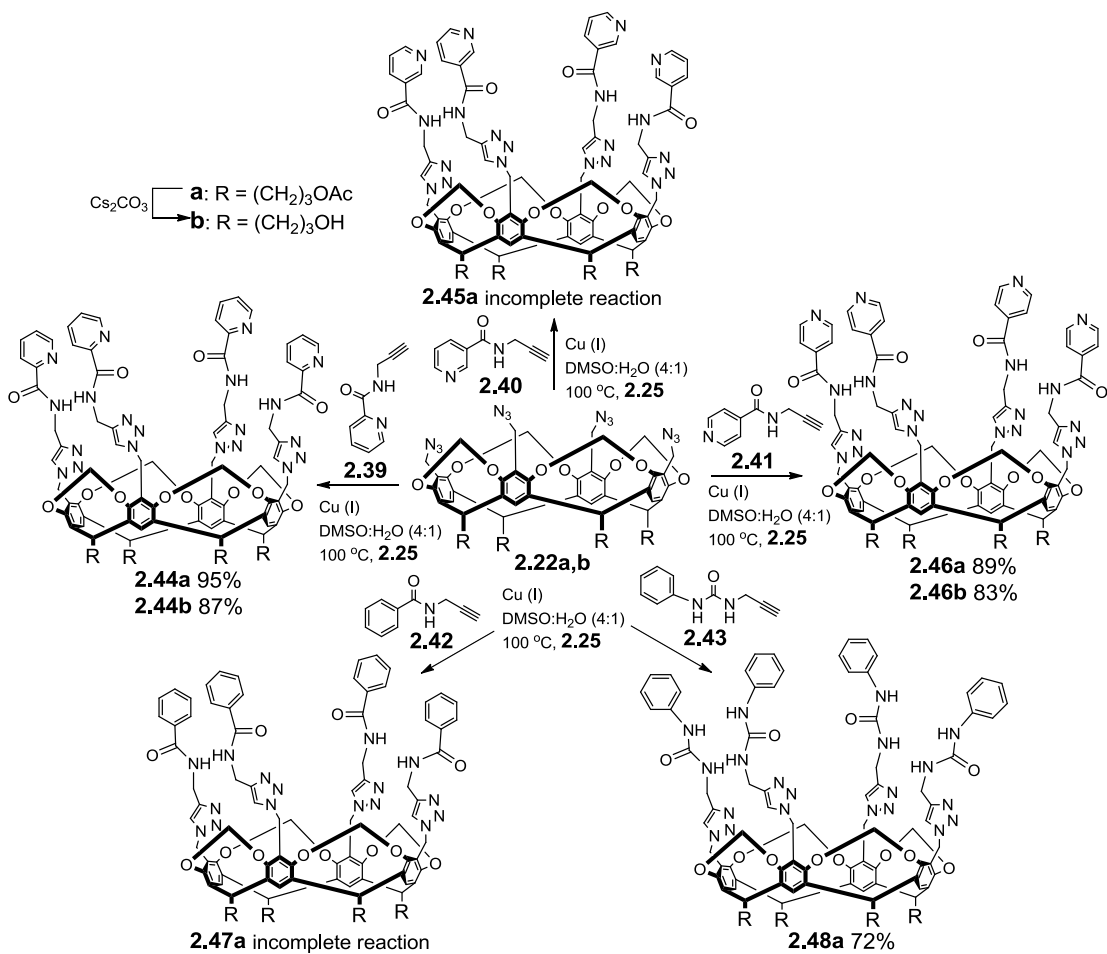


Figure 2.13 The synthesis of amide cavitands **2.44-2.48**

2.6 Molecular Baskets

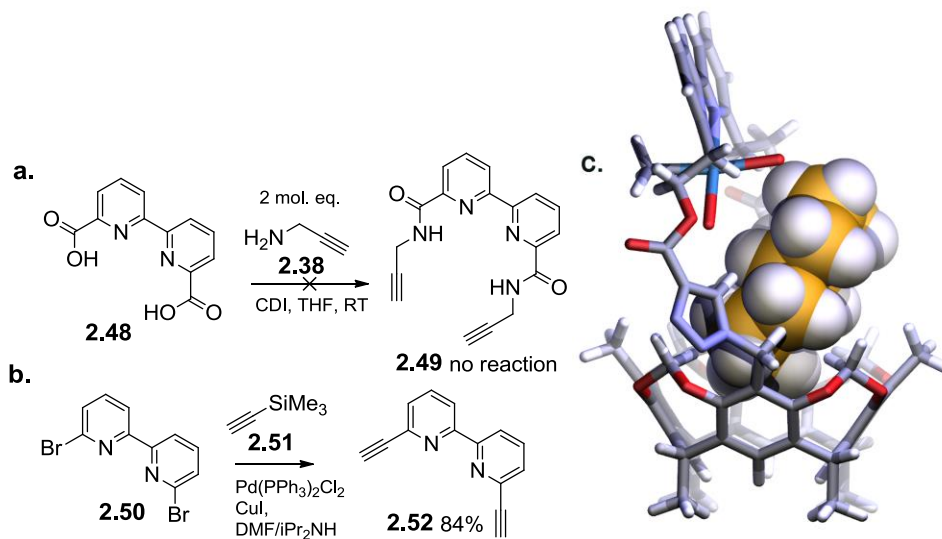


Figure 2.14: The synthesis of ligands (a) **2.49** and (b) **2.52** and (c) a model of a bipyridine-bridged molecular basket binding *trans*-decalin

We believed that selective oxidations could be achieved by orienting a single metal-coordinating bis-acetylene ligand such as **2.49** over the cavitand, forming a molecular basket (Figure 2.14c). By tailoring the size of bis-acetylene and using high dilution conditions, the biscyclization was expected to occur at the 1,3 cavitand rim positions. After the initial cyclization, only one azide on the cavitand rim would be accessible for the second reaction due to steric hindrance. The handle was expected to control oxidation so that only the C-H bonds closest to the metal center were oxidized. Bipyridylamide **2.49** was designed to coordinate methyltrioxorhenium (MTO) thereby orienting the metal center directly over the binding site; however bipyrindyl acid **2.48** was unreactive due to its insolubility in organic solvents. Instead the cyclization reaction was attempted with the simpler 2,2'-diethynylbipyridine **2.52** under standard click conditions (30 % CuSO₄, 60 % L-sodium ascorbate, DMSO:H₂O 4:1, 100 °C) using benzimidazole co-catalyst

2.25, and partially reacted cavitand was recovered. We wondered if the pyridyl motifs were inhibiting the reaction progress by coordinating the copper catalyst, and so the reaction was attempted a final time using 1,3-diethynylbenzene. The reaction with diethynylbenzene led to the collection of a completely insoluble white solid that could not be characterized – possibly a polymerized product.

2.7 Amine Cavitands

While the amide groups acted as potential metal coordinating groups and spacers for the formation of more flexible cavitands, we believed that attaching amine groups to the cavitand rim would allow for even stronger metal coordination. Because of the strong chelating abilities of amines, however, building cavitands with amine functional groups was significantly more challenging due to the tendency of the partially formed amine cavitands to coordinate the copper catalyst out of solution.

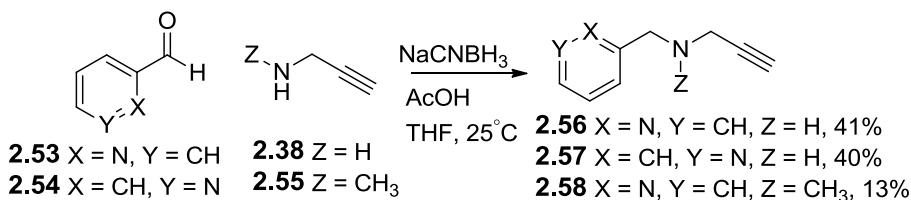


Figure 2.15: The synthesis of the amine ligands used to deepen the cavitands

Ligands **2.56-2.58** were synthesized in our laboratory from commercially available starting materials (Figure 2.15). The reactions of ligand **2.56** or **2.57** with **2.22a** did not go to completion, even under forcing conditions. The ¹H NMR of the partially reacted product was broad and poorly defined, which seemed to indicate that copper was being coordinated by the incompletely formed cavitand. To gain a better understanding of the

effect of the copper chelating groups, we tested the reaction of **2.22a** with **2.56** using stoichiometric copper (2 mol. eq). The increased copper loading improved the reaction progress, and MALDI mass spectrometry indicated that the desired product was formed, but pure product was never isolated. Further analysis of the partially reacted cavitands suggested decomposition of the amine ligands under the harsh reaction conditions.

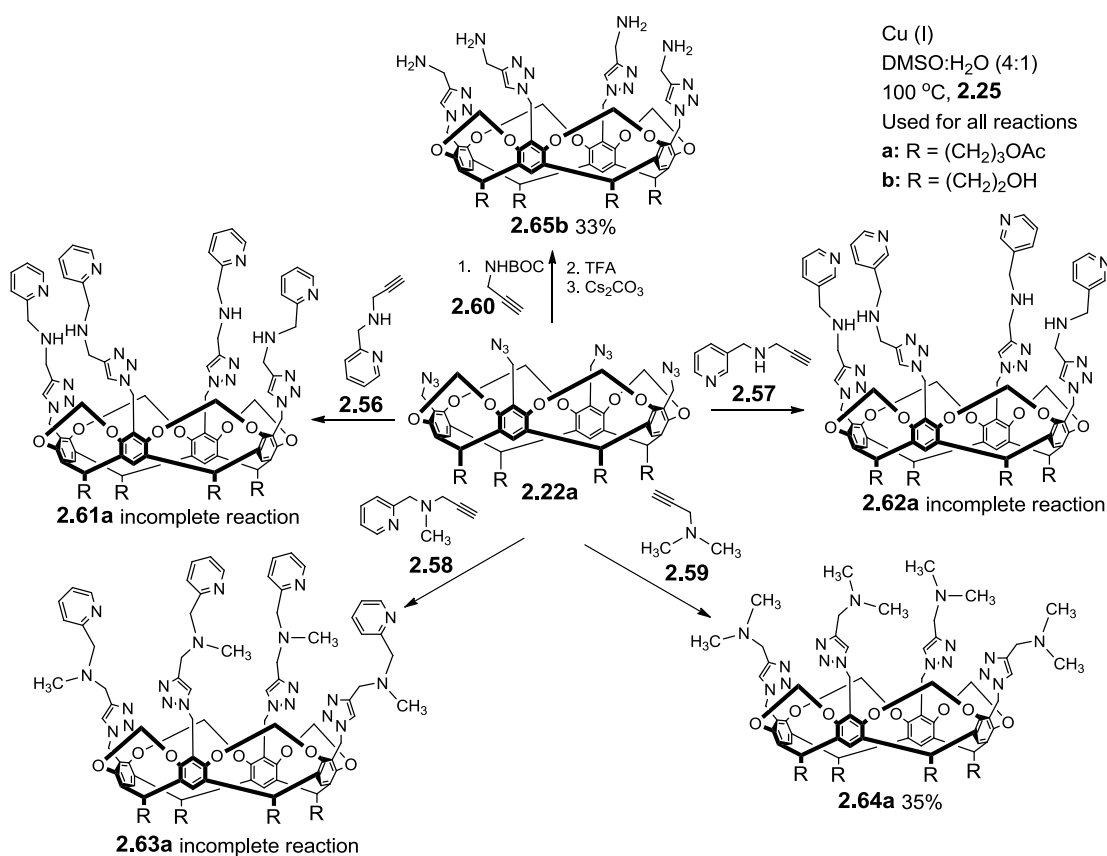


Figure 2.16 The synthesis of amine cavitands **2.61-2.65**

We predicted that if the problem with the reaction was coordination of the copper catalyst, these problems could be avoided by performing the click reaction with a less strongly coordinating amine such as **2.58**. This reaction to form **2.63** proceeded more readily than our previous attempts, but MALDI mass spectrometry showed a partially

formed, copper-coordinated cavitand where only 1 or 2 ligands had been added. Alternatively, the dimethylamine cavitand **2.64** could be formed in 35 % yield under our standard click conditions because the ligand does not decompose during the reaction.

Although the tertiary amine **2.59** could be added to the cavitand rim, the binding site of the product was not deep enough to be useful. Alternatively, the BOC-protecting group of **2.60** limited the coordination of the copper catalyst during the click reaction, and the BOC group could be removed once the product was fully formed. The click reaction with BOC-propargylamine proceeded smoothly under the standard click conditions, but treating the cavitand product with TFA to remove the BOC protecting groups partially removed the acyl groups on the feet. In order to obtain a single cavitand product, cavitand **2.65a** was treated with Cs_2CO_3 to remove the acyl groups completely and give the alcohol-footed **2.65b** in 33 % overall yield. Cavitand **2.65b**, however, was a poor nucleophile, and was not useful in the synthesis of deeper cavitands.

2.8 References

- 1) Hooley, R. J.; Biroš, S. M.; Rebek, J., Jr. "A Deep, Water-Soluble Cavitand Acts as a Phase-Transfer Catalyst for Hydrophobic Species." *Angew. Chem. Int. Ed.* **2006**, *45*, 3517–3519.
- 2) Gibb, B. C.; Chapman, R. G.; Sherman, J. C. "Synthesis of Hydroxyl-Footed Cavitands." *J. Org. Chem.* **1996**, *61*, 1505–1509.
- 3) Yanagihara, R.; Tominaga, M.; Aoyama, Y. "Chiral Host-Guest Interaction. A Water-Soluble Calix[4]resorcarene Having L-Proline Moieties as a Non-Lanthanide Chiral NMR Shift Reagent for Chiral Aromatic Guests in Water." *J. Org. Chem.* **1994**, *59*, 6865–6867.

- 4) Mezo, A. R.; Sherman, J. C. "Water-Soluble Cavitands: Synthesis of Methylene-Bridged Resorcin[4]arenes Containing Hydroxyls and Phosphates at Their Feet and Bromomethyls and Thiomethyls at Their Rims." *J. Org. Chem.* **1998**, *63*, 6824–6829.
- 5) Gui, X.; Sherman, J. C. "Host-guest Binding of Simple Cavitands in Water." *Chem. Commun.* **2001**, 2680–2681.
- 6) Hass, O.; Schierholt, A.; Jordan, M.; Lützen, A. "Improved Synthesis of Monohalogenated Cavitands and Their Use in the Synthesis of Further Functionalized Cavitands." *Synthesis* **2006**, 519–527.
- 7) Walker, S. D.; Barder, T. E.; Martinelli, J. R.; Buchwald, S. L. "A Rationally Designed Universal Catalyst for Suzuki–Miyaura Coupling Processes." *Angew. Chem. Int. Ed.* **2004**, *43*, 1871–1876.
- 8) Jude, H.; Sinclair, D. J.; Das, N.; Sherburn, M. S.; Stang, P. J. "Self-Assembly of Supramolecular Platinum Complexes with Bis-4-pyridyl Cavitands." *J. Org. Chem.* **2006**, *71*, 4155–4163.
- 9) Chan, T. R.; Hilgraf, R.; Sharpless, K. B.; Fokin, V. V. "Polytriazoles as Copper(I)-Stabilizing Ligands in Catalysis." *Org. Lett.* **2004**, *6*, 2853–2855.
- 10) Djernes, K. E.; Moshe, O.; Mettry, M.; Richards, D. D.; Hooley, R. J. "Metal-Coordinated Water-Soluble Cavitands Act as C–H Oxidation Catalysts." *Org. Lett.* **2012**, *14*, 788–791.

Chapter Three: Self-Assembly by Metal Coordination

3.1 Introduction

The four-walled cavitands such as **2.30-2.32** and **2.44-2.48** have free rotation and need to be held in a more rigid conformation to allow the binding of guests. This was accomplished via the self-assembly of bowl-shaped cavitands through metal coordination.¹ The metals served a three-fold purpose; they held the cavitands together, solubilized them in water, and the metals allowed the oxidation of hydrocarbons in the presence of stoichiometric oxidant. The cavitands that were selected for metal-binding studies are shown in Figure 3.1.

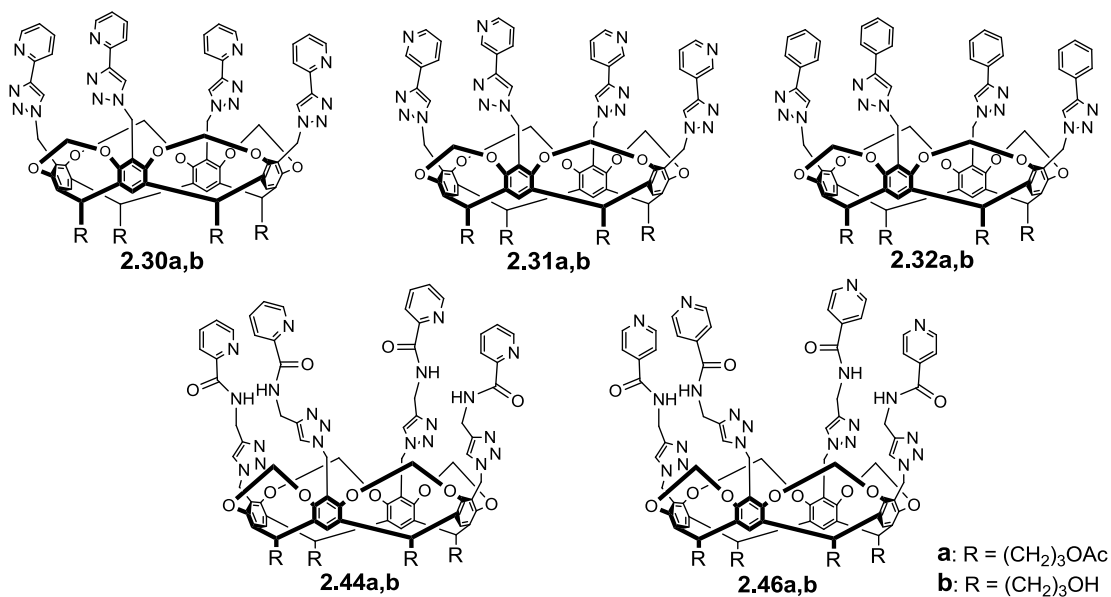


Figure 3.1: The cavitands selected for metal binding studies

3.2 Selection of Metals

We anticipated that the triazole groups of cavitands **2.30-2.32** would be able to coordinate metals, and so we performed binding studies by NMR to quickly gauge which metals had an affinity for the cavitand. ^1H NMR samples in CD_3CN of **2.31** were treated with various metal salts and the changes to the spectrum were observed (Figure 3.2). Treating **2.31** with $\text{Pd}(\text{OAc})_2$, $\text{Pd}(\text{NO}_3)_2$, or $\text{Pd}(\text{OTf})_2$ all led to the formation of insoluble precipitates that could not be analyzed; however the other metal salts led to observable changes in the ^1H NMR. Treating the cavitand with CuBF_4 or AgBF_4 caused an upfield change in chemical shift of up to 0.3 ppm. The change in chemical shift caused by $\text{Cu}(\text{NO}_3)_2$ was much smaller; the maximum change was < 0.1 ppm. Treating the cavitand with $\text{Zn}(\text{OAc})_2$ resulted in the coalescence of peaks in the aromatic region; while five distinct peaks are observed in the aromatic region for the cavitand alone, only two peaks are observed once $\text{Zn}(\text{OAc})_2$ is added.

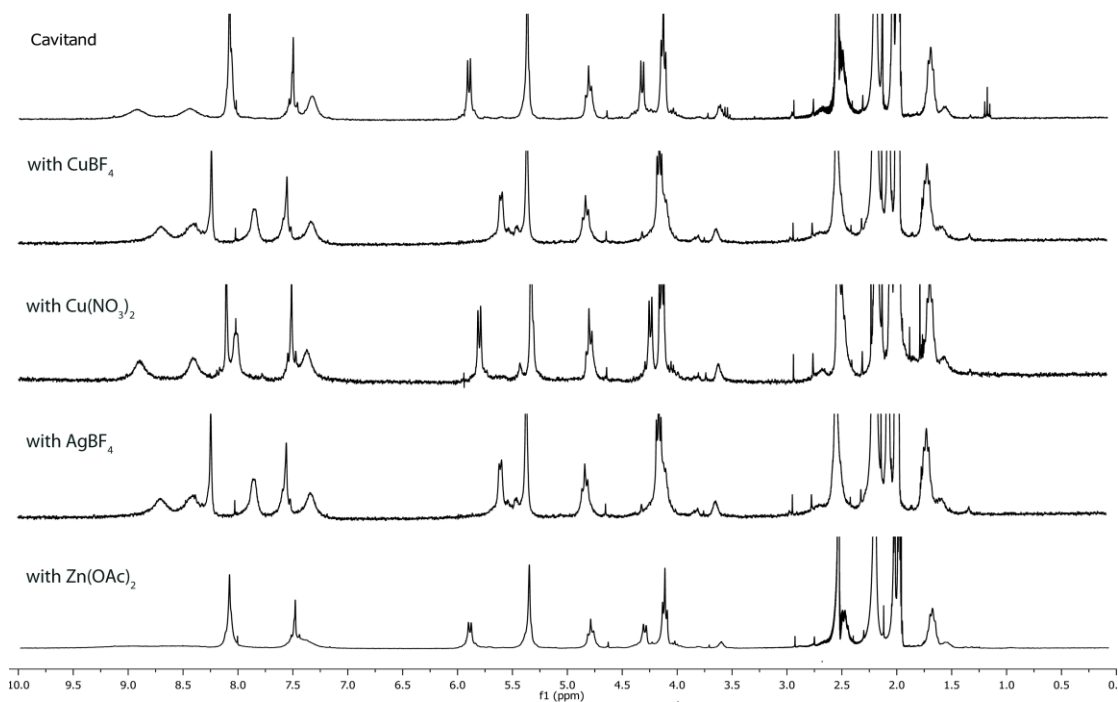


Figure 3.2: The preliminary metal-binding screen for **2.31** by ^1H NMR in CD_3CN

Preliminary binding studies also showed that **2.44a** also bound metals. The biggest changes to the ^1H NMR spectrum of **2.44a** were caused by AgBF_4 and CuBF_4 . In addition to broadening the peaks overall, addition of AgBF_4 shifted most of the peaks upfield, where the biggest change in chemical shift was in the methylene resonance that shifted from 5.74 ppm to 5.51 ppm (Figure 3.3b). CuBF_4 , on the other hand, did not cause an overall upfield or downfield shift, rather the resonances effectively merged into fewer, more poorly defined peaks. The largest change in chemical shift was on the pyridyl resonance that shifted from 8.67 ppm to 8.50 ppm (Figure 3.3f). Other metal salts, including $\text{Cr}(\text{NO}_3)_3$ and FeSO_4 caused overall broadening of the peaks, but no changes in chemical shift, whereas $\text{Al}(\text{NO}_3)_3$ and $\text{Ga}(\text{NO}_3)_3$ did not have any effect on the ^1H NMR spectrum at all.

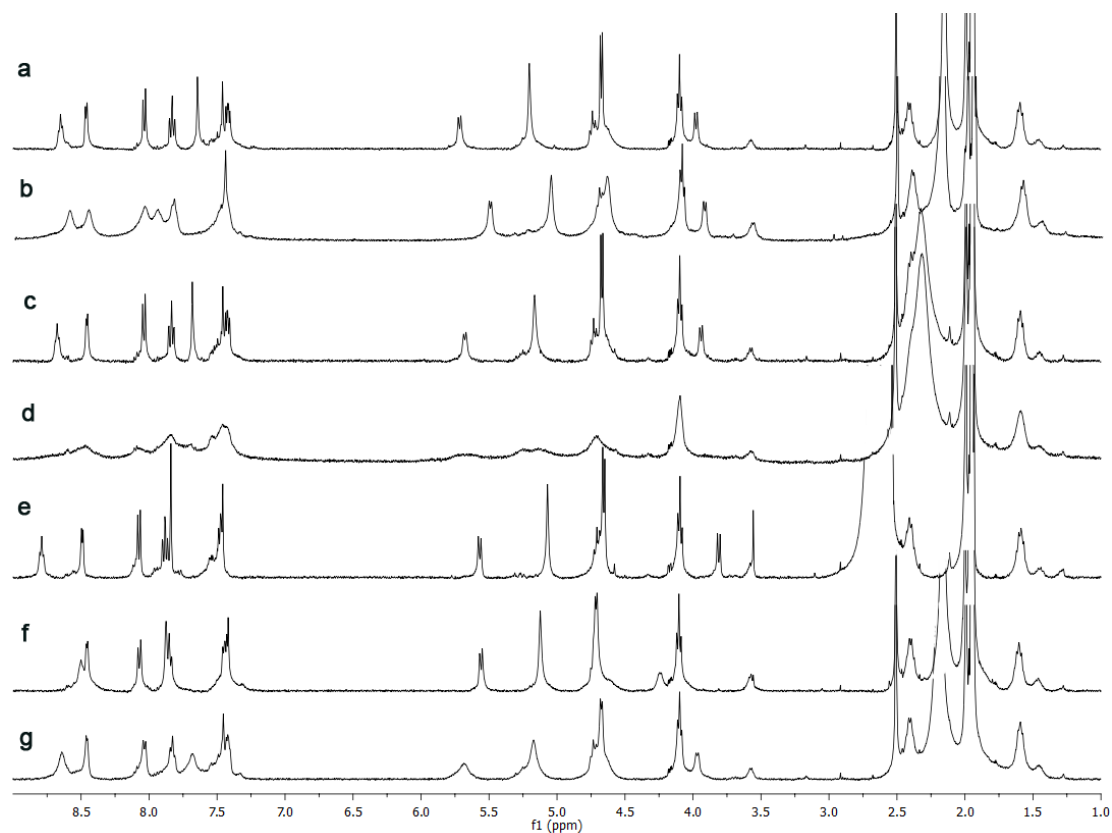


Figure 3.3: The preliminary metal-binding screen for **2.44a** by ^1H NMR in CD_3CN with (a) **2.44a** alone, (b) AgBF_4 , (c) $\text{Al}(\text{NO}_3)_3$, (d) $\text{Cr}(\text{NO}_3)_3$, (e) $\text{Ga}(\text{NO}_3)_3$, (f) CuBF_4 , and (g) FeSO_4

These changes in chemical shift and resolution suggested that the metals were being coordinated by the cavitand; but in order to confirm that these changes were not merely the effect of metal ions in solution, the metals were pre-coordinated to the cavitand and the formation of a complex was verified by MALDI mass spectrometry. These efforts focused on the ability of the cavitands to coordinate copper and iron since these metals had the greatest potential to perform oxidations.

3.3 Pyridyl and Phenyl Binding

The first binding studies were performed on the simplest cavitands made from commercially available alkynes. Molecular modeling suggested that the 2-pyridyl cavitand **2.30** would give the most desirable conformation, but the binding abilities of **2.31** and **2.32** were also tested. The metal-containing complexes could be isolated by reaction of either **2.22a** or **2.22b** with a weakly coordinated metal salt (e.g. $\text{Cu}(\text{CH}_3\text{CN})_4\text{BF}_4$, FeSO_4) in methanol. The ability of the cavitands to coordinate metals was not affected by the functional groups on the feet, however the OH footed cavitands gave cleaner MALDI spectra and so those cavitand derivatives were used primarily in the metal binding studies. The metal complexes precipitated from solution and could be isolated by simple filtration. Because the ^1H NMRs of the metal containing samples were broad, MALDI mass spectrometric analysis was used to analyze the metal binding properties of the system. MALDI mass spectrometry showed the number of metal cations that were coordinated, but it did not give information as to which functional groups were coordinating them. We were unable to grow X-ray quality crystals of the cavitands, however molecular modeling using Hartree-Fock calculations was used to determine the structures of the metal bound cavitands (Figure 3.4).

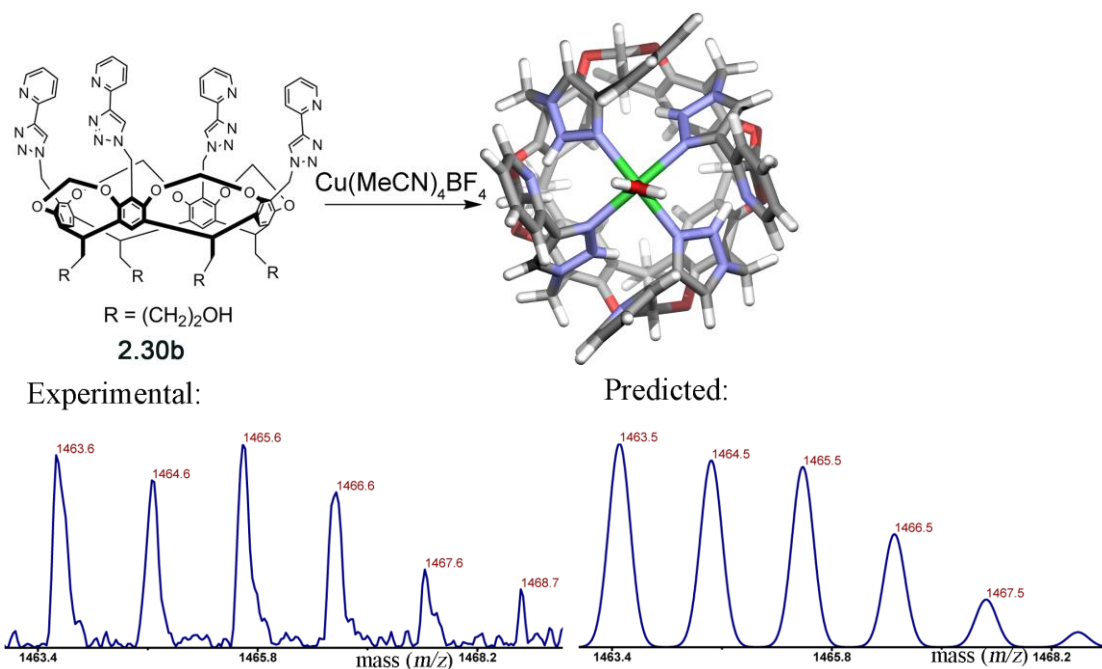


Figure 3.4: The formation of **2.30•Cu** and the experimental and predicted MALDI-MS spectra

Cavitanths **2.30**, **2.31**, and **2.32** all coordinated the copper catalyst during the click reaction, and it was determined that the coordination of copper could be completed by sonicating the partially coordinated cavitanths in methanol with $\text{Cu}(\text{CH}_3\text{CN})_4\text{BF}_4$ for 15 minutes. All three cavitanths showed the coordination of a single copper cation, which confirmed what we had predicted using models. Only the triazole nitrogens, were coordinated to the metal, and the pyridyl nitrogens of **2.30•Cu** and **2.31•Cu** were not. The minimized structure of **2.30•Cu** is shown in Figure 3.4, which shows the geometry of the bound copper that is common to **2.30•Cu**, **2.31•Cu**, and **2.32•Cu**.

We were happy to discover that cavitanths **2.30•Cu-2.32•Cu** were easily soluble (20 mM) in water or mixtures of water and an organic co-solvent such as acetonitrile. The feet played a small role in the solubility of the cavitant. The less polar acyl groups actually gave the cavitanths increased solubility in water:organic mixtures relative to the

alcohol counterparts, presumably due to increased solubility in an organic co-solvent. The more polar alcohol feet, however, did not increase the solubility of the cavitands in pure water.

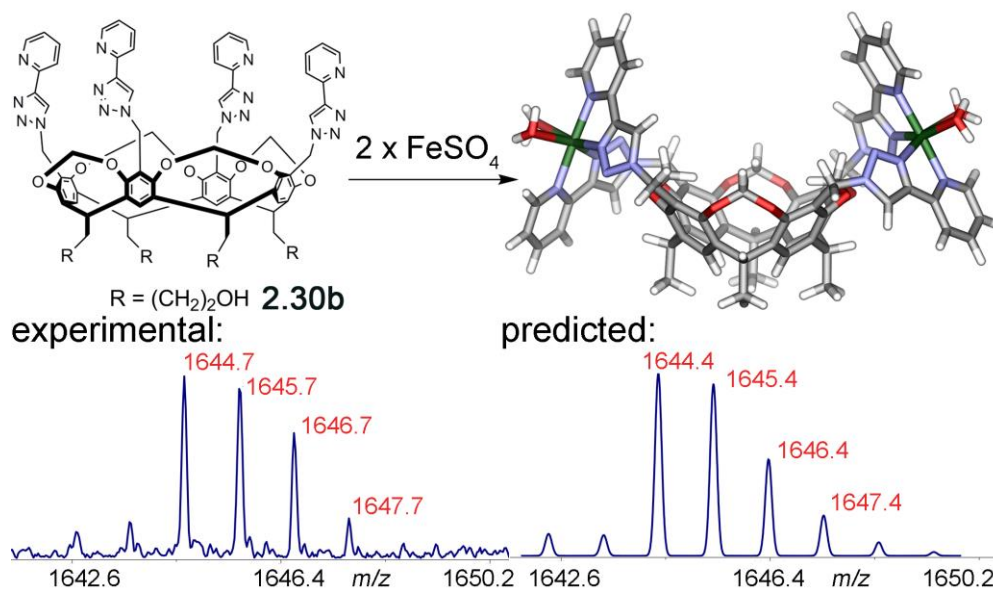


Figure 3.5: The formation of **2.30b·Fe₂** and confirmation of iron coordination by MALDI mass spectrometry

Despite the high affinity of the triazoles towards copper, they had limited affinity towards iron. Treating cavitands **2.31** and **2.32** with FeSO₄ did not allow the formation of a metal complex; however when **2.30** was treated with FeSO₄, MALDI-MS of the product showed the coordination of not one, but two iron cations (Figure 3.5). The fact that **2.31** and **2.32** had no affinity to iron suggested that having the pyridyl nitrogen at the 2-position was essential for binding and that the iron cations were coordinated by the bidentate ligands formed by the nitrogen atoms of the triazole and pyridyl groups. Again the coordination of the metals solubilized the cavitands in water or water/organic mixtures in excess of 50 mM.

3.4 Increasing Flexibility

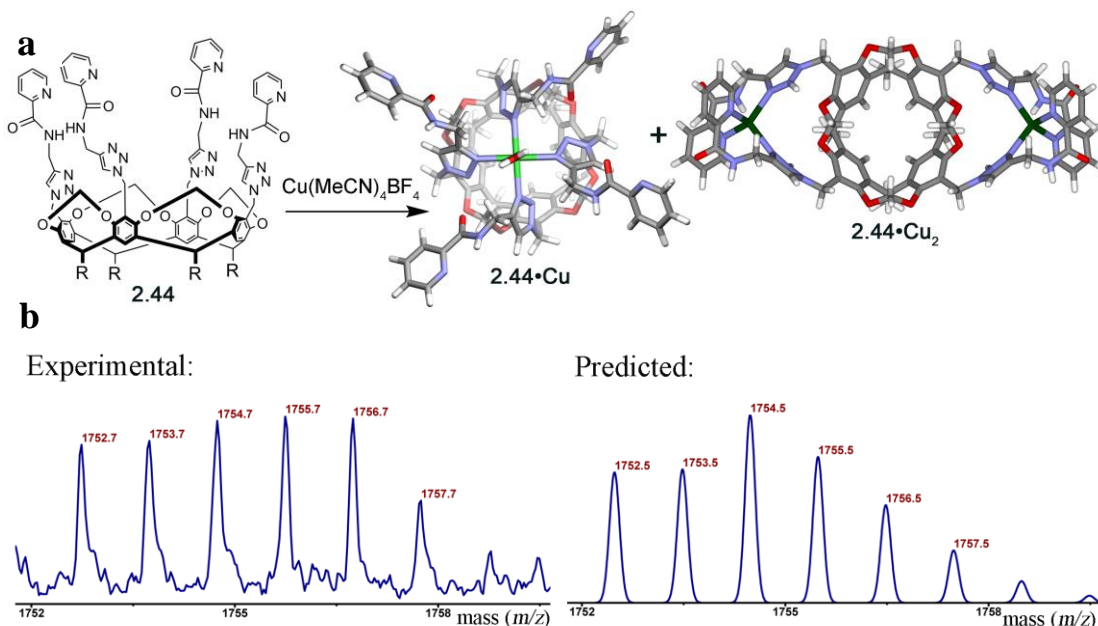


Figure 3.6: (a) The formation of cavitands **2.44•Cu** and **2.44•Cu₂** and (b) the experimental and predicted MALDI-MS spectra for the coordination of two copper cations in **2.44b•Cu₂**

Next the ability of the more flexible cavitands to coordinate metals was tested, and we found that the more flexible cavitands formed multiple metal-coordinated products. 2-Pyridyl amide cavitand **2.44** coordinated either one or two copper cations to form **2.44•Cu** and **2.44•Cu₂**, whereas the 4-pyridyl cavitand **2.46** only coordinated a single copper cation. In cavitand **2.44•Cu**, the single copper cation is coordinated at the triazoles, but in **2.44•Cu₂** two copper cations are coordinated at the bidentate ligands formed by the pyridyl nitrogens and the triazoles. The resulting mixture of products is annotated as **2.44•Cu_x** (Figure 3.6). Only a single copper cation is coordinated by **2.46** because the nitrogens on the pyridyl groups point upwards rather than inwards and therefore cannot coordinate a metal. All metal-coordinated cavitands existed as discrete molecules, and the formation of metal-cavitand dimers was not observed.

Cavitand **2.44**•Cu₂ formed a well-defined cavity with an open hydrophobic interior where the metal was fully coordinated to the cavitand. We believed that the octahedral geometry of iron would allow us to coordinate metals but also leave valences that could weakly coordinate solvent or oxidant.

Cavitand **2.46** had no affinity for iron because the pyridyl nitrogens were not at an angle that allowed coordination. **2.44** on the other hand, formed a mixture of products **2.44**•Fe and **2.44**•Fe₂ when treated with iron sulfate (the mixture is referred to as **2.44**•Fe_x). In **2.44**•Fe, only one iron was coordinated, presumably at the triazoles, whereas in **2.44**•Fe₂, the two irons were coordinated by the bidentate ligands formed by the 2-pyridyl nitrogens and the deprotonated amides (Figure 3.7).

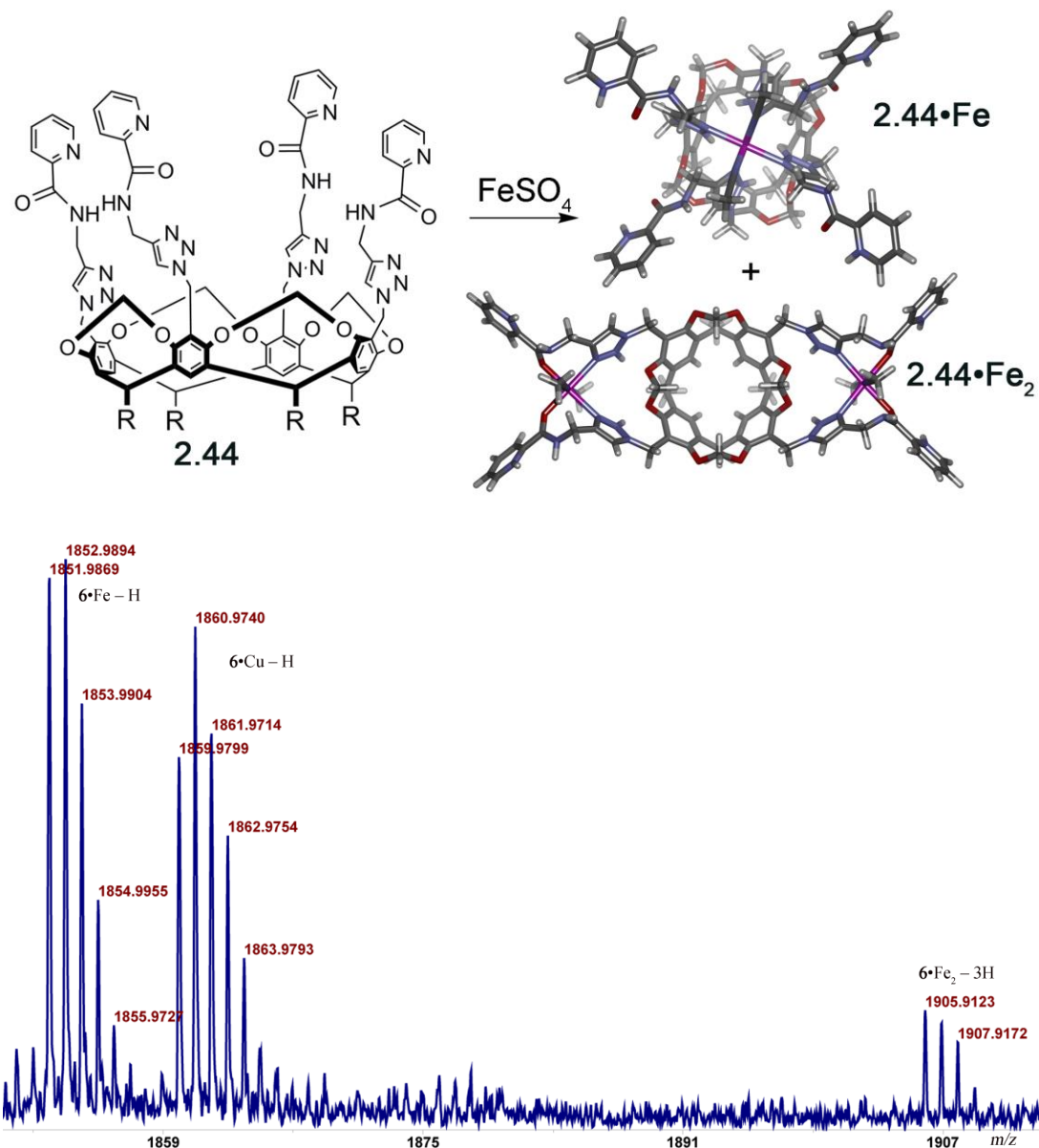


Figure 3.7: The formation of cavitands $2.44 \cdot \text{Fe}$ and $2.44 \cdot \text{Fe}_2$ and the MALDI-MS spectrum showing the formation of both products

Both $2.44 \cdot \text{Cu}_x$ and $2.44 \cdot \text{Fe}_x$ were soluble in water or water:organic mixtures, making the self-assembly of these host molecules using metals an extremely valuable approach to creating water-soluble supramolecular catalysts. Rather than taking a complex synthetic route towards the formation of our hosts, we can add freely rotating arms

relatively easily using click chemistry and then constrain these arms in a rigid conformation simply by adding an appropriate metal. The resulting metal cavitands are soluble in water, thereby eliminating the need for covalently added solubilizing groups; and in the case of **2.44•Fe_x**, an incompletely ligated transition metal is positioned over the binding site of the cavitand, which potentially allows the coordination of an oxidant and the formation of an active iron (V) oxo species for the oxidation of C-H bonds (see chapter 1).

3.5 Guest Binding Studies

The metal coordinated cavitands were challenging to characterize by NMR due to their broad peaks and/or paramagnetic properties. Nevertheless some binding studies were performed to ascertain whether or not the hydrophobic interior of the cavity was amenable to guest binding.

2.30•Fe₂ in D₂O was used to study guest binding of 4-ethyltoluene, cumene, cymene, benzene, adamantane, cyclohexane, methylcyclohexane, and cyclooctane (Figure 3.8). Only 4-ethyltoluene and *p*-cymene showed any upfield shifts of the guest resonances. Even then, no peaks were observed below 0 ppm, with the furthest upfield peak appearing at 0.62 ppm for 4-ethyltoluene and 0.85 for *p*-cymene. Both 4-ethyltoluene and *p*-cymene have a methyl group that can point directly downwards into the cavitand binding site. Previous studies have shown that substituted aromatic rings with alkyl groups in the *para*-position are especially good guests in resorcinarene-based cavitands due to the favorable hydrophobic interactions between host and guest.²

Methylcyclohexane also has a pendant methyl group that could potentially point into the cavity of the binding site, but binding of methylcyclohexane was not observed.

The limited number of guests that produce an observable change in chemical shift by ^1H NMR suggest that guest binding is not especially favorable and that the guest in/out rate is too fast to observe on the NMR timescale. Our models show that the binding sites of cavitands $2.30\cdot\text{Fe}_2$ and $2.44\cdot\text{Fe}_2$ are quite shallow. For improved guest binding, a deeper binding site is necessary.

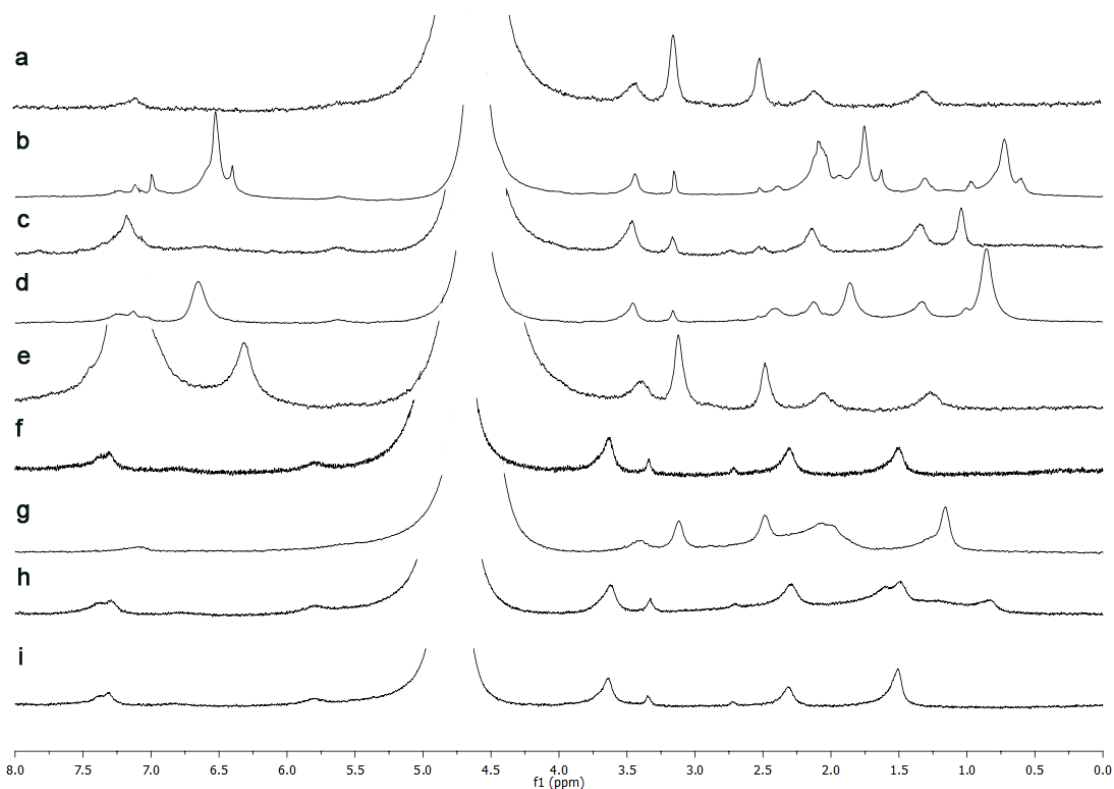


Figure 3.8: Guest-binding studies of $2.44\cdot\text{Fe}_2$ by ^1H NMR with (a) no guest, (b) 4-ethyltoluene, (c) cumene, (d) *p*-cymene, (e) benzene, (f) adamantane, (g) cyclohexane, (h) methylcyclohexane, (i) cyclooctane

3.6 References

- 1) Djernes, K. E.; Padilla, M.; Mettry, M.; Young, M. C.; Hooley, R. J. "Hydrocarbon Oxidation Catalyzed by Self-Folded Metal-Coordinated Cavitands." *Chem. Commun.* **2012**, *48*, 11576–11578.
- 2) Park, S. J.; Hong, J.-I. "The Cooperative Effect of Electrostatic and Hydrophobic Forces in the Complexation of Cationic Molecules by a Water-Soluble Resorcin[4]arene Derivative." *Tetrahedron Lett.* **2000**, *41*, 8311–8315.

Chapter Four: Oxidations

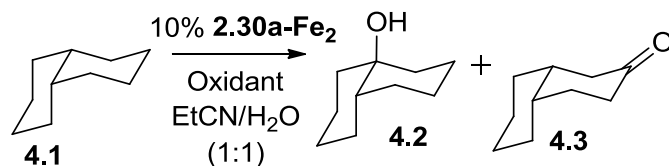
4.1 Introduction

After we had successfully built and characterized metal-coordinated cavitands **2.30•Fe₂** and **2.44•Fe_x**, the ability of these cavitands to perform oxidations was tested.¹ It was determined that the cavitands successfully oxidized unfunctionalized benzylic and aliphatic C-H bonds under mild aqueous conditions in the presence of stoichiometric ^tBuOOH. Cavitands **2.30•Fe₂** and **2.44•Fe_x** are extremely robust and can be reused multiple times without any decrease in reactivity. Both the acyl and alcohol footed derivatives catalyze hydrocarbon oxidations in approximately equal yields, although to rule out the possibility of the alcohol feet being oxidized during the reaction, acyl footed cavitands **2.30a•Fe₂** and **2.44a•Fe_x** were studied most thoroughly, and the yields that are reported in this chapter were obtained using **2.30a•Fe₂** and **2.44a•Fe_x** unless otherwise noted. The reusability of cavitand **2.44b•Fe_x** can be enhanced by derivatizing the alcohol feet with silyl groups and anchoring the cavitands to an SBA-15 surface. The resulting heterogeneous catalyst was found to be equally as reactive as the solution phase catalyst.

4.2 Optimization of Conditions

The initial test reactions using **2.44•Fe_x** were performed on *cis*-decalin as substrate to maximize solubility and minimize target volatility during the reaction (see Table 4.1). In order to prevent solvent oxidation, the reactions were performed in aqueous solution with an unreactive organic co-solvent such as acetonitrile or propionitrile. Multiple co-

oxidants were tested, but the only successful oxidant in the oxidation of *cis*-decalin was *tert*-butyl hydroperoxide. *Cis*-decalin was subjected to 10 equiv. ^tBuOOH and 10 % catalyst **2.44**•Fe_x in 1:1 MeCN/H₂O (substrate concentration of 180 mM) at ambient temperature for 24 hours, and the resulting products were analyzed by GC-MS. Under these conditions, two products were observed in 33 % overall conversion, *cis*-9-decalol (**4.2**) and *cis*-2-decalone (**4.3**). As propionitrile and water are immiscible at room temperature, no reaction occurred in that solvent mixture. Increasing the temperature greatly improved the conversion of the reaction, and allowed the more effective EtCN:H₂O solvent mixture to be used. At 60 °C, a 70 % overall conversion was attained, with oxidation at the tertiary bridgehead of *cis*-decalin favored in a ratio of almost 3:1. No multiple oxidation products were observed.



Eq. AcOH	T °C	Oxidant (10 eq.)	Time (h)	Overall Conv. (%)	Product ratio 4.2, 4.3 (%)
2	23	^t BuOOH	24	33	15, 18 ^b
2	23	^t BuOOH	24	n.r.	n.r.
0	60	^t BuOOH	24	70	46, 24 ^b
0	60	^t BuOOH	18	48	42, 6
2	60	^t BuOOH	24	69	51, 18
0	60	^t BuOOH	24	69	52, 17
5	60	^t BuOOH	24	68	49, 19
0	60	H ₂ O ₂	24	n.r.	n.r.
0	60	Oxone	24	n.r.	n.r.
0	60	(BzO) ₂	24	n.r.	n.r.
0	60	NMO	24	n.r.	n.r.
0	60	^t BuOOH	48	69	52, 17

^aReactions were performed in triplicate, and the average yield is reported. ^bH₂O:MeCN (1:1) as solvent.

Table 4.1: The optimization of catalyst **2.30•Fe₂** using *cis*-decalin

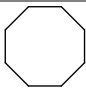
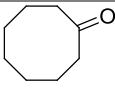
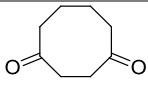
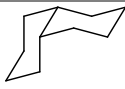
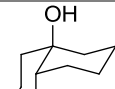

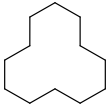
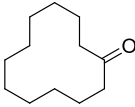

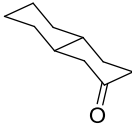

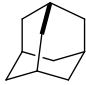
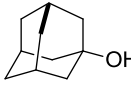
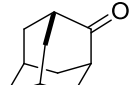
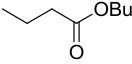
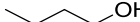
The optimal reaction time was 24 hours: a slight increase in product formation was observed by allowing the reaction to continue for 24 hours rather than 18 hours, but further increasing the reaction time did not increase the yield. Other co-oxidants were surprisingly inert. Benzoyl peroxide, hydrogen peroxide, oxone and *N*-methylmorpholine *N*-oxide all gave no reaction in the oxidation of *cis*-decalin. When testing more reactive substrates such as fluorene, the oxidant benzoyl peroxide was too reactive, causing the fragmentation of fluorene, rather than its oxidation. Furthermore, while hydrogen peroxide has been used successfully as a co-oxidant in other systems,² it was unreactive towards all unactivated hydrocarbons and only minimally active towards activated substrates such as styrene (20 % conversion to benzaldehyde) using **2.30•Fe₂**. Other

examples of Fe(II)-based hydrocarbon oxidation catalysts have shown that the addition of superstoichiometric amounts of weak acids can improve the effectiveness of the oxidation,³ but we did not observe this effect. Neither 2 nor 5 equivalents of acetic acid displayed any effect on conversion or selectivity. As a control experiment, FeSO₄ was tested as catalyst, but the unligated iron (II) species was unstable to the reaction conditions. Some conversion was observed, but catalysis was not: the maximal conversion was substoichiometric (~10 %).

4.3 Cyclic Oxidations

Unfortunately, linear alkanes such as n-octane were unreactive, as were branched acyclic alkanes such as 2,2,4-trimethylpentane, but we found that the catalysts were reactive towards cyclic and polycyclic hydrocarbons, specifically those benefitting from decreased ring strain upon oxidation (eg. cyclooctane). Cyclooctane could be oxidized at ambient temperature to cyclooctanone in 67 % yield. In this case, the diketone product 1,4-cyclooctanedione was also obtained in 12 % yield. No additional diketone products were seen. Cyclooctane is uniquely reactive due to ring strain and the relatively low ring strain of the ketone and diketone oxidation products. Eclipsing interactions with the two adjacent carbon atoms can be eliminated by oxidizing a methylene group to the corresponding ketone. Less strained rings such as cyclohexane and cyclododecane are less reactive, and no diketone oxidation products are observed. Cyclododecane was less reactive but at elevated temperature gave cyclododecanone in 47 % yield. Smaller ring oxidation was less successful, presumably due to increased ring strain in the products.

Interestingly, methylcyclohexane was oxidized in less than 10 % overall conversion while no oxidation occurred with cyclohexane. There was little difference in the effectiveness of catalysts **2.30**•Fe₂ and **2.44**•Fe_x, as can be seen in Table 4.2. Cavitand **2.30**•Fe₂ is slightly less effective in certain cases, possibly due to differences in catalyst solubility.

Substrate	Product	Total Yield	Substrate	Product	Total Yield
					
	a. 56%	a. 5%		a. 50%	a. 24%
	b. 70%	b. 16%		b. 54%	b. 17%
	c. 19%	c. 0%		c. 24%	c. 0%
		a. 61%			a. 74%
		b. 86%			b. 71%
		c. 19%			c. 24%
					
		a. 50%		a. 38%	a. 15%
		b. 45%		b. 42%	b. 17%
		c. 17%		c. 9%	c. 5%
		a. 50%			a. 53%
		b. 45%			b. 69%
		c. 17%			c. 14%
			Bu ₂ O		
	a. 44%	a. 25%		a. 49%	a. 21%
	b. 39%	b. 18%		b. 59%	b. 20%
	c. 3%	c. 4%		c. 8%	c. 4%
		a. 69%			a. 70%
		b. 57%			b. 79%
		c. 7%			c. 12%

Reactions were performed in H₂O:EtCN (1:1) using 10 mol% catalyst and 10 mol. eq. ^tBuOOH.

Table 4.2: The oxidations of hydrocarbon substrates as catalyzed by (a) **2.30**•Fe₂ (b) **2.44**•Fe_x, and (c) FeSO₄

Bi- and polycyclic substrates with both 2° and 3° C–H bonds were tested, namely *cis*-decalin (Table 4.1), *trans*-decalin and adamantane. Norbornane was unreactive while adamantane was readily converted to 1-adamantanol and 2-adamantanone. The oxidation

of these cyclic alkanes is determined largely by the amount of ring strain in the substrate and its corresponding oxidation product. Larger rings such as cyclooctane and cyclododecane are able to relieve ring strain by undergoing oxidation whereas the oxidation of norbornane increases ring strain and is therefore unfavorable. The product of *cis*-decalin oxidation favored the more sterically accessible C–H bonds, giving *cis*-9-decalol and *cis*-2-decalone in a 2.5:1 ratio. *Trans*-decalin, on the other hand, was oxidized to *trans*-2-decalone and *trans*-1-decalone in a 2:1 ratio with an overall yield of 53 %. No tertiary C–H oxidation was observed in this case due to the unfavorable 1,3-diaxial interactions in the product. The cavitands do not undergo observable self-oxidation or decomposition during the reaction: if the oxidation is quenched by addition of ether, the catalyst can be recovered by filtration, and still displays coordinated Fe as determined by MALDI-MS (Figure 4.1).

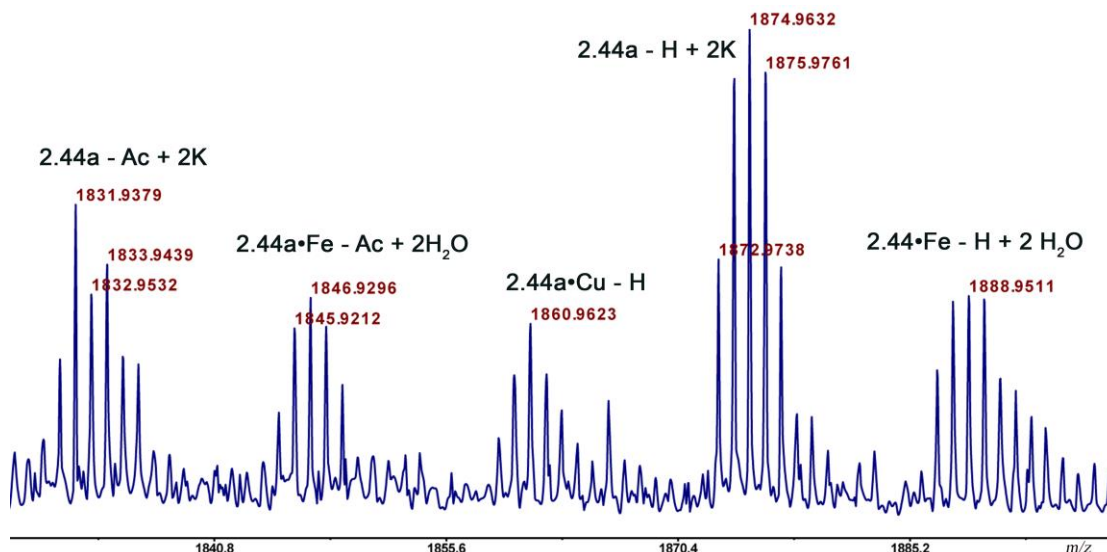


Figure 4.1: MALDI mass spectrometry of reclaimed **2.44•Fe_x**

4.4 Benzylic Oxidations

Using the optimized conditions (10 % catalyst, 10 eq. ^tBuOOH, ~200 mM), the selectivity of the oxidations was tested for an extended scope of substrates, as shown in Table 4.2. Because of the increased reactivity of benzylic substrates, oxidations were carried out in H₂O:MeCN (1:1) at ambient temperature. Yields (a) were obtained using **2.30**•Fe₂, yields (b) using **2.44**•Fe_x, (c) using FeSO₄, and (d) using the ligated iron control **4.4**. We found that the cavitand catalysts dramatically out-performed the controls. FeSO₄

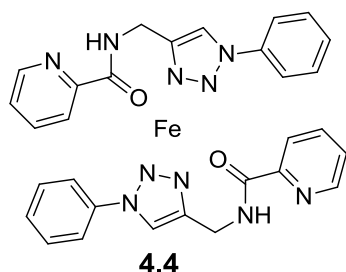


Figure 4.2: Iron control complex **4.4**

showed essentially stoichiometric oxidation of substrates. The ligated iron control **4.4** was more reactive than FeSO₄ alone, but it still fell short of the reactivity that was obtained using **2.30**•Fe₂ or **2.44**•Fe_x. The increase in reactivity that was achieved by using **4.4** rather than FeSO₄ was

minimal in the oxidation of fluorene. A more pronounced increase was observed in the oxidation of the more electron-rich, more sterically hindered 2,7-di-*tert*-butylfluorene. The cavitand catalysts were less reactive towards 2,7-di-*tert*-butylfluorene relative to fluorene, presumably due to steric hindrance; whereas the less bulky ligated control was more reactive towards the more electronically activated substrate.

In all substrates, the most electron rich position was favored. *p*-Xylene was unreactive, however the oxidation of cumene occurred in 80 % overall yield (with

2.30•Fe₂; 2.44•Fe_x gave 77 % conversion). Multiple products were observed, all stemming from initial tertiary C-H abstraction (Figure 4.3). 2-Phenyl-2-propanol was the major product formed, in 40 % yield, although the formation of acetophenone (via an oxidative benzylic C-C cleavage) and dicumyl peroxide were also observed. *p*-Cymene displayed similar reactivity, with overall oxidation proceeding in up to 90 % yield. The major products observed for the oxidation of *p*-cymene were 4-methylacetophenone and *p*- α -dimethylstyrene, and even though *p*-xylene was unreactive, small amounts of cuminaldehyde were detected. As expected, the oxidation of 4-ethyltoluene gave 4-methylacetophenone in high yield. The more reactive benzylic substrates were slightly more susceptible to oxidation with FeSO₄, but again, only stoichiometric quantities were observed. Bibenzyl was especially reactive. Shorter reaction times allowed the detection of products benzaldehyde and 2-phenylacetophenone, but increasing the reaction time to 24 hours or more led to decomposition.

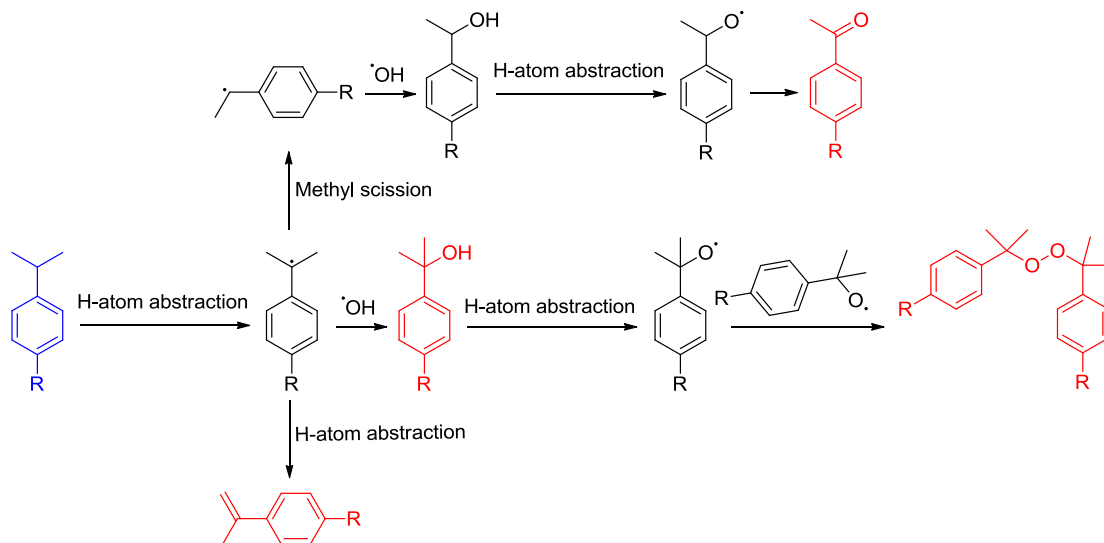


Figure 4.3: The mechanisms of oxidation for benzylic substrates. Starting substrate is shown in blue; products are shown in red, intermediates in black.

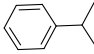
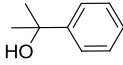
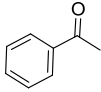
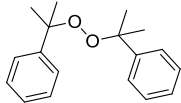
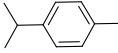
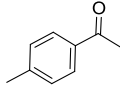
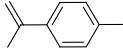
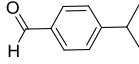
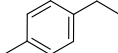
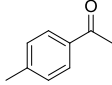
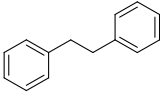
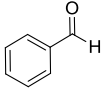
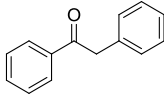
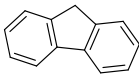
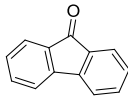
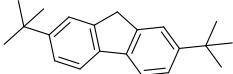
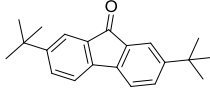
Substrate	Product(s)	Total Yield
	  	a. 42 % b. 46% c. 5%
	  	a. 63% b. 58% c. 16%
		a. 89% b. 88% c. 18%
	 	a. 6% ^a b. 16% ^a c. decomposition ^a
		a. 100% b. 91% c. 16% d. 19%
		a. 54% ^b b. 68% ^b c. 11% d. 40%

Table 4.3: The oxidations of benzylic substrates as catalyzed by (a) **2.30**•Fe₂ (b) **2.44**•Fe_x, (c) FeSO₄, and (d) **4.4**. ^aReaction time: 16 hrs. ^bData was obtained using cavitands **2.30b**•Fe₂ and **2.44b**•Fe_x.


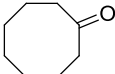
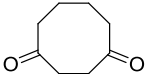
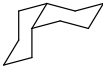
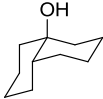

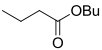
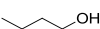

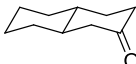
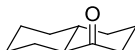

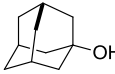
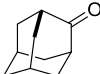
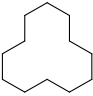
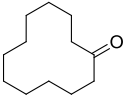
4.5 *n*-Alkyl Oxidations and Tolerance to Functional Groups

Given the success of catalysts **2.30**•Fe₂ and **2.44**•Fe_x for the oxidation of unfunctionalized hydrocarbons, we tested the tolerance for substrates with coordinating functional groups. Ethers were reactive: di-*n*-butyl ether was oxidized to butyl butyrate in greater than 50 % yield, (some saponification to *n*-butanol was also observed during the reaction), but cyclic ethers (e.g. tetrahydropyran) were not oxidized. While additives such as acetone or acetic acid have no deleterious effect on the oxidation, the presence of those functions in the substrate rendered the target unreactive. Species such as amides, lactones, carboxylic acids, and esters were all unreactive. Examples tested include methyldecanoate, methyl adamantane carboxylate, 1-adamantane carboxylic acid, octanoic acid, *N,N*-dihexyl-benzamide, *N*-hexylbenzamide, *N,N*-dihexyl-aceylamide, γ -valerolactone, butyryl lactone, δ -decanolactone, and cyclohexyl acetate. Iron-based synthetic catalysts have precedent for the intramolecular oxidation of carboxylic acids and esters to form lactones;³ however this oxidation is not observed using our catalysts, possibly due to the coordination of carboxylic acid to the metal center.

Given the exceptional reactivity of the cavitand catalysts for unactivated C-H bonds, it is noteworthy that the catalysts showed no activity towards olefins such as cyclooctene, which are typically thought of as being more reactive. Styrene and *trans*- β -methylstyrene were both oxidized, not to epoxides, but to benzaldehyde in 20 % and 68 % yields, respectively.

4.6 Copper Catalysis

Although copper cavitands **2.30•Cu** and **2.44•Cu₂** are coordinatively saturated by the cavitand, we tested the ability of **2.44•Cu₂** to catalyze the same oxidations as **2.30•Fe₂** and **2.44•Fe_x** and found that while **2.44•Cu₂** showed some reactivity, that reactivity was frequently matched by that of the copper sulfate control. Since cyclooctane and *n*-butyl ether were found to be reactive at room temperature using the iron catalysts, we carried those reactions out at room temperature using **2.44•Cu₂**, and in these cases, the cavitand catalyst dramatically outperformed the control, yielding the oxidized products in 90 % total yield while the yield from CuSO₄ was 6 % or less. At elevated temperatures, however, CuSO₄ actually out-performed **2.44•Cu₂** with yields as high as 61 % in the case of adamantane.

Substrate	Product	Total Yield	Substrate	Product	Total Yield
	 	a. 89% ^a b. 6% ^a		 	a. 46% b. 56%
Bu ₂ O	 	a. 90% ^a b. 5% ^a		 	a. 27% b. no rxn.
	 	a. 20% b. 61%			a. 30% b. 35%

Reactions were performed in H₂O:EtCN (1:1) using 10 mol% catalyst and 5 mol. eq. ^tBuOOH at 60°C.
^aReaction performed at 25°C.

Table 4.4: The oxidations of hydrocarbon substrates as catalyzed by (a) **2.44**•Cu_x, and (b) CuSO₄

4.7 Surface Chemistry

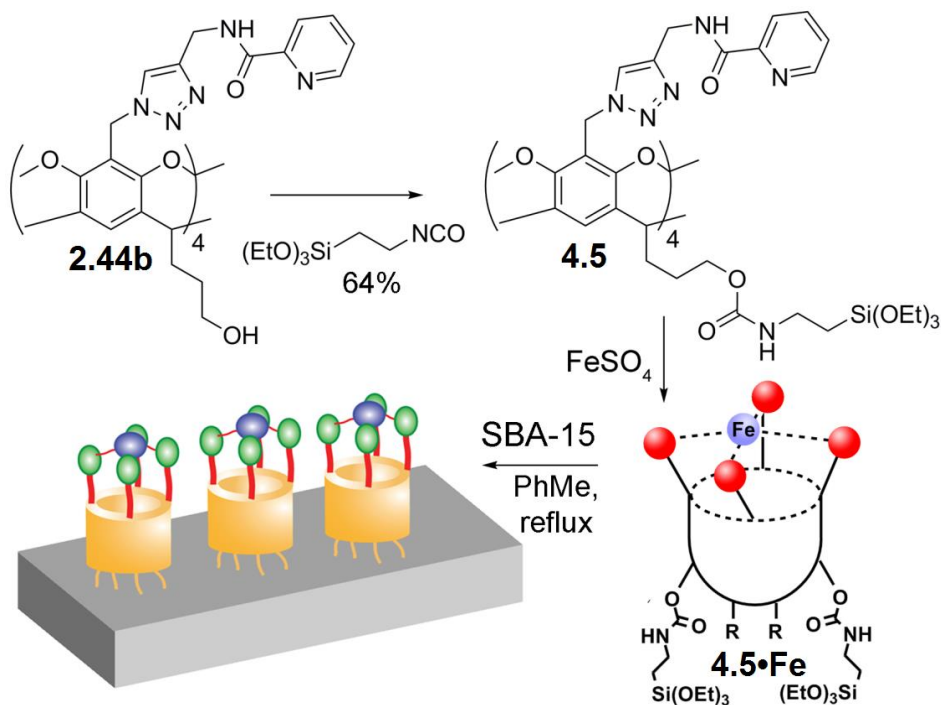


Figure 4.4: The synthesis of **4.5•Fe** and the formation of the heterogeneous catalyst

For solution-phase reactions, catalysts **2.30•Fe₂** and **2.44•Fe_x** were recovered by precipitating them out of solution with diethyl ether and recovering them by vacuum filtration. The recovered catalysts were then reused multiple times without any decrease in reactivity. The limiting factor in reusing catalysts **2.30•Fe₂** and **2.44•Fe_x** was in their recovery. Addition of diethyl ether after an oxidation reaction allowed the collection of catalyst in ~ 30 % recovery. We believed that we could increase the recoverability of the catalyst by anchoring it to a solid support, thereby creating a heterogeneous catalyst that could be recovered after a reaction by simple filtration. Treating **2.44b** with 3-(triethoxysilyl)propyl isocyanate, allowed access to the silyl derivative **4.5**. Following treatment with FeSO_4 to form **4.5•Fe**, the cavitand was anchored to mesoporous silica

nanoparticles (SBA-15) according to Figure 4.4. Refluxing **4.5•Fe** with SBA-15 cleaves the ethoxy groups on the cavitand and creates a Si-O-Si bond with the pores of the nanoparticle surface, thereby anchoring the cavitand to the solid support.

Catalyst **4.5•Fe** was equally as effective as its solution-phase counterpart, allowing the complete conversion of fluorene to fluorenone. Furthermore, rather than the 30 % catalyst recovery that we achieved using **2.44•Fe_x**, **4.5•Fe** could be recovered after a reaction in quantitative yield.

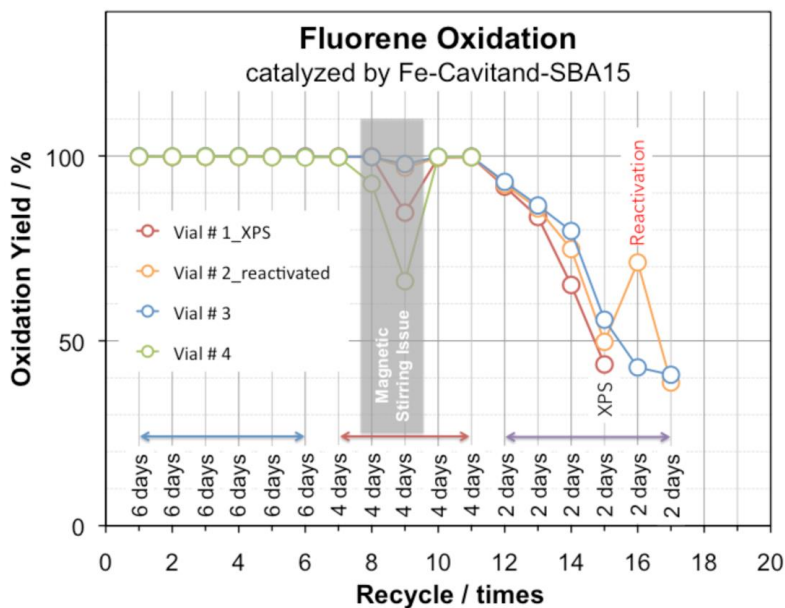


Figure 4.5: The oxidation of fluorene by **4.5•Fe** over 72 days and 17 reaction cycles

4.5•Fe was stable to the oxidation conditions for upwards of 60 days and could be reused more than 10 times without any decrease in efficiency or loss of iron. After 10-12 reaction cycles, some loss of iron and reactivity was observed. FeSO_4 could also be mounted to SBA-15. This iron control had some reactivity, but only for a single reaction cycle. The regeneration of the heterogenous catalyst was attempted by treating the SBA-15 bound cavitand with FeSO_4 , however the regenerated catalyst had only limited

reactivity for a single reaction cycle (Figure 4.5). This minimal activity of the regenerated catalyst suggested that the added iron was coordinated to the silica surface rather than the cavitand. It is significant that despite the many C-H bonds on **4.5•Fe**, no damage to the scaffold was observed, even after 17 uses.

4.8 References

- 1) Djernes, K. E.; Padilla, M.; Mettry, M.; Young, M. C.; Hooley, R. J. "Hydrocarbon oxidation catalyzed by self-folded metal-coordinated cavitands." *Chem. Commun.* **2012**, *48*, 11576–11578.
- 2) Chen, M. S.; White, M. C. "Combined Effects on Selectivity in Fe-Catalyzed Methylene Oxidation." *Science* **2010**, *327*, 566–571.
- 3) Bigi, M. A.; Reed, S. A.; White, M. C. "Directed Metal (Oxo) Aliphatic C–H Hydroxylations: Overriding Substrate Bias." *J. Am. Chem. Soc.* **2012**, *134*, 9721–9726.

Chapter Five: Deep Cavitands

5.1 Introduction

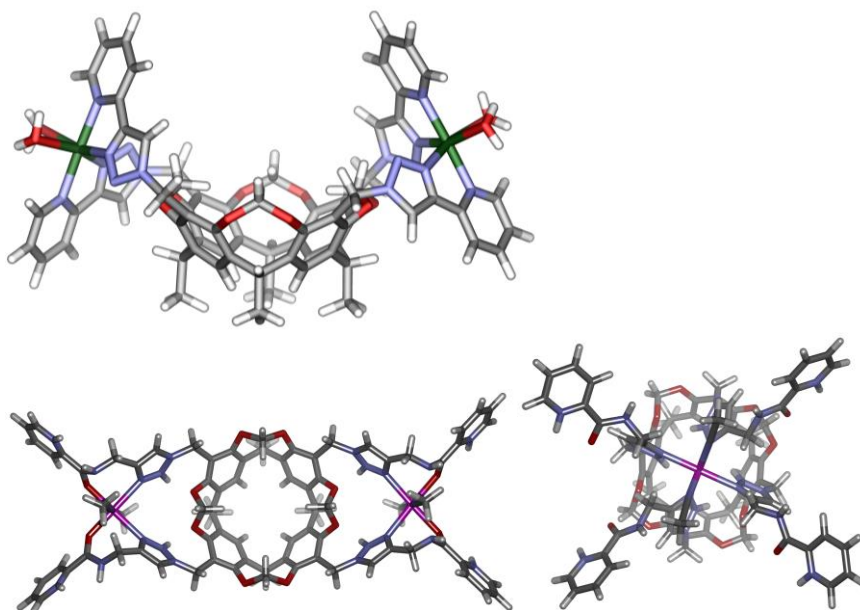


Figure 5.1: Cavitands $2.30\bullet\text{Fe}_2$, $2.44\bullet\text{Fe}$, and $2.44\bullet\text{Fe}_2$

Cavitands $2.30\bullet\text{Fe}_2$ and $2.44\bullet\text{Fe}_x$ successfully oxidized unactivated hydrocarbons with chemoselectivity towards the most electronically activated, least sterically hindered product; however regioselectivity was not observed. Models of $2.30\bullet\text{Fe}_2$ and $2.44\bullet\text{Fe}_x$ (Figure 5.1) show that three challenges with the self-assembly of the metallocavitands need to be overcome in order for the catalysts to exhibit regioselectivity. The first obstacle is the binding of iron at the triazole position where the metal blocks a guest from the hydrophobic binding site. Secondly the free valences of $2.30\bullet\text{Fe}_2$ and $2.44\bullet\text{Fe}_x$ are pointed away from the cavitand binding sites. Because oxidation occurs at the free valences, the hydrophobic binding site does not significantly impact the selectivity of the oxidations; and therefore chemoselectivity, but not regioselectivity, is observed. Finally,

cavitands $2.30 \cdot \text{Fe}_2$ and $2.44 \cdot \text{Fe}_x$ do not have an especially strong affinity for guests (Chapter 3). This chapter describes the work that is being done to synthesize new, deepened molecular receptors with unhindered binding sites where the free valences on iron are directed towards the cavitand binding site.

5.2 Development of a New Cavitand Scaffold

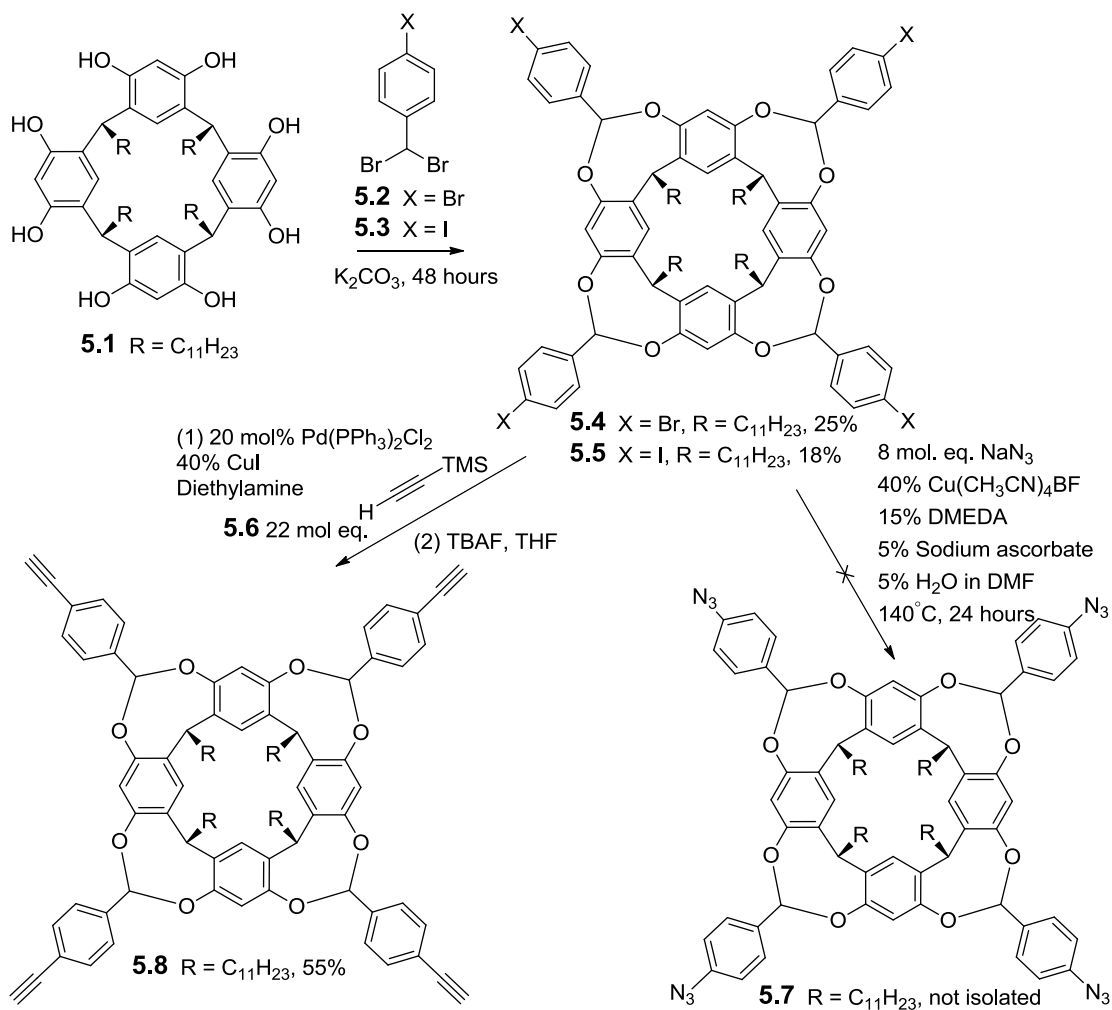


Figure 5.2: The synthesis of four-point cavitands

Because of the high affinity of the triazoles for metal coordination, we decided to design a new scaffold where the triazoles were remote from the binding site and were therefore less likely to limit the access of a guest. An additional challenge in the synthesis of deep cavitands is maintaining the concave shape of the cavitand. Even when employing weak forces to shape the receptor, the ligands must favor a concave shape rather than a more planar orientation. Molecular modeling suggested that bridging the rim phenol groups with a *para*-substituted benzal halide (**5.2** or **5.3**) would deepen the receptor while maintaining its shape (Figure 5.2). The *para*-substituted halides provide sites of attachment for iron-coordinating ligands that orient the free valences on iron towards the binding site.

The primary challenge with this approach was the low yields of the bridging reactions.¹ Bromocavitand **5.4** could be isolated in only 25 % yield, and the yield for iodocavitand **5.5** was even lower (18 %). Despite the low yields for **5.4** and **5.5**, the mass recovery was essentially 100 %. The main products of both reactions were cavitands with all of the expected ¹H NMR peaks, but where the peaks were very broad and poorly defined. The unintended major products were never definitively identified, but we suspected that they were either polymerized products or the result of adding more than four equivalents of benzal halide to the cavitand rim.

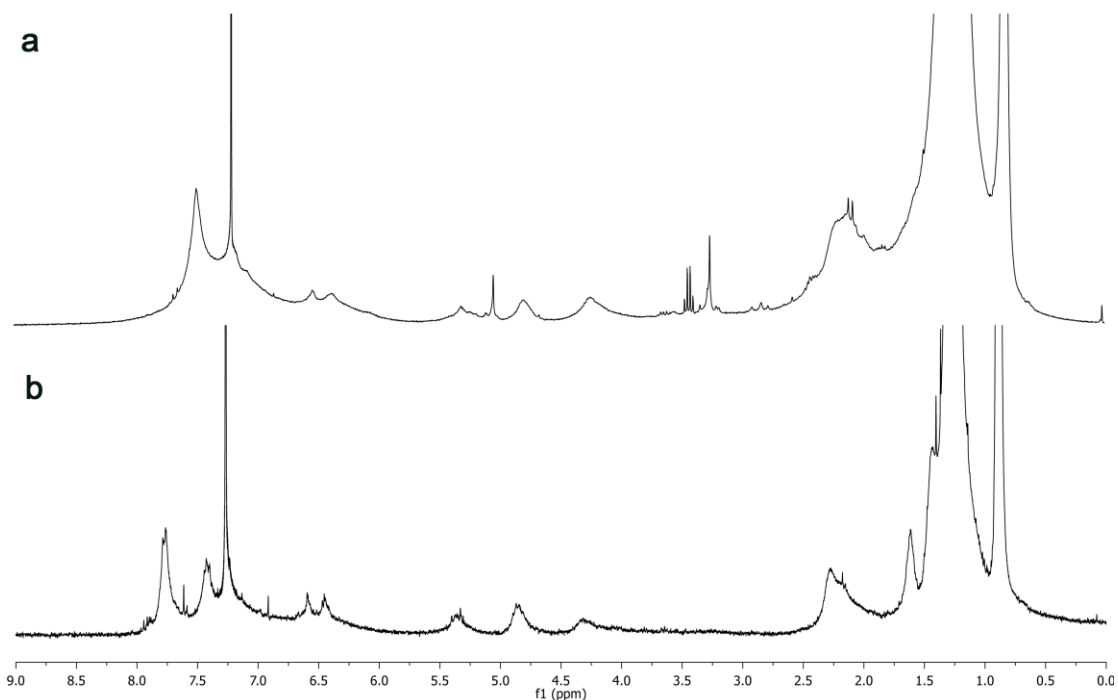


Figure 5.3: ^1H NMR spectra of the major bridging products for (a) **5.4** and (b) **5.5**

Multiple variables were tested to improve the yields, but with little success. Increasing the reaction time from 24 hours to 48 hours increased the yields by $\sim 50\%$, but further increasing the reaction time to 3 days or 1 week did not lead to any increase in product formation. Potassium carbonate, cesium carbonate, and 1,8-Diazabicycloundec-7-ene (DBU) were all tested as bases, but changing the base did not affect the reaction.² Finally, the amount of benzal halide that was used in the bridging reactions was tested. Increasing the number of molar equivalents from 4.4 to 6 did not affect the reaction, however increasing the amount of benzal halide to 10 equivalents lead to 100 % formation of the unintended major product and none of the desired product. This observation suggested that the unintended major product was in fact the result of adding more than 4 equivalents of benzal halide to the resorcinarene. Adding the benzal halide

slowly over several days did not bias the formation of the desired product, and the yields could not be raised above those shown in Figure 5.2.

5.3 Click Chemistry on the Deepened Scaffold

Our original plan was to substitute the aryl halide for an azide, forming **5.7** that could be further functionalized via click chemistry. When the formation of **5.7** was attempted from bromocavitand **5.4**, no reaction occurred. Iodocavitand **5.5** was more reactive, however the reaction did not go to completion under mild conditions. Under forcing conditions (140 °C, Figure 5.2), all of the starting material was consumed, but multiple cavitand products were formed. ¹H NMR of the products suggested that the forcing conditions that drove the reaction to completion also partially reduced the azides to amines (Figure 5.4) While this copper-catalyzed azide reduction was unexpected, it is known to occur at elevated temperatures.³ Alternatively, acetylene cavitand **5.8** was synthesized via a Sonagashira reaction. Cavitand **5.4** was unreactive, but **5.5** was easily converted to **5.8** in 55 % yield.

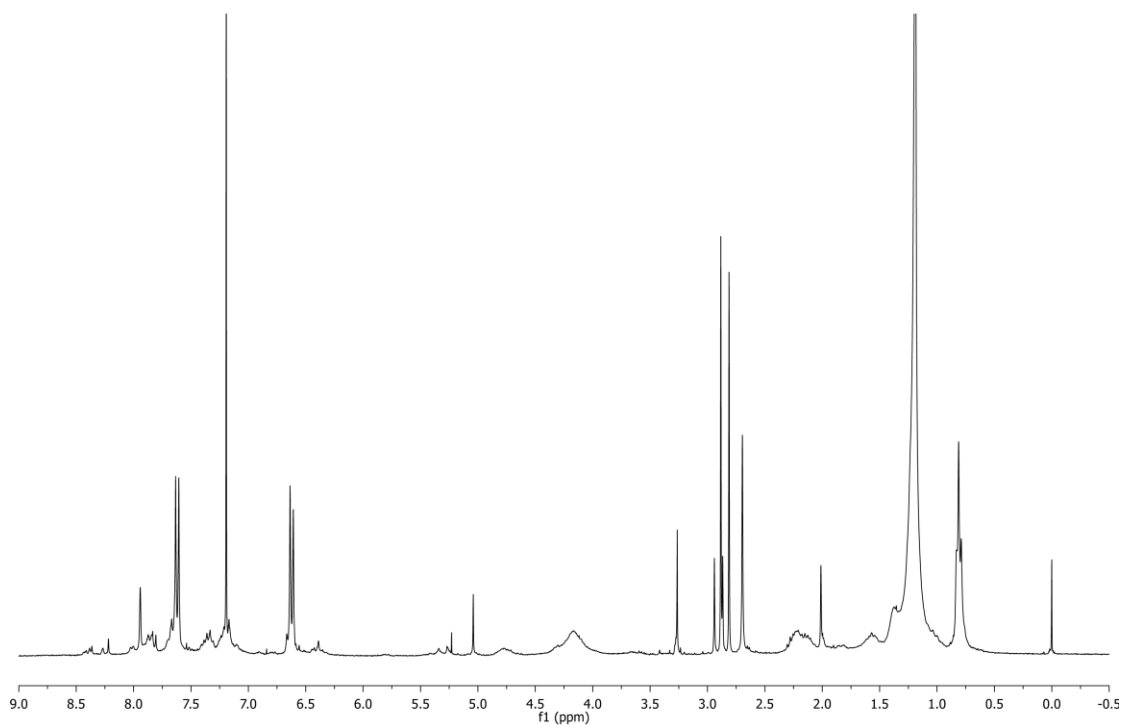


Figure 5.4: ^1H NMR spectra of **5.7**

5.4 Future Work

Cavitand **5.8** is a valuable scaffold that can be further derivatized by click chemistry. Our models suggest that cavitands such as that shown in Figure 5.5 can coordinate iron where four of the six sites are coordinated to the cavitand and the remaining two valences are oriented towards the cavitand interior. The deepened cavitand is designed to increase the binding affinity of neutral guests, and the improved orientation of the metals is expected to allow the regioselective oxidation of bound hydrocarbons.

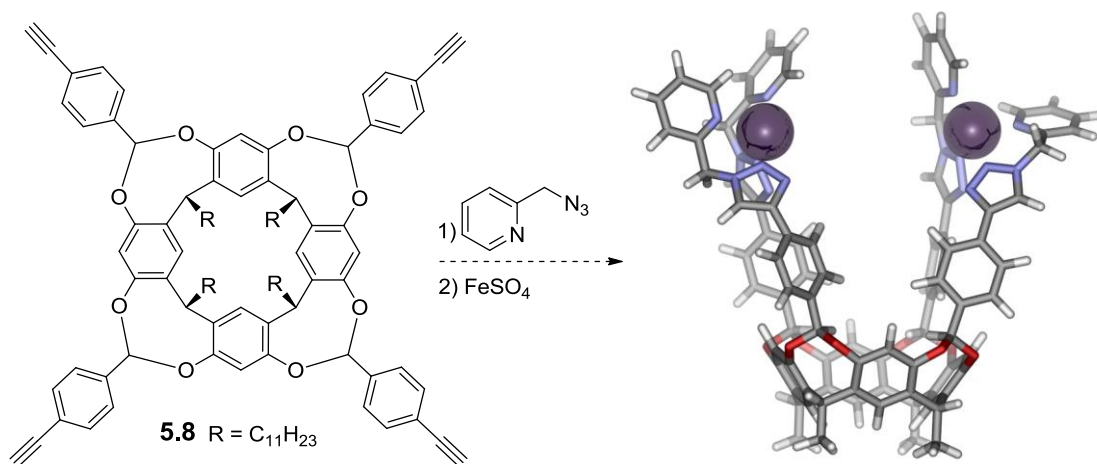


Figure 5.5: A model of a deep cavitant built from scaffold **5.8**

5.5 Conclusions

The work described in this thesis illustrates the importance of wide scope, selective C-H oxidations to the field of synthetic organic chemistry. A variety of cavitands were synthesized utilizing click chemistry and palladium catalyzed cross coupling reactions. These cavitands self-assemble in the presence of a metal to form metallocavitands where the metals simultaneously behave as structural elements, solubilizing groups, and catalytic groups. The resulting catalysts chemoselectively oxidize unactivated C-H bonds under mild conditions in aqueous solution. The catalysts are stable to the reaction conditions and can be used multiple times without any decrease in reactivity. Furthermore, the feet of the solution-phase catalysts can be altered in order to mount the cavitands on a solid support, thereby forming highly effective heterogeneous C-H oxidation catalysts in only two simple steps. The stability of these C-H oxidation

catalysts as well as their ability to catalyze reactions both in solution and the solid state is a significant advancement in this field.

5.6 References

- 1) Xi, H.; Gibb, C. L. D.; Gibb, B. C. "Functionalized Deep-Cavity Cavitands." *J. Org. Chem.* **1999**, *64*, 9286–9288.
- 2) Moran, J. R.; Karbach, S.; Cram, D. J. "Cavitands: Synthetic Molecular Vessels." *J. Am. Chem. Soc.* **1982**, *104*, 5826–5828.
- 3) Peng, H.; Dornevil, K. H.; Draganov, A. B.; Chen, W.; Dai, C.; Nelson, W. H.; Liu, A.; Wang, B. "An Unexpected Copper Catalyzed “Reduction” of an Arylazide to Amine through the Formation of a Nitrene Intermediate." *Tetrahedron* **2013**, *69*, 5079–5085.

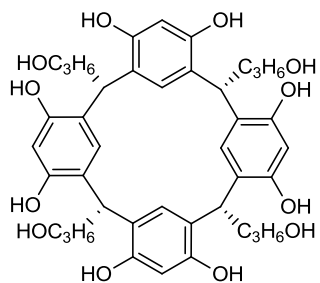
Chapter Six: Experimental

6.1 General Information

^1H and ^{13}C NMR spectra were recorded on a Varian Inova 300 or Inova 400 spectrometer. Proton (^1H) chemical shifts are reported in parts per million (δ) with respect to tetramethylsilane ($\text{Si}(\text{CH}_3)_4$, $\delta=0$), and referenced internally with respect to the protio solvent impurity. Carbon (^{13}C) chemical shifts are reported in parts per million (δ) with respect to tetramethylsilane ($\text{Si}(\text{CH}_3)_4$, $\delta=0$), and referenced internally with respect to the solvent ^{13}C signal (either CDCl_3 or $\text{DMSO}-d_6$). Deuterated NMR solvents were obtained from Cambridge Isotope Laboratories, Inc., Andover, MA, and used without further purification. All other materials were obtained from Aldrich Chemical Company, St. Louis, MO and were used as received. Solvents were dried through a commercial solvent purification system (SG Water, Inc.). Electrospray mass spectra were recorded on an Agilent 6210 LC TOF mass spectrometer using electrospray ionization and processed with an Agilent MassHunter Operating System. MALDI mass spectra were obtained using a PE Biosystems DE-STR MALDI TOF spectrometer operating in refractive mode at 2100 eV. Cyclic voltammetric experiments were performed on a CHI 650A Electrochemical Workstation (CH Instruments Inc.). All experiments were carried out using a conventional three-electrode system with the gold disc electrode as working, a platinum foil as auxiliary, and a saturated calomel electrode as reference. Molecular modeling (semi-empirical calculations) was performed using the AM1 force field using

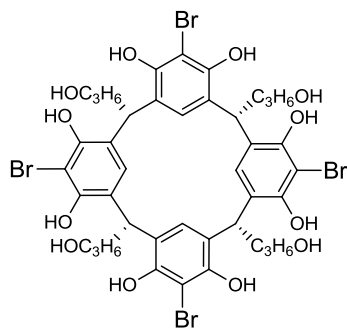
SPARTAN. All oxidation products were assigned by comparison (spectrometric or spectroscopic) to authentic samples.

6.2 Chapter Two Experimental



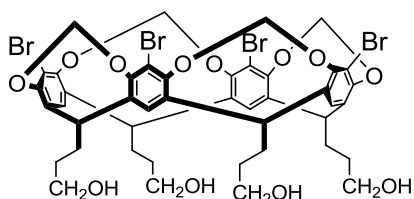
1.21a

Preparation of resorcinarene 1.21a: To a 120 mL round bottom flask equipped with a stir bar was added resorcinol (10.0 g, 81.0 mmol), methanol (60 mL), and concentrated HCl (15 mL). The solution was stirred on ice while 2,3-dihydrofuran (6.0 mL, 81.0 mmol) was added dropwise. After the addition of 2,3-dihydrofuran, the flask was equipped with a reflux condenser and heated to 60 °C for two d. The crude product precipitated from solution as a yellow solid and was collected by vacuum filtration. The crude product was recrystallized from methanol to give pure product as a white powder (6.14 g, 37 %). ¹H NMR (DMSO-*d*₆) δ 8.88 (s, 8H), 7.22 (s, 4H), 6.13 (s, 4H), 4.29 (t, *J* = 5.1 Hz, 4H), 4.18 (t, *J* = 7.8 Hz, 4H), 3.40 (q, *J* = 5.3 Hz, 8H), 2.08 (q, *J* = 5.3 Hz, 8H), 1.33 (qn, *J* = 7.2 Hz, 8H). Observed spectra consistent with literature values.¹



2.1

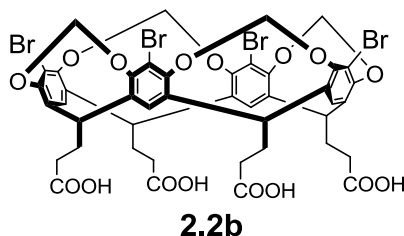
Preparation of bromoresorcinarene 2.1: To a 100 mL round bottom flask equipped with a stir bar was added **1.21a** (1.00 g, 1.43 mmol), *N*-bromosuccinimide (1.15 g, 6.45 mmol), and a solution of 30 % methanol in 2-butanone (20 mL). The top of the flask was capped, the flask was wrapped in foil, and the reaction was stirred at ambient temperature for 24 h. After 24 h, hexanes was added to precipitate the product as a white solid. The solid was collected by vacuum filtration and rinsed with ice cold acetone, leaving pure product (1.23 g, 82 %). ^1H NMR (DMSO- d_6) δ 9.11 (s, 8H), 7.40 (s, 4H), 4.34 (t, $J = 7.8$ Hz, 4H), 3.43 (t, $J = 6.5$ Hz, 8H), 2.21 (q, 8H $J = 6.5$ Hz), 1.34 (qn, $J = 6.5$ Hz, 8H). Observed spectra consistent with literature values.¹



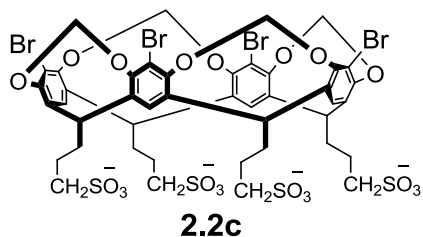
2.2a

Preparation of tetrabromocavitand 2.2a: To a 100 mL round bottom flask equipped with a stir bar was added **2.1** (1.63 g, 1.57 mmol), Cs_2CO_3 (6.69 g, 20.4 mmol), and dimethylacetamide (20 mL). The solution was stirred while bromochloromethane (1.36 mL, 20.4 mmol) was added. Following addition of bromochloromethane, a reflux

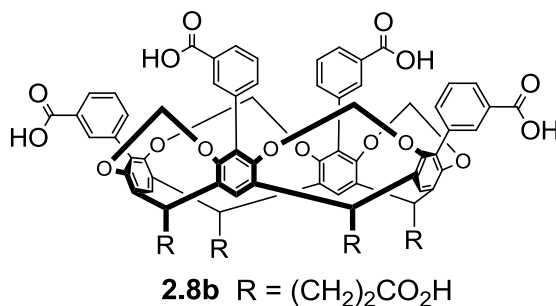
condenser was attached, and the reaction was heated to 65 °C for 3 d. The solution was cooled to ambient temperature, poured into 200 mL distilled water, and neutralized, allowing the crude product to precipitate as a sticky brown solid. The crude product was purified using column chromatography (10 % methanol in methylene chloride), allowing the collection of pure product as an off white solid (1.71 g, 67 %). ^1H NMR (DMSO- d_6) δ 7.65 (s, 4H), 5.99 (d, J = 7.6 Hz, 4H), 4.69 (t, J = 8.3 Hz, 4H), 4.50 (t, J = 4.8 Hz, 4H), 4.30 (d, J = 7.6 Hz, 4H), 3.50 (q, J = 7.0 Hz, 8H), 2.46 (q, J = 7.0 Hz, 8H), 1.44 (qn, J = 7.0 Hz, 8H). Observed spectra consistent with literature values.¹



Preparation of tetrabromocavitand 2.2b: To a 50 mL flask was added **2.2a** (1.00 g, 0.920 mmol), KMnO_4 (2.35 g, 15.0 mmol), and DMA: $^t\text{BuOH}$ (1:1, 20 mL). The mixture was stirred for 16 h at ambient temperature, allowing the formation of a brown precipitate. The precipitate was collected by vacuum filtration and rinsed with acetone to remove unreacted KMnO_4 . The precipitate was then sonicated in water (20 mL) to dissolve the product. The water was removed by lyophilization, leaving product as a white powder (0.700 g, 67 %). ^1H NMR (300 MHz, D_2O) δ 7.36 (br, 4H), 5.89 (br, 4H) 3.94 (br, 4H), 3.61 (br, 8H), 2.51 (br, 8H), 2.16 (br, 8H). ^{13}C NMR (100 MHz, D_2O) δ 173.56, 151.52, 138.73, 120.64, 112.43, 99.71, 38.35, 35.39, 26.27, 22.98, 20.37.

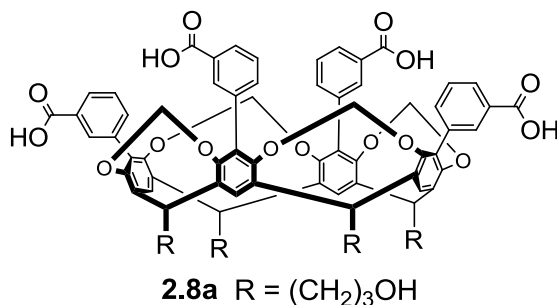


Preparation of tetrabromocavitand 2.2c: To a 10 mL flask was added **2.2a** (0.135 g, 0.130 mmol), DMF (2.5 mL), triethylamine (0.175 μ L), and mesyl chloride (70.0 μ L, 0.900 mmol). The reaction mixture was stirred at ambient temperature for 16 h, after which time the product was precipitated by adding 10 mL diethyl ether. The precipitate was collected by vacuum filtration (48 % yield), but the product was very sensitive to water, and pure product was never obtained. See Figure 6.3 for ^1H NMR.

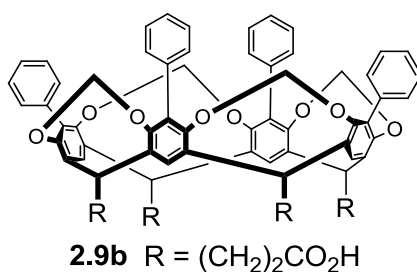


Attempted preparation of 2.8b: To a 10 mL round bottom flask was added **2.2b** (0.050 g, 0.044 mmol), 3-carboxyphenylboronic acid (0.030 g, 0.181 mmol), $\text{Pd}(\text{PPh}_3)_2\text{Cl}_2$ (0.010 g, 0.014 mmol), Cs_2CO_3 (0.171g, 0.530 mmol), and H_2O (2 mL). The solution was heated to 95 $^\circ\text{C}$ for 16 h, after which time the precipitate was removed by vacuum filtration. The filtrate was concentrated under a stream of air, allowing the collection of crude product. The crude product was purified by reverse-phase chromatography using a siliaprep SPE column and methanol:water (9:1) as elution solvent. The solvent was

removed *in vacuo*, allowing the collection of partially formed product in 10 % yield. ^1H NMR and ESI MS are shown in Figure 2.5.

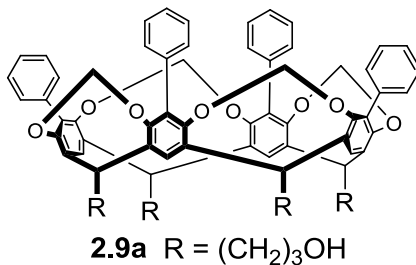


Attempted preparation of 2.8a: To a 10 mL round bottom flask was added **2.2a** (0.048 g, 0.043 mmol), 3-carboxyphenylboronic acid (0.044 g, 0.265 mmol), K₂CO₃ (0.080 g, 0.605 mmol), Pd(PPh₃)₂Cl₂ (0.011 g, 0.016 mmol), and toluene:methanol (4:1, 2.5 mL). The reaction mixture was heated to 100 °C for 16 h, and then the solvent was removed under a stream of air. Methanol (2 mL) was added to dissolve the product, and the insoluble material was filtered off. The filtrate was concentrated *in vacuo* and rinsed with acetone to remove unreacted starting material. Partially formed product was obtained in 92 % yield. ^1H NMR is shown in Figure 6.4.

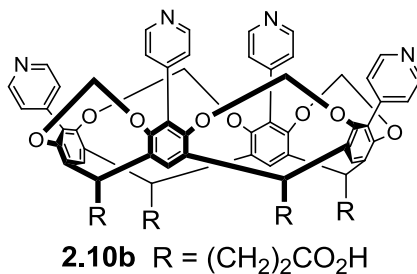


Attempted preparation of 2.9b: To a 10 mL round bottom flask was added **2.2b** (0.050 g, 0.044 mmol), phenylboronic acid (0.034 g, 0.263 mmol), Pd(PPh₃)₂Cl₂ (0.012 g, 0.013 mmol), K₂CO₃ (0.072 g, 0.526 mmol), and water:toluene (4:1, 2.5 mL). The reaction

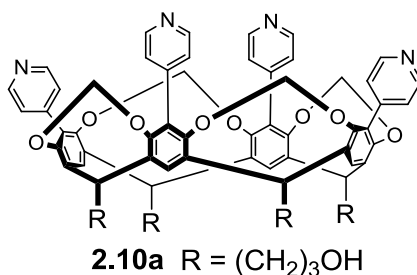
mixture was stirred at 100 °C for 16 h, and then the reaction was cooled to ambient temperature. The precipitate was filtered off and the filtrate was concentrated *in vacuo*. Methanol was added to dissolve the product, and the K₂CO₃ was removed by vacuum filtration. The methanol solution was concentrated *in vacuo*, allowing the collection of partially formed product in (80 % yield). ¹H NMR is shown in Figure 6.5.



Attempted preparation of 2.9a: To a 10 mL round bottom flask equipped with a stir bar was added **2.2a** (0.053 g, 0.046 mmol), phenylboronic acid (0.033 g, 0.277 mmol), Cs₂CO₃ (0.177 g, 0.550 mmol), and Ph(PPh₃)₂Cl₂ (0.010 g, 0.014 mmol). Toluene:water (4:1, 2 mL) was added, and the solution was heated to 100 °C under N₂ for 16 h. Ethyl acetate (5 mL) was added, and the reaction mixture was extracted 3 times with 5mL portions of water. The ethyl acetate solution was concentrated *in vacuo*, and the crude product was purified by column chromatography using 10 % acetone in methylene chloride. Partially formed cavitand was obtained in 77 % yield. ¹H NMR is shown in Figure 6.6.

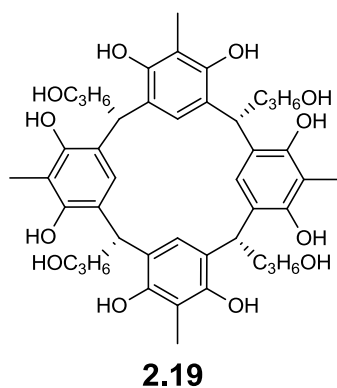


Attempted preparation of 2.10b: To a 10 mL round bottom flask equipped with a stir bar was added **2.2b** (0.098 g, 0.086 mmol), 4-pyridineboronic acid (0.068 g, 0.533 mmol), Pd(OAc)₂ (0.005 g, 0.022 mmol), tricyclohexylphosphine (0.016 g, 0.057 mmol), and K₃PO₄ (0.060 g). Water:dioxane (1:1, 4 mL) was added, and the reaction mixture was heated to 155 °C in a sealed tube for 2 d. After 2 d, the reaction was cooled to ambient temperature, and the solvent was removed under a stream of air. The remaining solid was triturated in methanol, and the insoluble material was filtered off and discarded. The methanol solution was concentrated in vacuo, and the crude product was purified by reverse-phase chromatography using a siliaprep SPE column and methanol:water (7:3) as elution solvent. The product containing fractions were concentrated under a stream of air, allowing the collection of almost, but not completely, pure product (0.018 g, 18 %). ¹H NMR and MALDI MS are shown in Figure 2.6.



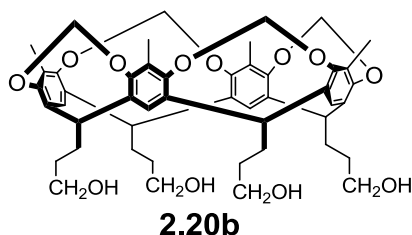
Attempted preparation of 2.10a: To a 10 mL round bottom flask equipped with a stir bar was added **2.2a** (0.050 g, 0.046 mmol), pyridine-4-boronic acid (0.036 g, 0.301

mmol), $\text{Ph}(\text{PPh}_3)_2\text{Cl}_2$ (0.010 g, 0.014 mmol), and K_2CO_3 (0.077 g, 0.557 mmol). Water:toluene:methanol (2:2:1, 2.5 mL) was added, and the reaction was heated to 100 °C for 16 h. After 16 h, the reaction was cooled to ambient temperature, and the solvent was removed under a stream of air. The crude product was rinsed with water and purified by reverse-phase chromatography using a siliaprep SPE column and methanol:water (9:1) as elution solvent. The product containing fractions were concentrated under a stream of air, allowing the collection partially formed product (0.040 g, 80 %). ^1H NMR is shown in Figure 6.7.

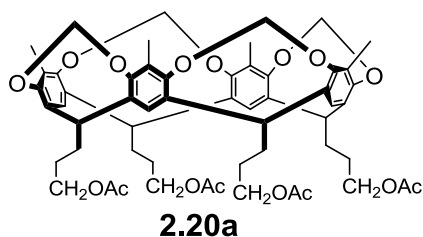


Preparation of resorcinarene 2.19: To a 250 mL flask was added 2-methylresorcinol (20.0 g, 0.161 mol), methanol (120 mL), and concentrated HCl (30 mL). 2,3-dihydrofuran (12.2 mL, 0.161 mol) was added slowly, and the reaction mixture was heated to 70 °C for 3 d. The product precipitated from solution as a yellow powder and was collected by vacuum filtration. The crude product was sonicated in acetone to dissolve impurities, allowing the pure product to be isolated by vacuum filtration as a white powder (27.85 g, 89 %). ^1H NMR ($\text{DMSO-}d_6$) δ 8.62 (s, 8H), 7.27 (s, 4H), 4.19 (t,

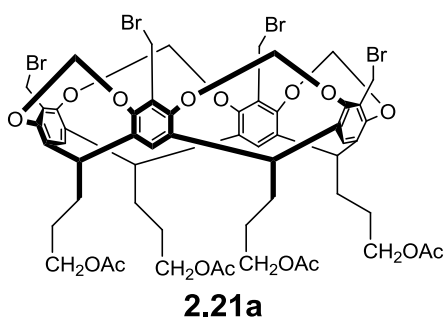
$J = 7.8$ Hz, 4H), 4.10 (br s, 4H), 3.44 (t, $J = 6.7$ Hz, 8H), 2.24 (q, $J = 6.7$ Hz, 8H), 1.94 (s, 12H), 1.35 (qn, $J = 6.7$ Hz, 8H). Observed spectra consistent with literature values.²



Preparation of cavitand 2.20b: To a 500 mL flask was added **2.19** (5.00 g, 6.44 mmol), K₂CO₃ (10.7 g, 77.2 mmol), and DMA (120 mL). Bromochloromethane (6.5 mL, 96.6 mmol) was added, and the solution was stirred at 65 °C for 3 d. The reaction was cooled to ambient temperature, poured into 500 mL water, and neutralized with 10 % aq. HCl. The product precipitated as a brown/orange oil and was purified by column chromatography using 10 % methanol in methylene chloride. When concentrating the product-containing fractions, pale-colored oil was sometimes obtained. Adding acetone to the oil allowed the collection of solid product. Product was collected as a white solid (2.03 g, 38 %). ¹H NMR (DMSO-*d*₆) δ 7.43 (s, 4H), 5.86 (d, $J = 7.4$ Hz, 4H), 4.59 (t, $J = 6.1$ Hz, 4H), 4.43 (t, $J = 5.1$ Hz, 4H), 4.19 (d, $J = 7.4$ Hz, 4H), 3.48 (q, $J = 5.9$ Hz, 8H), 2.35 (q, $J = 5.9$ Hz, 8H), 1.88 (s, 12H), 1.42 (qn, $J = 5.9$ Hz, 8H). Observed spectra consistent with literature values.²

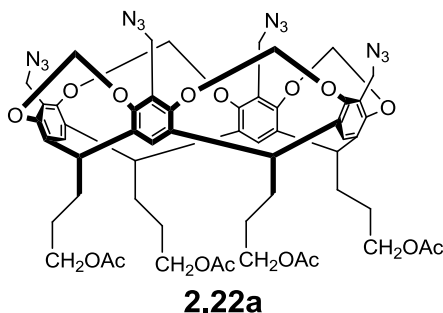


Preparation of cavitand 2.20a: To a 250 mL flask was added **2.20b** (4.05 g, 4.91 mmol), pyridine (60 mL), and acetic anhydride (60 mL). The mixture was stirred for 16 h at ambient temperature. After this time, the reaction mixture was poured into 200 mL of water in a beaker, and the mixture was allowed to cool to ambient temperature. The product stuck to the sides of the beaker, allowing the water to be decanted off. The sticky solid was sonicated in methanol, allowing the collection of pure product as a white powder (3.75 g, 77 %). $^1\text{H NMR}$ (CDCl_3) δ 6.93 (s, 4H), 5.86 (d, $J = 6.9$ Hz, 4H), 4.82 (t, $J = 9.1$ Hz, 4H), 4.23 (d, $J = 6.9$ Hz, 4H), 4.15 (t, $J = 6.5$ Hz, 8H), 2.26 (q, $J = 7.0$ Hz, 8H), 2.03 (s, 12H), 1.95 (s, 12H), 1.69 (qn, $J = 7.0$ Hz, 8H). Observed spectra consistent with literature values.²

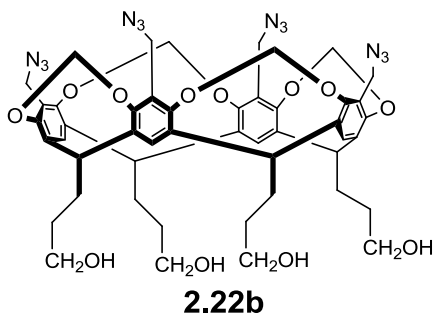


Preparation of tetrabromocavitand 2.21a: To a 250 mL round bottom flask was added **2.20a** (1.00 g, 1.01 mmol), *N*-bromosuccinimide (0.791 g, 4.44 mmol), benzoyl peroxide (0.049 g, 0.201 mmol), and CCl_4 (100 mL). The reaction mixture was refluxed vigorously

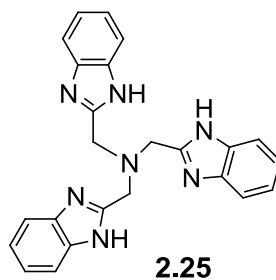
for 3 d. After this time, the precipitate was filtered off and discarded, and the filtrate was concentrated under vacuum, allowing the collection of pure product as a white powder (0.942 g, 71 %). ^1H NMR (CDCl_3) δ 7.09 (s, 4H), 6.01 (d, $J = 6.7$ Hz, 4H), 4.82 (t, $J = 8.1$ Hz, 4H), 4.55 (d, $J = 6.7$, 4H), 4.39 (s, 8H), 4.15 (t, $J = 6.5$ Hz, 8H), 2.28 (q, $J = 6.7$ Hz, 8H), 2.05 (s, 12H), 1.67 (qn, $J = 6.7$ Hz, 8H). Observed spectra consistent with literature values.²



Preparation of tetraazidecavitand 2.22a: To a 50 mL round bottom flask was added **2.21a** (1.50 g, 1.12 mmol), tetrahydrofuran (10mL), and sodium azide (0.5 M in DMSO, 10 mL). The reaction mixture was stirred at ambient temperature for 16 h. After that time, the product was obtained as a sticky white solid by pouring the reaction mixture into 50 mL of water. The sticky product was sonicated in 50 mL of pure water, causing the solid to become a pure, white powder (1.13 g, 87 %). ^1H NMR (300 MHz, CDCl_3) δ 7.13 (s, 4H), 5.95 (d, $J = 7.2$ Hz, 4H), 4.85 (t, $J = 7.0$ Hz, 4H), 4.39 (d, $J = 7.2$ Hz, 4 H), 4.33 (s, 8H), 4.18 (t, $J = 7.0$ Hz, 8H), 2.31 (q, $J = 7.0$ Hz, 8H), 2.07 (s, 12H), 1.70 (qn, $J = 7.0$ Hz, 8H). ^{13}C NMR (100 MHz, CDCl_3) δ 171.14, 153.95, 137.79, 122.85, 120.35, 99.76, 64.07, 45.06, 41.15, 36.52, 27.09, 21.03. MS (ESI) m/z 1179.4189 ($\text{M} + \text{Na}$)⁺, expected m/z 1179.4148 ($\text{M} + \text{Na}$)⁺.



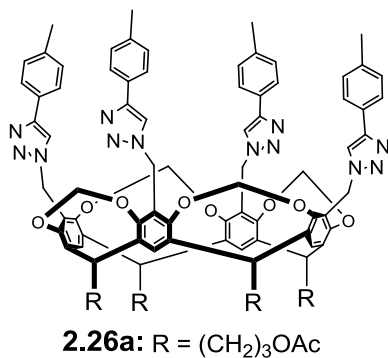
Preparation of tetraazidecavitand 2.22b: In a 50 mL round bottom flask, **2.22a** (0.262 g, 0.23 mmol) and cesium carbonate (0.443 g, 1.36 mmol) were dissolved in methanol:dichloromethane (1:1), and the reaction mixture was stirred at ambient temperature for 16 h. After that time, the solvent was removed *in vacuo*, leaving a sticky solid. The sticky product was sonicated in 10 mL of water, causing the solid to become a pure, white powder (0.163 g, 73 %). ¹H NMR (300 MHz, DMSO) δ 7.69 (s, 4H), 5.97 (d, $J = 7.5$ Hz, 4H), 4.63 (t, $J = 6.8$ Hz, 4H), 4.50 (b, 4H), 4.29 (s, 8H), 4.27 (d, $J = 7.5$ Hz, 4H), 3.50 (t, 6.8 Hz, 8H), 2.42 (q, $J = 6.8$ Hz, 8H), 1.44 (qn, $J = 6.8$ Hz, 8H). ¹³C NMR (100 MHz, DMSO) δ 153.58, 138.69, 123.39, 122.80, 99.89, 60.99, 44.84, 37.30, 31.49, 26.25. MS (ESI) m/z 1011.3755 ($M + Na$)⁺, expected m/z 1011.3720 ($M + Na$)⁺.



Preparation of benzimidazole co-catalyst 2.25: To a 100 mL round bottom flask equipped with a stir bar was added o-phenylenediamine (5.00 g, 42.3 mmol), nitrilotriacetic acid (2.95 g, 15.4 mmol), and ethylene glycol (33 mL). The solution was

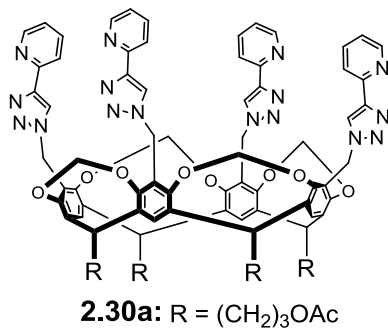
refluxed for 16 h at 200 °C and then cooled to ambient temperature. Upon cooling, the crude product precipitated from solution as a lavender-colored solid. The crude product was collected by vacuum filtration, rinsed with cold ethanol, and recrystallized from ethanol (30 mL). Pure product was collected as pale pink crystals (3.45 g, 60 %). ¹H NMR (300 MHz, DMSO-*d*₆) δ 7.60-7.58 (6H, m), 7.20-7.17 (6H, m) and 4.16 (6H, s). Observed spectra consistent with literature values.³

General procedure for the removal of copper from click products: In a round bottom flask, cavitand (0.20 mmol) and sodium EDTA dihydrate (0.20 mmol) were stirred in 4 mL DMSO:water (2:1) at 100 °C for 1 h. After cooling the solution to ambient temperature, a minimal amount of water was added to precipitate the cavitand product, and the product was collected by vacuum filtration.

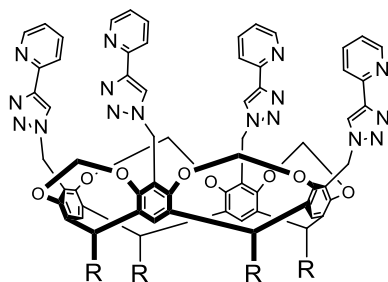


Preparation of tolylcavitand 2.26a: To a 10 mL round bottom flask equipped with a stir bar was added **2.22a** (0.018 g, 0.015 mmol), CuSO₄ (0.001 g, 0.005 mmol), L-sodium ascorbate (0.002 g, 0.010 mmol), **2.24** (0.003 g, 0.005 mmol), and DMSO:H₂O (4:1, 1 mL). *p*-tolylacetylene (0.009 mL, 0.068 mmol) was added, and the reaction was stirred at ambient temperature for 16 h. After that time, the reaction mixture was pipetted into 2 mL of water, and the product was collected by vacuum filtration (0.010 g, 40 %). ¹H

NMR (300 MHz, CDCl₃) δ 7.74-7.69 (m, 12 H), 7.24-7.17 (m, 12H), 5.83 (d, $J = 7.3$ Hz, 4H), 5.29 (s, 8H), 4.83 (t, $J = 8.1$ Hz, 4H), 4.18 (d, $J = 7.3$ Hz, 4H), 2.05 (s, 12H), 1.84 (m, 8H), 1.70 (m, 8H).

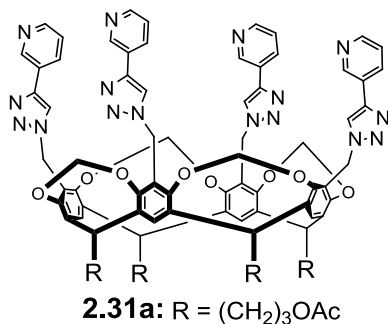


Preparation of 2-pyridyl cavitand 2.30a: In a 25 mL round bottom flask, **2.22a** (0.300 g, 0.260 mmol), copper (II) sulfate pentahydrate (0.012 g, 0.078 mmol), and L-sodium ascorbate (0.030 g, 0.160 mmol) were stirred in DMSO:H₂O (4:1, 3 mL) while 2-ethynylpyridine (0.129 mL, 1.14 mmol) was added. The reaction was stirred for 16 h at 100 ° C and then cooled to ambient temperature. The reaction mixture was pipetted into water (10 mL) in order to precipitate the product, and the product was collected as a pale brown powder (0.316 g, 78 %). ¹H NMR (300 MHz, CDCl₃) δ 8.51 (br d, $J = 3.5$ Hz, 4H), 8.14 (br d, $J = 5.5$ Hz, 4H), 8.10 (s, 4H), 7.70 (td, $J = 5.5, 0.9$ Hz, 4H), 7.22 (s, 4H), 7.17 (br dd, $J = 5.5, 0.9$ Hz, 4H), 5.80 (d, $J = 5.4$ Hz, 4H), 5.29 (s, 8H), 4.82 (t, $J = 5.3$ Hz, 4H), 4.32 (d, $J = 5.4$ Hz, 4H), 4.17 (t, $J = 5.3$ Hz, 8H), 2.30 (q, $J = 5.3$ Hz, 8H), 2.03 (s, 12H), 1.67 (qn, $J = 5.3$ Hz, 8H). ¹³C NMR (100 MHz, CDCl₃) δ 171.31, 154.23, 150.30, 149.49, 148.26, 137.97, 137.04, 123.08, 122.47, 121.05, 120.60, 99.60, 64.24, 44.40, 41.13, 36.74, 27.18, 26.91, 21.17. MS (MALDI) observed m/z 1591.8 (M + Na)⁺, expected m/z 1591.6 (M + Na)⁺.

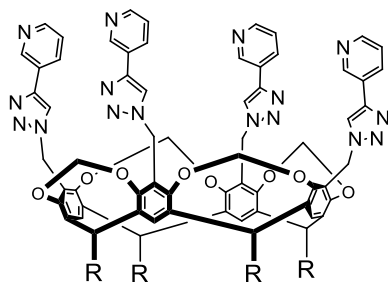


2.30b: R = (CH₂)₃OH

Preparation of 2-pyridyl cavitand 2.30b: In a 25 mL round bottom flask, **2.30a** (0.300 g, 0.190 mmol) and cesium carbonate (0.372 g, 1.14 mmol) were dissolved in methanol:dichloromethane (1:1, 6 mL) and stirred at ambient temperature for 12 h. The solvent was removed *in vacuo*, and the remaining solid was sonicated in water (10 mL) to remove the salt. The insoluble product (0.267 g, 99 %) was collected by vacuum filtration. ¹H NMR (300 MHz, DMSO) δ 8.58 (br d, *J* = 5.1 Hz, 4H), 8.51 (s, 4H), 7.97 (br d, *J* = 7.8 Hz, 4H), 7.87 (td, *J* = 7.8, 1.5 Hz, 4H), 7.77 (s, 4H), 7.33 (br ddd, *J* = 5.1, 1.5, 4H), 6.08 (d, *J* = 7.8 Hz, 4H), 5.40 (s, 8H), 4.64 (t, *J* = 6.8 Hz, 4H), 4.39 (d, *J* = 7.8 Hz, 4H), 3.47 (t, *J* = 6.8 Hz, 8H), 2.42 (q, *J* = 6.8 Hz, 8H), 1.42 (qn, *J* = 6.8 Hz, 8H). ¹³C NMR (100 MHz, CDCl₃) δ 153.80, 150.56, 150.17, 147.57, 138.84, 137.83, 124.38, 123.64, 122.04, 120.14, 100.10, 61.02, 44.25, 37.45, 31.55, 26.37. MS (MALDI) observed *m/z* 1423.3 (M + Na)⁺, expected *m/z* 1423.5 (M + Na)⁺.

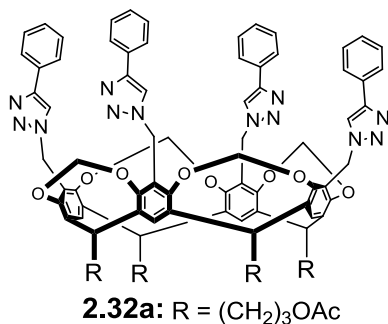


Preparation of 3-pyridyl cavitand 2.31a: In a 50 mL round bottom flask, **2.22a** (0.300 g, 0.260 mmol), 3-ethynylpyridine (0.120 g, 1.14 mmol), copper (II) sulfate pentahydrate (0.012 g, 0.078 mmol), and L-sodium ascorbate (0.030 g, 0.160 mmol) were dissolved in DMSO:H₂O (4:1, 10 mL) and heated for 16 h at 100 ° C. The reaction mixture was cooled to ambient temperature and then pipetted into water (50 mL) in order to precipitate the product, and the product was collected as a pale brown powder (0.405 g, 99 %). ¹H NMR (300 MHz, CDCl₃) δ 8.96 (br, 8H), 8.55 (br, 4H), 8.17 (br, 4H), 7.89 (s, 4H), 7.32 (br, 4H), 5.82 (d, *J* = 6.6 Hz, 4H), 5.33 (s, 8H), 4.86 (t, *J* = 6.8 Hz, 4H), 4.32 (d, *J* = 6.6 Hz, 4H), 4.15 (t, *J* = 6.8 Hz, 8H), 2.33 (q, *J* = 6.8 Hz, 8H), 2.03 (s, 12H), 1.67 (qn, *J* = 6.8 Hz, 8H). ¹³C NMR (100 MHz, CDCl₃) δ 171.26, 154.16, 149.31, 146.85, 144.69, 137.91, 133.13, 121.17, 120.85, 99.64, 64.13, 44.40, 41.08, 36.71, 27.08, 26.81, 21.13. MS (MALDI) observed *m/z* 1569.8 (M + H)⁺, expected *m/z* 1569.6 (M + H)⁺.

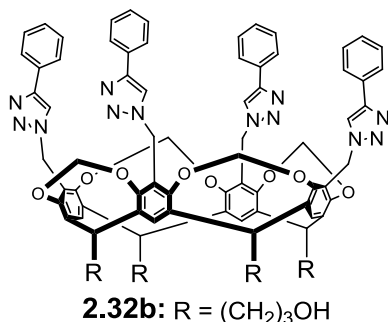


2.31b: R = (CH₂)₃OH

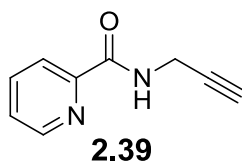
Preparation of 3-pyridyl cavitand 2.31b: In a 25 mL round bottom flask, **2.31a** (0.205 g, 0.131 mmol) and cesium carbonate (0.255 g, 0.780 mmol) were dissolved in methanol:dichloromethane (1:1, 4 mL) and stirred at ambient temperature for 12 h. The solvent was removed *in vacuo*, and the remaining solid was sonicated in water (10 mL) to remove the salt. The insoluble product (0.134 g, 73 %) was collected by vacuum filtration. Methyl acetate generated from the reaction could not be completely removed under vacuum. ¹H NMR (300 MHz, DMSO) δ 9.05 (br, 4H), 8.64 (s, 4H), 8.54 (br, 4H), 8.16 (d, *J* = 7.8 Hz, 4H), 7.76 (s, 4H), 7.46 (br, 4H), 6.11 (d, *J* = 7.5 Hz, 4H), 5.37 (s, 8H), 4.65 (t, *J* = 7.0 Hz, 4H), 4.46 (br, 4H), 4.33 (d, *J* = 7.5 Hz, 4H), 3.48 (t, *J* = 7.0 Hz, 8H), 2.42 (q, *J* = 7.0 Hz, 8H), 1.41 (qn, *J* = 7.0 Hz, 8H). ¹³C NMR (100 MHz, CDCl₃) δ 153.88, 149.38, 147.15, 143.99, 138.79, 138.48, 133.05, 123.95, 123.37, 121.97, 100.28, 61.06, 44.27, 37.45, 31.55, 27.39, 26.45. MS (MALDI) observed *m/z* 1401.6 (M + H)⁺, expected *m/z* 1401.6 (M + H)⁺.



Preparation of phenyl cavitand 2.32a: DMSO:H₂O (4:1, 6 mL) was added to a 25 mL round bottom flask containing **2.22a** (0.400 g, 0.350 mmol), copper (II) sulfate pentahydrate (0.015 g, 0.100 mmol), and L-sodium ascorbate (0.039 g, 0.210 mmol). While stirring, phenyl acetylene (0.228 mL, 2.08 mmol) was added. The reaction mixture was heated for 12 h at 100 ° C and then cooled to ambient temperature. The product was precipitated as a pale brown solid (0.445 g, 92 %) by pouring the solution into water (20 mL). ¹H NMR (300 MHz, CDCl₃) δ 7.82 (d, *J* = 5.2 Hz, 8H), 7.77 (s, 4H), 7.37 (t, *J* = 5.2 Hz, 8H), 7.29 (t, *J* = 5.2 Hz, 4H), 7.23 (s, 4H), 5.81 (d, *J* = 5.7 Hz, 4H), 5.30 (s, 8H), 4.87 (t, *J* = 6.3 Hz, 4H), 4.40 (d, *J* = 5.7 Hz, 4H), 4.18 (t, *J* = 5.1 Hz, 8H), 2.33 (q, *J* = 5.1 Hz, 8H), 1.70 (qn, *J* = 5.4 Hz, 8H). ¹³C NMR (100 MHz, CDCl₃) δ 171.30, 154.23, 147.83, 137.90, 130.59, 128.97, 128.37, 125.99, 121.44, 121.14, 120.21, 99.65, 64.22, 44.28, 36.76, 27.16, 26.93, 21.19. MS (ESI) observed *m/z* 1588.6103 (M + Na)⁺, expected *m/z* 1588.6052 (M + Na)⁺.

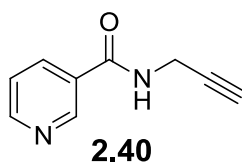


Preparation of phenyl cavitanol 2.32b: In a 25 mL round bottom flask, **2.32a** (0.252 g, 0.160 mmol) and cesium carbonate (0.315 g, 0.97 mmol) were dissolved in methanol:dichloromethane (1:1, 6 mL). The reaction mixture was stirred for 16 h at ambient temperature, and then the solvent was removed *in vacuo*. The remaining solid was sonicated in water (20 mL) to remove the salt, and the insoluble product (0.187 g, 83 %) was collected by vacuum filtration. ¹H NMR (300 MHz, DMSO) δ 8.51 (s, 4H), 7.85 (d, $J = 7.5$ Hz, 8H), 7.77 (s, 4H), 7.44 (t, $J = 7.5$ Hz, 8H), 7.33 (t, $J = 7.5$ Hz, 4H), 6.11 (d, $J = 7.5$ Hz, 4H), 5.36 (s, 8H), 4.67 (t, $J = 6.5$ Hz, 4H), 4.48 (br, 4H), 4.37 (d, $J = 7.5$ Hz, 4H), 3.49 (t, $J = 6.5$ Hz, 8H), 2.43 (q, $J = 6.5$ Hz, 8H), 1.41 (qn, $J = 6.5$ Hz, 8H). ¹³C NMR (100 MHz, DMSO-*d*₆) δ 153.79, 150.41, 150.17, 147.53, 138.84, 137.88, 124.35, 123.97, 123.70, 122.06, 120.20, 100.14, 61.04, 44.19, 37.45, 31.50, 26.35. MS (MALDI) observed m/z 1397.1 (M + H)⁺, expected m/z 1397.6 M (M + H)⁺.



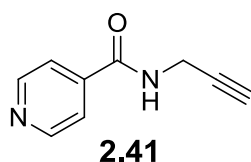
Preparation of 2-pyridyl amide ligand 2.39: Picolinic acid (1.00 g, 8.12 mmol) was added to a 50 mL round bottom flask of carbonyldiimidazole (1.32 g, 8.12 mmol) in 15

mL of tetrahydrofuran. Once the carbonyldiimidazole had fully dissolved, propargylamine (0.892 mL, 8.12 mmol) was added, and the solution was stirred at ambient temperature for 16 h. The reaction mixture was concentrated *in vacuo* and extracted with methylene chloride (2 x 50 mL) and water (50 mL) to isolate the impure product. The product was purified by column chromatography using 10 % methanol in methylene chloride as elution solvent (0.450 g, 35 %). ^1H NMR (300 MHz, CDCl_3) δ 8.53 (ddd, $J = 3.6, 1.2, 0.9$, 1H), 8.21 (b, 1H), 8.16 (dt, $J = 5.7, 0.9$, 1H), 7.82 (td, $J = 5.7, 1.2$, 1H), 7.41 (ddd, $J = 5.7, 3.6, 0.9$, 1H), 4.24 (dd, $J = 5.7, 2.4$ Hz, 2H), 2.25 (t, $J = 2.4$ Hz, 1H). ^{13}C NMR (100 MHz, CDCl_3) δ 163.86, 148.93, 147.86, 137.01, 126.11, 121.91, 79.31, 71.32, 28.70. MS (ESI) observed m/z 160.0718 ($\text{M} + \text{H}$) $^+$, expected m/z 160.0715 ($\text{M} + \text{H}$) $^+$.

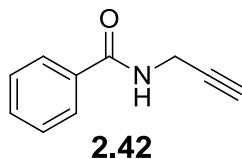


Preparation of 3-pyridyl amide ligand 2.40: To a 25 mL round bottom flask was added nicotinic acid (0.384 g, 3.12 mmol), carbonyldiimidazole (0.506 g, 3.12 mmol), and 5 mL of tetrahydrofuran. Once the carbonyldiimidazole had fully dissolved, propargylamine (0.200 mL, 3.12 mmol) was added, and the solution was stirred at ambient temperature for 16 h. The solvent was removed *in vacuo*, leaving the crude product. The crude product was purified by column chromatography (7 % methanol in methylene chloride) and then by recrystallization using ethyl acetate and hexanes. Pure product was obtained as colorless prisms (0.198 g, 39 %). ^1H NMR (300 MHz, DMSO) δ 9.01 (t, $J = 1.0$ Hz, 1H), 8.64 (dt, $J = 4.8, 1.0$ Hz, 1H), 8.18 (dt, $J = 7.8, 1.0$ Hz, 1H), 7.42 (dd, $J = 7.8, 4.8$

Hz, 1H), 5.05 (br, 1H), 3.57 (dd, $J = 2.6, 1.2$ Hz, 2H), 3.33 (t, $J = 2.6$ Hz, 1H). ^{13}C NMR (100 MHz, CDCl_3): δ 165.80, 152.06, 148.64, 135.62, 129.90, 123.59, 79.87, 71.54, 29.67. MS (ESI) observed m/z 160.0716 ($\text{M} + \text{H}$) $^+$, expected m/z 160.0715 ($\text{M} + \text{H}$) $^+$.

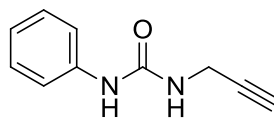


Preparation of 4-pyridyl amide ligand 2.41: To a 25 mL round bottom flask was added isonicotinic acid (0.384 g, 3.12 mmol), carbonyldiimidazole (0.506 g, 3.12 mmol), and 5 mL of tetrahydrofuran. Once the carbonyldiimidazole had fully dissolved, propargylamine (0.200 mL, 3.12 mmol) was added, and the solution was stirred at ambient temperature for 16 h. The solvent was removed *in vacuo*, leaving the crude product. The crude product was purified by column chromatography (7 % methanol in methylene chloride) and then by recrystallization using ethyl acetate and hexanes. Pure product was obtained as colorless prisms (0.200g, 40 %). ^1H NMR (300 MHz, CDCl_3) δ 8.71 (dd, $J = 4.5, 1.2$ Hz, 2H), 7.61 (dd, $J = 4.5, 1.2$ Hz, 2H), 6.76 (b, 1H), 4.24 (dd, $J = 3.9, 1.8$ Hz, 2H), 2.28 (t, $J = 1.8$ Hz, 1H). ^{13}C NMR (100 MHz, CDCl_3) δ 165.45, 150.81, 141.07, 121.15, 79.02, 72.52, 30.11. MS (ESI) observed m/z 160.0731 ($\text{M} + \text{H}$) $^+$, expected m/z 160.0715 ($\text{M} + \text{H}$) $^+$.



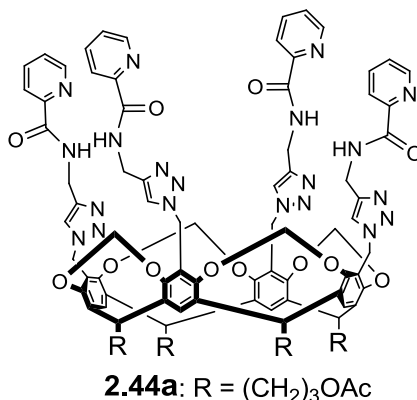
Preparation of phenyl amide ligand 2.42: A two-neck 25 mL round bottom flask equipped with a stir bar was evacuated and filled with nitrogen. Methylene chloride (1

mL, anhydrous), benzoyl chloride (0.100 mL, 0.086 mmol), propargylamine (0.055 mL, 0.086 mmol), and triethylamine (0.180 mL, 1.29 mmol) were added through a septum via syringe, and the reaction mixture was stirred at ambient temperature for 16 h. The solvent was removed in vacuo, leaving pure product as a pale pink solid (0.136 g, 99 %). ^1H NMR δ 7.79 (d, 2H, $J = 7.3$ Hz), 7.56-7.40 (m, 3H), 6.35 (br, 1H), 4.26 (dd, 2H, $J = 5.1$, 2.5 Hz), 2.29 (t, 1H, $J = 2.4$ Hz). Observed spectra consistent with literature values.⁴

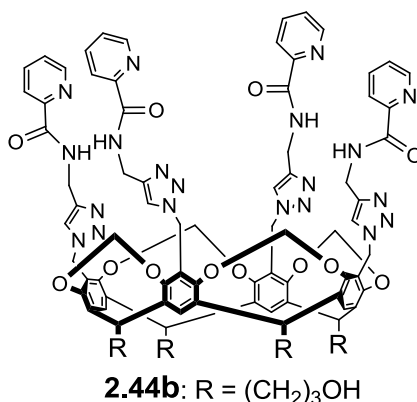


2.43

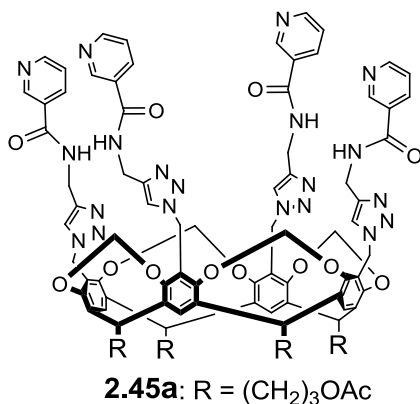
Preparation of phenyl urea ligand 2.43: A two-neck 25 mL round bottom flask equipped with a stir bar was evacuated and filled with nitrogen. DMF (1 mL, anhydrous), propargylamine (0.100 mL, 0.015 mmol), and phenylisocyanate (0.117 mL, 0.015 mmol) were added through a septum via syringe, and the reaction mixture was heated to 90 °C for 16 h. After this time, the reaction mixture was cooled to ambient temperature and poured into 3 mL of water, causing the product to precipitate as a white powder. The product was collected by vacuum filtration and dried (0.131 g, 52 %). ^1H NMR (300 MHz, DMSO- d_6) δ 8.65 (s, 1H), 7.38 (d, $J = 7.7$ Hz, 2H), 7.23 (t, $J = 7.7$ Hz, 2H), 6.90 (t, $J = 7.3$ Hz, 1H), 6.43 (t, $J = 5.6$ Hz, 1H), 3.88 (dd, $J = 5.6$, 2.4, Hz, 2H), 3.09 (t, $J = 2.4$ Hz, 1H). Observed spectra consistent with literature values.⁵



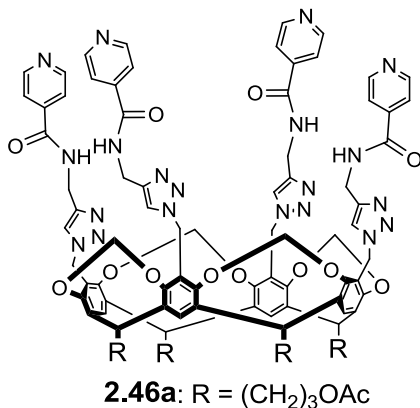
Preparation of 2-pyridyl amide cavitand 2.44a: To a 10 mL round bottom flask was added **2.22a** (0.308 g, 0.270 mmol), **2.39** (0.187 g, 1.17 mmol), benzimidazole catalyst **2.25** (0.033 g, 0.080 mmol), copper (II) sulfate pentahydrate (0.013 g, 0.080 mmol), L-sodium ascorbate (0.032 g, 0.160 mmol), and 4:1 DMSO: H₂O (6 mL). The reaction mixture was stirred at 100 °C for 16 h. The reaction mixture was poured into water (20 mL), causing the product to precipitate as an off-white solid. (0.452 g, 95 %). ¹H NMR (300 MHz, CD₃CN) δ 8.65 (t, *J* = 4.4 Hz, 4 H), 8.46 (br d, *J* = 3.0 Hz, 4H), 8.03 (br d, *J* = 5.7 Hz, 4H), 7.83 (td, *J* = 5.7, 1.2 Hz, 4H), 7.64 (s, 4H), 7.45 (s, 4H), 7.42 (ddd, *J* = 5.7, 3.6, 0.9, 4H), 5.71 (d, *J* = 5.7 Hz, 4H), 5.20 (s, 8H), 4.73 (t, *J* = 6.0 Hz, 4H), 4.67 (d, *J* = 4.4 Hz, 8H), 4.10 (t, *J* = 6.0 Hz, 8H) 3.97 (d, *J* = 5.7 Hz, 4H), 2.41 (q, *J* = 6.0 Hz, 8H), 1.98 (s, 12H), 1.59 (qn, *J* = 6.0 Hz, 8H). ¹³C NMR (100 MHz, CDCl₃) δ 171.21, 164.60, 153.95, 149.62, 148.29, 144.75, 137.49, 126.45, 123.14, 122.28, 121.32, 120.89, 99.65, 64.11, 43.91, 41.03, 36.58, 35.03, 27.05, 21.07. MS (MALDI) observed *m/z* 1819.4 (M + Na)⁺, expected *m/z* 1819.7 (M + Na)⁺.



Preparation of 2-pyridyl amide cavitand 2.44b: To a 25 mL round bottom flask containing **2.44a** (0.900 g, 0.500 mmol) and cesium carbonate (0.980 g, 3.01 mmol) was added methanol (5 mL) and dichloromethane (5 mL). The reaction was stirred at ambient temperature for 16 h. After that time, the solvent was removed by rotary evaporation, and the remaining solid was sonicated in water (30 mL) to dissolve the salt. The insoluble product was collected as a brown solid (0.711 g, 87 %). ¹H NMR (300 MHz, DMSO-*d*₆) δ 9.19 (t, *J* = 5.4 Hz, 4H), 8.60 (ddd, *J* = 5.7, 2.4, 1.5 Hz, 4H), 8.00 (dt, *J* = 7.8, 0.9), 7.92 (td, *J* = 7.8, 1.8 Hz, 4H), 7.89 (s, 4H), 7.70 (s, 4H), 7.55 (ddd, *J* = 7.5, 4.8, 1.5, 4H), 5.89 (d, *J* = 7.6 Hz, 4H), 5.21 (s, 8H), 4.56 (t, *J* = 7.8 Hz, 4H), 4.52 (d, *J* = 6.0, 8H), 4.44 (br t), 4.17 (d, *J* = 7.6 Hz, 4H), 3.45 (br q, *J* = 6.5 Hz, 8H), 2.38 (q, *J* = 6.5 Hz, 8H), 1.38 (qn, *J* = 6.5, 8H). ¹³C NMR (100 MHz, DMSO-*d*₆) δ 164.03, 153.08, 150.42, 149.08, 145.24, 138.69, 138.38, 127.21, 124.13, 122.55, 122.09, 99.42, 60.42, 43.20, 36.78, 34.67, 30.93, 25.77. MS (MALDI) observed *m/z* 1651.3 (M + Na)⁺, expected *m/z* 1651.6 (M + Na)⁺.

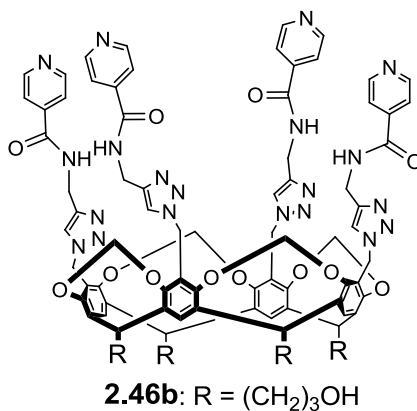


Attempted preparation of 3-pyridyl amide cavitand 2.45a: To a 10 mL round bottom flask was added **2.22a** (0.500 g, 0.432 mmol), **2.40** (0.305 g, 1.90 mmol), **2.25** (0.053 g, 0.130 mmol), CuSO₄ (0.021g, 0.130 mmol), L-sodium ascorbate (0.052 g, 0.260 mmol), and DMSO:H₂O (4:1, 7 mL). The reaction mixture was stirred at 100 °C for 16 h. After this time, the reaction mixture was cooled to ambient temperature and poured into 30 mL of water, allowing the product to precipitate as a brown solid (0.698 g, 90 %). ¹H NMR showed that the reaction had not gone to completion (shown in Figure 6.35).



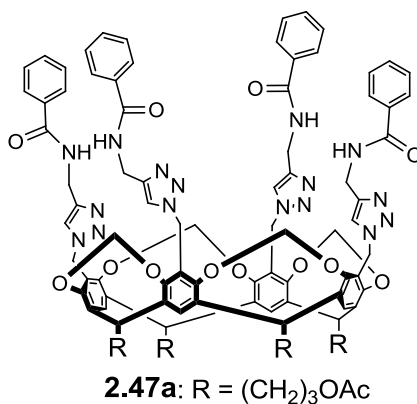
Preparation of 4-pyridyl amide cavitand 2.46a: To a 25 mL round bottom flask was added **2.22a** (0.300 g, 0.260 mmol), **2.41** (0.187 g, 0.120 mmol), copper (II) sulfate pentahydrate (0.013 g, 0.080 mmol), benzimidazole catalyst **2.25** (0.033 g, 0.080 mmol),

L-sodium ascorbate (0.032 g, 0.160 mmol), and DMSO:H₂O (4:1, 6 mL). The reaction mixture was heated for 12 h at 100 ° C and then cooled to ambient temperature. The product was precipitated as a pale brown solid (0.413 g, 89 %) by pouring the solution into water (20 mL). ¹H NMR (300 MHz, CDCl₃) δ 8.65 (d, *J* = 5.1 Hz, 8H), 8.49 (br t, 4H), 7.65 (d, *J* = 5.1 Hz, 8H), 7.53 (s, 4H), 7.14 (s, 4H), 5.62 (d, *J* = 6.6 Hz, 4H), 5.10 (s, 8H), 4.77 (t, *J* = 6.0 Hz, 4H), 4.65 (d, *J* = 2.4 Hz, 8H), 4.15 (t, *J* = 6.0 Hz, 8 H), 3.88 (d, *J* = 6.6 Hz, 4H), 2.23 (q, *J* = 6.0 Hz, 8H). 1.67 (qn, *J* = 6.0 Hz, 8H). ¹³C NMR (100 MHz, CDCl₃) δ 171.19, 166.02, 154.08, 150.48, 144.96, 141.36, 137.75, 123.70, 121.23, 100.11, 64.08, 43.90, 41.17, 36.66, 35.61, 27.03, 21.16. MS (MALDI) observed *m/z* 1820.0 (M + Na)⁺, expected *m/z* 1819.7 (M + Na)⁺.

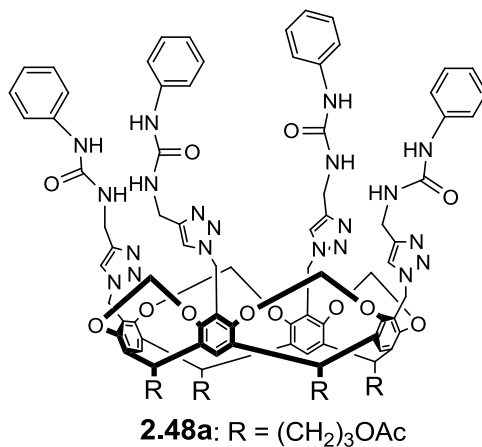


Preparation of 4-pyridyl amide cavitand 2.46b: In a 25 mL round bottom flask containing **2.46a** (0.413 g, 0.230 mmol) and cesium carbonate (0.449 g, 1.38 mmol) was added methanol:dichloromethane (1:1, 4mL), and the reaction was stirred at ambient temperature for 12 h. The solvent was removed *in vacuo*, and the remaining solid was sonicated in water (10 mL) to dissolve the salts. The insoluble cavitand was collected as a pale brown solid (0.312 g, 83 %). ¹H NMR (300 MHz, DMSO-*d*₆) δ 9.27 (br, 8H), 8.68

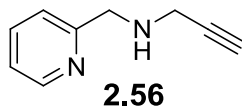
(br, 8H), 7.94 (br, 4H), 7.72 (s, 4H), 7.70 (s, 4H), 5.92 (d, $J = 6.6$ Hz, 4H), 5.18 (s, 8H), 4.57 (t, $J = 6.0$ Hz, 4H), 4.50 (br, 8H), 4.16 (d, $J = 6.6$ Hz, 4 H), 3.45 (t, $J = 6.0$ Hz, 8H), 2.38 (q, $J = 6.0$ Hz, 8H). 1.38 (br qn, 8H). ^{13}C NMR (100 MHz, $\text{DMSO-}d_6$) δ 165.52, 153.70, 150.82, 144.85, 141.79, 138.69, 124.35, 123.82, 122.12, 100.11, 61.01, 43.79, 37.37, 35.61, 31.51, 26.37. MS (ESI) observed m/z 1651.6449 ($\text{M} + \text{Na}$) $^+$, expected m/z 1651.6272 ($\text{M} + \text{Na}$) $^+$.



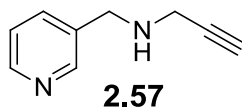
Attempted preparation of phenyl amide cavitand 2.47a: To a 10 mL round bottom flask was added **2.22a** (0.100 g, 0.086 mmol), **2.42** (0.061 g, 0.380 mmol), copper (II) sulfate pentahydrate (0.004 g, 0.026 mmol), **2.25** (0.011, 0.026 mmol), L-sodium ascorbate (0.010 g, 0.052 mmol), and $\text{DMSO:H}_2\text{O}$ (4:1, 2 mL). The reaction mixture was heated for 16 h at 100 °C and then cooled to ambient temperature. Partially completed product was precipitated as a pale brown solid (0.079 g, 51 %) by pouring the solution into water (8 mL). ^1H NMR is shown in Figure 6.40.



Preparation of phenyl urea cavitand 2.48a: To a 10 mL round bottom flask equipped with a stir bar was added **2.22a** (0.100 g, 0.086 mmol), **2.43** (0.066 g, 0.380 mmol), copper (II) sulfate pentahydrate (0.004 g, 0.026 mmol), **2.25** (0.011 g, 0.026 mmol), L-sodium ascorbate (0.010 g, 0.052 mmol), and DMSO:H₂O (4:1, 2 mL). The reaction mixture was heated for 16 h at 100 ° C and then cooled to ambient temperature. The product was precipitated as a pale brown solid (0.116 g, 72 %) by pouring the solution into water (8 mL). ¹H NMR (300 MHz, CDCl₃) δ 7.87 (br, 4H), 7.63 (br, 4H), 7.35 (m, 8H), 7.16 (m, 12H), 6.85 (t, *J* = 7.5 Hz, 4H), 6.53 (br, 4H), 5.95 (d, *J* = 7.6 Hz, 4H), 5.23 (s, 8H), 4.60 (t, *J* = 6.0 Hz, 4H), 4.29 (s, 8H), 4.22 (d, *J* = 7.6 Hz, 4H), 4.05 (t, *J* = 6.0 Hz, 8H), 2.39 (m, 8H), 1.94 (s, 12H), 1.55 (m, 8H). ¹³C NMR (100 MHz, CDCl₃): δ 154.10, 137.91, 137.57, 129.10, 123.74, 122.91, 120.39, 119.27, 99.88, 64.20, 45.20, 41.14, 36.64, 27.10, 26.79, 21.19.

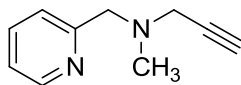


Preparation of 2-pyridyl amine ligand 2.56: To a 10 mL round bottom flask equipped with a stir bar was added NaCNBH₃ (0.201 g, 3.21 mmol), THF (8 mL), 2-pyridinecarboxaldehyde (0.300 mL, 3.21 mmol), propargylamine (0.204 mL, 3.21 mmol), and glacial acetic acid (0.183 mL, 3.21 mmol). The reaction was stirred at ambient temperature for 16 h. After this time, 10 mL methylene chloride was added, and the reaction mixture was extracted three times with 10 mL of 10 % aq. NaOH. The organic layer was dried, concentrated *in vacuo*, and purified by column chromatography using 5 % methanol in methylene chloride. The product containing fractions were concentrated *in vacuo*, leaving product as an orange oil (0.210 g, 41 %). ¹H NMR (300 MHz, CDCl₃): δ = 8.56 (d, J = 4.9 Hz, 1H), 7.65 (td, J = 7.8, 1.8 Hz, 1H), 7.32 (d, J = 4.9 Hz, 1H), 7.17 (t, J = 4.9 Hz, 1H), 4.00 (s, 2H), 3.50 (d, J = 2.4 Hz, 2H), 2.24 (t, J = 2.4 Hz, 1H), 1.89 ppm (bs, 1H). Observed spectra consistent with literature values.⁶



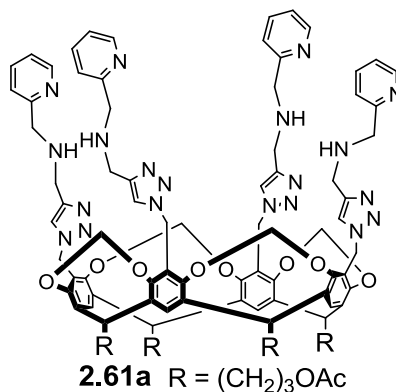
Preparation of 3-pyridyl amine ligand 2.57: To a 10 mL round bottom flask equipped with a stir bar was added NaCNBH₃ (0.201 g, 3.21 mmol), THF (8 mL), 3-pyridinecarboxaldehyde (0.300 mL, 3.21 mmol), propargylamine (0.204 mL, 3.21 mmol), and glacial acetic acid (0.183 mL, 3.21 mmol). The reaction was stirred at ambient temperature for 16 h. After this time, 10 mL methylene chloride was added, and the reaction mixture was extracted three times with 10 mL of 10 % aq. NaOH. The

organic layer was dried, concentrated *in vacuo*, and purified by column chromatography using 5 % methanol in methylene chloride. The product containing fractions were concentrated *in vacuo*, leaving product as a yellow oil (0.206 g, 40 %). ^1H NMR (300 MHz, CDCl_3): δ = 8.59 (m, 2H), 7.70 (td, J = 8.4, 1.5 Hz, 1H), 7.28 (dd, J = 8.4, 4.8 Hz, 1H), 3.89 (s, 2H), 3.40 (d, J = 2.4 Hz, 2H), 2.30 (t, J = 2.4 Hz, 1H), 1.89 ppm (bs, 1H). Observed spectra consistent with literature values.⁷

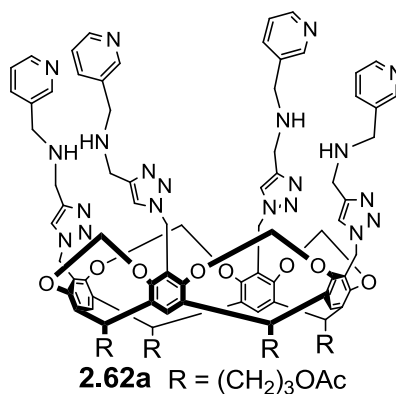


2.58

Preparation of 2-pyridyl methyl amine ligand 2.58: To a 10 mL round bottom flask equipped with a stir bar was added NaCNBH_3 (0.201 g, 3.21 mmol), THF (8 mL), 2-pyridinecarboxaldehyde (0.300 mL, 3.21 mmol), N-methylpropargylamine (0.271 mL, 3.21 mmol), and glacial acetic acid (0.183 mL, 3.21 mmol). The reaction was stirred at ambient temperature for 16 h. After this time, 10 mL methylene chloride was added, and the reaction mixture was extracted three times with 10 mL of 10 % aq. NaOH. The organic layer was dried, concentrated *in vacuo*, and purified by column chromatography using 3 % methanol in methylene chloride. The product containing fractions were concentrated *in vacuo*, leaving product as an orange oil (0.067 g, 13 %). ^1H NMR (300 MHz, CDCl_3): δ 8.56 (d, J = 3.8 Hz, 1H), 7.62 (td, J = 7.6, 1.5 Hz, 1H), 7.37 (d, J = 7.7 Hz, 1H), 7.15 (t, J = 6.9 Hz, 1H), 3.71 (s, 2H), 3.36 (s, 2H), 2.35 (s, 3H), 2.25 (t, J = 2.2 Hz, 1H).⁸ Observed spectra consistent with literature values.

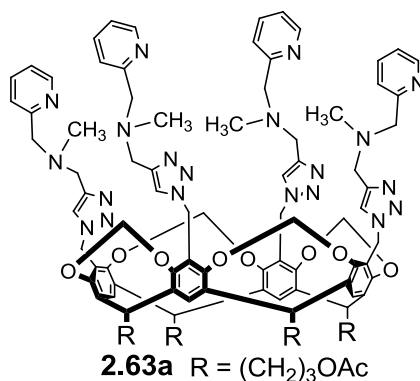


Attempted preparation of 2-pyridyl amine cavitand 2.61a: To a 50 mL round bottom flask was added **2.22a** (0.110 g, 0.095 mmol), **2.56** (0.109 g, 0.746 mmol), copper (II) sulfate pentahydrate (0.008 g, 0.051 mmol), **2.25** (0.021g, 0.051 mmol), L-sodium ascorbate (0.020 g, 0.10 mmol), and DMSO:H₂O (4:1, 10 mL). The reaction mixture was heated for 16 h at 100 ° C and then cooled to ambient temperature. Crude product was obtained by removing the solvent under a stream of air. The crude product was sonicated in water and then collected by vacuum filtration, 0.054 g. ¹H NMR showed that the reaction went to partial completion (Figure 6.43).

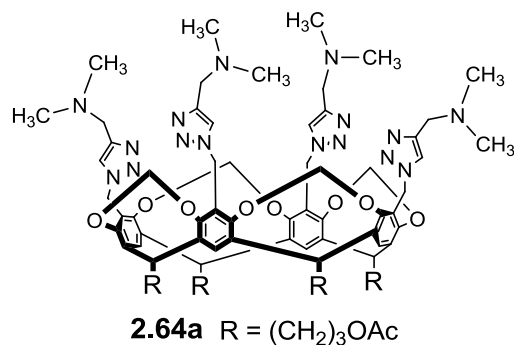


Attempted preparation of 3-pyridyl amine cavitand 2.62a: To a 10 mL round bottom flask was added **2.22a** (0.100 g, 0.087 mmol), **2.57** (0.056 g, 0.381 mmol), copper (II)

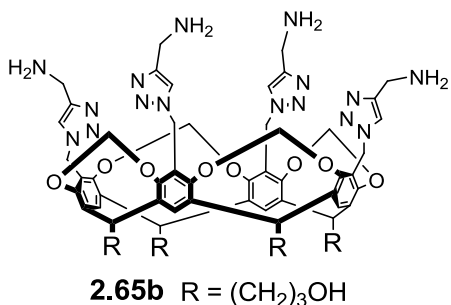
sulfate pentahydrate (0.043 g, 0.173 mmol), L-sodium ascorbate (0.069 g, 0.346 mmol), and DMSO:H₂O (4:1, 4 mL). The reaction mixture was heated for 16 h at 100 ° C and then cooled to ambient temperature. The product was precipitated from solution by pouring the reaction mixture into 15 mL of water. The brown solid (0.120 g) was collected by vacuum filtration, and ¹H NMR showed that the reaction went to partial completion (Figure 6.44).



Attempted preparation of 2-pyridyl methyl amine cavitand 2.63a: To a 10 mL round bottom flask was added **2.22a** (0.110 g, 0.095 mmol), **2.58** (0.067 g, 0.418 mmol), copper (II) sulfate pentahydrate (0.005 g, 0.029 mmol), **2.25** (0.012 g, 0.029 mmol), L-sodium ascorbate (0.011 g, 0.057 mmol), and DMSO:H₂O (4:1, 2 mL). The reaction mixture was heated for 16 h at 100 ° C and then cooled to ambient temperature. Crude product was obtained by removing the solvent under a stream of air. ¹H NMR showed that the reaction went to partial completion (Figure 6.45).



Preparation of dimethylamine cavitand 2.64a: To a 10 mL round bottom flask equipped with a stir bar was added **2.22a** (0.100 g, 0.086 mmol), **2.59** (0.047 mL, 0.432 mmol), copper (II) sulfate pentahydrate (0.005 g, 0.029 mmol), L-sodium ascorbate (0.010 g, 0.058 mmol), and DMSO:H₂O (4:1, 2 mL). The reaction mixture was heated for 16 h at 100 ° C and then cooled to ambient temperature. Crude product was obtained by removing the solvent under a stream of air. Crude product was sonicated in water and then collected by vacuum filtration (0.110 g). ¹H NMR (300 MHz, CDCl₃): δ 7.42 (s, 4H), 7.12 (s, 4H), 5.73 (d, *J* = 6.6 Hz, 4H), 5.20 (s, 8H), 4.73 (br, 4H), 4.22 (d, *J* = 6.6 Hz), 4.11 (br, 8H), 3.51 (s, 8H), 2.00 (s, 12H), 1.75 (m, 8H), 1.62 (m, 8H). ¹³C NMR (100 MHz, CDCl₃): δ171.26, 154.14, 137.92, 121.29, 99.62, 64.16, 41.43, 36.70, 27.13, 26.76, 21.15. MS (ESI) observed *m/z* 1511.7108 (M + Na)⁺, expected *m/z* 1511.7082 (M + Na)⁺.



Attempted preparation of amine cavitand 2.65b: To a 10 mL round bottom flask was added **2.22a** (0.050 g, 0.043 mmol), **2.60** (0.033 g, 0.216 mmol), copper (II) sulfate pentahydrate (0.002 g, 0.013 mmol), L-sodium ascorbate (0.005 g, 0.026 mmol), and DMSO:H₂O (4:1, 2 mL). The reaction mixture was heated for 16 h at 100 ° C and then cooled to ambient temperature. BOC-protected cavitand was obtained by removing the solvent under a stream of air. The remaining solid was triturated in water, and the cavitand product was collected by vacuum filtration. The cavitand product was stirred in a 10 mL round bottom flask with trifluoroacetic acid (1 mL) for 6 h. TFA was removed under a stream of air, leaving 0.17 g product as a brown solid (33 %). The ¹H NMR was broad and poorly defined due to copper that was coordinated from the click reaction, and a completely pure sample was never obtained.

6.3 Chapter Three Experimental

Preparation of 2-pyridyl cavitand 2.30b•Cu: In a 10 mL round bottom flask, **2.30b** (0.142 g, 0.100 mmol) and tetrakis(acetonitrile)copper(I) tetrafluoroborate (0.191 g, 0.610 mmol) were sonicated in methanol (4 mL) until a homogenous suspension was formed. The precipitate was filtered off and rinsed with methanol (0.114 g, 77 %). The

NMR peaks were broad and poorly defined so no integral values or coupling constants were obtained. The product did not have sufficient solubility to obtain ^{13}C NMR data. ^1H NMR (300 MHz, DMSO) δ 7.63, 4.48, 3.50, 1.42. MS (MALDI) observed m/z 1463.6 M^+ , expected m/z 1463.5 M^+ .

Preparation of 3-*pyridyl* cavitand 2.31b•Cu: In a 10 mL round bottom flask, **2.31b** (0.079 g, 0.056 mmol) and tetrakis(acetonitrile)copper(I) tetrafluoroborate (0.106 g, 0.340 mmol) were sonicated in methanol (2 mL) until a homogenous suspension was formed. The product was collected by simple filtration (0.076 g, 92 %). The NMR peaks were broad and poorly defined so no integral values or coupling constants were obtained. The product did not have sufficient solubility to obtain ^{13}C NMR data. ^1H NMR (300 MHz, DMSO) δ 8.50, 7.70, 6.09, 5.30, 4.59, 4.43, 4.17, 3.45, 2.37, 1.38. MS (MALDI) observed m/z 1463.5 M^+ , expected m/z 1463.5 M^+ .

Preparation of phenyl cavitand 2.32b•Cu:

In a 10 mL round bottom flask, **2.32b** (0.140 g, 0.100 mmol) and tetrakis(acetonitrile)copper(I) tetrafluoroborate (0.189 g, 0.600 mmol) were sonicated in methanol (3 mL) until a homogenous suspension was formed, and the precipitate was collected by vacuum filtration (0.127 g, 87 %). The NMR peaks were broad and poorly defined so no integral values or coupling constants were obtained. The product did not have sufficient solubility to obtain ^{13}C NMR data. ^1H NMR (300 MHz, DMSO) δ 8.62, 8.16, 7.65, 5.48, 4.50, 2.05, 1.41. MS (MALDI) observed m/z 1459.7 M^+ , expected m/z 1459.5 M^+ .

Preparation of 2-pyridyl cavitand 2.30a•Fe₂: In a 20 mL scintillation vial, cavitand **2.30a** (0.375 g, 0.240 mmol) and iron (II) sulfate (0.370 g, 1.43 mmol) were sonicated in 15 mL of methanol for 20 minutes until a yellow precipitate formed. The precipitate was collected by vacuum filtration, rinsed with 3 x 50 mL portions of methanol, and dried under vacuum. The product was collected as a yellow solid (0.460 g, 99 %). The product did not have sufficient solubility to obtain ¹³C NMR data in a realistic amount of time. MS (MALDI) *m/z* calculated for C₈₄H₈₃Fe₂N₁₆O₂₂S (M + H₂O + OH – SO₄)⁺ 1811.4287; found 1812.9724.

Preparation of 2-pyridyl cavitand 2.30b•Fe₂: In a 10 mL round bottom flask, **2.30b** (0.089 g, 0.064 mmol) and iron (II) sulfate heptahydrate (0.106 g, 0.380 mmol) were sonicated in methanol (3mL) until a homogeneous suspension was formed. The precipitate was filtered off and rinsed with methanol (0.096 g, 99 %). The NMR peaks were broad and poorly defined so no integral values or coupling constants were obtained. The product did not have sufficient solubility to obtain ¹³C NMR data. ¹H NMR (300 MHz, DMSO) δ 8.60, 7.99, 7.90, 7.78, 7.33, 6.09, 5.40, 4.64, 4.45, 1.42. MS (MALDI) observed *m/z* 1644.7 (M + 2H₂O +SO₄)⁺, expected *m/z* 1644.4 (M + 2H₂O +SO₄)⁺.

Preparation of 2-pyridyl amide cavitand 2.44a•Cu_x: Methanol (2 mL) was added to a 10 mL round bottom flask containing **2.44a** (0.100 g, 0.056 mmol) and tetrakis(acetonitrile)copper(I) tetrafluoroborate (0.105 g, 0.330 mmol), and the solution was sonicated for 5 minutes until a green, homogenous suspension was observed. The product was collected by vacuum filtration (0.074 g, 74 %). The NMR peaks were broad and poorly defined so no integral values or coupling constants were obtained. The

product did not have sufficient solubility to obtain ^{13}C NMR data. ^1H NMR (300 MHz, CD_3CN) δ 8.57, 8.15, 7.90, 7.45, 5.59, 5.18, 4.75, 4.29, 4.13, 3.62, 2.44, 2.00, 1.63. MS (MALDI) observed m/z 1922.1 M^+ , expected m/z 1922.5 M^+ .

Preparation of 2-pyridyl amide cavitand 2.44b•Cu_x: In a 25 mL round bottom flask, **2.44b** (0.300 g, 0.180 mmol) and tetrakis(acetonitrile)copper(I) tetrafluoroborate (0.347 g, 1.10 mmol) were sonicated in methanol (6 mL) until a homogeneous suspension was formed. The pale green precipitate was collected by simple filtration (0.310 g, 99 %). The NMR peaks were extremely broad and poorly defined so no integral values or coupling constants were obtained. The product did not have sufficient solubility to obtain ^{13}C NMR data. ^1H NMR (300MHz, D_2O) δ 6.86, 4.07, 2.99, 1.70, 0.78. MS (MALDI) observed m/z 1754.7 M^+ , expected m/z 1754.5 M^+ .

Preparation of 4-pyridyl amide cavitand 2.46b•Cu: To a 25 mL round bottom flask was added **2.46b** (0.112 g, 0.068 mmol), tetrakis(acetonitrile)copper(I) tetrafluoroborate (0.139 g, 0.440 mmol), and methanol (4 mL). The reaction mixture was sonicated until a homogenous, dark green suspension was formed. The solid (0.101 g, 87 %) was collected by vacuum filtration. The NMR peaks were broad and poorly defined so no integral values or coupling constants were obtained. The product did not have sufficient solubility to obtain ^{13}C NMR data. ^1H NMR (300 MHz, DMSO) δ 9.27, 8.09, 7.67, 5.64, 5.21, 4.60, 4.53, 4.43, 3.66, 3.44, 2.35, 2.68, 1.37. MS (ESI) observed m/z 1691.5689 M^+ , expected m/z 1691.5670 M^+ .

Preparation of 2-pyridyl amide cavitand 2.44a•Fe_x: In a 20 mL scintillation vial, **2.44a** (0.550 g, 0.310 mmol) and iron (II) sulfate (0.475 g, 1.80 mmol) were sonicated in 15 mL

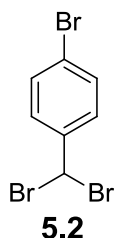
of methanol for 20 minutes. The product was collected via vacuum filtration, rinsed with 3 x 50 mL excess methanol, and dried under vacuum. The product was collected as a reddish solid (0.642 g, 99 %, calculation based on the mass of the bis-iron species **2.44a**•Fe₂•(SO₄)₂). The NMR peaks were broad and poorly defined so no integral values or coupling constants were obtained. The product did not have sufficient solubility to obtain ¹³C NMR data in a realistic amount of time. Due to the extremely high affinity of **2.44** for copper, residual copper-coordinated cavitand **2.44**•Cu is also observed. Copper could not be completely removed from **2.44** even after refluxing **2.44** in water with NaEDTA and then with NaSH. It should be noted that the copper-coordinated side-product **2.44**•Cu is observed in the MS analysis of pure **2.44**, and **2.44**•Cu has a far higher ionization potential than both **2.44** and **2.44**•Fe/**2.44**•Fe₂. The actual amount of copper present in **2.44**•Fe/**2.44**•Fe₂ is minimal. MS (MALDI) observed *m/z* 1851.9865, expected for C₉₂H₉₁FeN₂₀O₂₀ (M – H – SO₄)⁺ *m/z* 1851.6068; and observed *m/z* 1905.9123, expected for C₉₂H₈₉Fe₂N₂₀O₂₀ (M – 3H – 2SO₄)⁺ *m/z* 1905.5261.

Preparation of 2-pyridyl amide cavitand 2.44b•Fe_x: In a 25 mL round bottom flask, **2.44b** (0.300 g, 0.180 mmol) and iron (II) sulfate heptahydrate (0.310 g, 1.10 mmol) were sonicated in methanol (5 mL) until a homogenous suspension was formed. The red-brown precipitate was collected as a brown solid (0.309 g, 99 %). The ¹H NMR peaks were broad and poorly defined so no integral values or coupling constants were obtained. The product did not have sufficient solubility to obtain ¹³C NMR data. ¹H NMR (300 MHz, D₂O) δ 7.91, 7.41, 7.21, 6.93, 6.85, 5.16, 4.54, 4.50, 3.96, 3.47, 3.19, 2.95, 1.64, 0.80. MS (MALDI) observed *m/z* 1684.0 M⁺, expected *m/z* 1684.6 M⁺.

6.4 Chapter Four Experimental

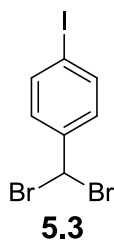
General Oxidation Procedures: In a 2 mL scintillation vial, catalyst (3.77×10^{-3} mmol, 10 mol %) was dissolved in 0.150 mL solvent (water:acetonitrile or water:propionitrile 1:1). Oxidant (0.377 mmol) and substrate (3.77×10^{-2} mmol) were added, and the reaction was stirred for 24 h (25°C or 60°C). Aliquots (75 μ L) were taken and passed through a silica/magnesium sulfate plug with 1.5 mL ether before being analyzed by GCMS. The reactions were performed in triplicate, and the average yield is reported. All yields are based on recovered starting material.

6.5 Chapter Five Experimental

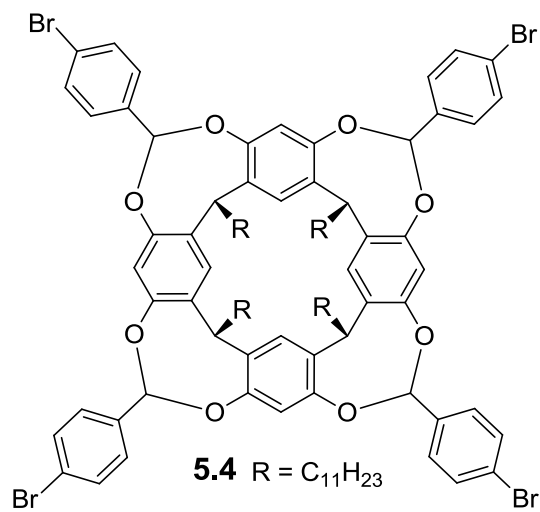


Preparation of 4-bromobenzal bromide 5.2: To an oven dried 50 mL round bottom flask equipped with a stir bar was added 4-bromobenzaldehyde (1.00 g, 5.40 mmol), anhydrous methylene chloride (20 mL), and boron tribromide (0.564 mL, 5.95 mmol). The reaction mixture was stirred at ambient temperature for 16 h, and after this time, the reaction was quenched by the slow addition of water (20 mL). The methylene chloride layer was collected, and the aqueous layer was extracted with 10 mL of methylene chloride an additional 2 times. The organic layers were dried and concentrated *in vacuo*,

leaving 1.37 g (77 %) pure product as a white powder. ^1H NMR (300 MHz, D_2O) δ 7.51 (d, $J = 8.4$ Hz, 2H), 7.45 (d, $J = 8.4$ Hz, 2H), 6.59 (s, 1H). Observed spectra consistent with literature values.⁹

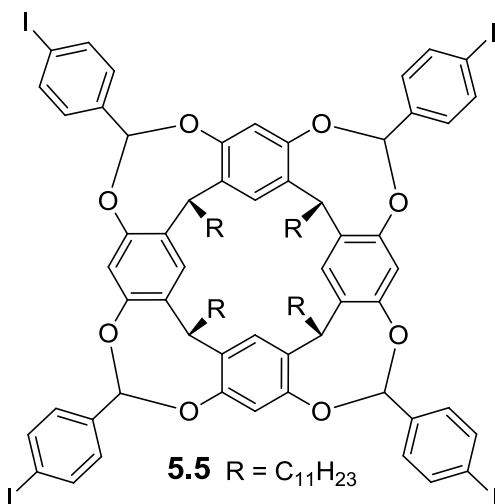


Preparation of 4-iodobenzal bromide 5.3: To an over dried 250 mL round bottom flask equipped with a stir bar was added 4-iodobenzaldehyde (3.35 g, 14.4 mmol), anhydrous methylene chloride (70 mL), and boron tribromide (1.51 mL, 15.9 mmol). The reaction mixture was stirred at ambient temperature for 16 h, and after this time, the reaction was quenched by the slow addition of water (70 mL). The precipitate was filtered off and discarded. The methylene chloride layer was collected, and the aqueous layer was extracted with 50 mL of methylene chloride an additional two times. The organic layers were dried and concentrated *in vacuo*, leaving 4.75 g (88 %) pure product as a white powder. ^1H NMR (300 MHz, D_2O) δ 7.72 (d, $J = 8.4$ Hz, 2H), 7.32 (d, $J = 8.4$ Hz, 2H), 6.58 (s, 1H). Observed spectra consistent with literature values.⁹



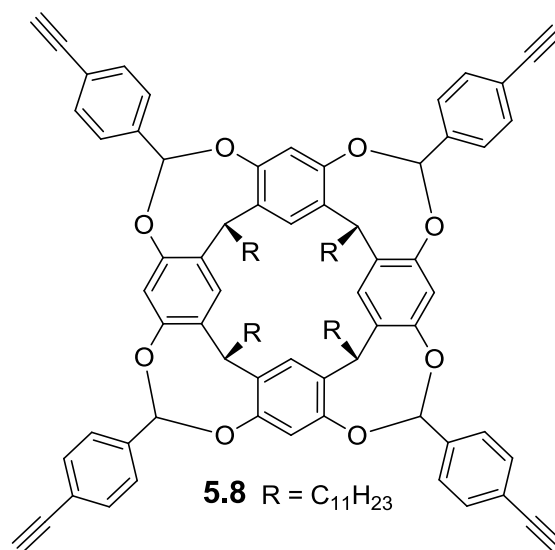
Preparation of bromide cavitand 5.4: To a 100 mL round bottom flask equipped with a stir bar was added **5.1** (0.619 g, 0.560 mmol), **5.2** (1.11 g, 3.36 mmol), DMA (25 mL, degassed), and 1,8-Diazabicyclo[5.4.0]undec-7-ene (DBU, 0.67 mL, 4.47 mmol). The reaction mixture was stirred under nitrogen at 60 °C for 48 h. After this time, the reaction was cooled to ambient temperature, and the DMA was removed under a stream of air. The remaining oil was extracted with 25 mL of methylene chloride and 25 mL of water. The aqueous layer was rinsed with 25 mL of methylene chloride an additional two times, and the combined organic layers were dried and concentrated *in vacuo*. The crude oil was purified by column chromatography using hexanes and methylene chloride as elution solvent (starting with pure hexanes, product eluted in 1:1 hexanes: methylene chloride). The product-containing fractions were concentrated *in vacuo*, leaving product (0.248 g, 25 %) as a white solid. ¹H NMR (300 MHz, CDCl₃): δ 7.54 - 7.48 (m, 16H), 7.19 (s, 4H), 6.57 (s, 4H), 5.34 (s, 4H), 4.87 (t, *J* = 8.1 Hz, 4H), 2.25 (q, *J* = 6.6 Hz, 8 H), 1.39 (m, 8H), 1.22 (br s, 64 H), 0.83 (t, *J* = 6.3 Hz, 12H). ¹³C NMR (100 MHz, CDCl₃): δ 154.47,

139.23, 137.56, 131.90, 128.20, 123.54, 121.17, 116.75, 107.19, 36.49, 31.99, 29.95, 28.17, 22.93, 14.34.



Preparation of iodo cavitand 5.5: To a 100 mL round bottom flask equipped with a stir bar was added **5.1** (1.00 g, 0.900 mmol), **5.3** (1.49 g, 3.98 mmol), DMA (50 mL, degassed), and DBU (1.08 mL, 7.24 mmol). The reaction mixture was stirred under nitrogen at 60 °C for 48 h. After this time, the reaction was cooled to ambient temperature and poured into a beaker with 100 mL of water, causing the product to precipitate as a brown oil on the sides of the beaker. After approximately 2 h, the water was decanted, and the remaining oil was purified by column chromatography using hexanes and methylene chloride as elution solvent (starting with pure hexanes, product eluted in 20 % methylene chloride in hexanes). The product-containing fractions were concentrated *in vacuo*, leaving product (0.305 g, 18 %) as a white solid. ¹H NMR (300 MHz, CDCl₃): δ 7.78 (d, *J* = 8.3 Hz, 8 H), 7.41 (d, *J* = 8.3 Hz, 8H), 7.25 (s, 4H), 6.62 (s, 4H), 5.38 (s, 4H), 4.91 (t, *J* = 7.8 Hz, 4H), 2.31 (q, *J* = 6.3 Hz, 8H), 1.45 (m, 8H), 1.28 (br s, 64 H), 0.90 (t,

$J = 6.0$ Hz, 12H). ^{13}C NMR (100 MHz, CDCl_3): δ 154.43, 139.22, 138.32, 137.85, 128.35, 121.15, 116.77, 107.15, 95.37, 36.70, 32.16, 29.94, 28.16, 22.92, 14.35.



Preparation of acetylene cavitand 5.8: To a 10 mL round bottom flask equipped with a stir bar was added **5.5** (0.119 g, 0.061 mmol), Pd(PPh₃)₂Cl₂ (0.009 g, 0.012 mmol), CuI (0.005 g, 0.024 mmol), diethylamine (2 mL), and trimethylsilylacetylene **5.6** (0.190 mL, 1.33 mmol). The reaction mixture was refluxed in a sealed tube at 60 °C for 16 h and then cooled to ambient temperature. Water and hexanes (10 mL each) were added to the reaction mixture, and the product was extracted into hexanes. The aqueous layer was rinsed with 5 mL of hexanes an additional two times, and the combined organic layers were rinsed with 10 % aq. HCl (20 mL) and water (20 mL). The organic layers were dried and concentrated *in vacuo*, leaving the crude product. The crude product was triturated in methanol, and the TMS-protected product was collected by vacuum filtration as a white solid (0.062 g). The TMS-protected product was dissolved THF (2 mL) with tetrabutylammonium fluoride (10 eq) and stirred at ambient temperature for 16 h. After

this time, water and hexanes were added (10 mL each) and the product was extracted into hexanes. The aqueous layer was rinsed with hexanes (5 mL) an additional two times, and the combined organic layers were dried and concentrated *in vacuo*, leaving product as a white solid (0.052 g, 55 % overall). ^1H NMR (300 MHz, CDCl_3): δ 7.64 (d, $J = 8.4$ Hz, 8H), 7.57 (d, $J = 8.4$ Hz, 8H), 7.26 (s, 4H), 6.66 (s, 4H), 5.45 (s, 4H), 4.93 (t, $J = 7.8$ Hz, 4H), 2.33 (m, 8H), 1.46 (m, 8H), 1.28 (br, 64 H), 0.89 (t, 12H). ^{13}C NMR (100 MHz, CDCl_3): δ 154.49, 139.19, 132.45, 126.46, 123.10, 121.09, 116.80, 107.27, 83.29, 78.16, 58.99, 36.70, 32.14, 29.92, 28.15, 22.89, 14.31.

6.6 Selected NMR Spectra

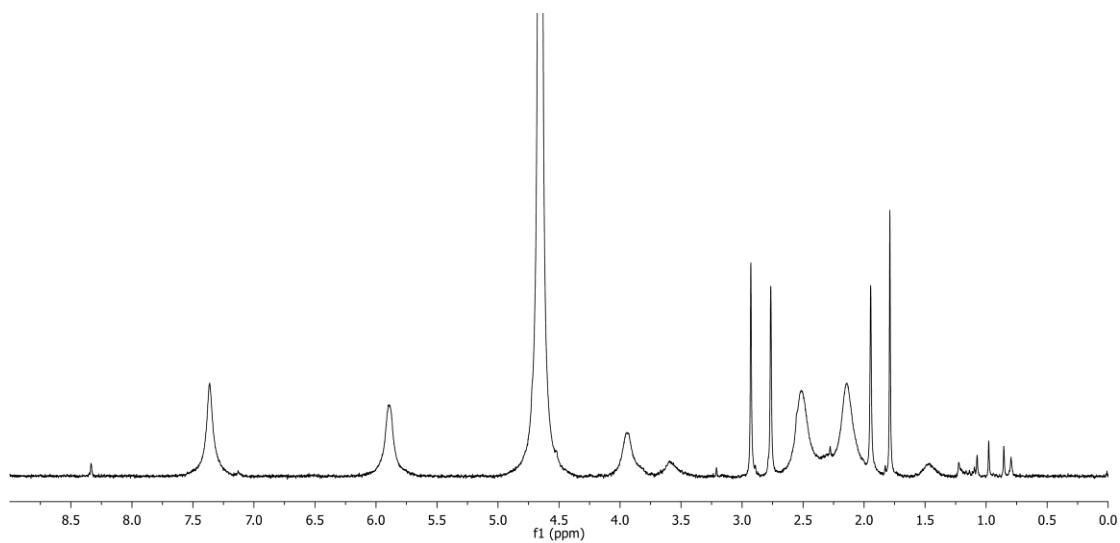
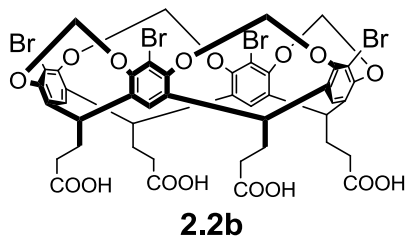


Figure 6.1: ¹H NMR spectrum (300 MHz, D₂O, 298K) of **2.2b**

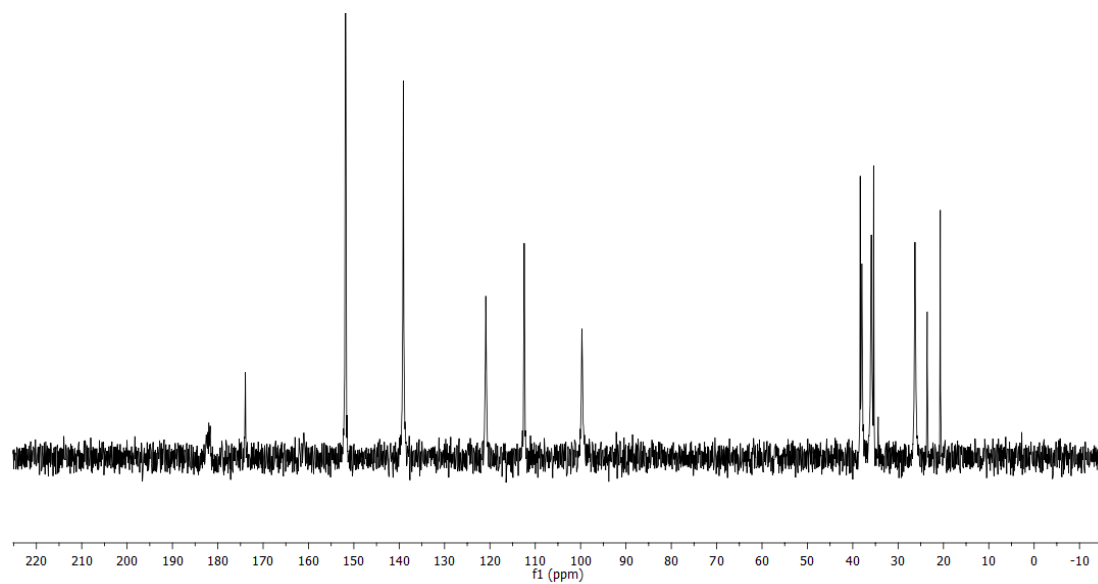


Figure 6.2: ¹³C NMR spectrum (100 MHz, D₂O, 298K) of **2.2b**

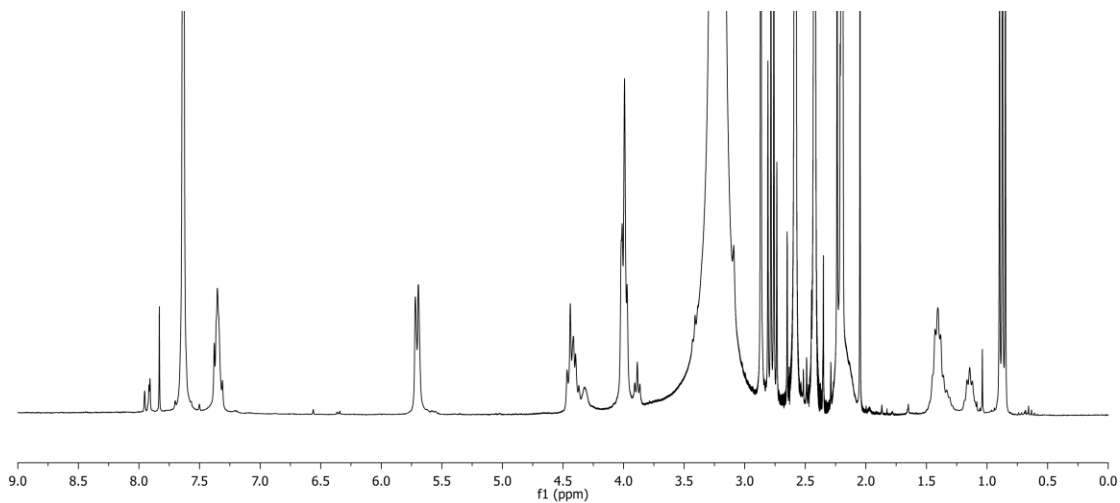
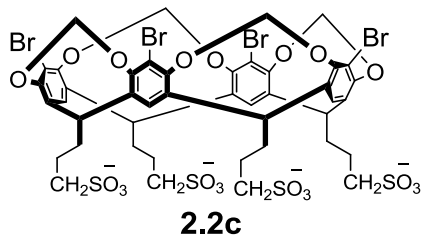


Figure 6.3: ¹H NMR spectrum (300 MHz, DMSO, 298K) of **2.2c**

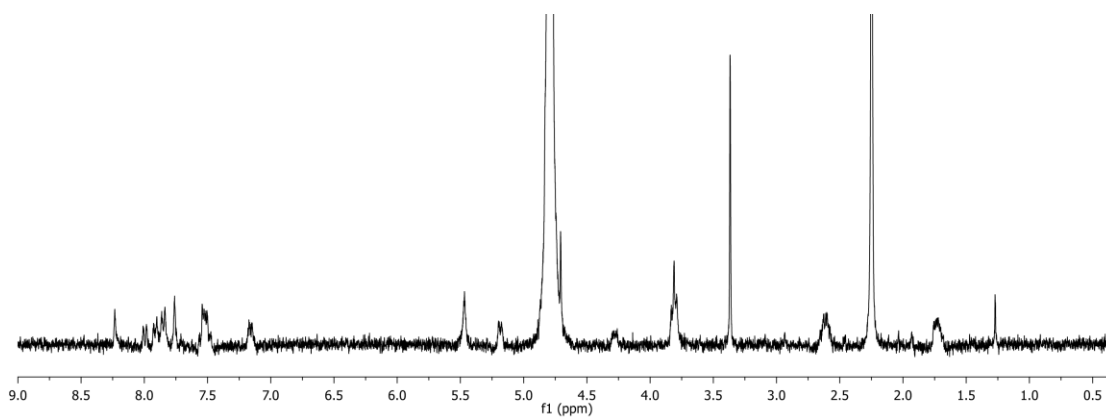
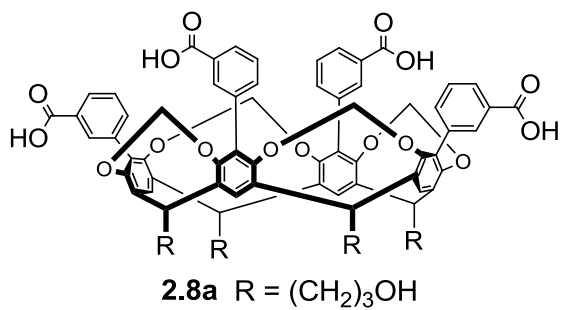


Figure 6.4: ^1H NMR spectrum (300 MHz, D_2O , 298K) of **2.8a**

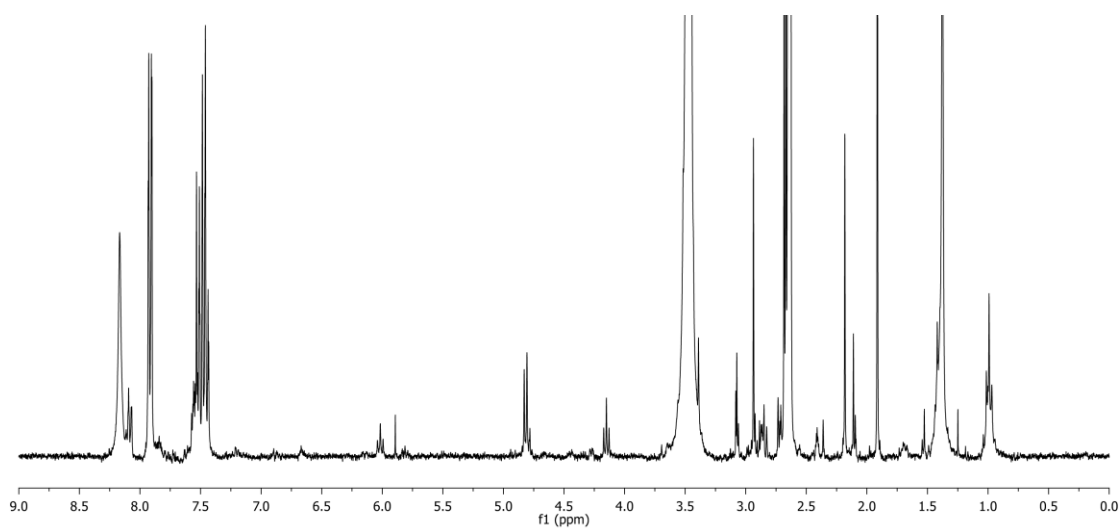
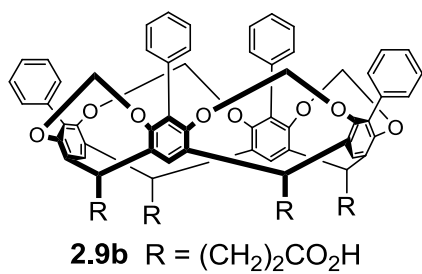


Figure 6.5: ¹H NMR spectrum (300 MHz, DMSO, 298K) of **2.9b**

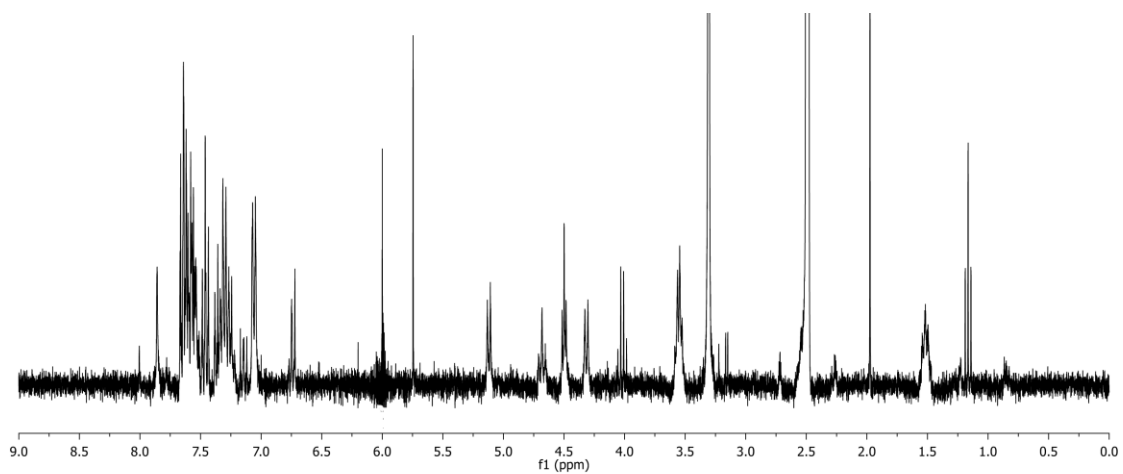
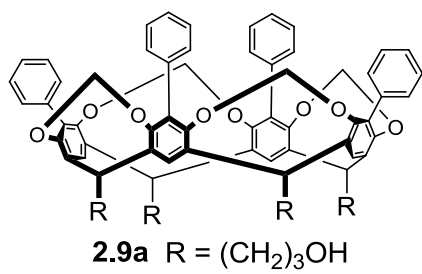


Figure 6.6: ^1H NMR spectrum (300 MHz, DMSO, 298K) of **2.9a**

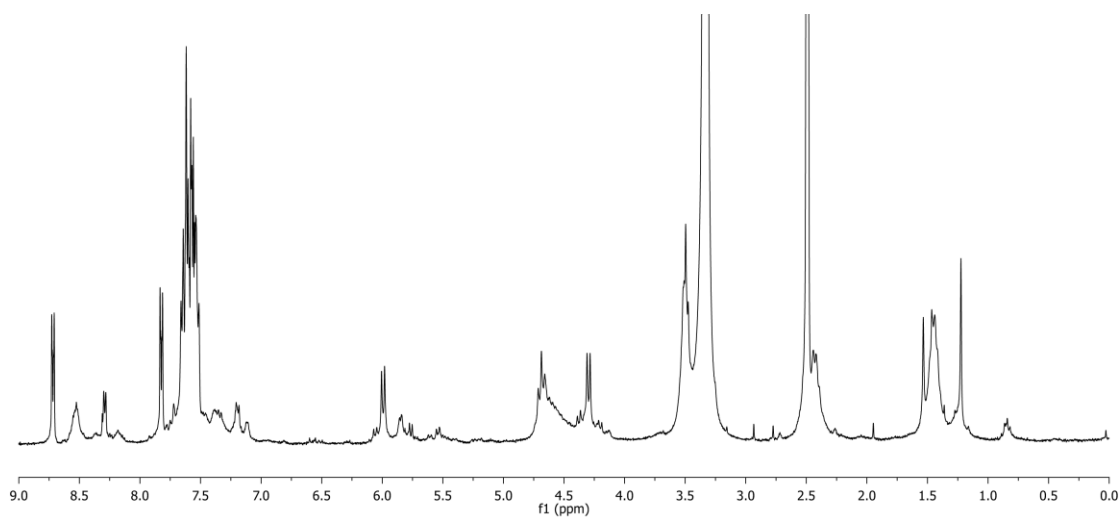
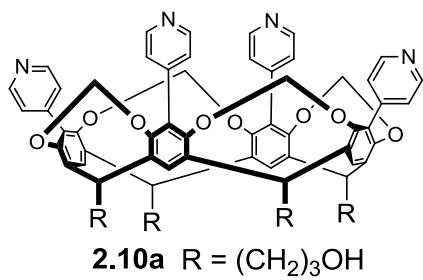


Figure 6.7: ¹H NMR spectrum (300 MHz, DMSO, 298K) of **2.10a**

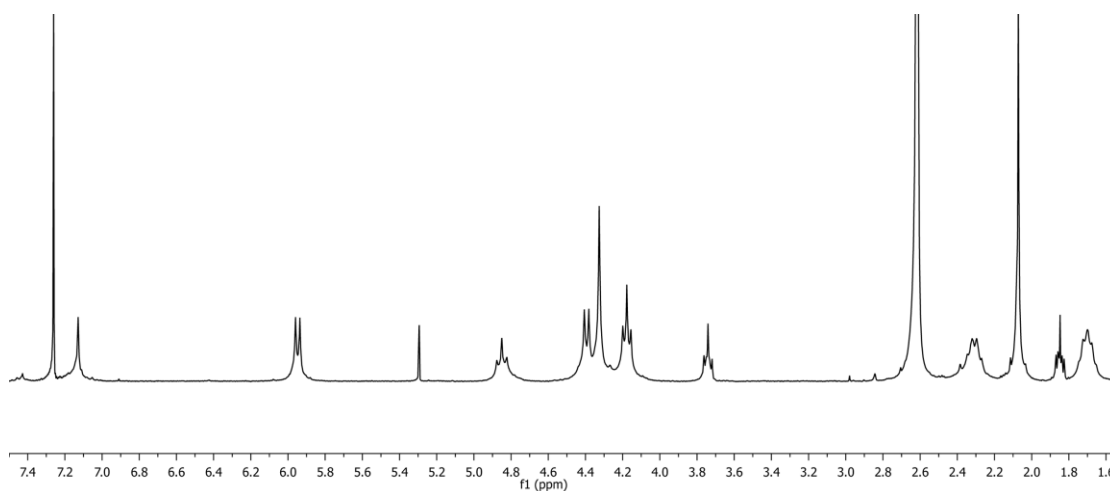
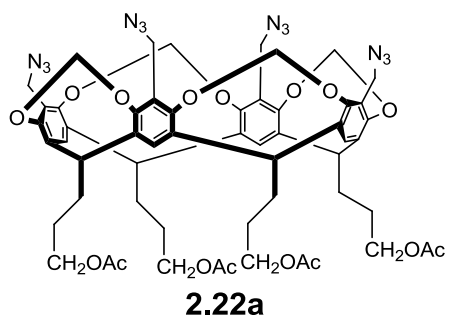


Figure 6.8: ^1H NMR spectrum (300 MHz, CDCl_3 , 298K) of **2.22a**

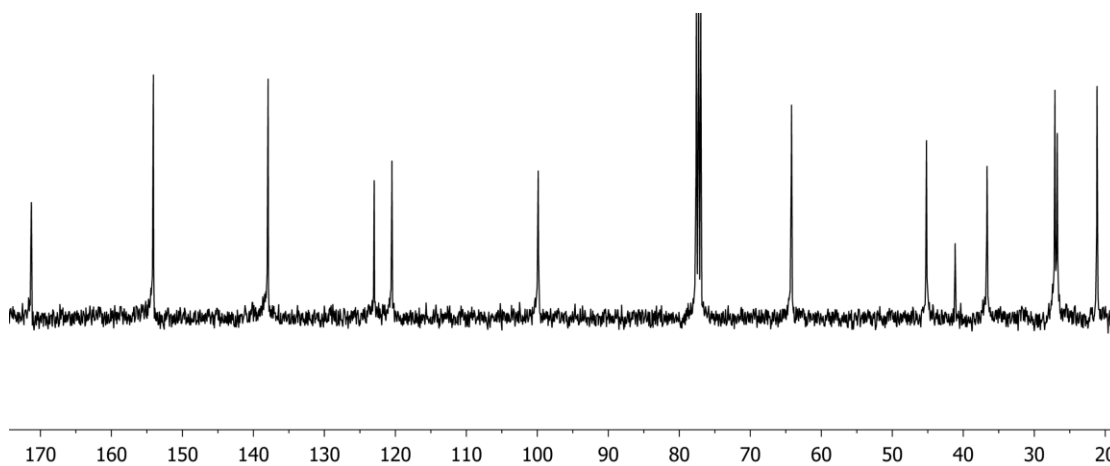


Figure 6.9: ^{13}C NMR spectrum (100 MHz, CDCl_3 , 298K) of **2.22a**

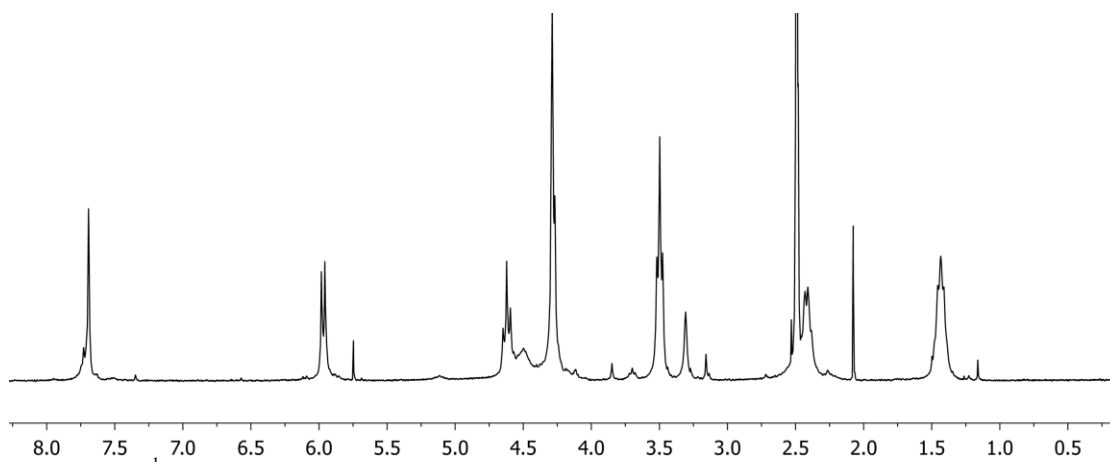
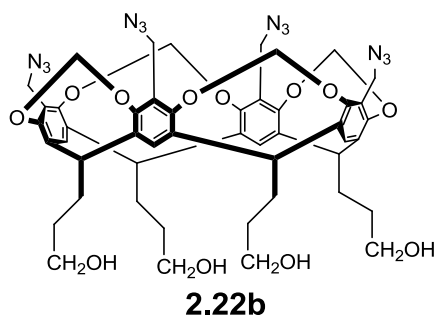


Figure 6.10. 1H NMR spectrum (300 MHz, $CDCl_3$, 298K) of **2.22b**

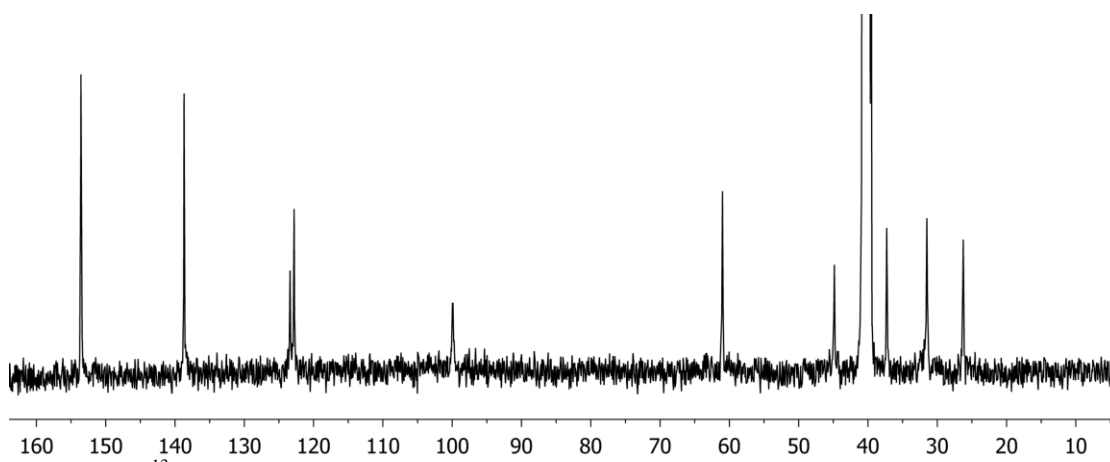
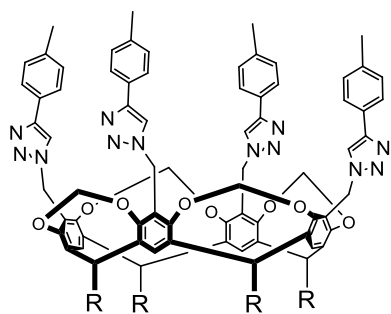


Figure 6.11. ^{13}C NMR spectrum (100 MHz, $CDCl_3$, 298K) of **2.22b**



2.26a: $R = (\text{CH}_2)_3\text{OAc}$

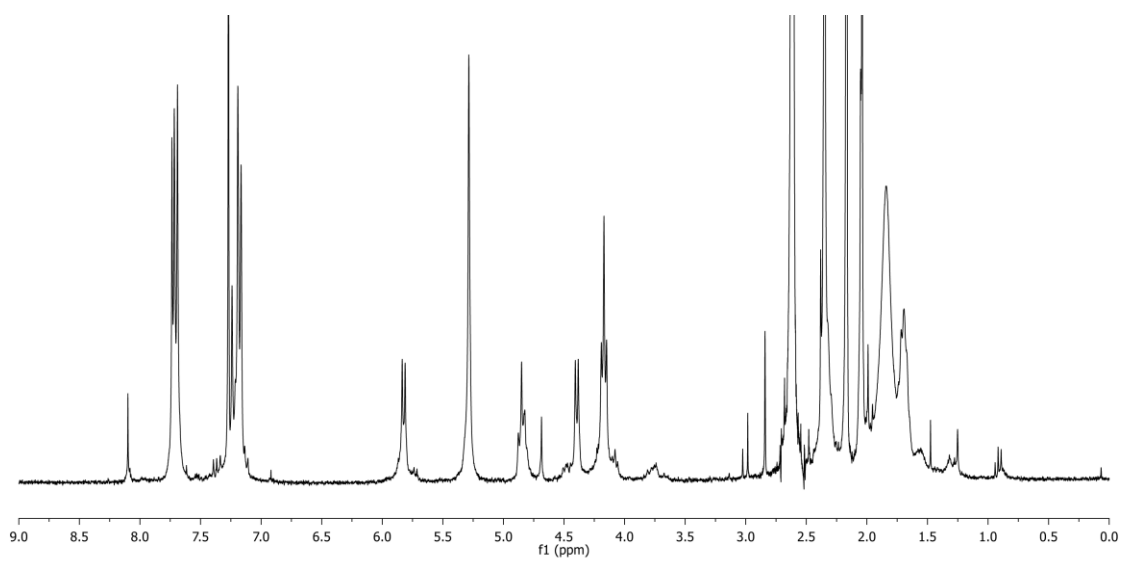


Figure 6.12. ^1H NMR spectrum (300 MHz, CDCl_3 , 298K) of **2.26a**

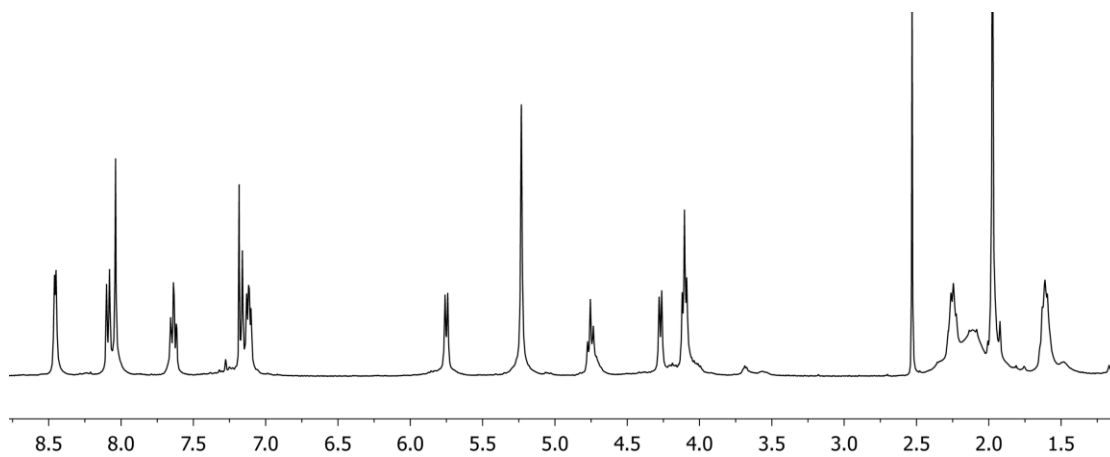
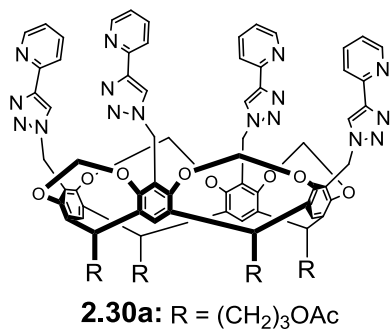


Figure 6.13. ¹H NMR spectrum (300 MHz, CDCl₃, 298K) of **2.30a**

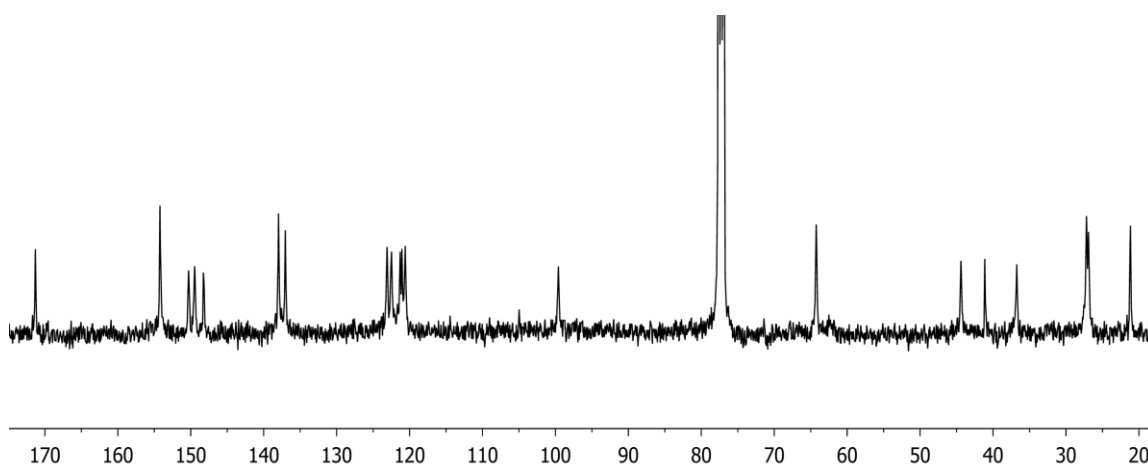


Figure 6.14. ¹³C NMR spectrum (100 MHz, CDCl₃, 298K) of **2.30a**

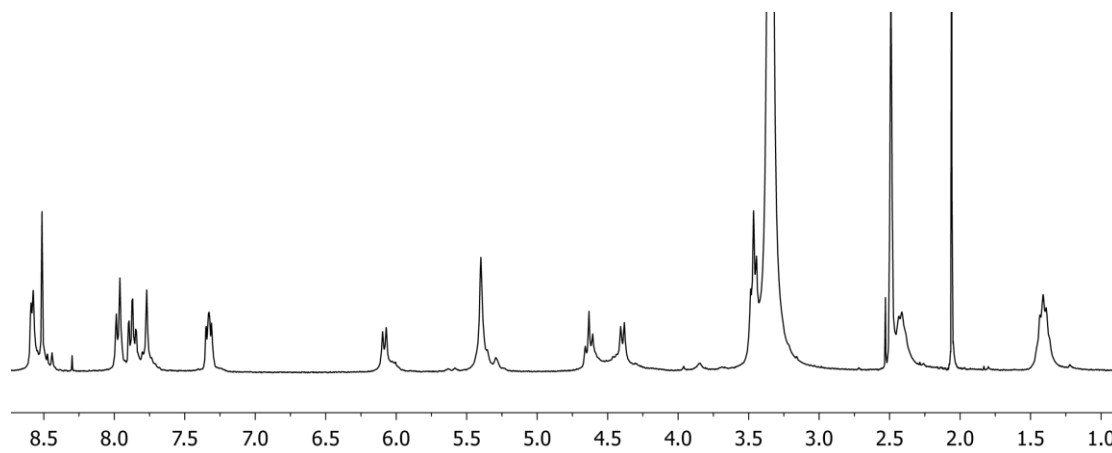
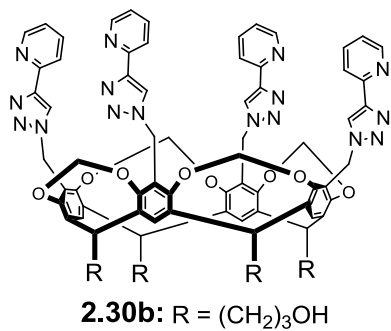


Figure 6.15. ¹H NMR spectrum (300 MHz, DMSO, 298K) of **2.30b**

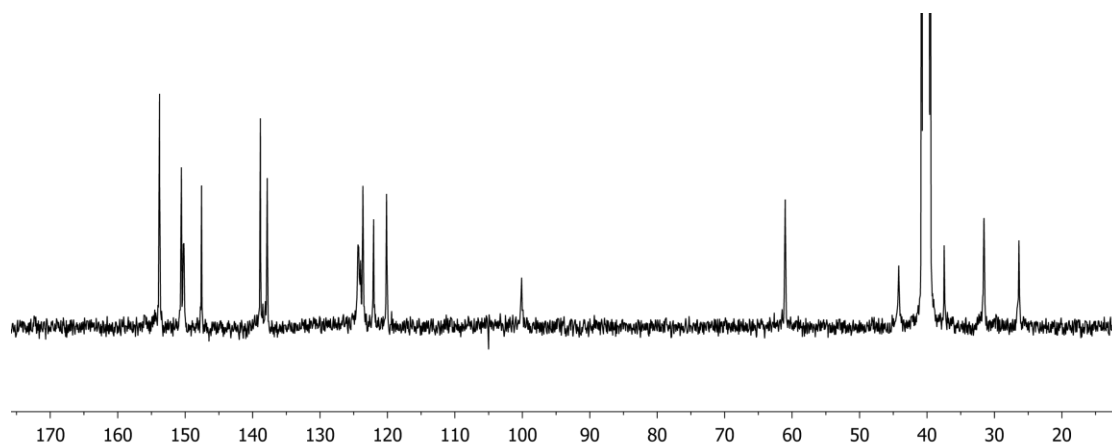


Figure 6.16. ¹³C NMR spectrum (100 MHz, DMSO, 298K) of **2.30b**

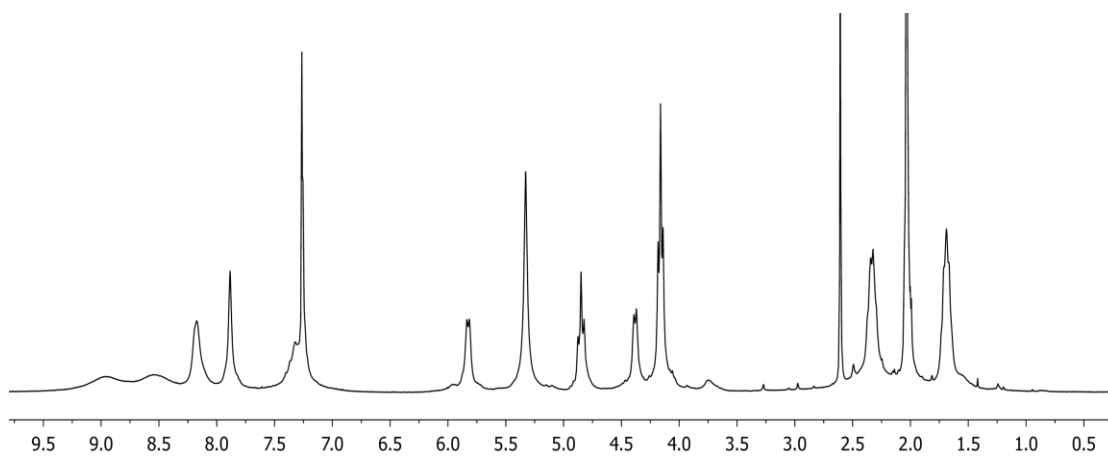
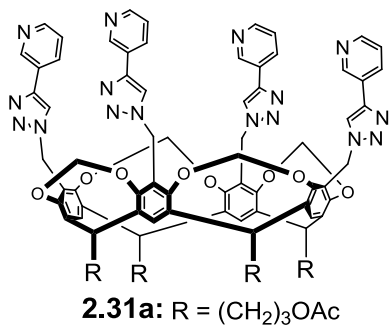


Figure 6.17. ¹H NMR spectrum (300 MHz, CDCl₃, 298K) of **2.31a**

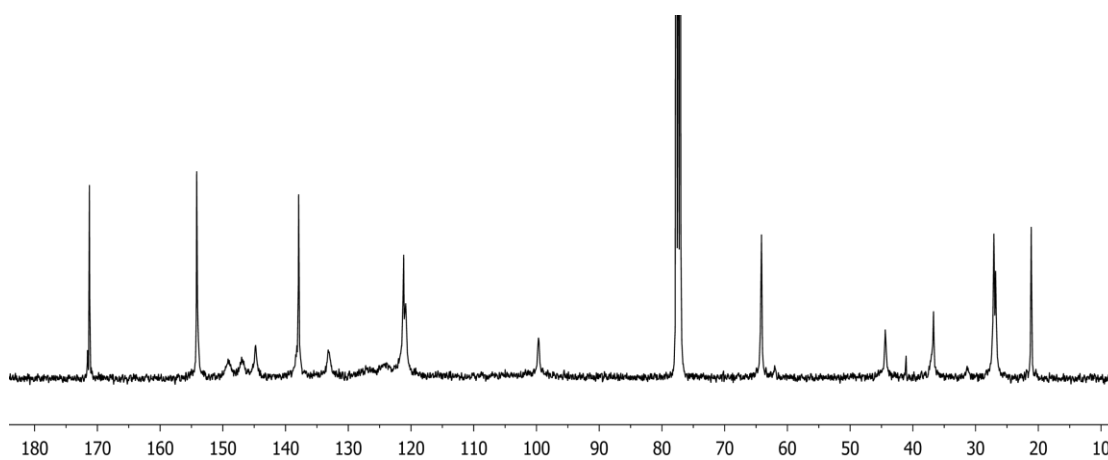


Figure 6.18. ¹³C NMR spectrum (100 MHz, CDCl₃, 298K) of **2.31a**

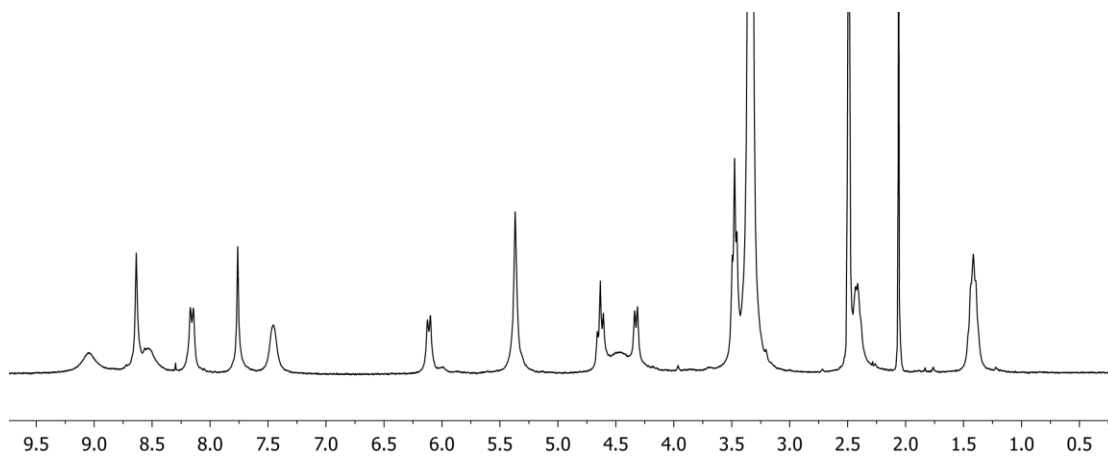
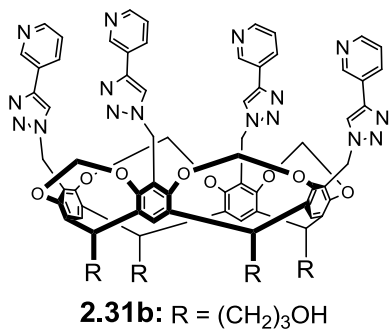


Figure 6.19. ¹H NMR spectrum (300 MHz, DMSO, 298K) of **2.31b**

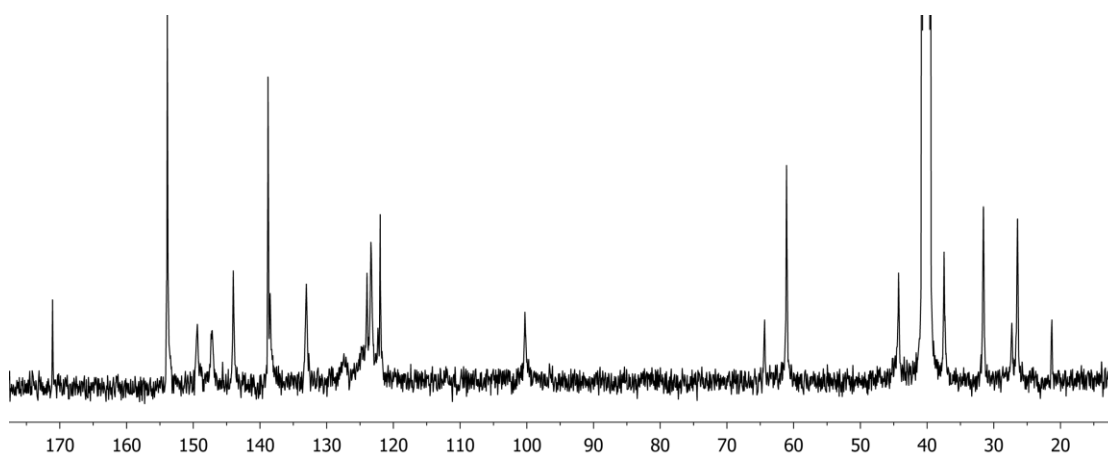


Figure 6.20. ¹³C NMR spectrum (100 MHz, DMSO, 298K) of **2.31b**

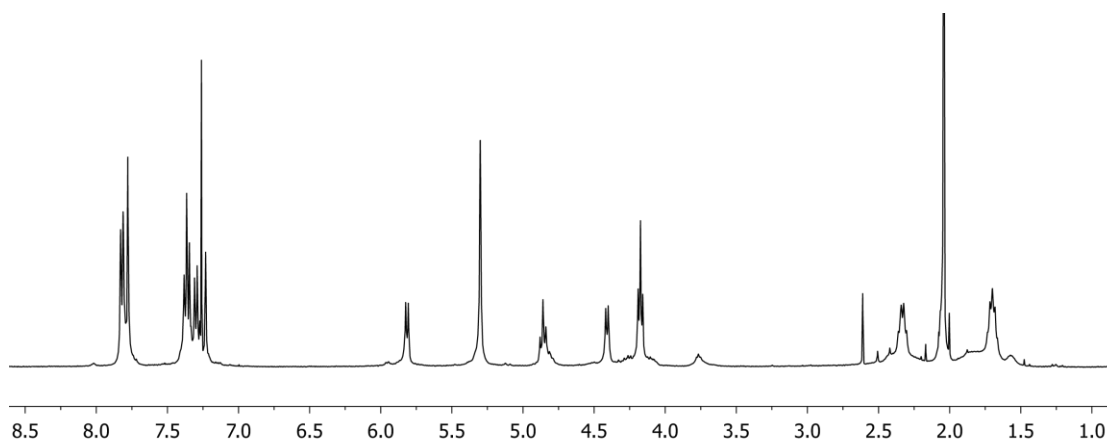
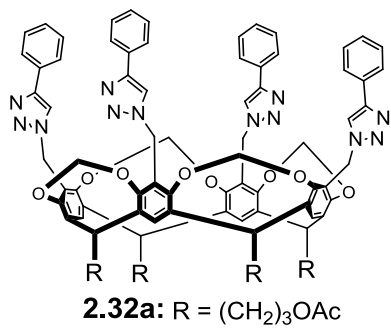


Figure 6.21. ¹H NMR spectrum (300 MHz, CDCl₃, 298K) of **2.32a**

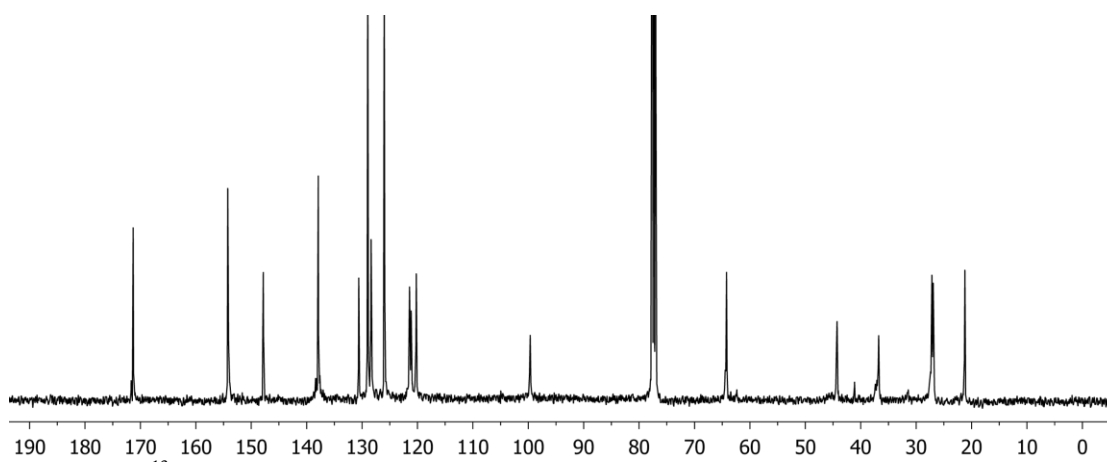


Figure 6.22. ¹³C NMR spectrum (100 MHz, CDCl₃, 298K) of **2.32a**

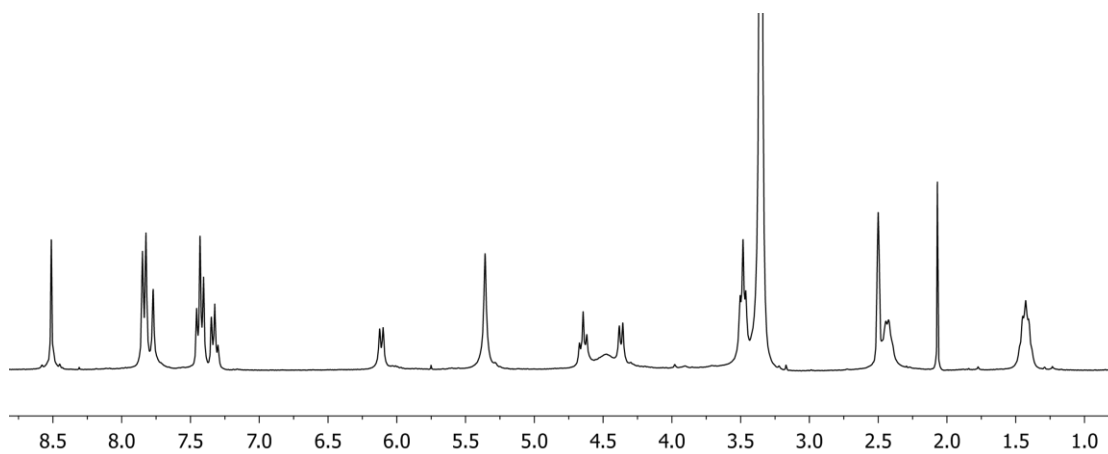
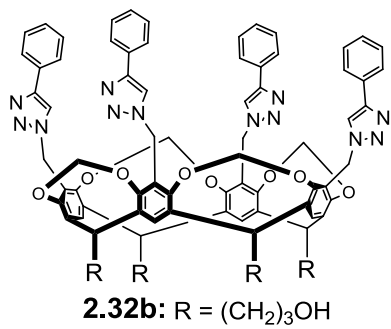


Figure 6.23. ^1H NMR spectrum (300 MHz, DMSO, 298K) of **2.32b**

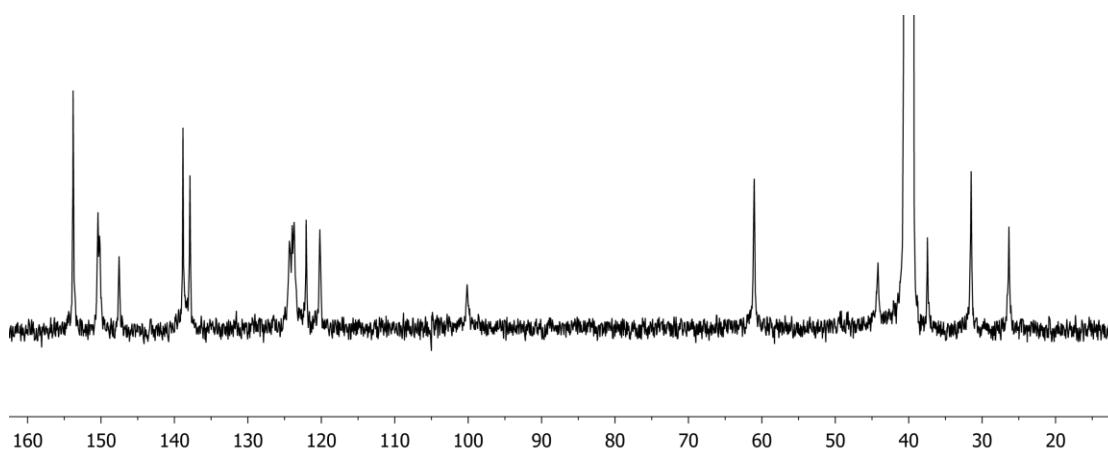


Figure 6.24. ^{13}C NMR spectrum (100 MHz, DMSO, 298K) of **2.32b**

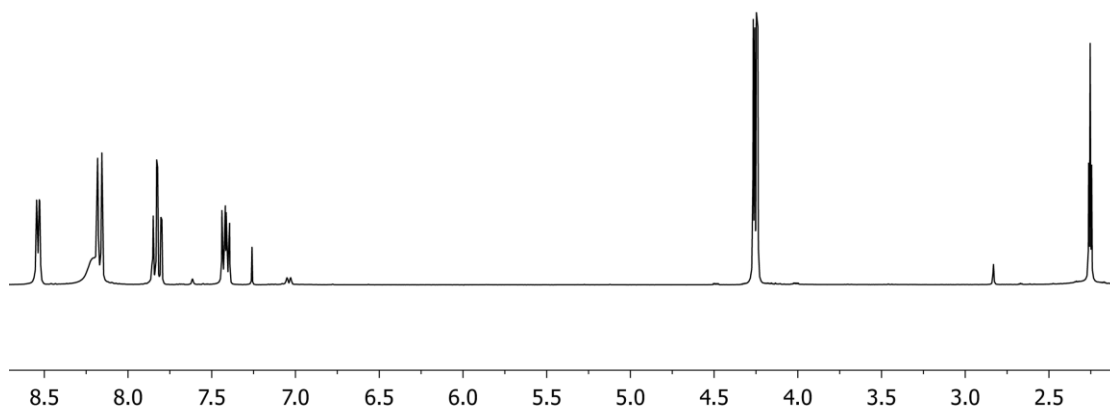
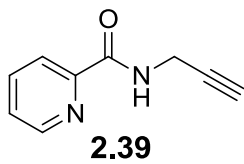


Figure 6.25. ¹H NMR spectrum (300 MHz, CDCl₃, 298K) of **2.39**

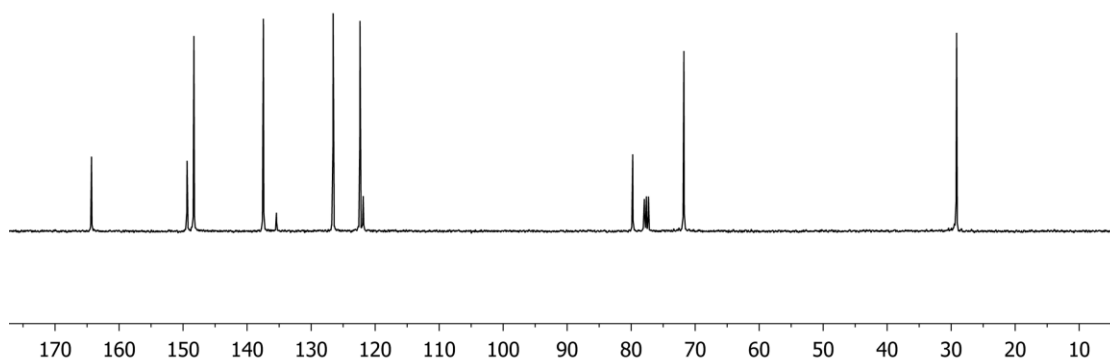


Figure 6.26. ¹³C NMR spectrum (100 MHz, CDCl₃, 298K) of **2.39**

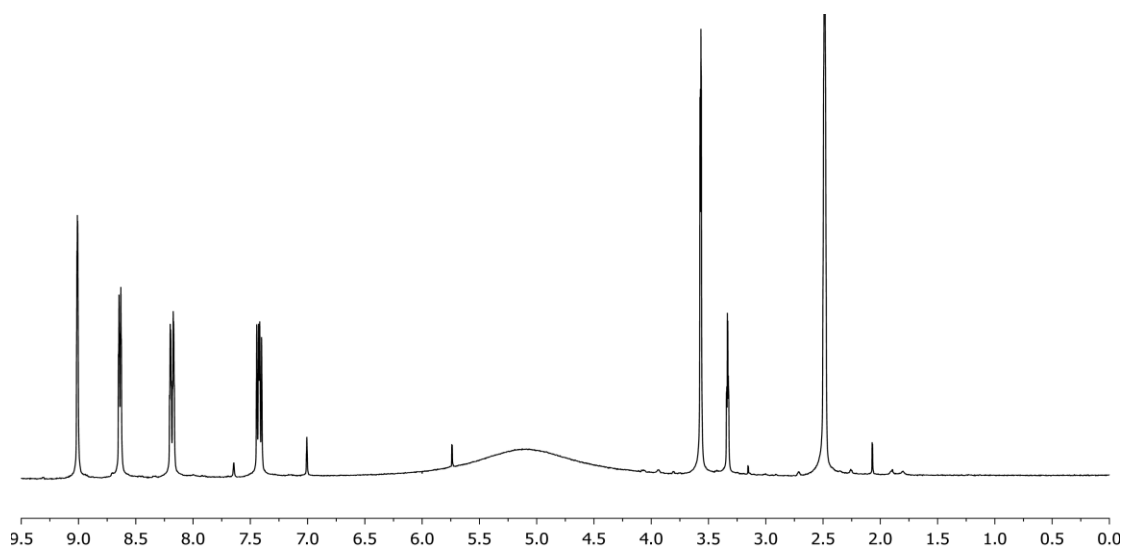
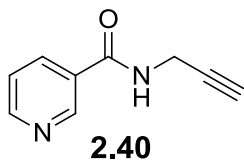


Figure 6.27. ^1H NMR spectrum (300 MHz, DMSO, 298K) of **2.40**

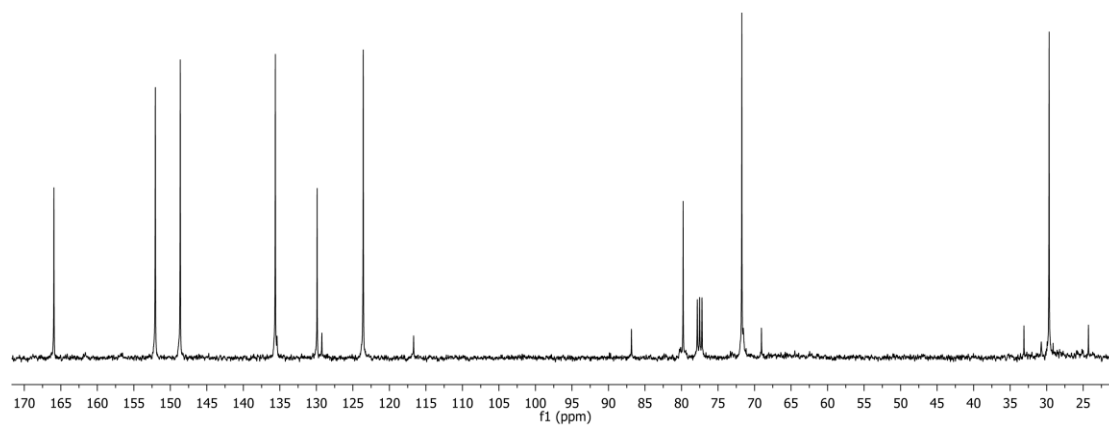


Figure 6.28. ^{13}C NMR spectrum (100 MHz, CDCl_3 , 298K) of **2.40**

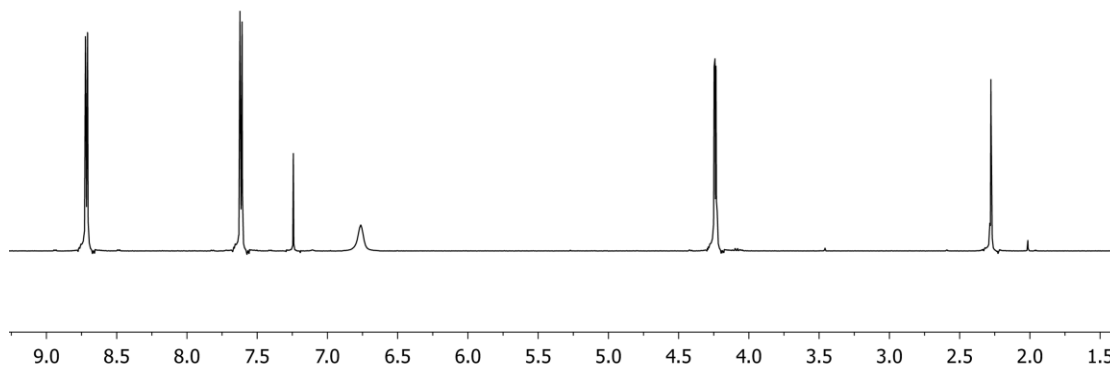
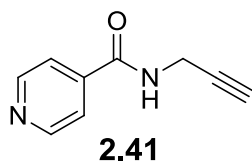


Figure 6.29. ¹H NMR spectrum (300 MHz, CDCl₃, 298K) of **2.41**

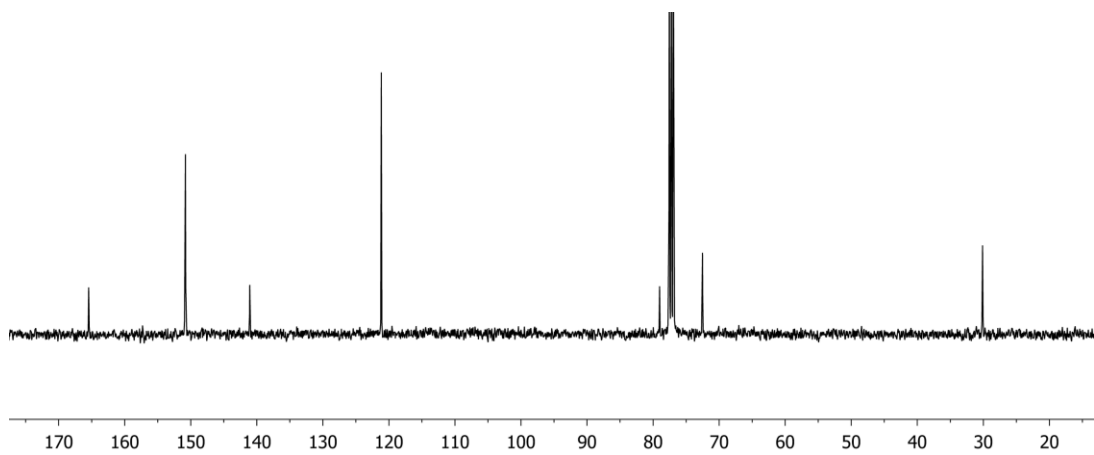


Figure 6.30. ¹³C NMR spectrum (100 MHz, CDCl₃, 298K) of **2.41**

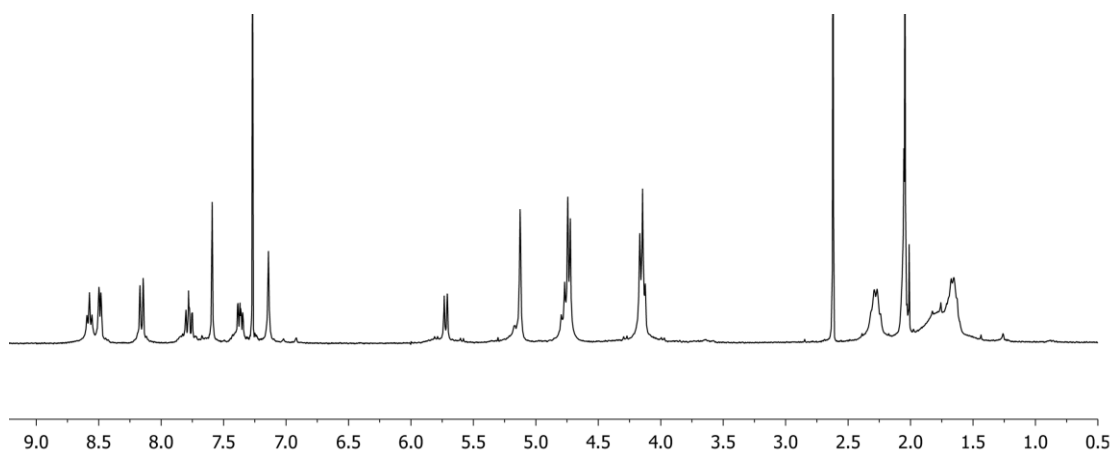
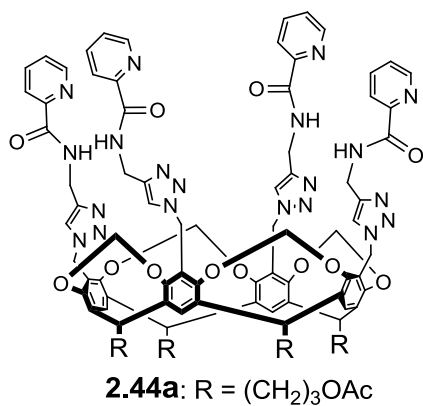


Figure 6.31. ¹H NMR spectrum (300 MHz, CDCl₃, 298K) of **2.44a**

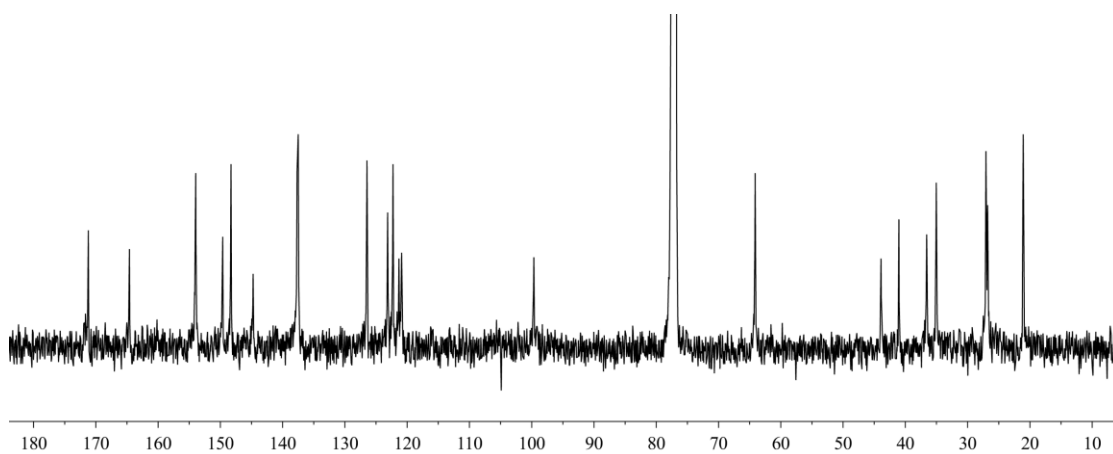


Figure 6.32. ¹³C NMR spectrum (100 MHz, CDCl₃, 298K) of **2.44a**

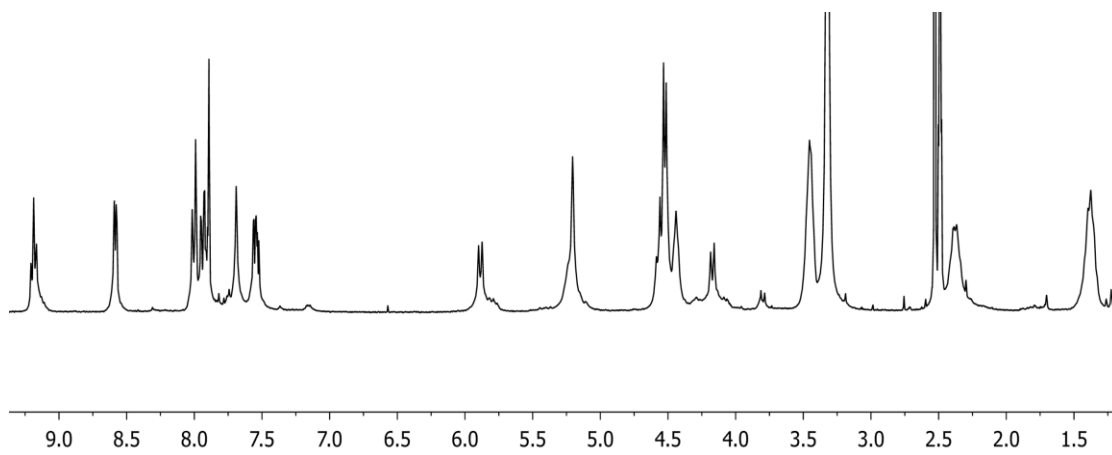
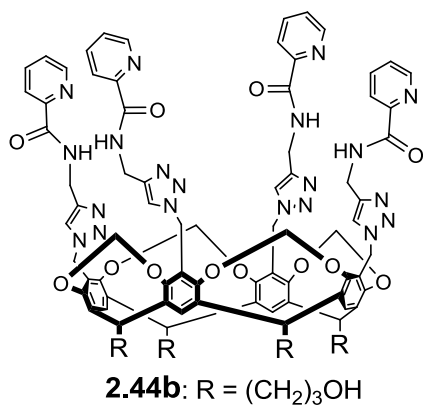


Figure 6.33. ¹H NMR spectrum (300 MHz, DMSO, 298K) of **2.44b**

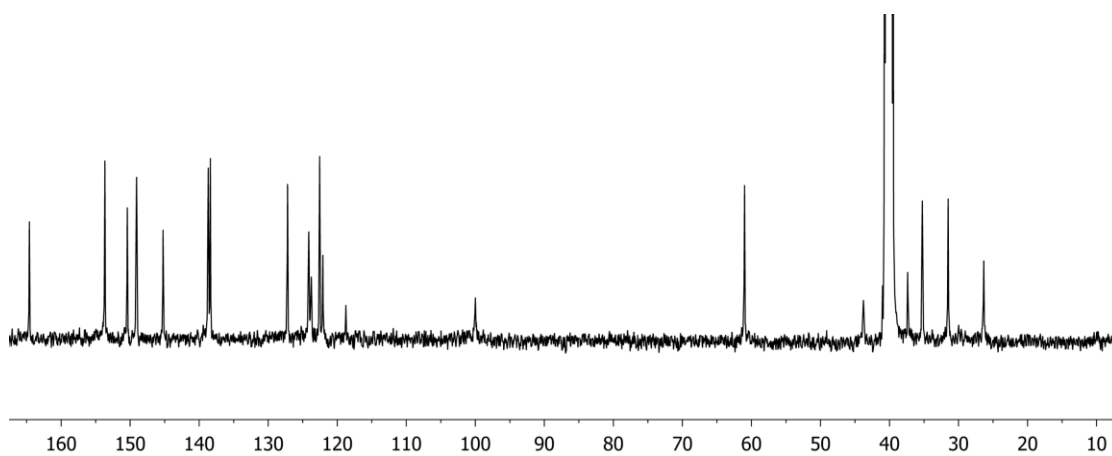


Figure 6.34. ¹³C NMR spectrum (100 MHz, DMSO, 298K) of **2.44b**

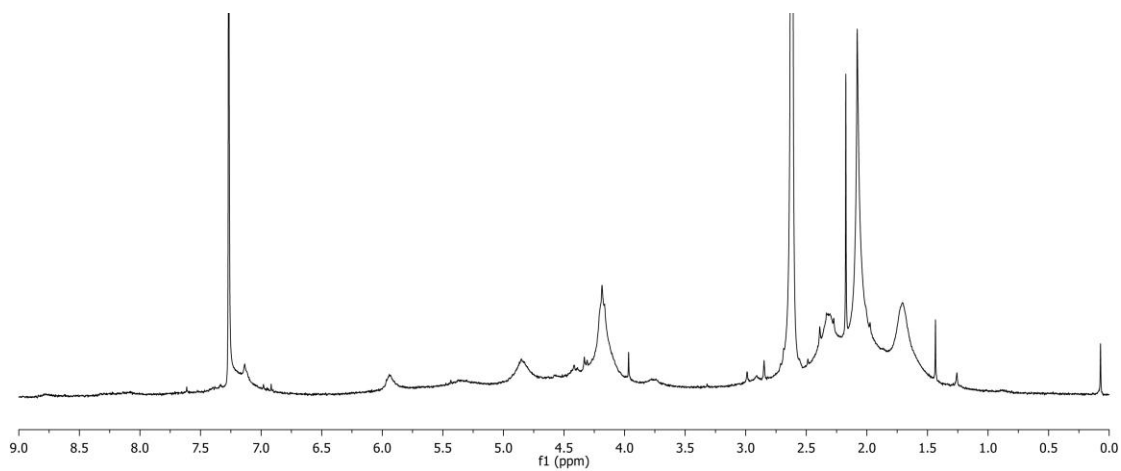
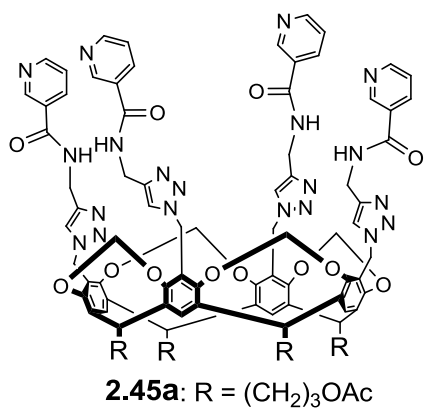
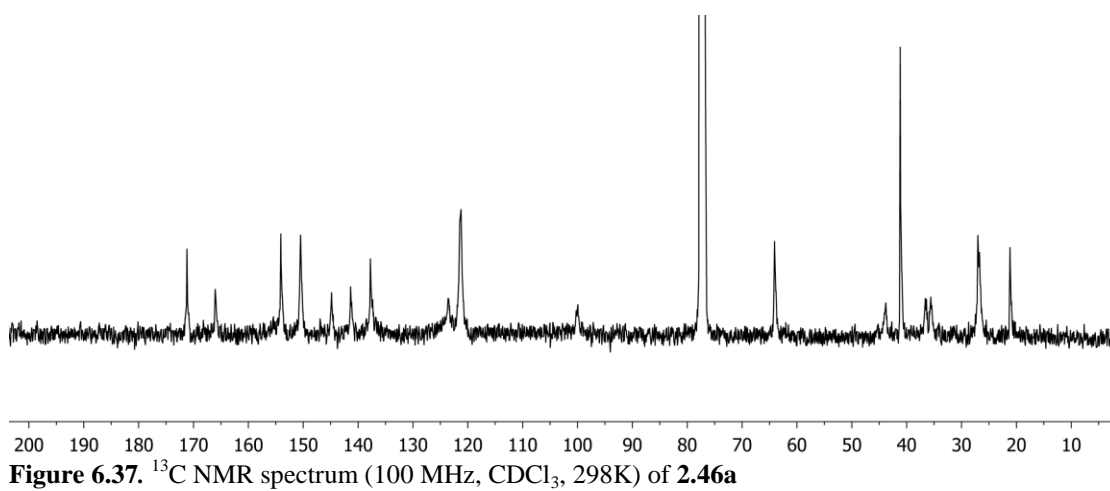
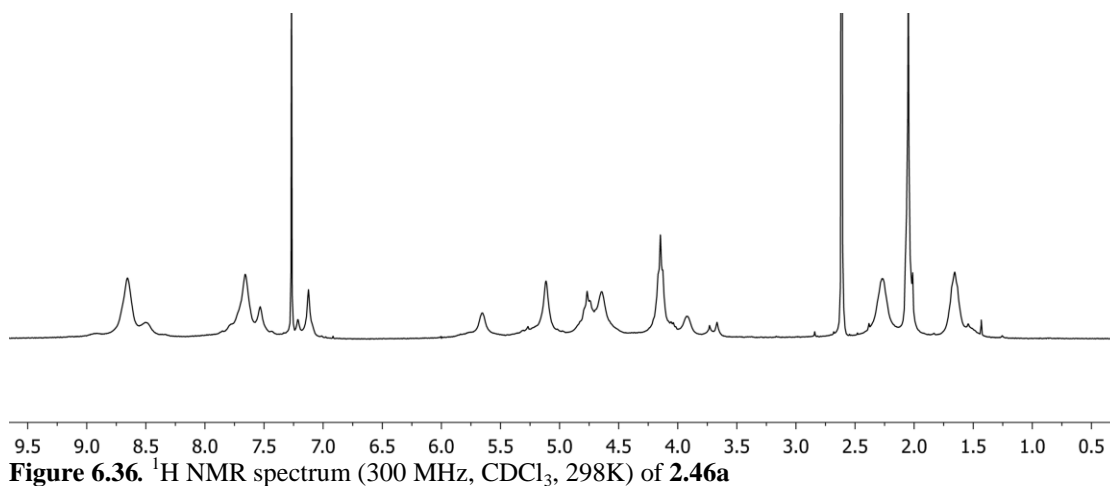
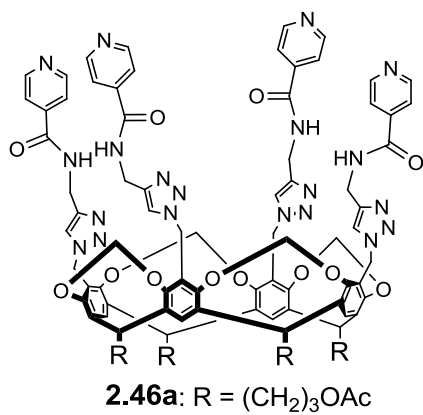
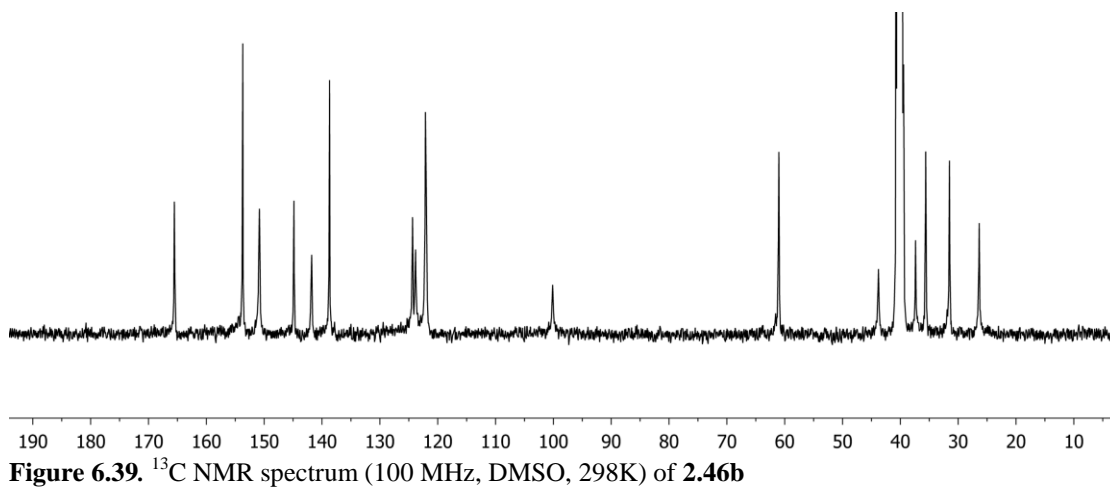
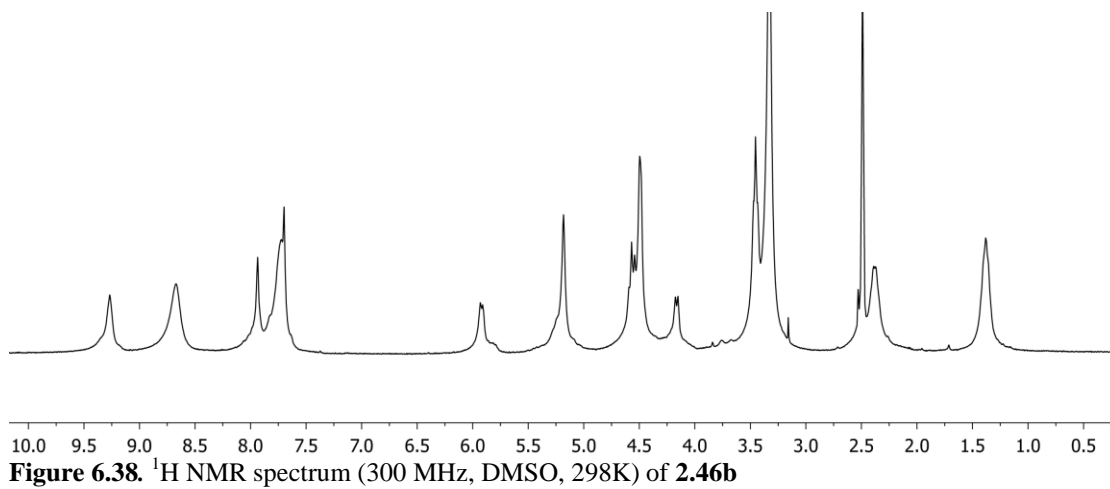
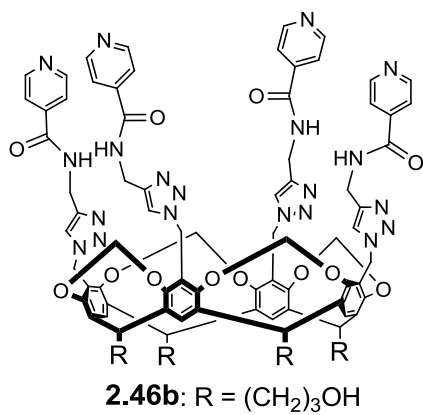


Figure 6.35. ^1H NMR spectrum (300 MHz, CDCl_3 , 298K) of **2.45a**





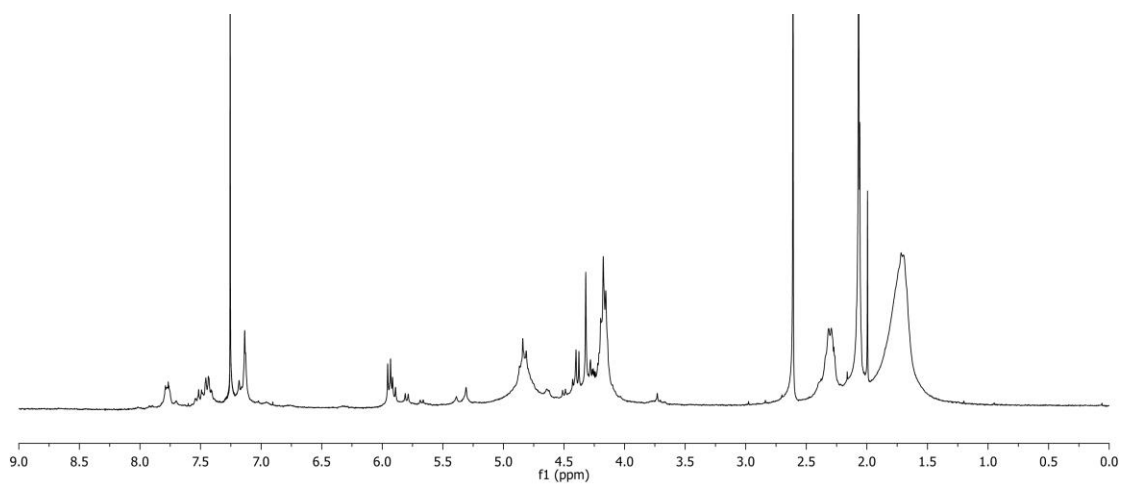
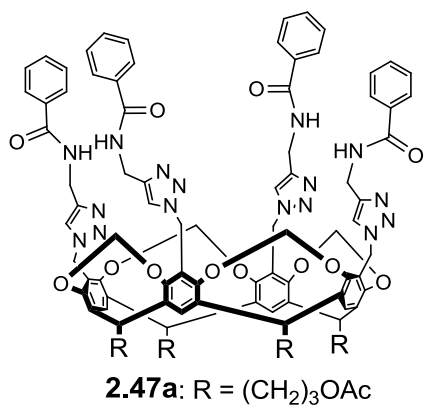


Figure 6.40. ¹H NMR spectrum (300 MHz, CDCl₃, 298K) of **2.47a**

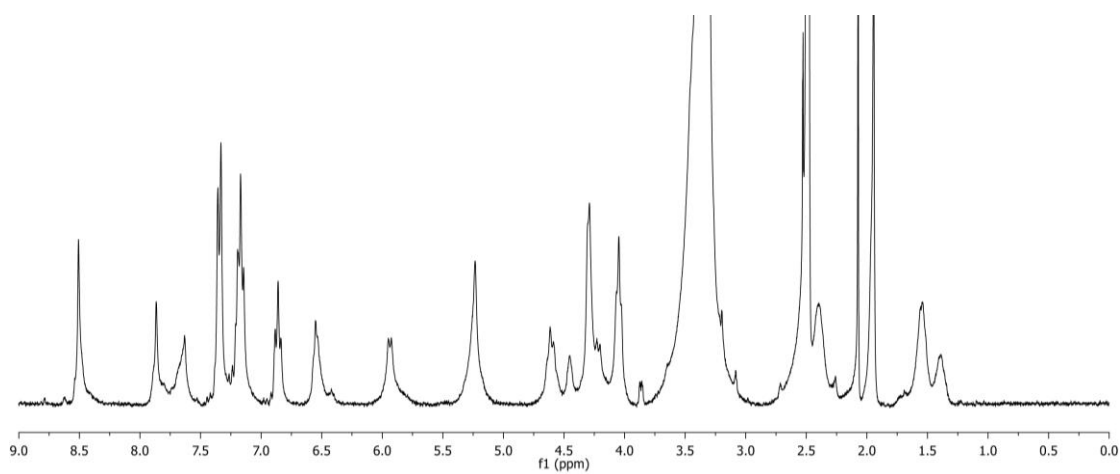
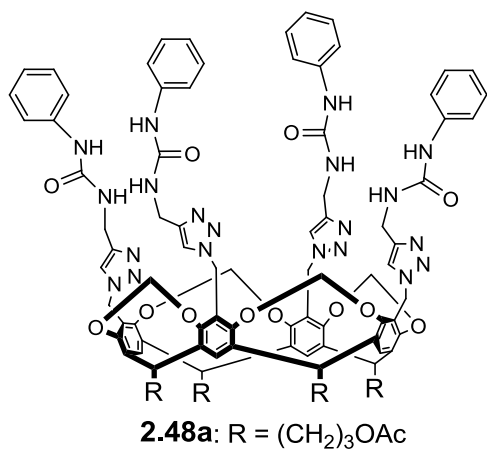


Figure 6.41. ¹H NMR spectrum (300 MHz, DMSO, 298K) of **2.48a**

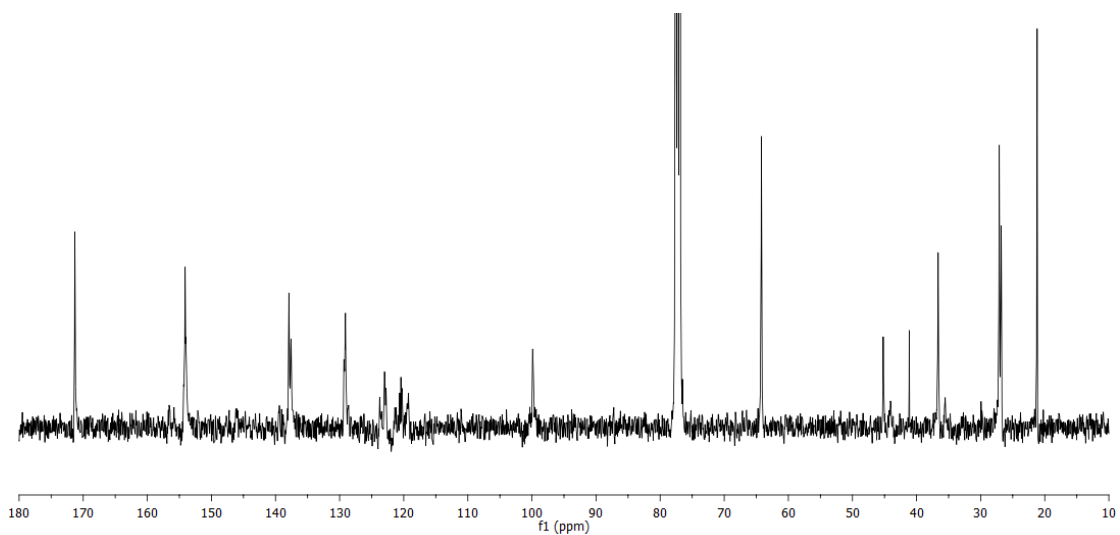


Figure 6.42. ¹³C NMR spectrum (100 MHz, DMSO, 298K) of **2.48a**

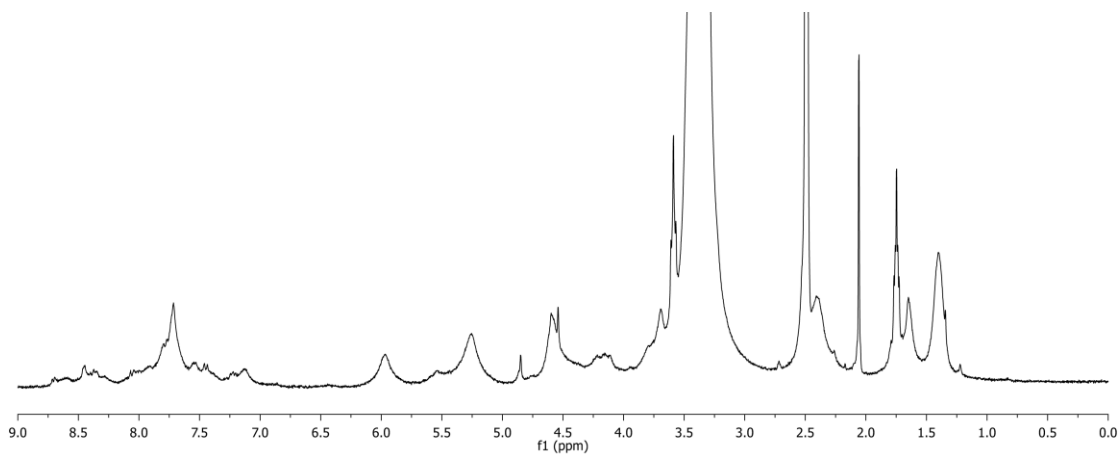
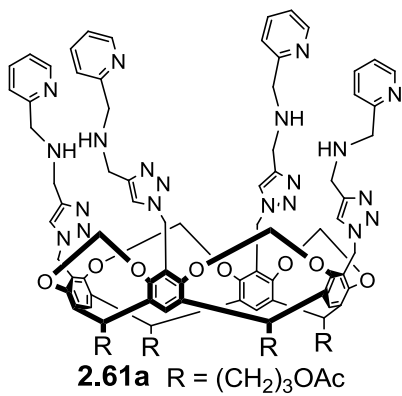


Figure 6.43. ¹H NMR spectrum (300 MHz, CDCl₃, 298K) of **2.61a**

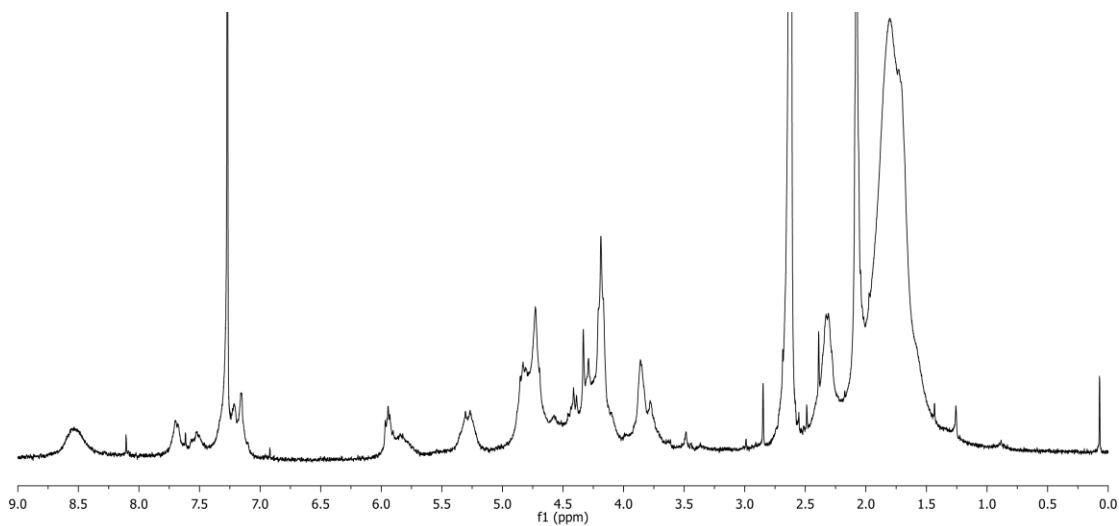


Figure 6.44. ¹H NMR spectrum (300 MHz, CDCl₃, 298K) of **2.62a**

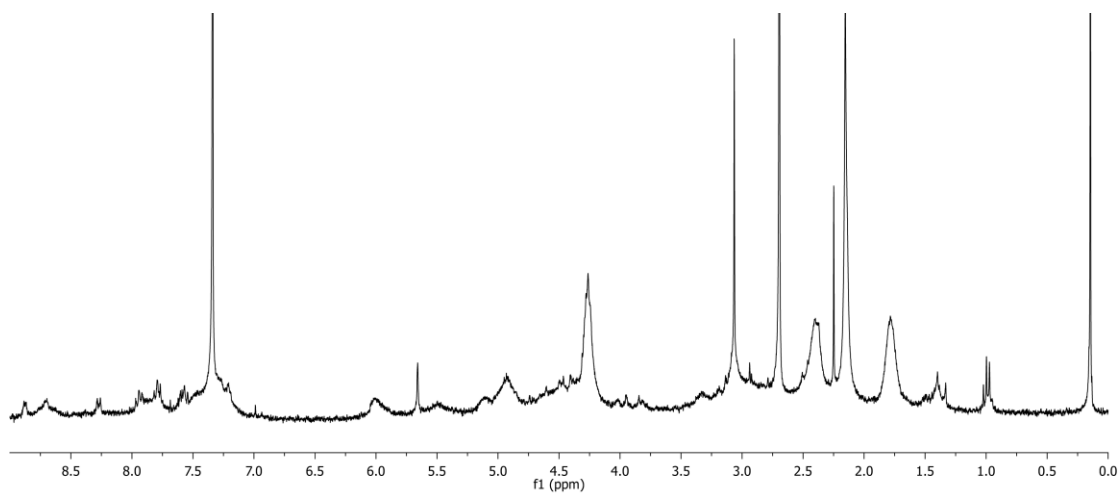
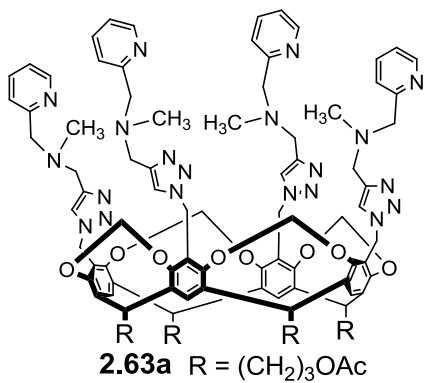


Figure 6.45. ¹H NMR spectrum (300 MHz, CDCl₃, 298K) of **2.63a**

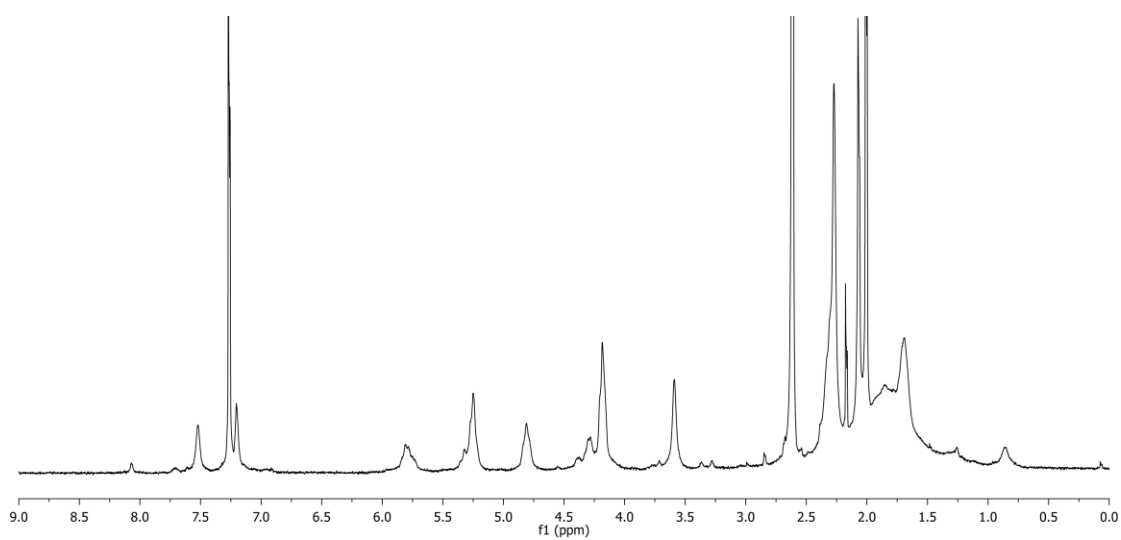
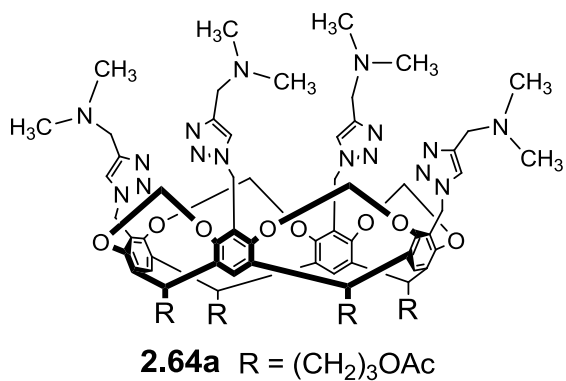


Figure 6.46. ¹H NMR spectrum (300 MHz, CDCl₃, 298K) of **2.64a**

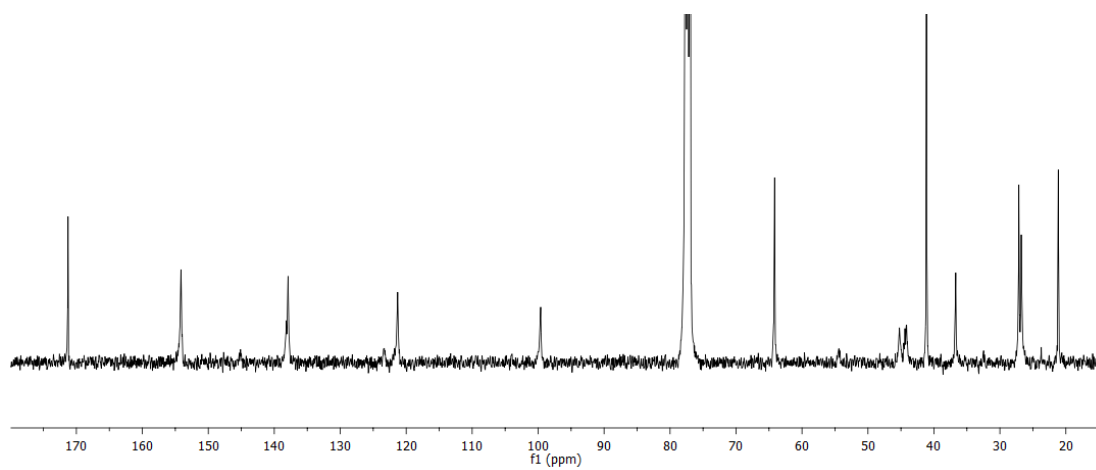


Figure 6.47. ¹³C NMR spectrum (100 MHz, CDCl₃, 298K) of **2.64a**

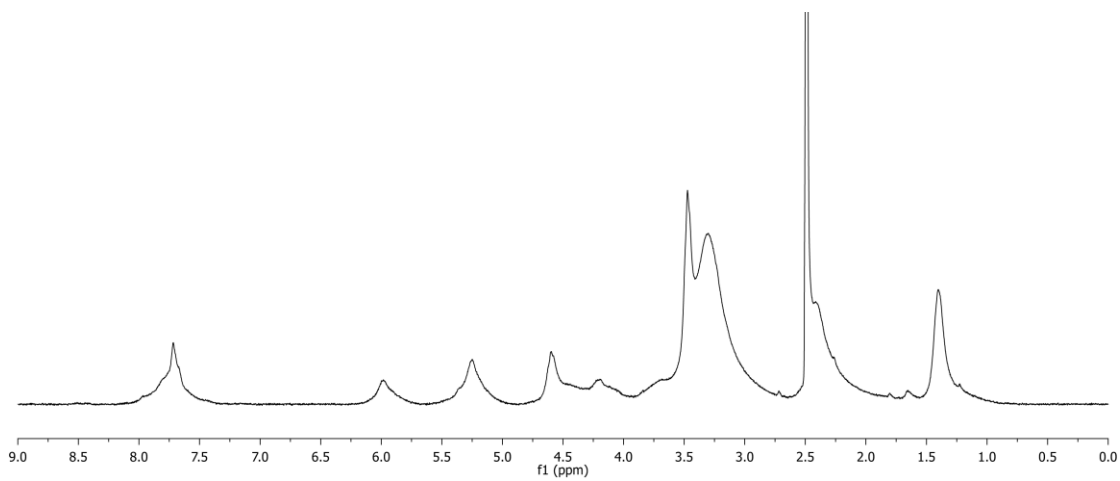
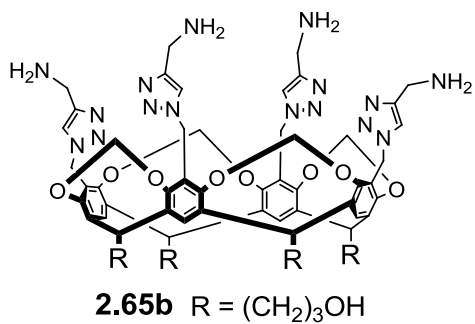


Figure 6.48. ¹H NMR spectrum (300 MHz, DMSO, 298K) of **2.65b**

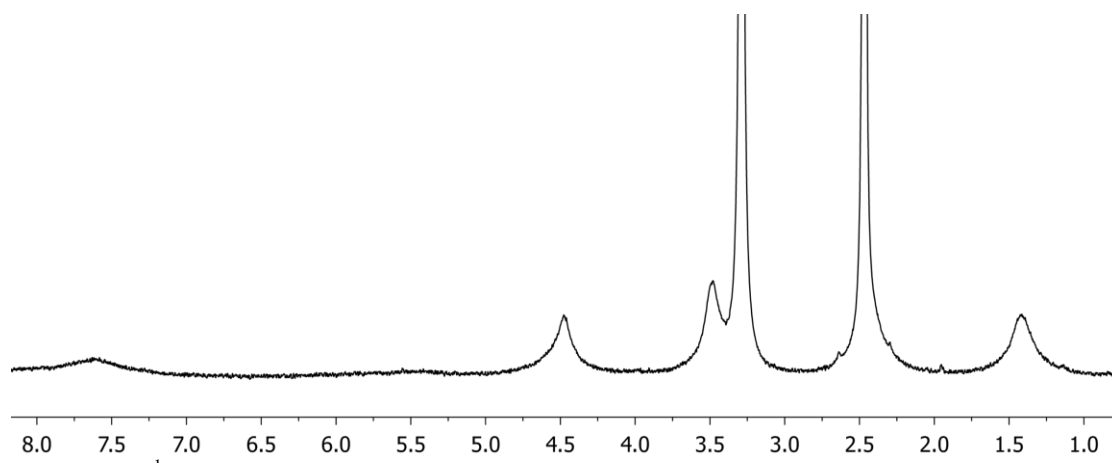
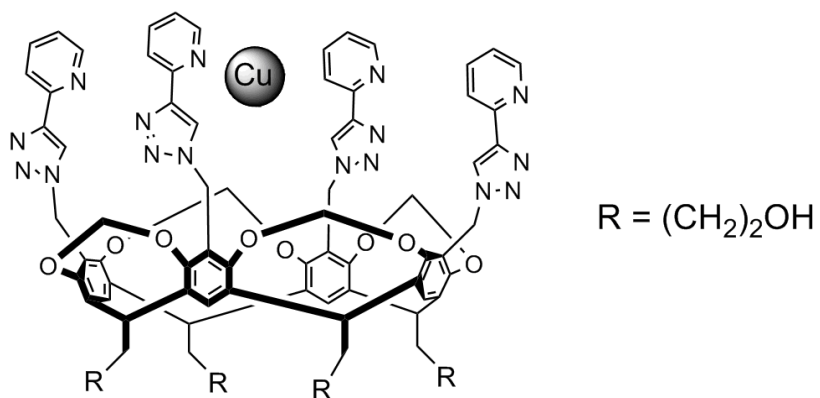


Figure 6.49. ¹H NMR spectrum (300 MHz, DMSO, 298K) of **2.30b•Cu**

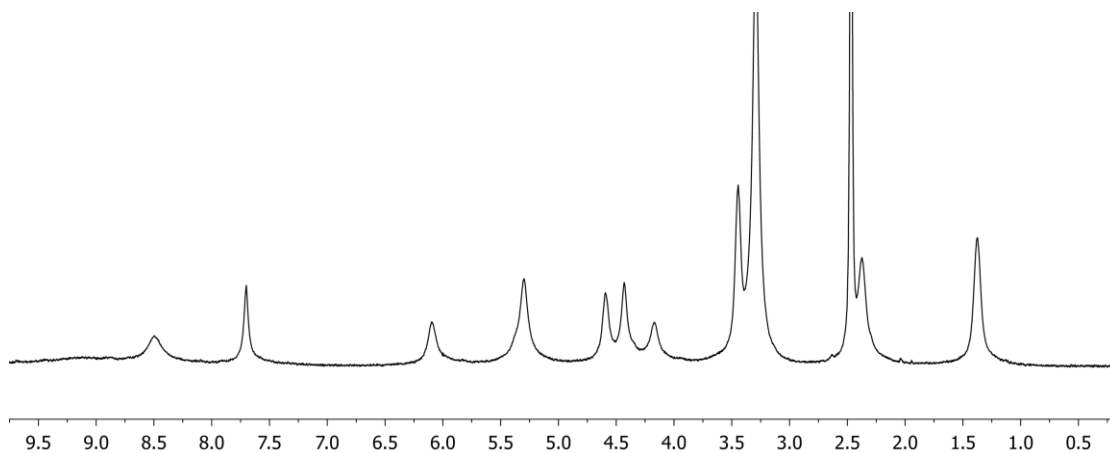
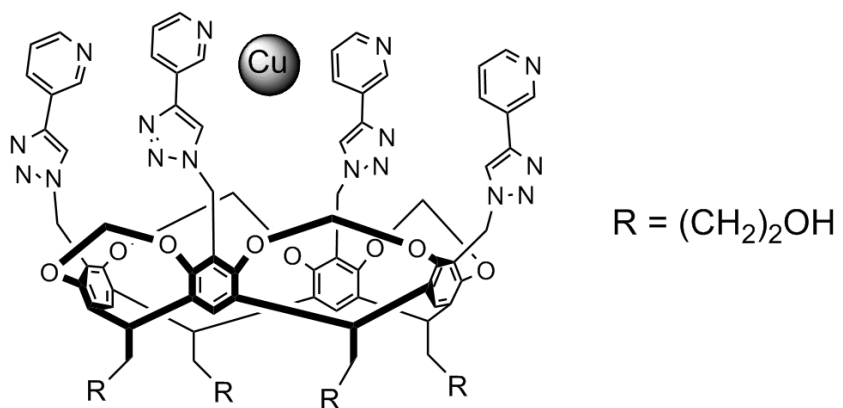


Figure 6.50. ^1H NMR spectrum (300 MHz, DMSO, 298K) of **2.31b**•Cu

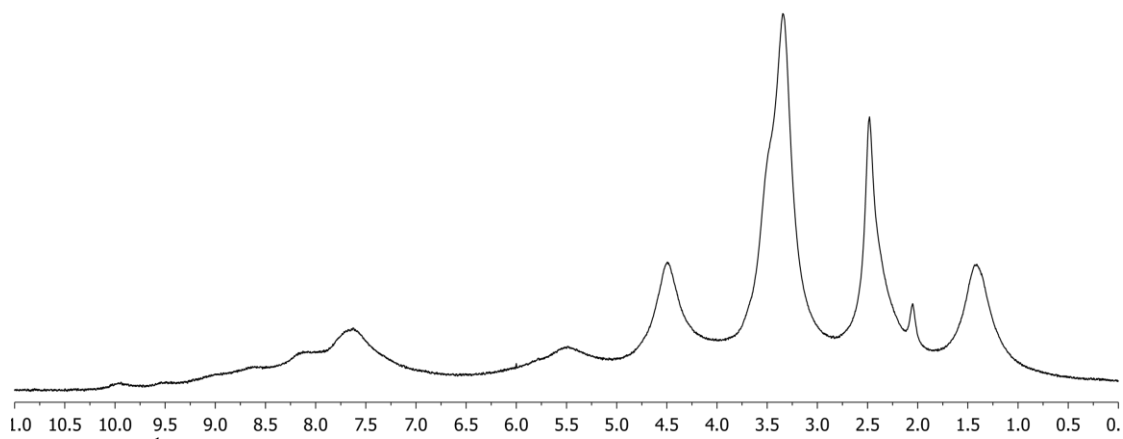
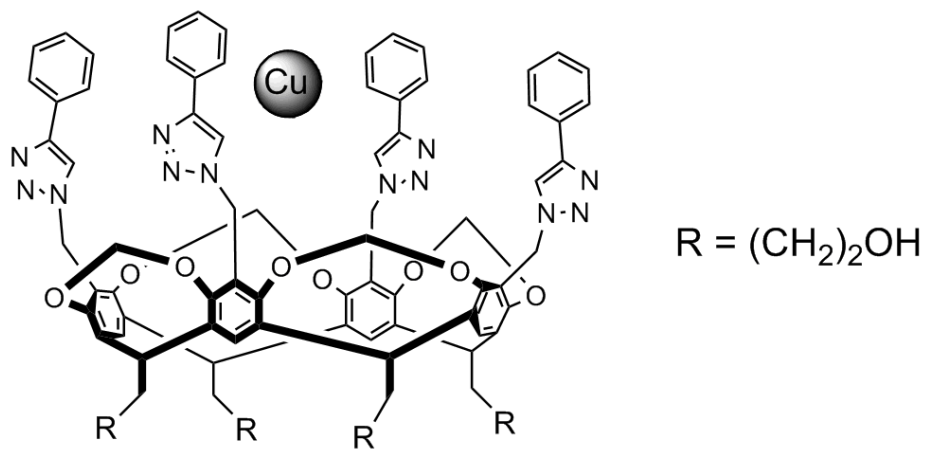
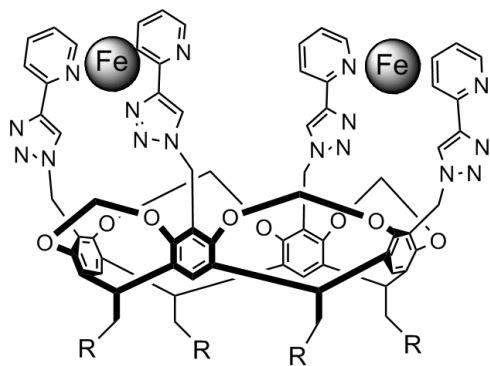


Figure 6.51. ^1H NMR spectrum (300 MHz, DMSO, 298K) of **2.32b**•Cu



2.30•Fe₂ a. R = (CH₂)₂OAc b. R = (CH₂)₂OH

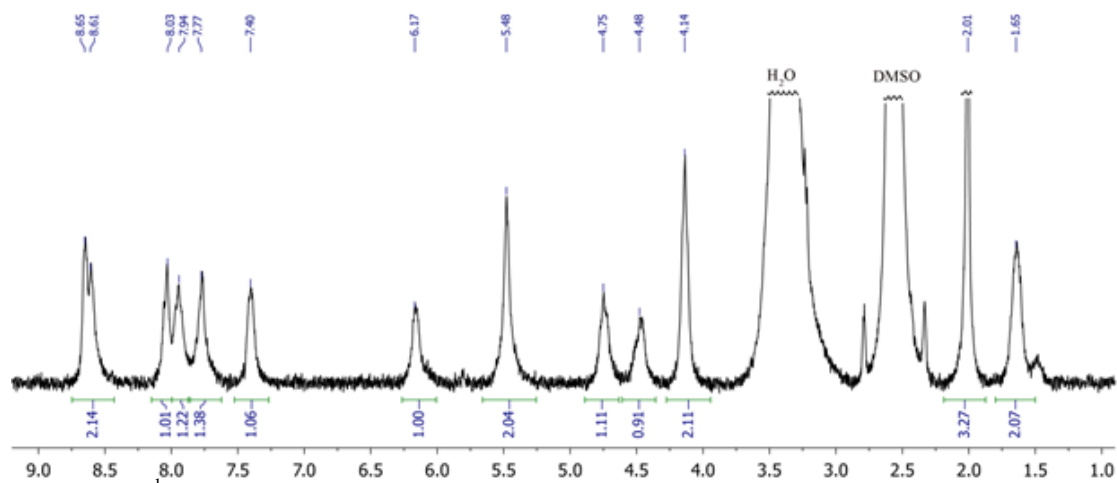


Figure 6.52. ¹H NMR spectrum (300 MHz, DMSO, 298K) of **2.30a**•Fe₂

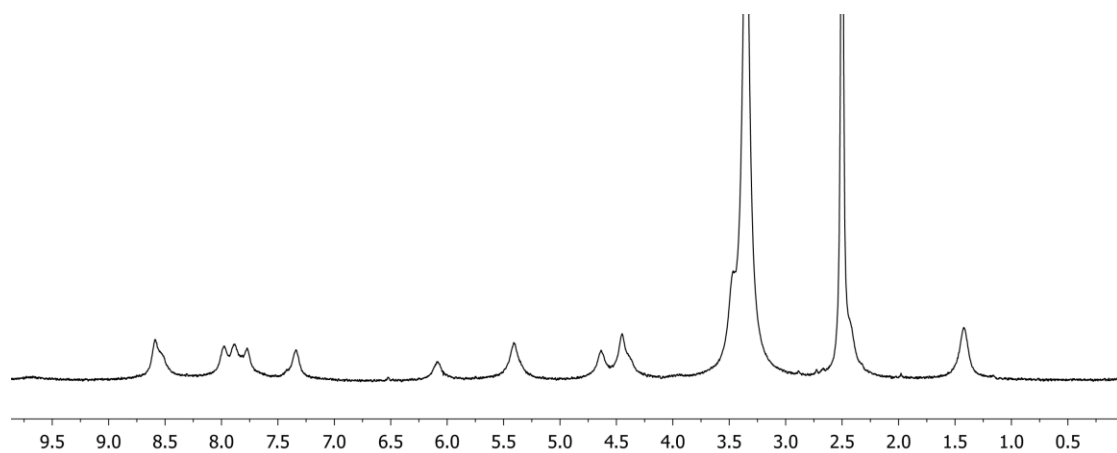


Figure 6.53. ¹H NMR spectrum (300 MHz, DMSO, 298K) of **2.30b**•Fe₂

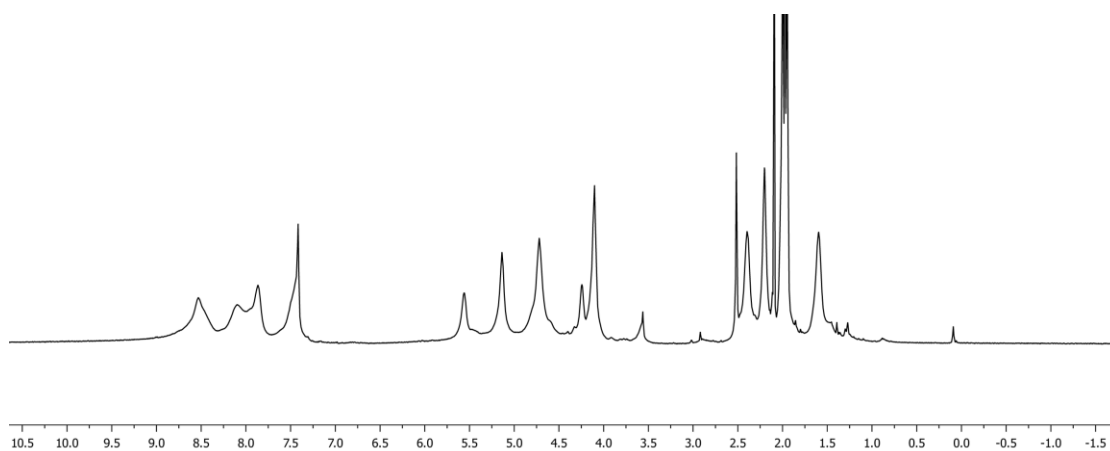
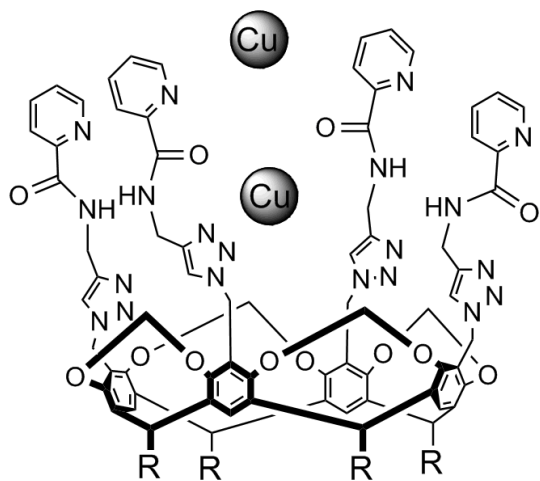


Figure 6.54. ¹H NMR spectrum (300 MHz, CD₃CN, 298K) of 2.44a•Cu_x

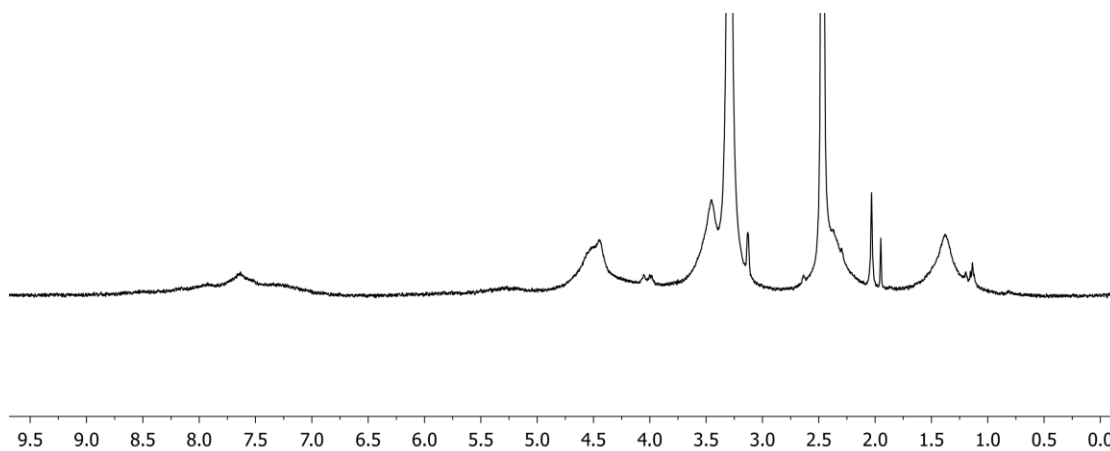


Figure 6.55. ¹H NMR spectrum (300 MHz, DMSO, 298K) of 2.44b•Cu_x

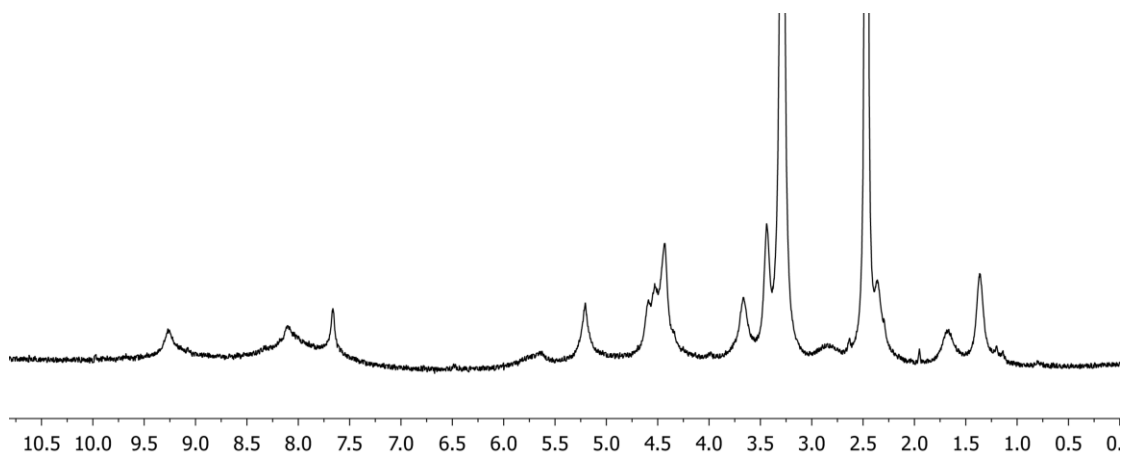
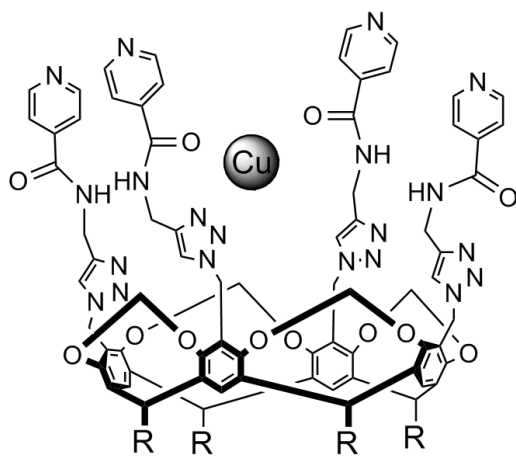
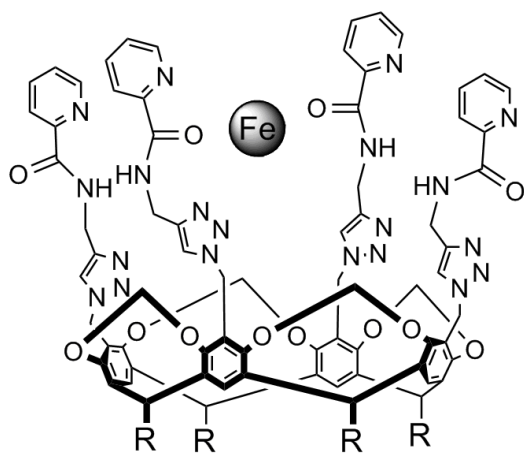


Figure 6.56. ¹H NMR spectrum (300 MHz, DMSO, 298K) of **2.46b**•Cu_x



2.44•Fe_x a. R = (CH₂)₃OAc b. R = (CH₂)₃OH

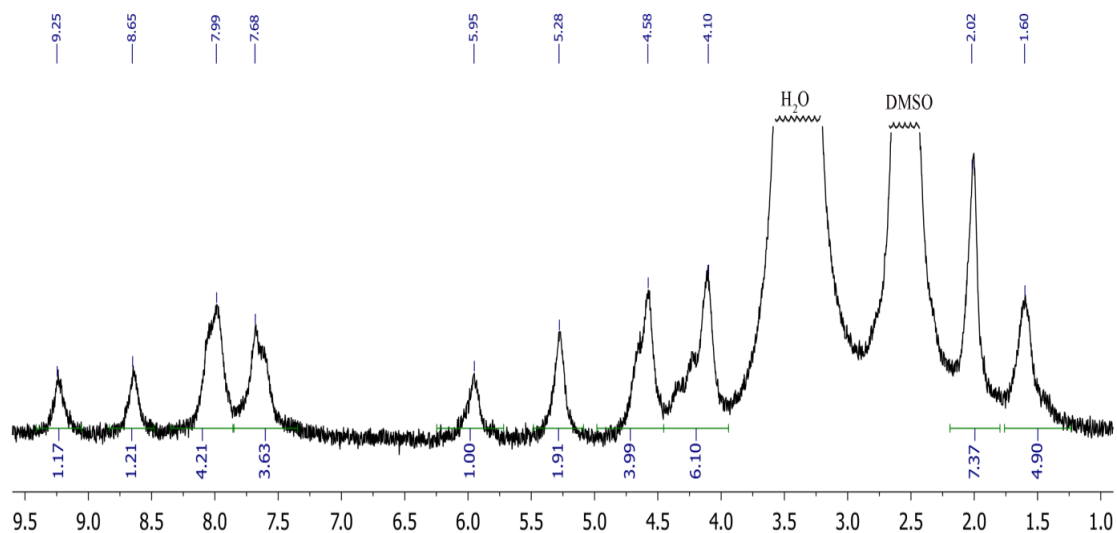


Figure 6.57. ¹H NMR spectrum (300 MHz, DMSO, 298K) of **2.44a•Fe_x**

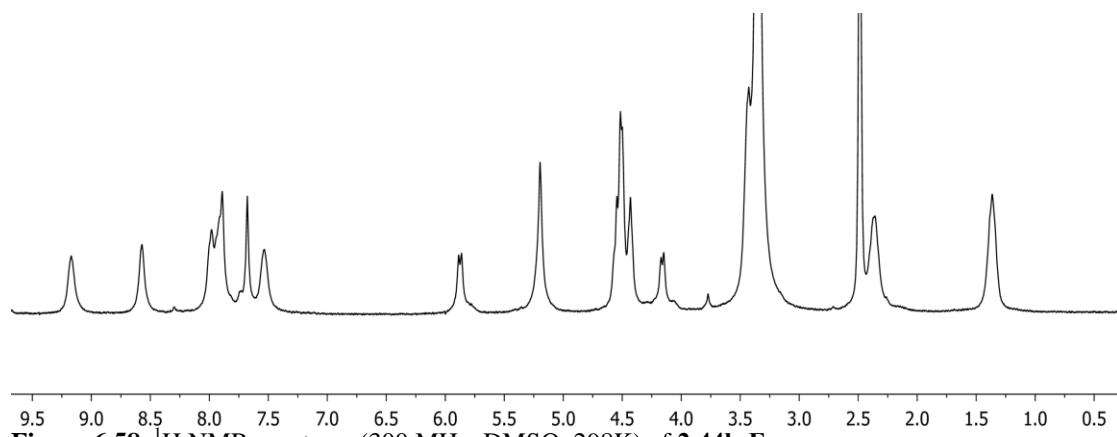


Figure 6.58. ¹H NMR spectrum (300 MHz, DMSO, 298K) of **2.44b•Fe_x**

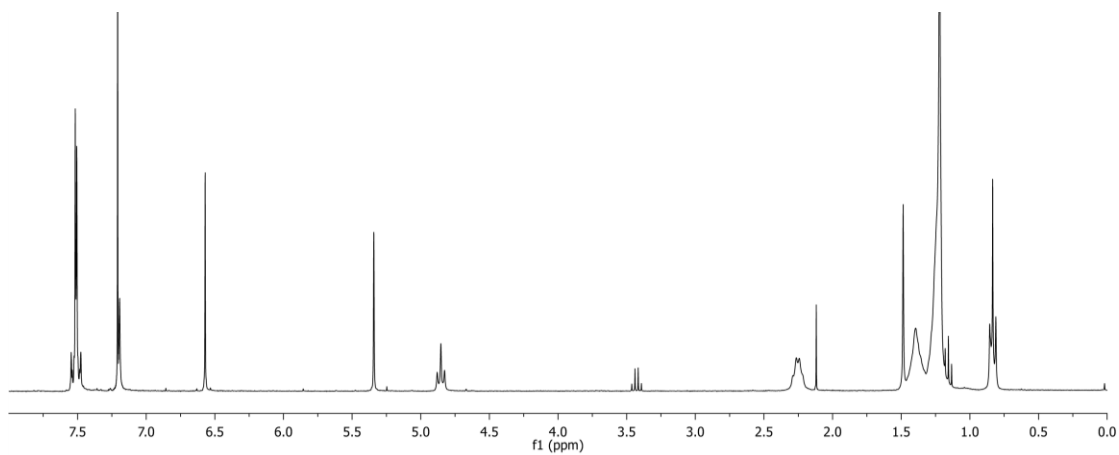
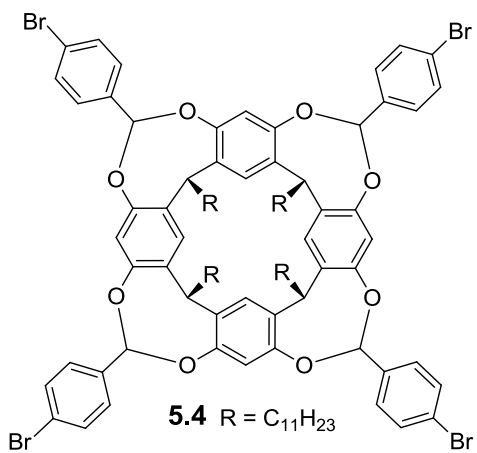


Figure 6.59. ¹H NMR spectrum (300 MHz, CDCl₃, 298K) of 5.4

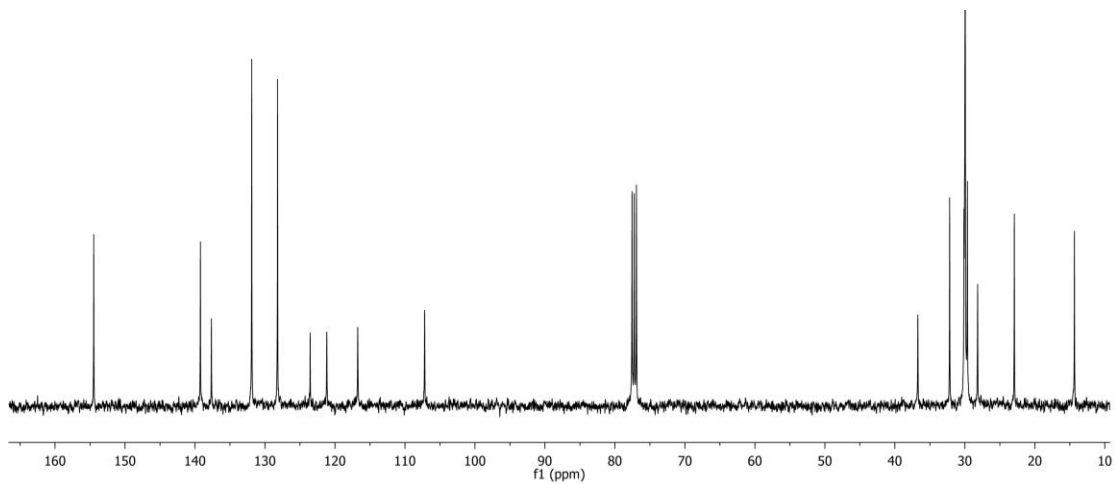


Figure 6.60. ¹³C NMR spectrum (100 MHz, DMSO, 298K) of 5.4

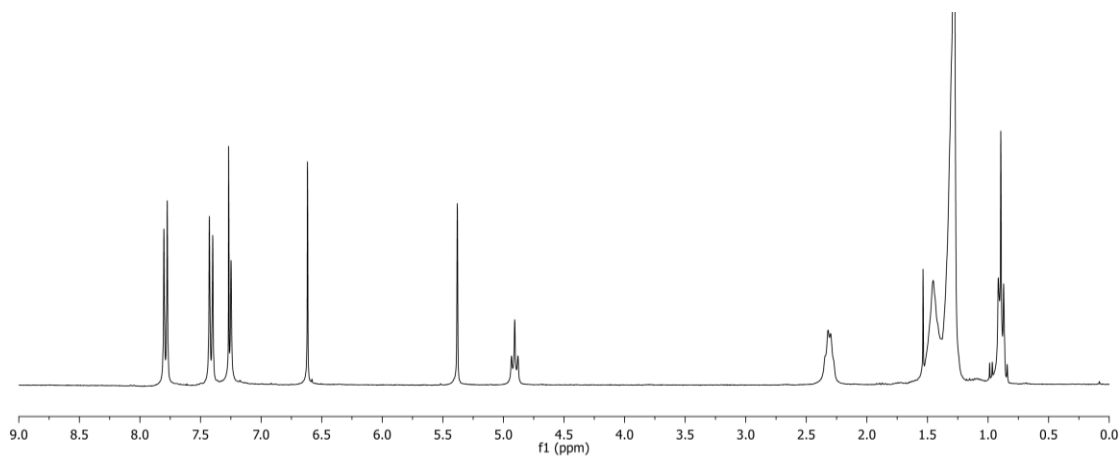
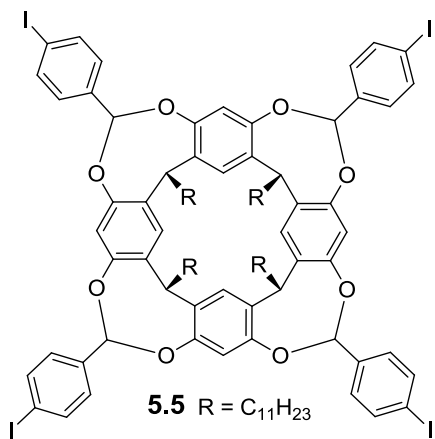


Figure 6.61. ¹H NMR spectrum (300 MHz, CDCl₃, 298K) of **5.5**

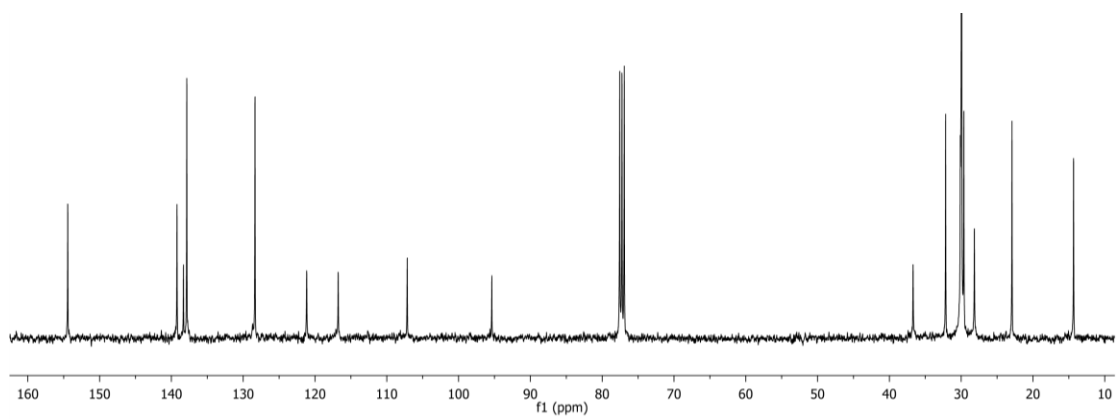


Figure 6.62. ¹³C NMR spectrum (100 MHz, DMSO, 298K) of **5.5**

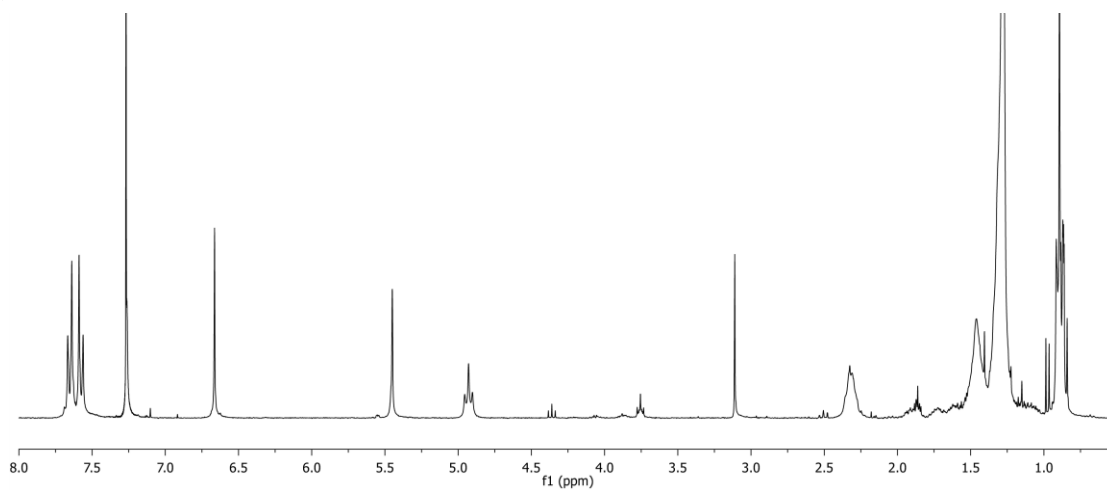
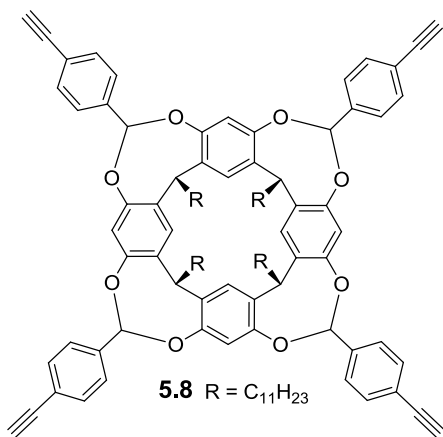


Figure 6.63. ¹H NMR spectrum (300 MHz, CDCl₃, 298K) of **5.8**

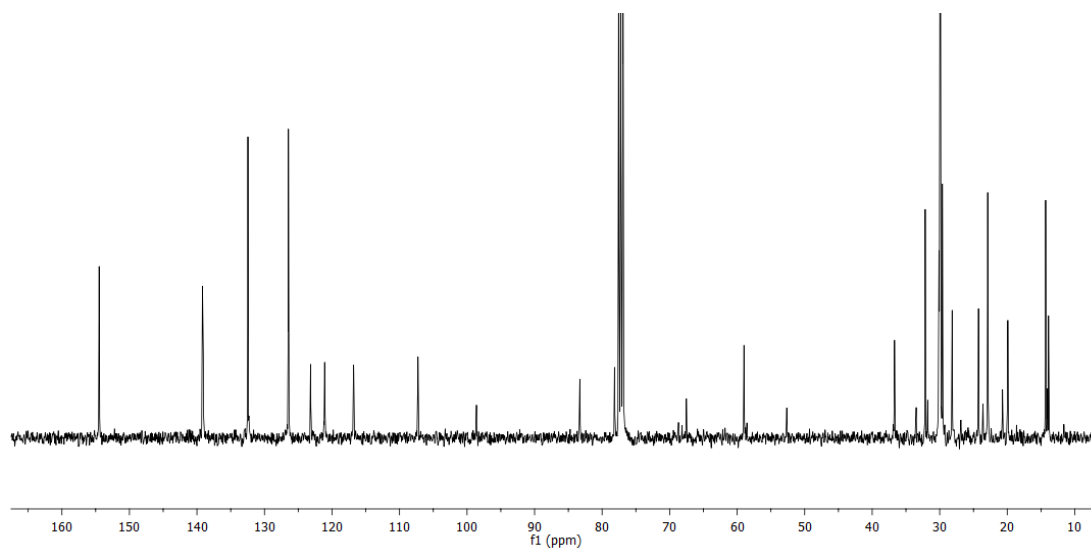


Figure 6.64. ¹³C NMR spectrum (100 MHz, DMSO, 298K) of **5.8**

6.7 Selected Mass Spectra

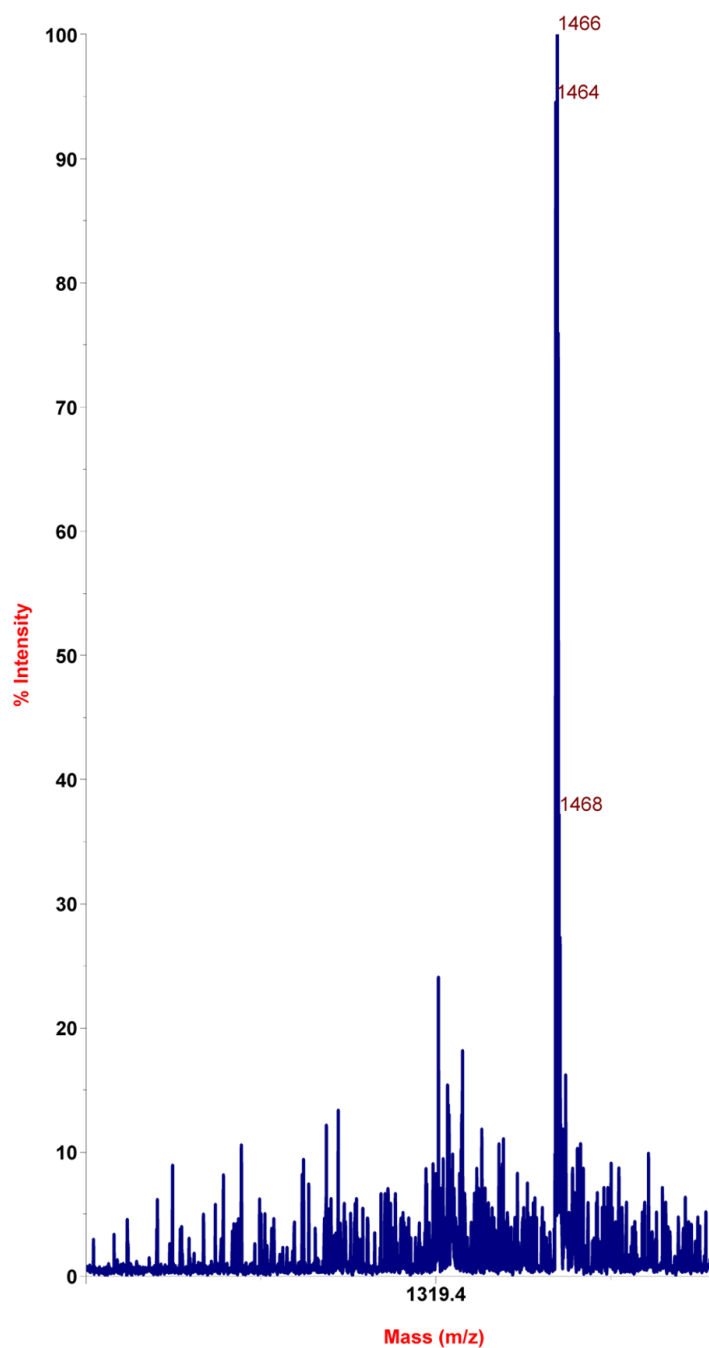


Figure 6.65. MALDI spectra of 2.30b•Cu

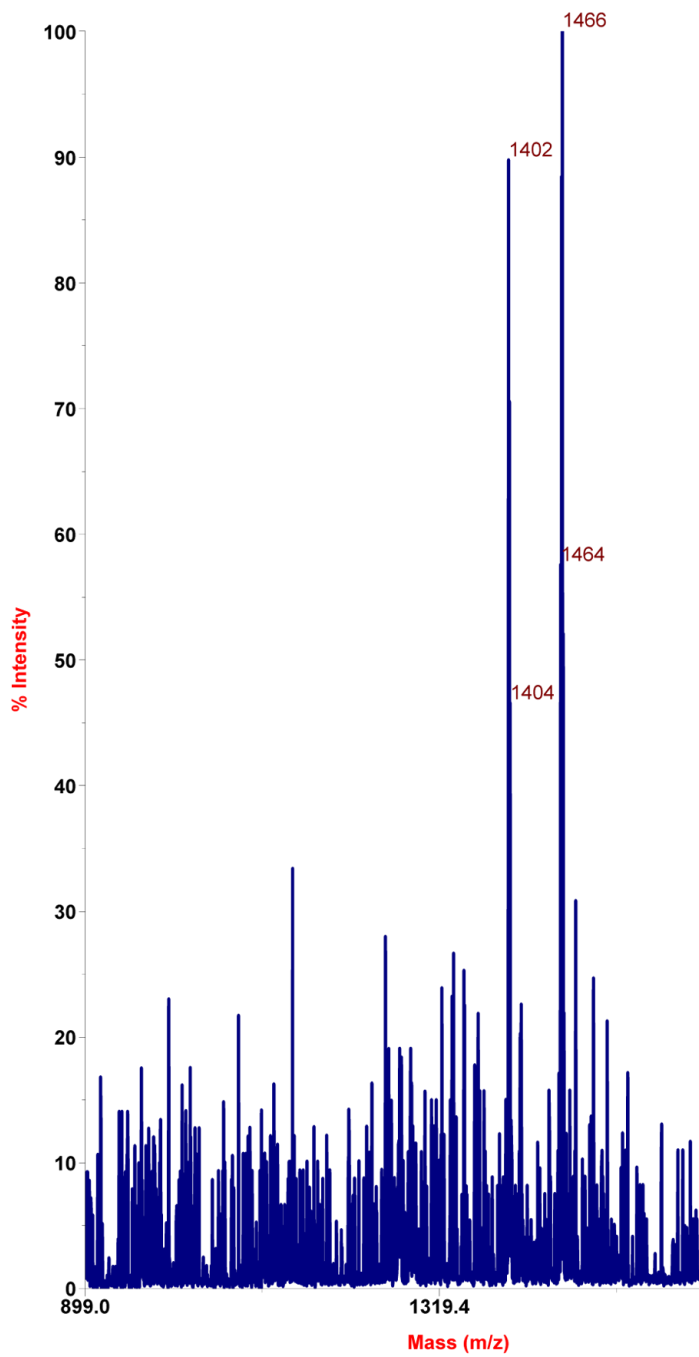


Figure 6.66. MALDI spectra of 2.31b•Cu

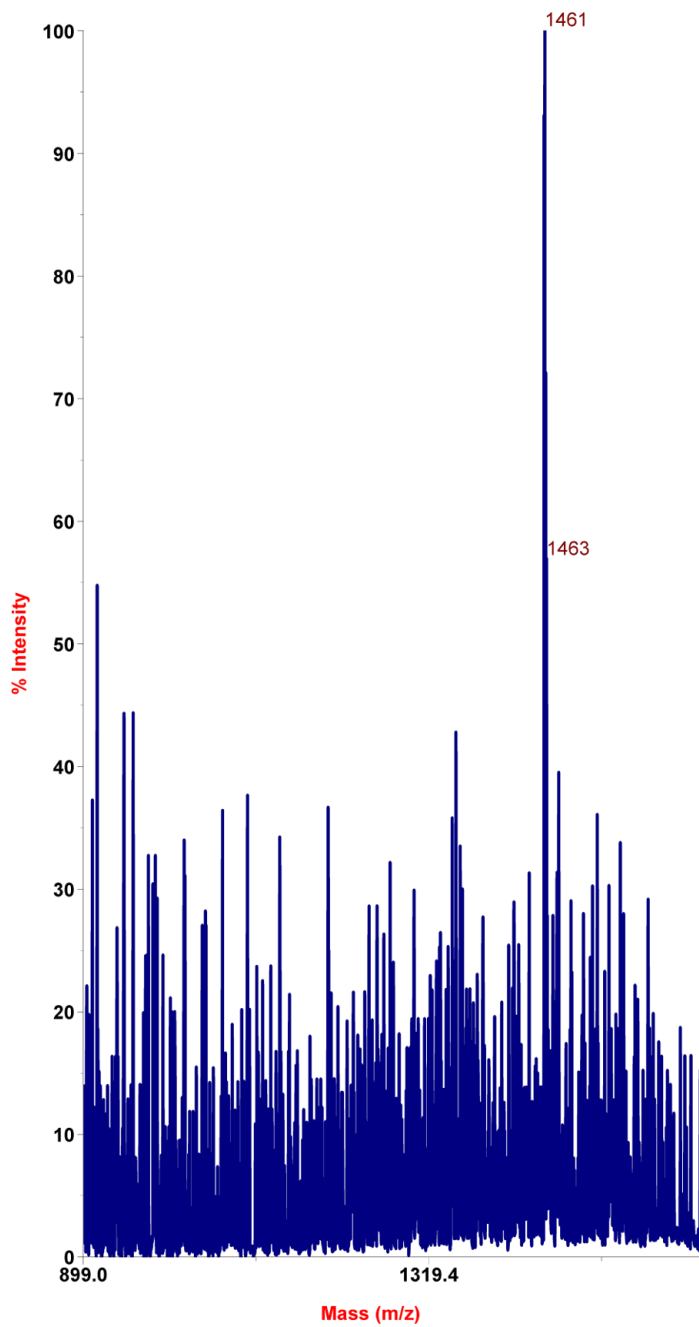


Figure 6.67. MALDI spectra of 2.32b•Cu

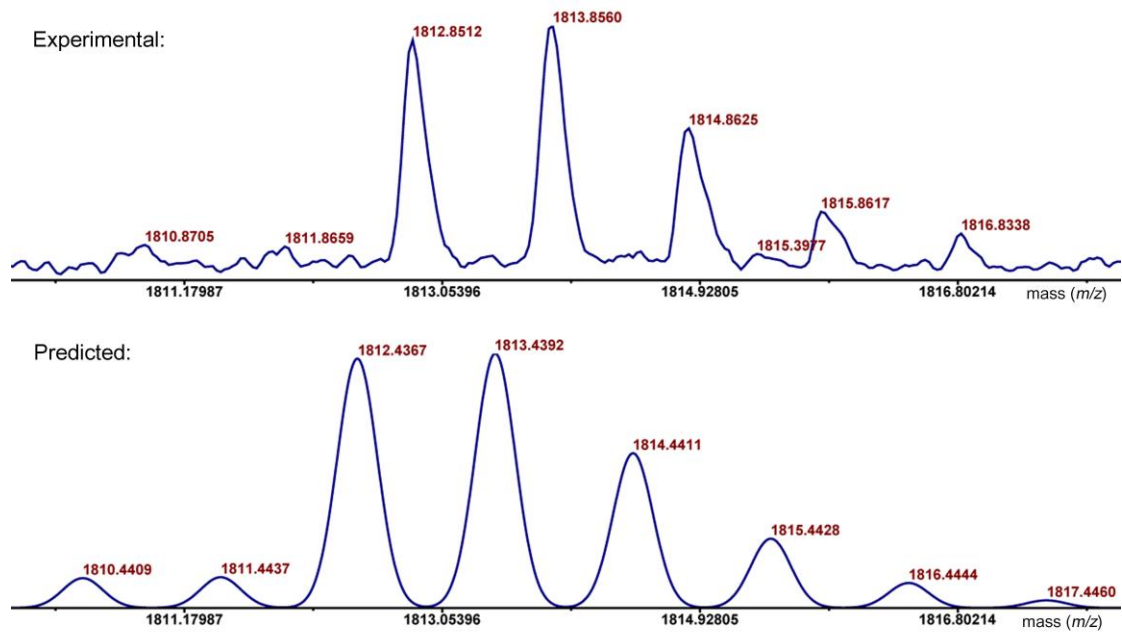


Figure 6.68. Experimental and predicted MALDI spectra of $2.30a \cdot Fe_2$

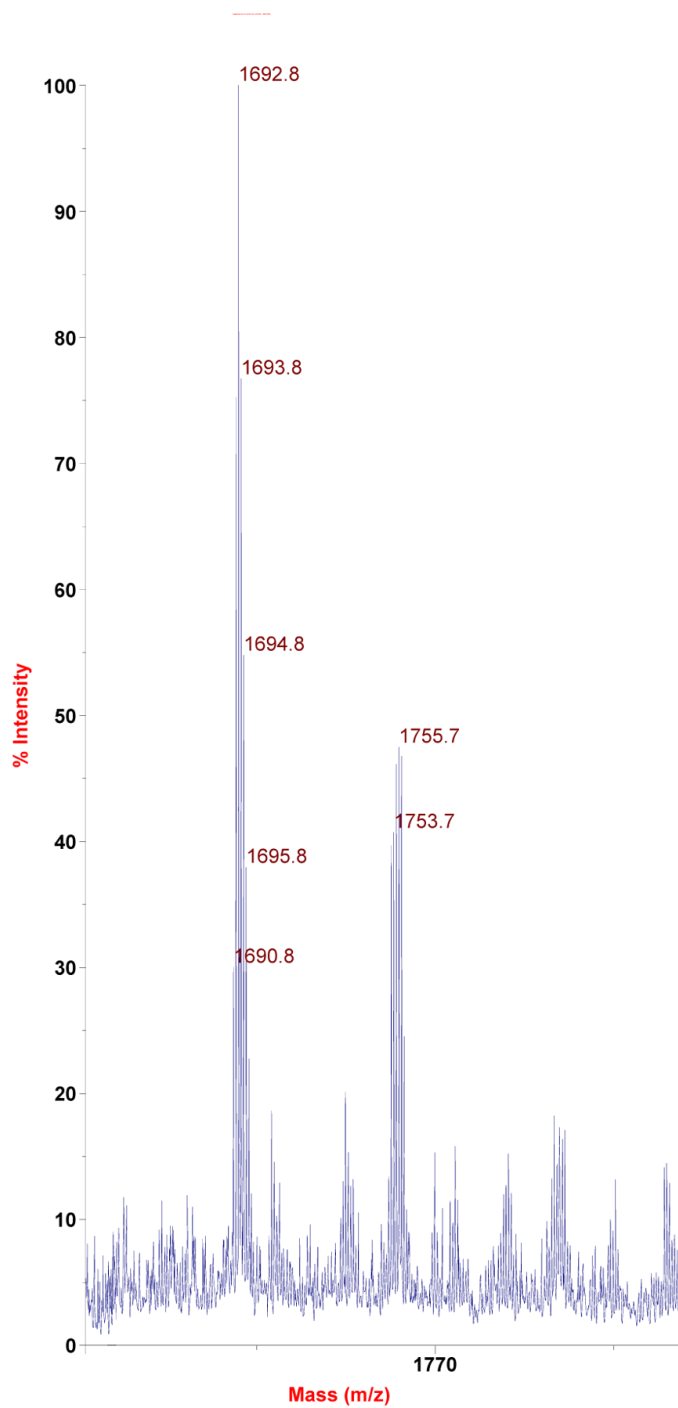


Figure 6.69. Experimental and predicted MALDI spectra of $2.44b \cdot Cu_x$

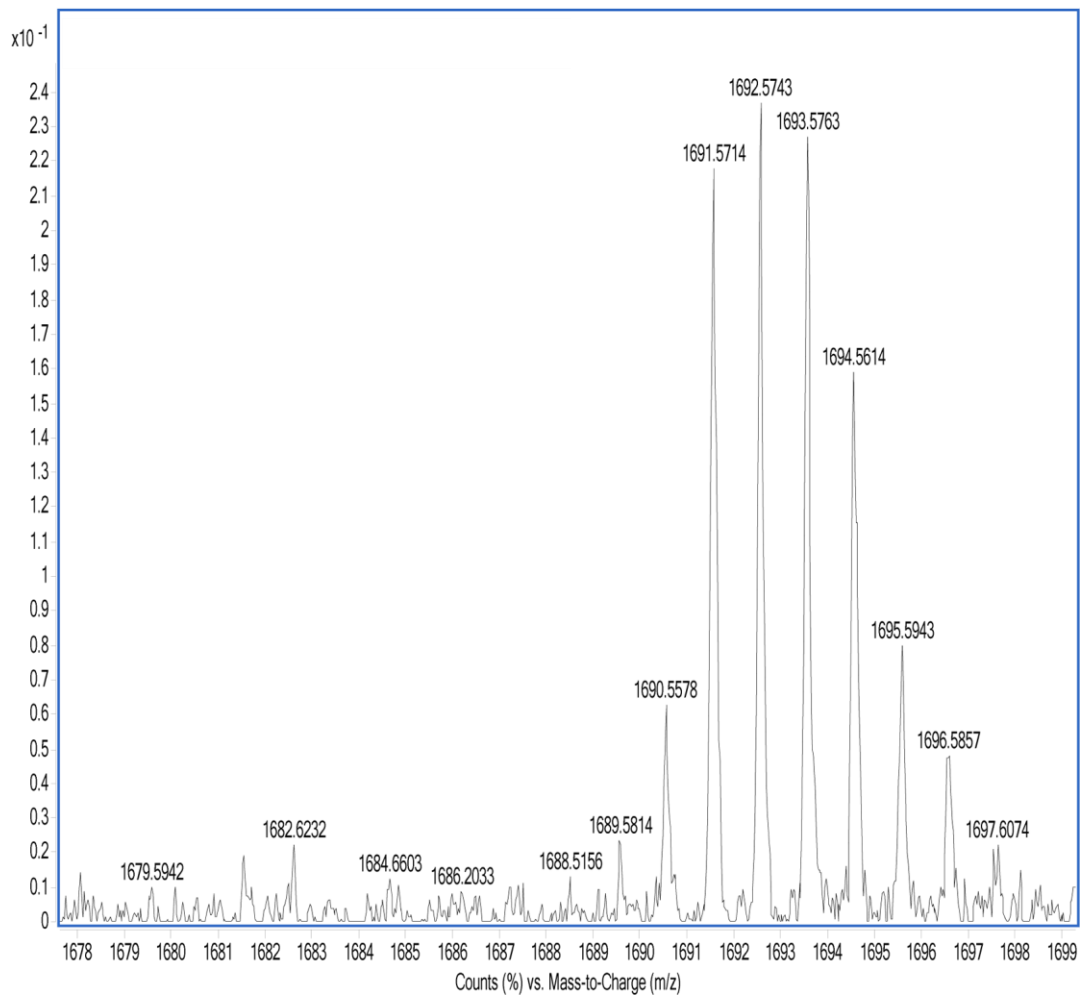


Figure 6.70. ESI spectrum of **2.46b•Cu**

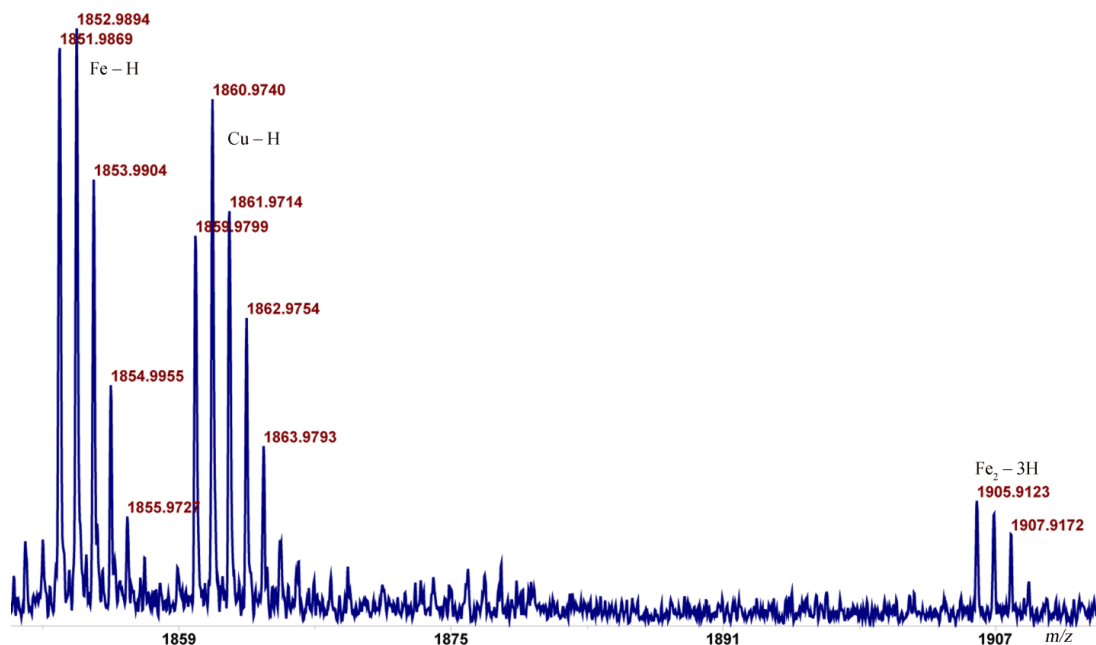


Figure 6.71. ESI spectrum of $2.44a \cdot Fe_x$

6.8 X-ray Crystallographic Data

A colorless prism fragment ($0.51 \times 0.47 \times 0.12 \text{ mm}^3$) was used for the single crystal X-ray diffraction study of $C_{48}H_{52}N_{12}O_{12} \cdot [CHCl_3]_2$ (cavitand **2.22b**). The crystal was coated with paratone oil and mounted on to a cryo-loop glass fiber. X-ray intensity data were collected at 100(2) K on a Bruker APEX2¹⁰ platform-CCD X-ray diffractometer system (fine focus Mo-radiation, $\lambda = 0.71073 \text{ \AA}$, 50KV/30mA power). The CCD detector was placed at a distance of 5.0500 cm from the crystal.

A total of 3600 frames were collected for a sphere of reflections (with scan width of 0.3° in ω , starting ω and 2θ angles at -30° , and ϕ angles of 0° , 90° , 120° , 180° , 240° , and 270° for every 600 frames, 40 sec/frame exposure time). The frames were integrated using the Bruker SAINT software package¹¹ and using a narrow-frame integration algorithm. Based on a monoclinic crystal system, the integrated frames yielded a total of

109550 reflections at a maximum 2θ angle of 56.56° (0.75 \AA resolution), of which 13725 were independent reflections ($R_{\text{int}} = 0.0401$, $R_{\text{sig}} = 0.0235$, redundancy = 8.0, completeness = 99.9 %) and 10499 (76.5 %) reflections were greater than $2\sigma(I)$. The unit cell parameters were, $\mathbf{a} = 22.5261(15) \text{ \AA}$, $\mathbf{b} = 12.1649(8) \text{ \AA}$, $\mathbf{c} = 20.9584(14) \text{ \AA}$, $\beta = 105.425(1)^\circ$, $V = 5536.3(6) \text{ \AA}^3$, $Z = 4$, calculated density $D_c = 1.473 \text{ g/cm}^3$. Absorption corrections were applied (absorption coefficient $\mu = 0.383 \text{ mm}^{-1}$; max/min transmission = 0.9569/0.8292) to the raw intensity data using the SADABS program.¹²

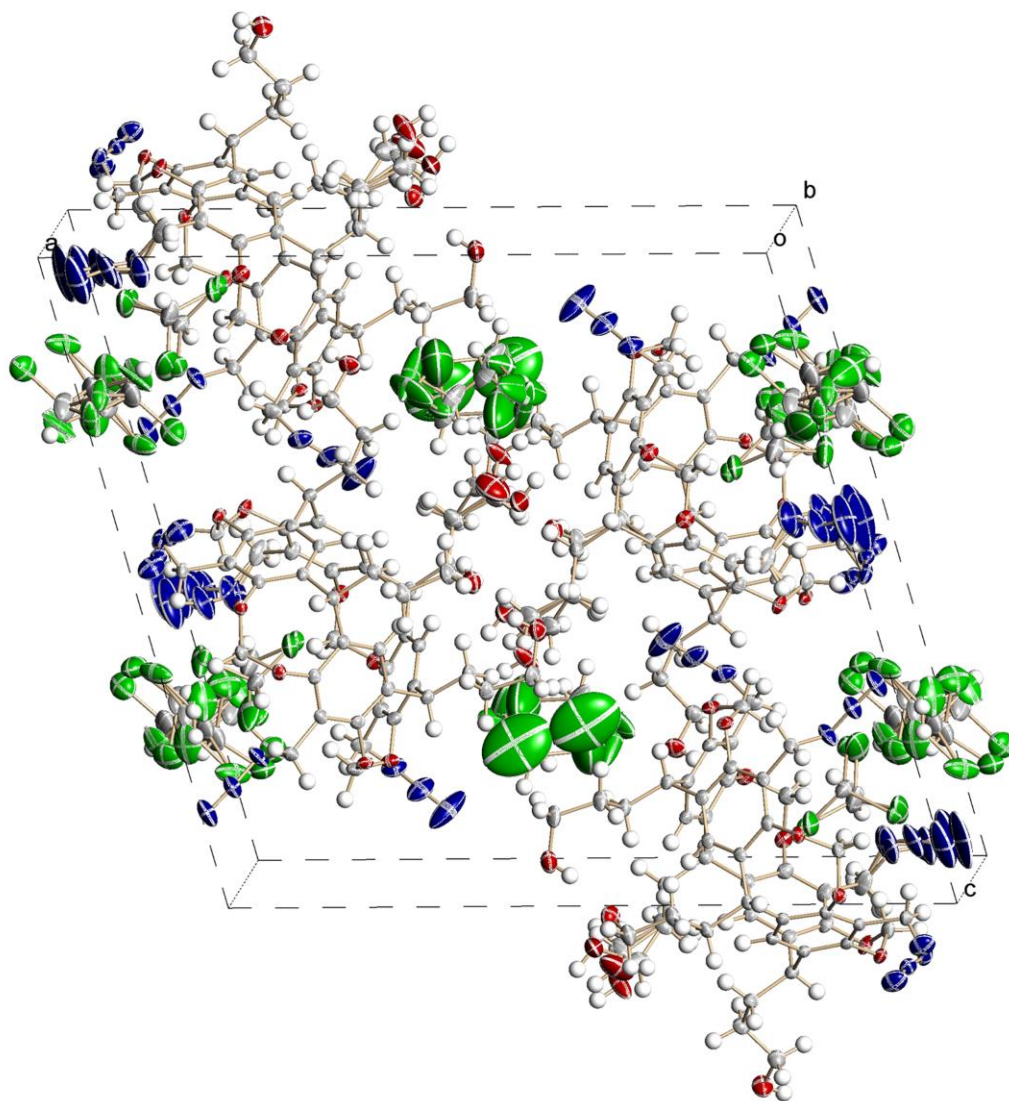


Figure 6.72. ORTEP representation on the unit cell of azidocavitanol **2.22b**

The Bruker SHELXTL software package¹³ was used for phase determination and structure refinement. The distribution of intensities ($E^2-1 = 0.976$) and systematic absent reflections indicated two possible space groups, P2/c and Pc. The space group P2/c (#13) was later determined to be correct. Direct methods of phase determination followed by

two Fourier cycles of refinement led to an electron density map from which most of the non-hydrogen atoms were identified in the asymmetry unit of the unit cell. With subsequent isotropic refinement, all of the non-hydrogen atoms were identified, including the disordered azides and disordered CHCl_3 solvent molecules. There were one molecule of $\text{C}_{48}\text{H}_{52}\text{N}_{12}\text{O}_{12}$ (with two azides and one $-\text{CH}_2\text{OH}$ disorder), one disordered molecule of CHCl_3 , and two disordered half-molecules of CHCl_3 present in the asymmetry unit of the unit cell. Two of the four azides were modeled with disorder (disordered site-occupancy ratios were 92 %/ 8 % and 43 %/ 30 %/ 27 %). One of the four $-\text{CH}_2\text{OH}$ groups was modeled with disorder ($-\text{CH}_2\text{OH}$ disordered site occupancy ratio was 39 %/ 34 %/ 27 %). All the three CHCl_3 solvents were modeled with disorder. Two disordered half-molecules of CHCl_3 were located at the two-fold rotation axis parallel to the **b**-axis (the two half-molecule of CHCl_3 disordered site occupancy ratios were 35 %/ 15 % and 20 %/ 19 %/ 11 %). The disordered site occupancy ratio for the whole CHCl_3 molecule located in general position was 80 %/ 20 %. One of the four $-\text{OH}$ groups was involved in intra-molecular hydrogen bonding and three were involved in intermolecular hydrogen bonding. The hydrogen bond distances and angles are given in Table 6.1. The following restraints, SUMP, DFIX, SADI, DELU, SIMU, FVAR and EADP were used to stabilize the final refinement of the disordered azides, disordered $-\text{CH}_2\text{OH}$, and disordered CHCl_3 .

Atomic coordinates, isotropic and anisotropic displacement parameters of all the non-hydrogen atoms were refined by means of a full matrix least-squares procedure on F^2 . The H-atoms were included in the refinement in calculated positions riding on the atoms to which they were attached. The refinement converged at $R1 = 0.0587$, $wR2 = 0.1620$,

with intensity $I > 2\sigma(I)$. The largest peak/hole in the final difference map was 0.872/-0.594 e/Å³.

Table 6.1: Crystal data and structure refinement for cavitand **2.22b**

Identification code	cavitand 2.22b	
CCDC Submission No.	862080	
Empirical formula	C ₅₀ H ₅₄ Cl ₆ N ₁₂ O ₁₂	
Formula weight	1227.75	
Temperature	100(2) K	
Wavelength	0.71073 Å	
Crystal system	Monoclinic	
Space group	<i>P2/c</i>	
Unit cell dimensions	a = 22.5261(15) Å	α = 90 °.
	b = 12.1649(8) Å	β = 105.4250(10)°.
	c = 20.9584(14) Å	γ = 90 °.
Volume	5536.3(6) Å ³	
Z	4	
Density (calculated)	1.473 Mg/m ³	
Absorption coefficient	0.383 mm ⁻¹	
F(000)	2544	
Crystal size	0.51 x 0.47 x 0.12 mm ³	
Theta range for data collection	1.88 to 28.28 °.	
Index ranges	-30 ≤ h ≤ 30, -16 ≤ k ≤ 16, -27 ≤ l ≤ 27	
Reflections collected	109550	
Independent reflections	13725 [<i>R</i> (int) = 0.0401]	
Completeness to theta = 28.28 °	99.9 %	
Absorption correction	Semi-empirical from equivalents	
Max. and min. transmission	0.9569 and 0.8292	
Refinement method	Full-matrix least-squares on F ²	
Data / restraints / parameters	13725 / 420 / 968	
Goodness-of-fit on F ²	1.050	
Final R indices [<i>I</i> > 2σ(<i>I</i>)]	R1 = 0.0587, wR2 = 0.1620	

R indices (all data)

R1 = 0.0788, wR2 = 0.1815

Largest diff. peak and hole

0.872 and -0.594 e.Å⁻³

Table 6.2: Atomic coordinates ($\times 10^4$) and equivalent isotropic displacement parameters ($\text{\AA}^2 \times 10^3$) for cavita nd **2.22b** is defined as one third of the trace of the orthogonalized U^{ij} tensor.

	x	y	z	U(eq)
O(1)	8229(1)	12157(1)	1227(1)	23(1)
C(1)	7808(1)	11405(2)	1352(1)	20(1)
C(2)	7903(1)	11024(2)	1998(1)	22(1)
C(2B)	8445(1)	11410(2)	2537(1)	27(1)
N(1B)	8945(1)	10574(2)	2640(1)	44(1)
N(2B)	9407(1)	10864(2)	3077(1)	44(1)
N(3B)	9846(1)	11054(3)	3463(2)	62(1)
C(3)	7464(1)	10320(2)	2136(1)	22(1)
O(3)	7548(1)	9984(1)	2789(1)	25(1)
C(4)	6933(1)	10022(2)	1654(1)	21(1)
C(5)	6862(1)	10415(2)	1015(1)	20(1)
C(6)	7290(1)	11108(2)	849(1)	19(1)
C(7)	7775(1)	8910(2)	2959(1)	27(1)
O(7)	7304(1)	8108(1)	2894(1)	28(1)
C(8)	6472(1)	9248(2)	1836(1)	22(1)
C(8A)	5796(1)	9454(2)	1463(1)	26(1)
C(9A)	5559(1)	10549(2)	1651(1)	33(1)
C(10A)	4863(1)	10668(2)	1422(1)	38(1)
O(10A)	4611(1)	10585(2)	721(1)	43(1)
C(9)	7110(1)	7577(2)	2283(1)	24(1)
C(10)	7326(1)	6518(2)	2229(1)	26(1)
C(10B)	7769(1)	5966(2)	2808(1)	34(1)
N(4B)	7450(1)	5290(2)	3201(1)	47(1)
N(5B)	7144(2)	5799(2)	3506(2)	60(1)
N(6B)	6837(3)	6151(4)	3795(2)	112(2)
C(11)	7110(1)	5970(2)	1627(1)	24(1)
C(12)	6689(1)	6442(2)	1087(1)	22(1)
O(11)	7299(1)	4881(1)	1592(1)	28(1)

C(13)	6485(1)	7505(2)	1167(1)	21(1)
C(14)	6684(1)	8082(2)	1758(1)	22(1)
C(15)	7778(1)	4683(2)	1277(1)	29(1)
O(15)	7550(1)	4442(1)	596(1)	28(1)
C(16)	6492(1)	5832(2)	432(1)	22(1)
C(17A)	5840(1)	6139(2)	20(1)	27(1)
C(18A)	5626(1)	5475(2)	-618(1)	40(1)
C(19A)	4946(5)	5647(12)	-961(12)	47(3)
O(19A)	4884(6)	6750(10)	-1189(7)	93(4)
C(19D)	5163(4)	6127(10)	-1155(5)	47(3)
O(19D)	4612(3)	6094(10)	-929(4)	80(4)
C(19E)	4988(4)	5872(7)	-1022(6)	40(3)
O(19E)	4766(3)	5181(6)	-1576(3)	64(3)
C(17)	7496(1)	5339(2)	173(1)	24(1)
C(18)	7958(1)	5505(2)	-149(1)	27(1)
C(18B)	8481(1)	4709(2)	-62(2)	44(1)
N(7B)	9011(4)	5194(11)	451(6)	57(3)
N(8B)	9505(5)	4748(14)	501(8)	101(4)
N(9B)	9962(5)	4314(15)	555(13)	183(8)
N(7D)	8978(8)	4953(19)	551(10)	74(3)
N(8D)	9365(6)	4270(12)	494(10)	74(3)
N(9D)	9779(7)	3692(15)	620(16)	137(6)
N(7E)	8963(8)	4841(18)	579(10)	74(3)
N(8E)	9382(6)	5513(11)	640(8)	74(3)
N(9E)	9806(6)	6003(14)	616(13)	137(6)
C(19)	7906(1)	6400(2)	-570(1)	25(1)
C(20)	7393(1)	7092(2)	-708(1)	22(1)
C(21)	6943(1)	6892(2)	-377(1)	21(1)
C(22)	6982(1)	6023(2)	64(1)	21(1)
O(19)	8375(1)	6586(1)	-876(1)	30(1)
C(23)	8794(1)	7433(2)	-588(1)	28(1)
O(23)	8644(1)	8462(1)	-911(1)	24(1)
C(24)	7346(1)	8047(2)	-1182(1)	21(1)
C(24A)	6682(1)	8269(2)	-1602(1)	24(1)

C(25A)	6397(1)	7322(2)	-2056(1)	30(1)
C(26A)	6729(1)	7110(2)	-2586(1)	34(1)
O(26A)	6381(1)	6348(2)	-3053(1)	46(1)
C(25)	8286(1)	9187(2)	-657(1)	20(1)
C(26)	8581(1)	10097(2)	-308(1)	20(1)
C(26B)	9260(1)	10273(2)	-199(1)	24(1)
N(10B)	9410(1)	10933(2)	-735(1)	34(1)
N(11B)	9186(1)	11843(2)	-834(1)	33(1)
N(12B)	8992(2)	12685(2)	-990(2)	55(1)
N(11D)	9433(15)	11898(11)	-537(16)	33(1)
N(12D)	9525(18)	12806(13)	-432(17)	55(1)
C(27)	8225(1)	10851(2)	-68(1)	20(1)
C(28)	7592(1)	10717(2)	-170(1)	19(1)
C(29)	7317(1)	9806(2)	-534(1)	20(1)
C(30)	7649(1)	9039(2)	-793(1)	19(1)
O(27)	8523(1)	11779(1)	254(1)	23(1)
C(31)	8693(1)	11741(2)	956(1)	24(1)
C(32)	7226(1)	11506(2)	144(1)	20(1)
C(32A)	6557(1)	11623(2)	-265(1)	24(1)
C(33A)	6201(1)	12478(2)	3(1)	32(1)
C(34A)	5510(1)	12363(2)	-284(2)	37(1)
O(34A)	5280(1)	11371(2)	-75(1)	46(1)
C(1S)	1185(1)	8409(3)	3351(2)	35(1)
Cl(1)	583(1)	8606(2)	3731(1)	42(1)
Cl(2)	1892(2)	8167(2)	3961(2)	40(1)
Cl(3)	1035(1)	7323(2)	2774(1)	51(1)
C(1D)	1128(8)	7577(17)	3576(10)	59(5)
Cl(1D)	508(7)	8428(15)	3671(8)	92(5)
Cl(2D)	1789(8)	8207(15)	3886(9)	69(4)
Cl(3D)	905(8)	7314(16)	2792(8)	134(7)
C(2S)	4728(4)	3362(7)	-2686(5)	59(4)
Cl(4)	4382(1)	2089(2)	-2925(1)	48(1)
Cl(5)	5487(2)	3191(5)	-2185(2)	104(2)
Cl(6)	4286(2)	4091(5)	-2254(4)	159(4)

C(2D)	5435(9)	3356(14)	-2060(12)	59(4)
Cl(4D)	5510(16)	2008(12)	-2330(20)	339(18)
Cl(5D)	4656(8)	3660(20)	-2118(14)	265(12)
Cl(6D)	5763(7)	4317(14)	-2492(7)	182(9)
C(3S)	9522(6)	4052(10)	2410(8)	72(3)
Cl(7)	10109(2)	3045(4)	2653(4)	59(2)
Cl(8)	9099(3)	4213(5)	2995(4)	68(2)
Cl(9)	9818(4)	5261(5)	2172(5)	98(3)
C(3D)	10173(5)	4558(13)	2209(5)	72(3)
Cl(7D)	9570(7)	3610(20)	2086(7)	159(8)
Cl(8D)	10671(3)	4226(7)	1716(3)	74(2)
Cl(9D)	10530(4)	4729(8)	3053(3)	81(2)
C(3E)	10079(6)	4846(15)	2396(8)	72(3)
Cl(7E)	9347(5)	4234(11)	2110(9)	73(5)
Cl(8E)	10326(5)	5388(8)	1728(4)	79(4)
Cl(9E)	10613(6)	3890(9)	2854(6)	64(5)

6.9 References

- 1) Gibb, B. C.; Chapman, R. G.; Sherman, J. C. "Synthesis of Hydroxyl-Footed Cavitands." *J. Org. Chem.* **1996**, *61*, 1505–1509.
- 2) Mezo, A. R.; Sherman, J. C. "Water-Soluble Cavitands: Synthesis of Methylene-Bridged Resorcin[4]arenes Containing Hydroxyls and Phosphates at Their Feet and Bromomethyls and Thiomethyls at Their Rims." *J. Org. Chem.* **1998**, *63*, 6824–6829.
- 3) Woollard-Shore, J. G.; Holland, J. P.; Jones, M. W.; Dilworth, J. R. "Nitrite Reduction by Copper Complexes." *Dalton Trans.* **2010**, *39*, 1576–1585.
- 4) Wipf, P.; Aoyama, Y.; Benedum, T. E. "A Practical Method for Oxazole Synthesis by Cycloisomerization of Propargyl Amides." *Org. Lett.* **2004**, *6*, 3593–3595.
- 5) Sanphanya, K.; Wattanapitayakul, S. K.; Prangsaengtong, O.; Jo, M.; Koizumi, K.; Shibahara, N.; Priprem, A.; Fokin, V. V.; Vajragupta, O. "Synthesis and Evaluation

- of 1-(Substituted)-3-prop-2-ynylureas as Antiangiogenic Agents." *Bioorg. Med. Chem. Lett.* **2012**, *22*, 3001–3005.
- 6) Struthers, H.; Spingler, B.; Mindt, T. L.; Schibli, R. "Click-to-Chelate: Design and Incorporation of Triazole-Containing Metal-Chelating Systems into Biomolecules of Diagnostic and Therapeutic Interest." *Chem. Eur. J.* **2008**, *14*, 6173–6183.
 - 7) Biedrzycki, M.; de Bie, D. A.; van der Plas, H. C. "Dihydroisobenzofurans and Isoindolines by Intramolecular Inverse Diels-Alder Reactions of Pyridines." *Tetrahedron* **1990**, *46*, 607–614.
 - 8) Michaels, H. A.; Murphy, C. S.; Clark, R. J.; Davidson, M. W.; Zhu, L. "2-Anthryltriazolyl-Containing Multidentate Ligands: Zinc-Coordination Mediated Photophysical Processes and Potential in Live-Cell Imaging Applications." *Inorg. Chem.* **2010**, *49*, 4278–4287.
 - 9) Xi, H.; Gibb, C. L. D.; Gibb, B. C. "Functionalized Deep-Cavity Cavitands." *J. Org. Chem.* **1999**, *64*, 9286–9288.
 - 10) *APEX 2*, version 2010.11-3, Bruker (2010), Bruker AXS Inc., Madison, Wisconsin, USA.
 - 11) *SAINT*, version V7.60A, Bruker (2009), Bruker AXS Inc., Madison, Wisconsin, USA.
 - 12) *SADABS*, version 2008/1, Bruker (2008), Bruker AXS Inc., Madison, Wisconsin, USA.
 - 13) *SHELXTL*, version 2008/4, Bruker (2008), Bruker AXS Inc., Madison, Wisconsin, USA.